NASA CONTRACTOR REPORT

NASA CR-1475

NASA CR-1475

A COLD CATHODE ION SOURCE MASS SPECTROMETER EMPLOYING ION COUNTING TECHNIQUES

by F. L. Torney, Jr., P. Blum, P. Fowler, and J. R. Roehrig

Prepared by
NORTON RESEARCH CORPORATION
Cambridge, Mass.
for Langley Research Center

NATIONAL AERONAUTICS AND SPACE ADMINISTRATION • WASHINGTON, D. C. • DECEMBER 1969

NASA CR-1475

A COLD CATHODE ION SOURCE MASS SPECTROMETER EMPLOYING ION COUNTING TECHNIQUES

By F. L. Torney, Jr., P. Blum, P. Fowler, and J. R. Roehrig

Prepared under Contract No. NAS 1-5347, Task 8 by
NORTON RESEARCH CORPORATION
Cambridge, Mass.

for Langley Research Center

NATIONAL AERONAUTICS AND SPACE ADMINISTRATION

For sale by the Clearinghouse for Federal Scientific and Technical Information
Springfield, Virginia 22151 – Price $3.00

TABLE OF CONTENTS

Page

Page

LIST OF FIGURES

A COLD CATHODE ION SOURCE MASS SPECTROMETER EMPLOYING ION COUNTING TECHNIQUES

By F. L. Torney, Jr., P. Blum, P. Fowler and J. R. Roehrig
Norton Research Corporation

SUMMARY

A need has existed for some time to improve the performance of ultrahigh vacuum (UHV) residual gas analyzers. Consequently, a comprehensive research and development program has been undertaken (under NAS1-2691 and NAS1-5347) to improve the primary elements of UHV residual gas analyzers; namely the ion source, mass analyzer and ion detector. As a result of this effort, a new type of spectrometer has been developed employing a cold-cathode source of ions, a quadrupole mass analyzer, and an ion counting detector. The instrument is called a cold-cathode ion source/quadrupole (CCIS/Quad) mass spectrometer. In its present form, it is designed for general laboratory use. With appropriate miniaturization, the instrument is particularly suitable for space flight applications which emphasize low power and weight.

The new instrument features a cold-cathode ion source adapted for use with a purchased quadrupole mass analyzer. The detector of the instrument has also been modified to enhance the output signal-to-noise (S/N) ratio by means of ion counting techniques. Although the analyzer is not theoretically optimal for use with the CCIS, the performance of the overall instrument displays notable improvements in sensitivity, S/N ratio and spectral cleanliness which are important to the problems of UHV residual gas analysis.

Resolution of the new instrument is identical to that obtained from a comparable hot-filament instrument and appears limited only by the design of the quadrupole analyzer.

Response characteristics of the CCIS/Quad (output vs. partial pressure) have been studied for N_2, Ar, and Ne in the range 4 x 10^{-12} Torr (nitrogen) to approximately 10^{-10} Torr using dc current and ion counting techniques. Good agreement was noted between the methods and with previously published data. Additionally, response characteristics have been measured for He and Kr in the range of 3 x 10^{-9} Torr to 1 x 10^{-7} Torr. The upper limit of partial pressure analysis using counting techniques is primarily established by the speed of the ion counting electronics. In the present work this limit is approximately 10^6 counts per minute, corresponding to a nitrogen partial pressure of 1 x 10^{-10} Torr.

The ion counting S/N ratio of the instrument has been studied as a function of certain operating parameters such as anode voltage, magnetic field, retarding voltage, multiplier gain and ion accelerating voltage. An optimal choice of these parameters has been made. A small photon noise background has been discovered emanating from the CCIS. Unlike the familiar Bayard-Alpert (B-A) gauge x-ray current, the CCIS noise is pressure dependent. This background can be overcome by locating the multiplier off axis and by electrostatically deflecting the ion beam to the first dynode. This method has been used successfully to avoid x-ray induced noise in a commercial hot-filament quadrupole.

In other recent studies, it has been shown that the use of ion counting techniques offers promise of major improvements in instrument S/N ratio when compared with conventional ion current detection methods. Moreover, if recently improved electron multipliers are used, the counting detector also promises to eliminate uncertainties in multiplier gain. Additionally, anomalous responses of the multiplier to ionic mass, structure, and momentum can probably be circumvented.

This report will, therefore, describe in detail all phases of the research and development programs pertaining to the development of the new instrument. Complete construction and assembly drawings of the CCIS are included together with instructions for adapting the source to a commercial analyzer. Instructions are also included for the installation, preparation and operation of the instrument as an UHV residual gas analyzer. Finally, detailed descriptions of the equipment and techniques used to modify the instrument for ion counting detection are included together with the results of a recently completed evaluation of the ion counting detection method.

INTRODUCTION

Residual gas analysis in ultrahigh vacuum is still a problem of sizeable importance in space research instrumentation although residual gas analyzers (RGA's) find widespread use in laboratory and in spaceflight applications. In general, these instruments have certain fundamental problems which have not been adequately solved for all potential applications. The first problem is one of instrument sensitivity. The resolved ion beam typically

represents an output current sensitivity of the order of 10^{-5} to 10^{-4} amps/Torr. While some loss of ions is anticipated within the analyzer, the basic ion source sensitivity is not exceptionally high. Furthermore, the type of ion source most widely used contains a hot-filament electron emitter. In UHV applications, this type of source is known to generate objectionable amounts of various gases which essentially obliterate the measurement of these same gases which are in the test environment. This characteristic limits the effective sensitivity of the instrument. This is the second problem area encountered. The third problem involves the use of electron multipliers which are required at the analyzer output to amplify the small ion currents. Typical electron multipliers are often characterized by large and unpredictable variations in gain. As a result, the ion detector has a pronounced influence on instrument sensitivity, which is proportional to multiplier gain.

It was realized a few years ago that the cold-cathode total pressure ionization gauge has certain desirable characteristics which might be brought to bear on two of these three problem areas. First, these gauges have much larger sensitivity than hot-filament ionization gauges. For instance, the familiar Redhead magnetron ionization gauge is 45 times more sensitive (4.5 amps/Torr) than a B-A ionization gauge (0.1 amps/Torr) in the region above approximately 10^{-10} Torr. Furthermore, it is not limited

by the equivalent of the well known x-ray limit in B-A gauges, since its x-ray limit is actually pressure dependent. Most important, however, is the fact that the gauge is typically less troublesome with regard to the generation of internal gas (outgassing).

Accordingly, contract work was undertaken to study the feasibility of using a cold-cathode discharge as an ion source for UHV RGA's. This preliminary work investigated the characteristics of ion beams extracted from the CCIS to ascertain such important parameters as average ion energy, distribution of ion energies and the ultimate sensitivity that might be anticipated. In addition, the selection of a suitable mass-to-charge (m/e) analyzer was also considered. The quadrupole analyzer was chosen as a result of the rather broad energy distribution encountered in the CCIS studies. Furthermore, certain favorable modes of operating the quardupole were also investigated and a tentative analyzer design was chosen which represented an optimum design for laboratory use.

Following these initial studies, improvements in source design were made and evaluated, with particular emphasis placed on increasing the sensitivity of the source. A lens system for focusing ions into the quadrupole was studied but was discarded, when it was found that the geometry of the extracted ion beam was inappropriate. The program did, however, effect an order of magnitude improvement in sensitivity over the previous source design. A simplified quadrupole design chart was devised for selecting the optimum future quadrupole design parameters. This chart was drawn up to simplify trade-off studies in future quadrupole designs.

Nearly coincidental with the development of the improved CCIS, three quadrupole mass spectrometers were announced in the commercial market. While none of these instruments were designed in accordance with the original design goals for a CCIS/Quadrupole, their general performance was close to these goals. The notable exception involved sensitivity which is fundamentally related to quadrupole size (resolution held constant). Since these events presented an opportunity to expeditiously evaluate and compare the CCIS with a hot-filament instrument, a commercial quadrupole was eventually selected as the analyzer.

In the next stage of development, one of the commercial quadrupoles was selected for adaptation to the CCIS. The instrument was briefly studied using its hot-filament ion source to form a baseline for future comparison with the CCIS. The CCIS was adapted to the quadrupole and performance studies of the new instrument began. After optimizing certain CCIS operating parameters, resolution, sensitivity, linearity, transmission, and cleanliness of the instrument were evaluated. In general, the instrument shows improved sensitivity and reduced outgassing effects. Resolution is excellent and is largely limited by the quardupole design and not by the ion source. In these investigations, an electron multiplier was not used as the ion detector. Instead, a simple Faraday cup detector was used, to permit more reliable evaluation of sensitivity, transmission, and other instrument characteristics.

The final contract effort reported herein centered around a study of the use of ion counting techniques to improve instrument S/N ratio at extremely low pressures. An electron multiplier was purchased and installed in the instrument. A background current was noted which is traceable to a form of photon emission from the ion source. The source was modified slightly and a noticeable reduction in the noise level was made. This noise is pressure-dependent, unlike the pressure-independent x-ray photons encountered in hot-filament RGA's and is therefore, generally less objectionable. After studying the ion source and counting detector operating parameters to maximize S/N ratio, the ion counting detector performance was evaluated. Counting efficiency, S/N ratio, signal and noise pulse height distribution, multiplier gain and other important characteristics have been thoroughly investigated. Although detector performance is not theoretically perfect, future success for this detection technique can be predicted. In general, this work is not only applicable to the CCIS/Quadrupole but is also of interest in improving other UHV spectrometers and total pressure gauges.

LIST OF SYMBOLS AND ABBREVIATIONS

B-A gauge	Bayard-Alpert gauge
CCIS	cold-cathode ion source
CCIS/Quad	cold-cathode ion source/quadrupole
cpm	counts per minute
FWHM	full width at half maximum
G_m	gain of multiplier
G_n	gain of multiplier for noise
I^+	magnetron cathode ion current (amperes)
I^-	electron emission current (amperes)
I_1	ion collector current (modulator at grid potential, amperes)
I_2	ion collector current (modulator at ground potential, amperes)
i_c	collector current (amperes)
I_{in}	multiplier ion input current (amperes)
i_j^+	cathode current due to jth species (amperes)
I_n	multiplier output noise current (amperes)
I_o	Multiplier output current (amperes)
K	gauge constant ($Torr^{-1}$)
K_1	cathode #1
K_2	cathode #2

k_j	sensitivity constant for jth species (amps/Torr)
K_n	counting sensitivity (cpm/Torr)
M	mass
MBAG	modulated Bayard-Alpert gauge
M/c	mass-to-charge ratio
n	exponent
P, p	pressure (Torr)
P_j	partial pressure of jth species (Torr)
P_T	true pressure (Torr)
R	multiplier input ion arrival rate (ions/sec)
RGA's	residual gas analyzers
R_n	multiplier output noise counting rate (counts/sec)
R_o	observed counting rate (ions/sec)
r_o	radius of circle inscribed within quadrupole rod structure (meter)
R_t	true counting rate (ions/sec)
S	multiplier sensitivity (cpm/Torr)
S_{28}	multiplier sensitivity for mass 28 (cpm/Torr)
S/N	signal-to-noise ratio
U	dc rod potential (volts)
UHV	ultra high vacuum (pressure $<10^{-9}$ Torr)

$U_{T_{max}}$	maximum allowable transverse ion energy (eV)
V	rf rod potential (peak volts)
V_A	anode potential (volts)
V_R	retarding potential (volts)
V_{K_1}	cathode K_1 potential (volts)
V_{K_2}	cathode K_2 potential (volts)
α	modulation coefficient for MBAG
ΔM	peak width in amu expressed at 5% peak height
ε	ion counting efficiency
γ	secondary emission ratio
ν	rf frequency (Hz)

SYNOPSIS OF PREVIOUS DESIGN AND DEVELOPMENT EFFORTS

General Organization of the Report

It is recognized that the most recent developments are likely to be of greatest immediate interest. Earlier studies which background the present developments are briefly synopsized below. Complete discussions of earlier work appear in Appendices A and B. Following the synopsis three main sections will discuss: (1) the CCIS/ Quadrupole and its performance, (2) the improved ion counting detector studies, and (3) a detailed description of the design, construction and operation of the CCIS/ Quadrupole spectrometer.

The final section will summarize the general conclusions which can be drawn from this work and will suggest areas of future study or development.

Program Goals and Objectives

Spectrometer problems. - The primary objective of the program is to develop an improved mass spectrometer for general laboratory use in UHV space simulation and related laboratory vacuum studies. The instrumentation previously available was deficient in three important areas associated with the ion source and detector elements such as: (1) relatively low ion source sensitivity, (2) outgassing of the hot-filament ion source under UHV conditions, and (3) detector instabilities which impede quantitative measurements in UHV.

Approach to the problem. - It was recognized at the outset that a new type of ion source was required to overcome these difficulties. The new source should be "cold", to eliminate both thermal desorption and dissociation of residual gas by the heated filament. Additionally, the source should exhibit greater ionization efficiency to markedly improve overall instrument sensitivity. Such improvement would reduce the reliance on very sensitive dc ion detectors. Finally, a more stable detector was required to permit reliable quantitative UHV measurements.

The cold-cathode ion source suggested itself as an appropriate candidate because of its lack of a high temperature filament and because of its large ionization efficiency. Although cold-cathode discharge gauges have found widespread application in UHV measurement, scanty information exists on their application as ion sources. It was anticipated that such devices would yield ions widespread in energy. Very little definitive information existed, however, on the ion energy distribution following extraction from cold-cathode sources.

Accordingly, NRC proposed to NASA/Langley Research Center that a modest program be instituted to evaluate the cold-cathode ion source for application in UHV mass spectrometry. A program was conceived in which the unknown characteristics of the ion source would be studied first. Contingent on the successful outcome of this work,

an improved source would be developed and tested under the program. Simultaneous to the ion source investigations, the mass analyzer and detection systems would be considered and recommendations made regarding the optimal design of these elements. The suggestions were funded and the program work was begun. This work, although preliminary in extent and application, has important bearing on the final design and performance of the CCIS/Quad spectrometer particularly to the analyzer section. Therefore, the program results are included in their entirety in Appendices A and B. A brief summary of the salient results of this work will also be given to synopsize the results and to emphasize the design criteria of the spectrometer.

Preliminary Ion Source and Analyzer Studies

Ion source design. - A number of configurations of the cold-cathode ion source (CCIS) were considered for possible application in the proposed spectrometer. These sources all involved a magnetically confined electrical discharge in a low pressure gas. Radioactive and other cold discharges were also considered but rejected primarily for sensitivity reasons. Of the numerous types of cold-cathode discharge devices, the magnetron type discharge (after Redhead) was selected, primarily because of its large sensitivity.

An ion source was designed and built using the Redhead magnetron structure, but with a small remmant stub replacing the normal cathode spool construction. A complete description of the source is given in Appendix A. The preliminary source was designed to study the properties of ion beams extracted from the source. To this end, retarding field techniques were used in conjunction with a simple Faraday cup ion collector to measure the emergent beam. After preliminary investigation of various extraction methods, studies were made of the energy spread of the ion beam. A relatively large flux of low energy ions was noted under optimum conditions. This flux of ions was measured after passing through an aperture of 3mm. The resultant ion source sensitivity was approximately 5 mA/Torr (nitrogen). The total energy spread of 96.8% of the ions was between 0 and 31.5 eV. This figure is within the acceptable limits for axial energy spread for a small quadrupole analyzer. However, the transverse component of ion energy is a more critical criterion for ion rejection within a quadrupole analyzer and the experiments were not capable of yielding information of this type. Since very limited information existed on the total energy distribution of ions extracted from a magnetron, primary emphasis was placed on obtaining this data.

Quadrupole design. - It became obvious from early investigations of the ion source that the only analyzer capable of dealing with the relatively large CCIS energy spread was a quadrupole. It was not obvious which of the number of quadrupole operating modes would be most favorable for the CCIS, or if, indeed, any modes were. A careful analysis was, therefore, made of the quadrupole theory to define the optimum conditions. The results of this study showed that one mode is preferable to the others. A complete discussion of the quadrupole operating modes and the reasons for the choice of one specific mode are detailed in Appendix A. Summarized briefly, it was shown that the so-called "constant peak width" (Δm = constant) mode is preferable for the following reasons:

(a) Peak width is nearly independent of mass.

(b) Mass scale is linear throughout the mass range.

(c) Maximum allowable transverse ion energy (for 100% transmission) is independent of mass.

(d) Maximum allowable axial ion energy is also independent of mass.

(e) For 100% transmission, the selected mode will permit a larger beam diameter (higher sensitivity) than other modes.

(f) Requirements of frequency and voltage stability are less stringent for the chosen mode, particularly at lower mass.

A design study of a quadrupole suitable for use with the CCIS was made. The design assumed that a resolution of 1 amu (10% valley criterion) would be required and that 100% transmission of all ions in the mass range 1-100 amu would also be necessary. These two criteria define a quadrupole of laboratory size and power consumption. The rod radius, for instance, was 2.32 cm and rod length was 25 cm. Although the projected analyzer is larger than the purchased analyzer eventually chosen, the theory predicts that the projected design is capable of taking full advantage of the high sensitivity of the CCIS. In fact, it has been shown that the sensitivity with the commercial quadrupole is less than 10% of the full capability of the ion source because of the smaller size, etc. of the commercial instrument. Despite this fact, it will be shown that the CCIS is nearly six times more sensitive than the hot-filament instrument. Thus, in comparing the sensitivities of the CCIS/Quad with other hot-filament spectrometers, it should be remembered that the smaller analyzer does not display the full sensitivity potential of the CCIS.

Briefly summarized then, the feasibility study of the CCIS has shown that the new ion source is capable of delivering a large flux of ions to an appropriately designed quadrupole analyzer. The next section will summarize the improvements made in the source design.

Improved Ion Source Design

Having demonstrated that a cold-cathode ion source will produce a beam of ions acceptable to a quadrupole analyzer, further work was begun in improving the source design to its fullest extent.

The purpose of this work was to investigate methods of increasing the source sensitivity obtained in the feasibility study, compatible with the requirements of a quadrupole mass spectrometer. Appendix B gives complete details of the program. The improved source contained a probe for measuring ion energy distribution through a very small (1 mm) simulated quadrupole entrance aperture. The probe's position was adjustable relative to the ion exit aperture. The design included an electrostatic lens and provision for comparing sensitivities with and without the lens. Also included was a provision for defining optimum ion extraction conditions. Modifications were also made in the magnetic field geometry used in the feasibility study source. Cylindrical ceramic magnets were used to reduce external bulk. Elimination of internal pole pieces improved beam geometry at the ion exit aperture and generally reduced internal sources of outgassing.

Methods of optimizing sensitivity without the lens were studied first. The sensitivity and ion energy distribution were examined (using retarding potential methods) as a function of extraction conditions. It was discovered that a large electron component was present in the beam and that certain abnormally large sensitivities observed were connected with the electron beam component. Subsequent data was, therefore, examined critically for possible misconceptions of this nature.

A family of ion energy distributions was obtained as a function of distance from the ion exit aperture. The energy distributions for all distances and all cathode potentials used (both positive and negative) showed ions predominating at low energies and decreasing continuously with increased energy, a situation beneficial to high quadrupole spectrometer sensitivity. Maximum sensitivity occurred nearest the exit aperture and again at a point more distant.

The highest sensitivity obtained with optimum ion extraction conditions and for an energy distribution acceptable to a quadrupole (0-30 eV) was 5.5 mA/Torr (nitrogen). This value was measured at two nodes along the axis of the exiting beam. This sensitivity, obtained through the 1 mm diameter probe aperture compares very favorably with a somewhat lower figure obtained with a 3 mm diameter aperture used in the feasibility study. A minimum sensitivity improvement of one decade was achieved without the use of a lens.

Improvements in sensitivity through the use of an electrostatic lens were also investigated. A three-aperture einzel lens was designed for this purpose. It has the necessary characteristic of focusing without increasing ion energy. Analytical investigations conducted to determine optimum lens design and operation revealed that a lens would not provide an increase in source sensitivity, compared to placing the quadrupole close to the source, unless an especially favorable beam geometry existed (e.g., a nearly parallel and mono-energetic beam). To validate this prediction, studies

were conducted for several positions of the lens and probe relative to the ion exit aperture. A large range of lens focusing potentials were applied and ion energy distributions were obtained. The effect of various ion extraction conditions was also studied. It was concluded for each situation that the lens provided no sensitivity improvement. However, certain anomalies in lens operation were also observed. These were attributed to the presence of electrons in the beam and their resulting focusing and/or reflection by the lens.

A quadrupole mass analyzer design chart was constructed covering a wide range of possible design values. Their interdependence, which is rather complicated, is thereby made evident. As a result, a set of design parameters were determined which are optimally matched to both the experimentally determined characteristics of the cold-cathode ion source and the general program objectives.

In summary then, the improved ion source design study demonstrated a noticeable improvement in source sensitivity. Approximately the same sensitivity (5 mA/Torr) was observed through a simulated aperture 1/9 are large in area as that used in the earlier studies. Pronounced electron fluxes were observed in the extracted beam, which made retarding potential measurements of ion beam energy distribution difficult to evaluate.

In the next main section the culmination of these preliminary investigations will be described. The improved source was adapted to a quadrupole analyzer and the resultant spectrometer is described and discussed.

DEVELOPMENT OF THE CCIS/QUAD MASS SPECTROMETER

Selection of the Quadrupole Analyzer

It has been previously noted that during the feasibility study phase, a design study was made of the optimal quadrupole for use with the CCIS. Coincident with this work, three quadrupole mass spectrometers were introduced on the market. Previously such instruments were built entirely by individuals and/or agencies to suit particular needs. In the interest of economy it was decided to examine the alternative of purchasing a suitable analyzer and its electronics rather than designing and building a new instrument.

The design and performance characteristics of the three commercial instruments were examined as critically as available information would allow. It was recognized that certain trade-offs would be necessary if a physically smaller analyzer were chosen. For instance, a loss in sensitivity and variation in quadrupole transmission with mass was immediately anticipated with a smaller instrument.

The final selection was by no means straightforward since each design approached the problem differently. The sensitivity of all instruments was similar. One design was theoretically more favorable to larger axial energy distribution, while another was more favorable to larger transverse energies. The final choice was made primarily on the basis of operating mode and of availability. The instrument chosen* operated in the desired mode (constant

---

*An Ultek/EAI Quad Model 200, Ultek Corp., Palo Alto, Calif.

peak width) which, as explained, is more favorable to the CCIS. It was purchased with a so-called axial beam ionizer (hot-filament) together with the electronics required to operate the ionizer and the quadrupole analyzer. An electron multiplier was not included, since absolute sensitivity measurements were desired. A comparative study could, therefore, be made of the hot and cold-cathode sources without involving multiplier variables.

Once received, the commercial instrument was installed on an UHV system (to be described in connection with the CCIS/Quad), and performance testing begun using the hot-filament ionizer. This information was required for future comparisons with the CCIS/Quad version. The preliminary tests which were made using the hot-filament ionizer will be described next.

Evaluation Studies of Hot-Filament Quadrupole

Purposes of tests. - The Ultek/EAI Model 200 Quadrupole was operated in accordance with instructions supplied by the manufacturer. The primary objective was to establish performance comparisons between the hot-cathode and cold-cathode ion sources using the same quadrupole analyzer. The following characteristics were examined using the hot-cathode source:

(a) Sensitivity vs. atomic mass number

(b) Linearity vs. partial pressure.

(c) Resolution vs. mass number from 1 to 150 amu

(d) Spectrometer cleanliness, noise and response time.

The purchased hot-filament quadrupole spectrometer automatically scans the mass spectrum in the most favorable mode (constant Δ M) for the cold-cathode ion source. It is also important to note that the entrance aperture is nearly equal to the dimension r_o. Figure A-17 of Appendix A shows that this larger aperture can lead to a pronounced variation in transmission as a function of mass number. This variation would lead to exaggerated peak heights for the lighter gases.

One of the main purposes of testing the spectrometer was, therefore, to discover how the quadrupole transmission varied over the desired mass range (1-150 amu). Closely related to this question is the absolute sensitivity of the spectrometer, since the product of the ion source sensitivity and quadrupole transmission factor determines the over-all sensitivity.

Since the sensitivity and resolution are inversely related in any spectrometer, it was first necessary to set the spectrometer to a prescribed resolution and to maintain these conditions throughout the test program. For this purpose, the isotopes of Xenon are nearly ideal. Xe^{131} and Xe^{132} are one mass unit apart and of nearly the same abundance. Therefore, the resolution was set so that the valley between these peaks was 10% of the height of the Xe^{132} peak. This now defines and fixes the resolution for all subsequent tests of the hot-filament quadrupole.

The spectrometer has three mass ranges:

Low:	1 - 50 amu
Medium:	10 - 150 amu
High:	50 - 500 amu

The performance was not studied on the 50 - 500 amu range. However, both the "low" and "medium" ranges were studied in detail. Before describing the results of these tests, a brief description of the test methods will be given.

Test methods. - The spectrometer was allowed to warm up for 2 - 3 hours before the start of each test. The electron emission current was set to 3×10^{-3} amps (recommended value) and the various dials peaked for maximum response for mass 28 (CO^+, N_2^+). A Modulated Bayard-Alpert (MBAG) gauge was used as a reference pressure standard and was set to the correct emission for the gas being tested. These emission values were derived as follows:

$$i_A^- = i_N^- \times \frac{S_n}{S_a} \qquad (1)$$

where i_A^- is the correct emission current for gas "A" and i_N^- is the correct emission for N_2 (0.3 mA for an MBAG sensitivity of .01 amps/Torr). S_n/S_a is the ratio of gauge sensitivity for nitrogen and gas "A" respectively. This

ratio was derived from Dushman and Lafferty (ref. 1) by normalizing the sensitivities to nitrogen. After appropriate system bake-out, gauge outgassing, and subsequent pumpdown, the test gas was admitted. The ion pump located in the test section of the UHV system was valved off during the gas admission. The spectrometer was carefully tuned to the appropriate mass peak. The following gases were admitted in the order listed: He, Ne, N_2, Ar, Kr, and Xe. The UHV system was permitted a 24-hour pumping period between exposures to each gas. The residual system pressure was between 1-2 x 10^{-9} Torr (N_2) before each gas was admitted. An X-Y recorder was used to plot the observed ion current at the selected mass as a function of the Modulated Bayard-Alpert gauge total pressure of that gas. Pressures up to 10^{-6} Torr of the test gas were used. Data at higher pressures was not taken because the program emphasis is on UHV measurements.

Using the methods described, it is possible to determine both linearity and sensitivity for the spectrometer, over a limited range. This was done for both the "low" and "medium" mass ranges. For the isotopic gases, suitable corrections were made for the isotope abundances. Table I summarizes this data.

The X-Y recorder traces displayed a very linear relationship between resolved ion current and pressure for He, Ne, N_2 and argon. For Kr and Xe, a small amount of non-linearity was noted. This problem was also observed during previous tests wherein the UHV ion pump was not valved off. In this instance, the non-linear response was much more pronounced. Although not proven, it is believed

that desorption (within the ion pump) of previously pumped gases by the calibration gas produced the observed increase in the MBAG response. A similar, but smaller effect may have occurred within the MBAG.

TABLE I

SENSITIVITIES OF QUADRUPOLE 200 FOR VARIOUS GASES

Gas (Mass No.)	Sens. (Low Range) A/Torr at 3mA	Sens. (Medium Range) A/Torr at 3mA
He^4	0.42×10^{-4}	0.18×10^{-4}
Ne^{20}	0.68×10^{-4}	0.45×10^{-4}
$N_2{}^{28}$	2.50×10^{-4}	1.98×10^{-4}
Ar^{40}	2.63×10^{-4}	2.86×10^{-4}
Kr^{84}		3.52×10^{-4}
Xe^{132}		1.42×10^{-4}

Table I displays some interesting results. Note that the overall spectrometer sensitivity increases markedly as the mass number increases, and for the "medium" mass range decreases again at mass 132 (Xe). It would be anticipated that the ion source sensitivity would increase monotonically with increasing mass due to the increasing ionization efficiency of the gases. It would also be inferred from Figure A-17 of Appendix A that the transmission efficiency of the quadrupole will fall sharply with increasing mass

number, particularly for this instrument, in which the r_o^2/d^2 value is approximately unity.

Qualitatively, it would be anticipated that the overall sensitivity of the spectrometer might display a maximum sensitivity at some intermediate mass number. This is because the overall sensitivity will be proportional to the product of the ionizer sensitivity and the transmission factor.

Using the data given in Table I, it is possible, with certain assumptions, to derive relative transmission factors normalized with respect to nitrogen. For this calculation, the following relation is used:

$$\frac{S_o}{S_n} = \frac{S_a}{S_n} \sigma_a T_r \qquad (2)$$

In this equation, S_a/S_n is the sensitivity of the ionizer for gas "A" relative to nitrogen. σ_a is the abundance fraction for the mass being resolved. S_o/S_n is the overall sensitivity of the spectrometer for the mass peak being resolved relative to nitrogen. T_r is the transmission factor for the particular mass relative to the nitrogen transmission.

S_a/S_n values are derived from Dushman and Lafferty by normalizing their published sensitivity factors for nitrogen. The assumption is made that the hot-filament

ionizer will exhibit the same sensitivity factors. This assumption is reasonable since the electron energies used in the quadrupole ionizer are nearly equal to those used in Bayard-Alpert gauges (90 volts).

Rearranging equation (2),

$$T_r = \frac{S_o}{S_n} \times \frac{S_n}{S_a} \sigma_a \qquad (3)$$

Table II below shows how the relative transmission, calculated from the data of Table I varies with mass number.

TABLE II

QUADRUPOLE TRANSMISSION VS. MASS
(Normalized to Nitrogen)

Gas (Mass No.)	σ_a	S_o/S_n (low)	S_o/S_n (med)	$\frac{S_n}{S_a} \times \sigma_a$	T_r(low)	T_r(med)
He^4	1.00	0.17	0.09	6.45	1.08	0.58
Ne^{20}	0.91	0.27	0.23	4.64	1.26	1.07
N_2^{28}	1.00	1.00	1.00	1.00	1.00	1.00
Ar^{40}	1.00	1.05	1.45	0.84	0.88	1.22
Kr^{84}	0.57	--	1.78	0.95	--	1.69
Xe^{132}	0.27	--	0.72	1.36	--	0.98

Using eq. (3), the transmission factors (T_r) have been calculated and normalized with respect to nitrogen. These factors are shown in the last two columns of this Table, for both the "low" and "medium" mass ranges of the instrument. It is apparent from these data that the quadrupole transmission is not varying with mass number in the manner predicted by the theory. In fact, it is nearly constant, at least for the "low" mass range.

The manufacturer was questioned regarding this unexpected variation of transmission vs. mass number. It was disclosed that certain bias voltages have been employed in the electronics which supply the dc quadrupole potentials. These small potentials are provided to compensate for increased quadrupole transmission at the low mass numbers only. Compensation is accomplished by essentially improving the resolution at the expense of lowered transmission. Therefore, the transmission for the lower masses can be adjusted to be more nearly equal to the transmission at the higher masses. A noticeable reduction in peak width, ΔM, should coincide with this reduction in the transmission factor.

Figures 1 and 2 show spectra of a mixture of inert gases taken on the "low" (1-50 amu) and "medium" (10-150 amu) mass ranges of the hot-filament quadrupole. A careful examination of Fig. 2 reveals some interesting qualitative information. Xenon 131 and 132 have been clearly resolved with a valley between these peaks of approximately 10%. However, krypton 82 and 83 have not been as well resolved. At the low end of the mass scale,

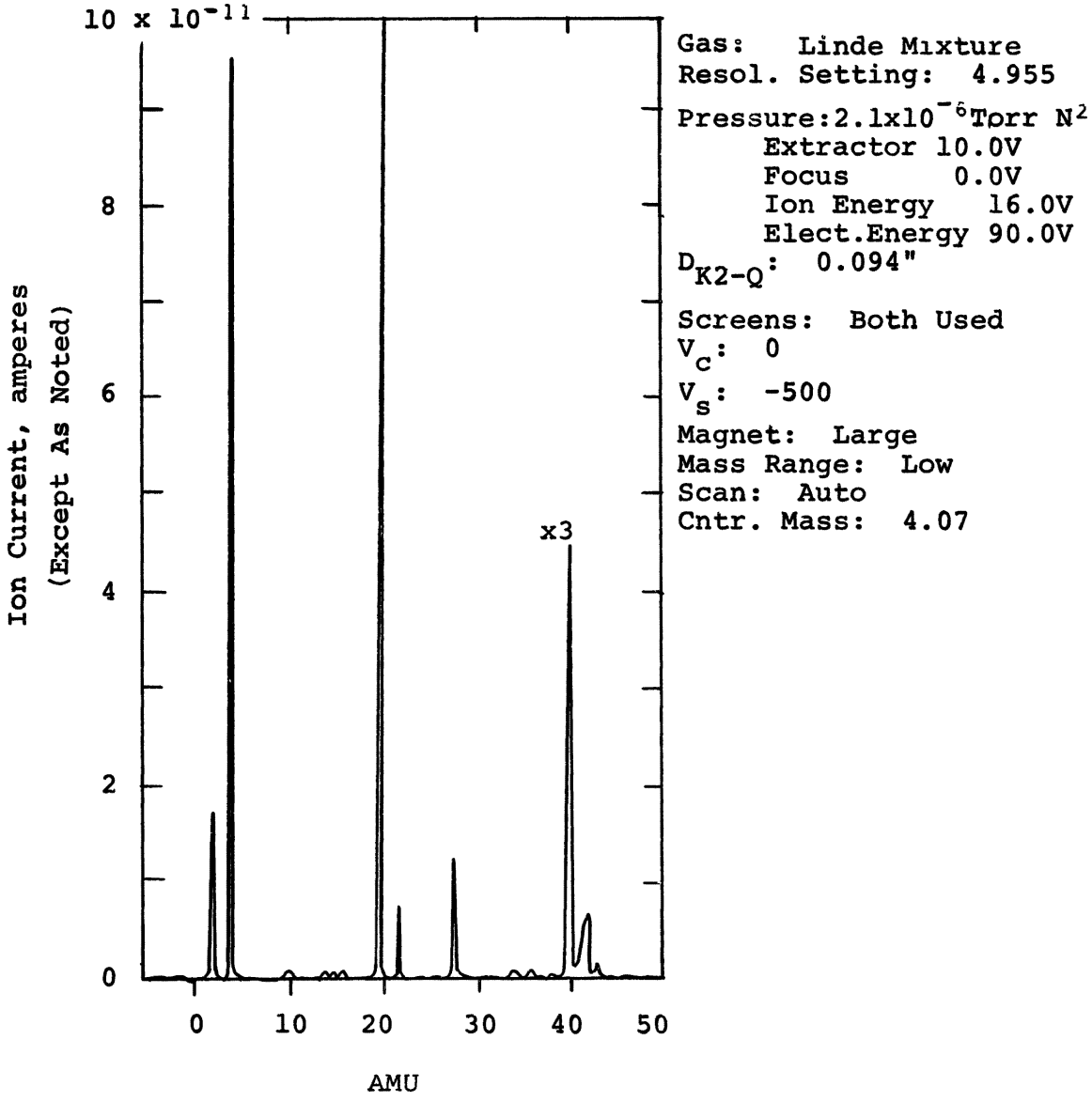

Fig. 1 Low Mass Range Spectrum Taken with the Hot Filament Spectrometer.

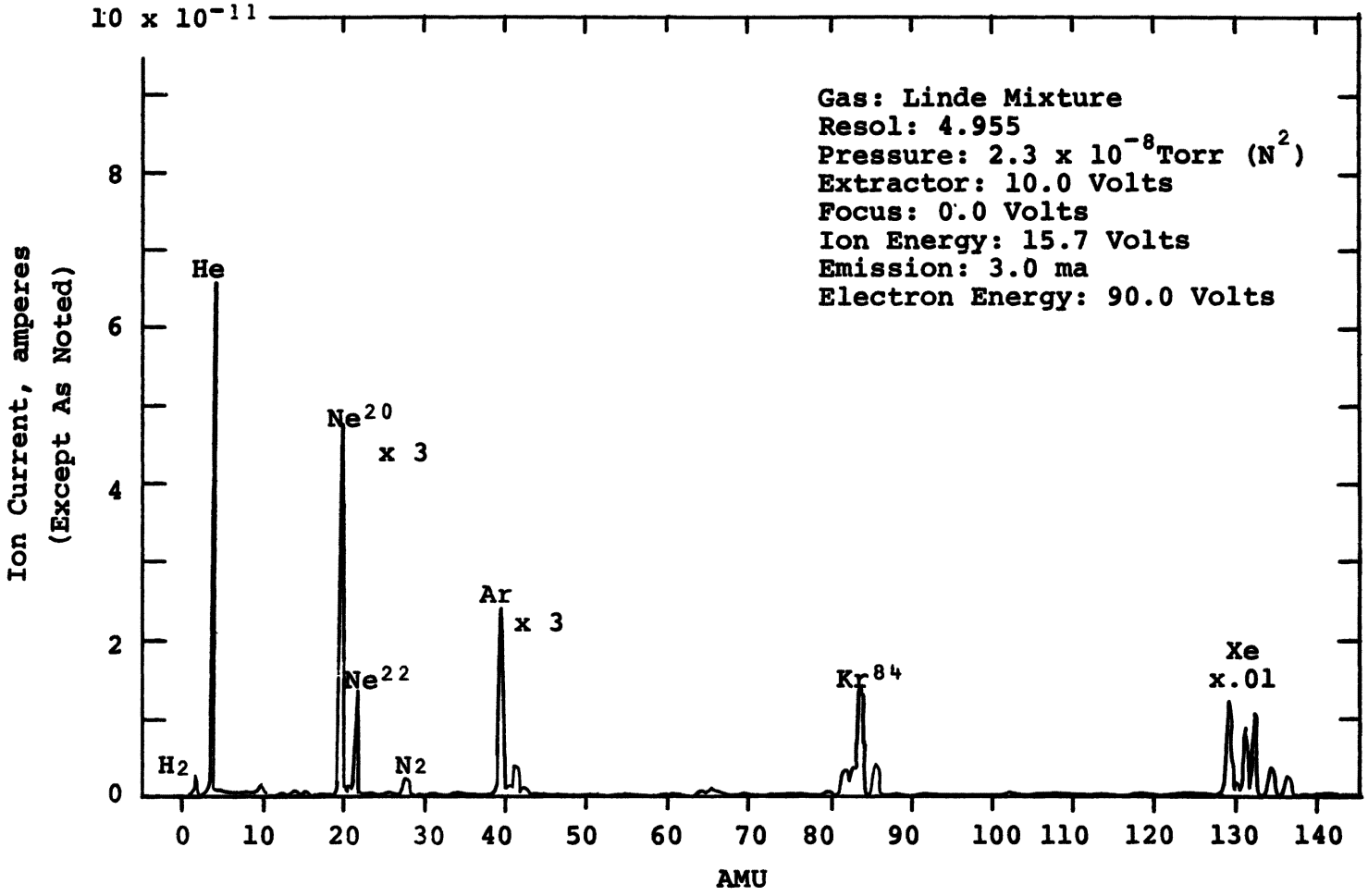

Fig. 2
Medium Mass Range Spectrum Taken with the Hot Filament Spectrometer.

the hydrogen and helium peaks are more narrow than those at any other part of the entire mass range. If these results are correlated with the Table II transmission factors (medium range), we see the anticipated inverse relationship between resolution and transmission. Similarly, a comparison can be made between Table II transmission factors and Fig. 1. As both Fig. 1 and Table II show, however, the variation in resolution is less for the "low" mass range than for the "medium" range.

Thus far, the absolute values of the quadrupole transmission have not been discussed. It is of importance to know what these absolute relations are, since transmission is closely related to spectrometer sensitivity. Furthermore, absolute data should be available in order to compare the hot and cold-cathode ionizers. The absolute transmission factor is difficult to determine, however, since the ion beam which enters the aperture hole cannot be measured directly. This beam is not perfectly collimated and, therefore, some ions will be lost on the rods and other structures even though the quadrupole voltages are off. Under these circumstances, it is necessary to measure the ion current at the specified resolution and at zero resolution. The transmission factor is then the resolved current divided by the unresolved current. In making this measurement, it is important to measure only one gas at a time. Also, appropriate corrections must be made for the abundance of the isotope being resolved.

The data shown in Table III below was obtained using this method of determining absolute transmission.

TABLE III

ABSOLUTE TRANSMISSION VS. MASS NUMBER

Gas (Mass No.)	σ_a	T_a (Low Range)	T_a (Med. Range)
He^4	1.000	Not Measured	0.222
Ne^{20}	0.905	" "	0.283
$N_2{}^{28}$	1.000	" "	0.286
Ar^{40}	1.000	" "	0.344
Kr^{84}	0.569	" "	0.435
Xe^{132}	0.269	" "	0.299

If the data of Table III is normalized for T_a (nitrogen), the results are in reasonably close agreement with the values given in the last column of Table II. Similar absolute transmission factors were not determined for the "low" mass range because significant changes were not evident in Table II.

Thus, it is seen that the performance of the hot-filament quadrupole is in agreement with quadrupole theory and with the manufacturer's specifications. In order to derive quantitative results from the instrument, more attention should be given to the proper adjustment of the controls which effect quadrupole transmission and resolution for the lighter gases.

Test Apparatus for Evaluation of CCIS/Quad

Vacuum system. - The vacuum system used is shown schematically in Fig. 3. It is divided into upper and lower manifold units, which allows the upper portion to be oven baked while being pumped from below. After bakeout, the upper manifold is valved off and pumped by the upper ion pump.

The upper manifold consists of the quadrupole spectrometer, a modulated Bayard-Alpert gauge, an 11 liter per second Ultek Model 10-252 ion pump, a bakeable Varian ultrahigh vacuum valve for isolating the upper manifold from the lower and a bakeable Varian valve for isolating the upper ion pump. A thermostatically controlled oven is used for baking the upper manifold system. Figures 4 and 5 show two views of the experimental apparatus.

The lower manifold consists of a 20 liter/second Ultek Model 10-354 ion pump, a small mechanical pump, a Varian zeolite sorption pump, a port for admitting gas to the system and associated valves for closing off the pumps and gas supply inlet. The pumping speed of the system was intentionally made small to detect outgassing in the CCIS spectrometer.

Quadrupole spectrometer. - On the basis of a feasibility study of the cold-cathode ion source*, it was concluded that a quadrupole mass spectrometer would be most suitable for mass analysis of the source's higher ion energies

---

*See Appendix A and a previous section entitled, "Selection of a Quadrupole Analyzer".

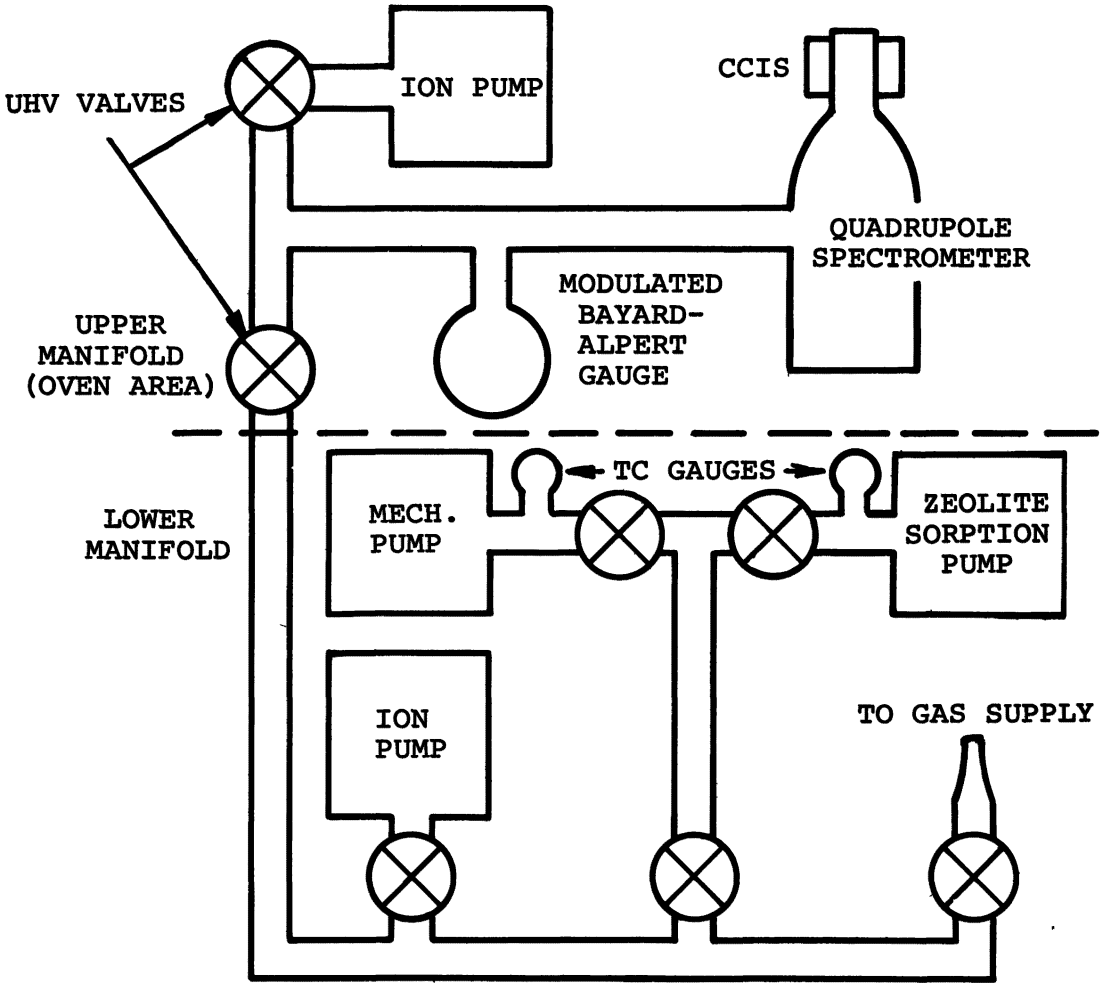

Figure 3

Vacuum System Schematic

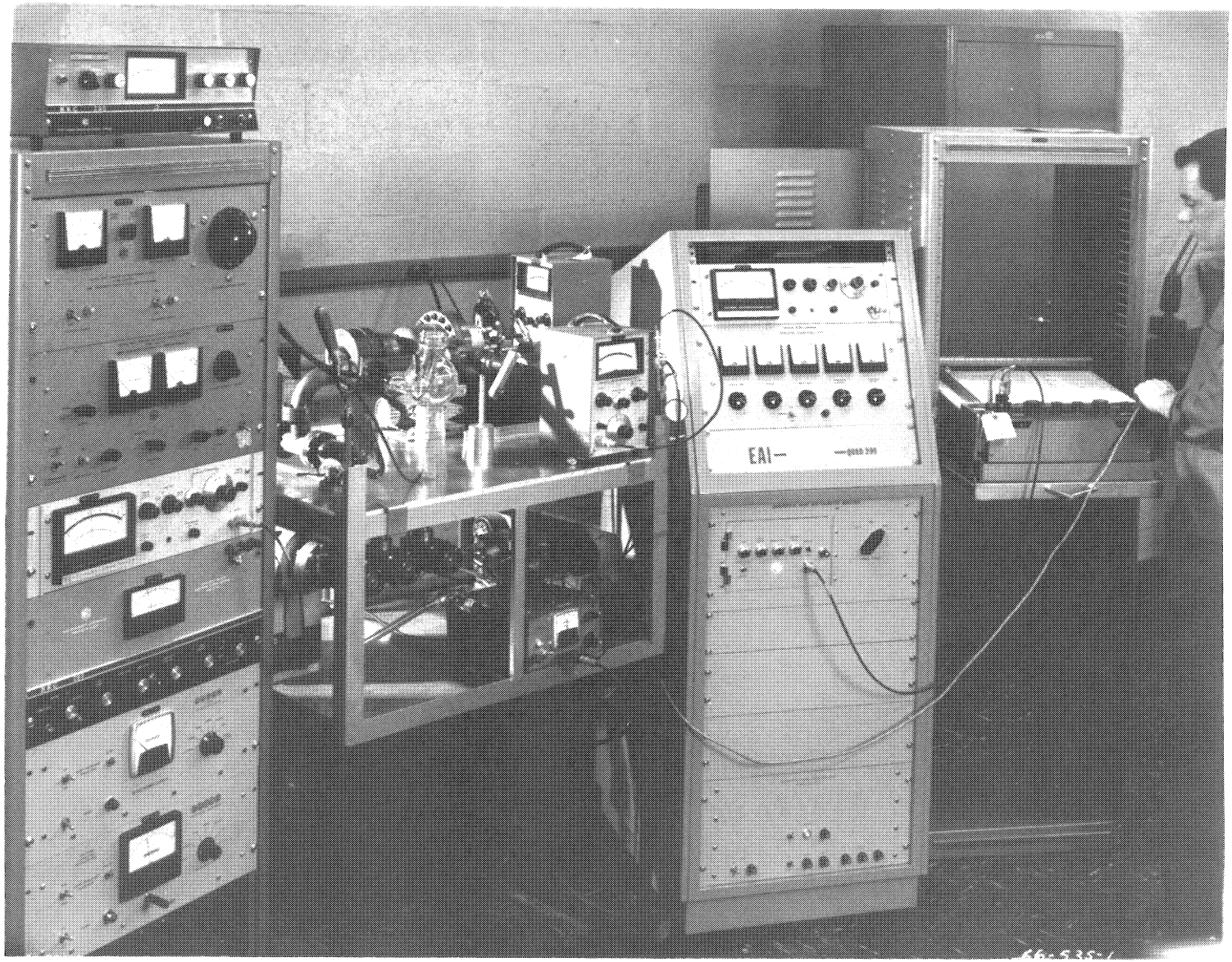

Fig. 4

Experimental Test Apparatus

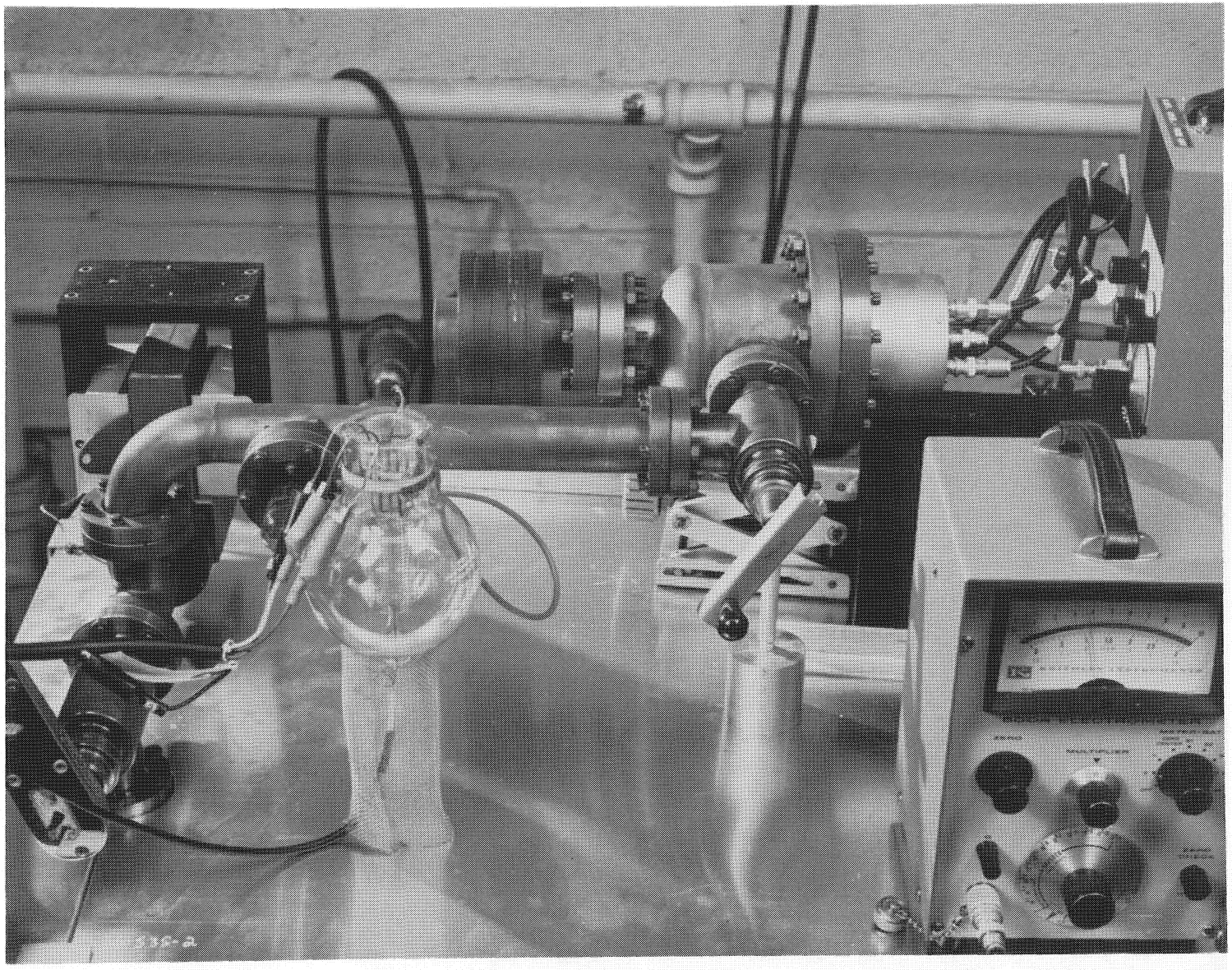

Fig. 5

CCIS/Quadrupole and UHV System as Arranged for Cleanliness Tests

and larger beam cross section. A commercial quadrupole was purchased equipped with a standard hot-filament ionizer. The latter permitted spectrometer performance comparisons between both types of sources.

Quadrupole specifications pertinent to a theoretical analysis of results are as follows: operating frequencies (ν) are 5.3 mHz and 3.3 mHz on the low and medium mass ranges, respectively. Maximum available rf potential (V) is 1000 volts. The radius (r_o) of the circle inscribed by the quadrupole rods is 2.7 mm. The entrance aperture diameter is also 2.7 mm. Rod lengths are 11.3 mm.

Cold Cathode Ion Source

Description. - The cold-cathode ion source (CCIS) is a modification of the Redhead (ref.2) magnetron gauge. An assembly drawing of the source attached to the quadrupole is shown in Fig. 6. To allow ion extraction, the single spool shaped cathode design used in the gauge is separated into two cathodes, one with a remnant stub (K_1) which is 9.7 mm long and 3.1 mm in diameter. All remaining electrode dimensions remain as in the gauge. The horseshoe magnet ordinarily used has been replaced by hollow cylindrical ceramic magnets. Dimensions and field strengths of the magnets used are given in later sections. Figure 7 shows two views of the CCIS/Quadrupole without its external housing.

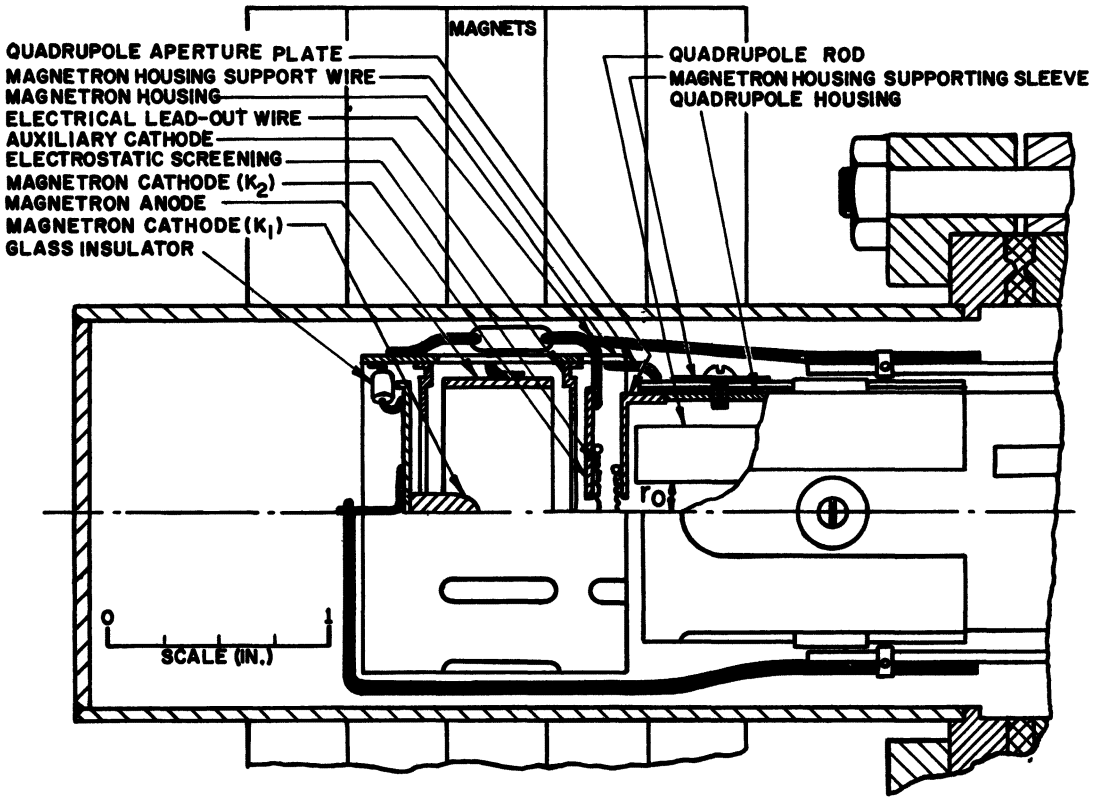

Fig. 6

Cross-Section of Cold Cathode Ion Source
Showing Attachment to Quadrupole Analyzer.

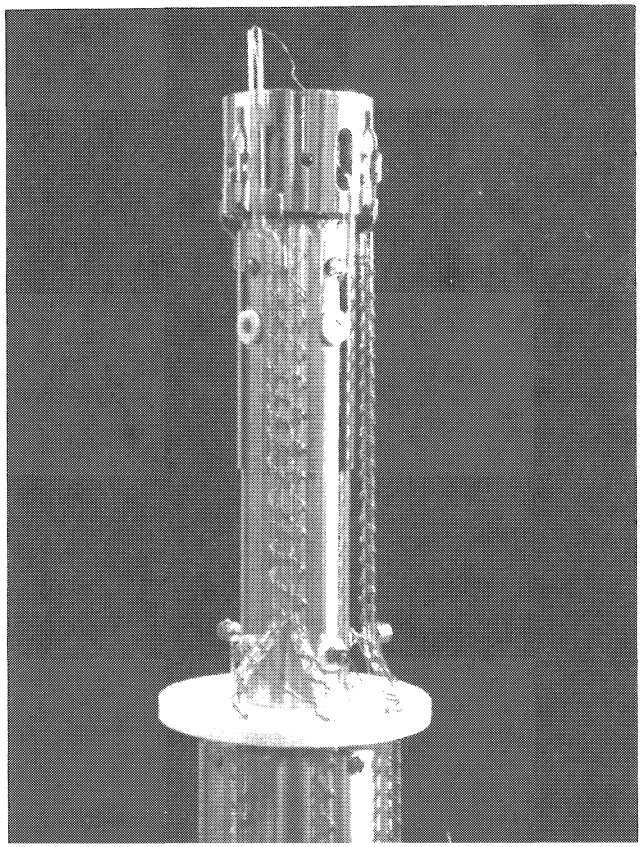

(a) Overall View

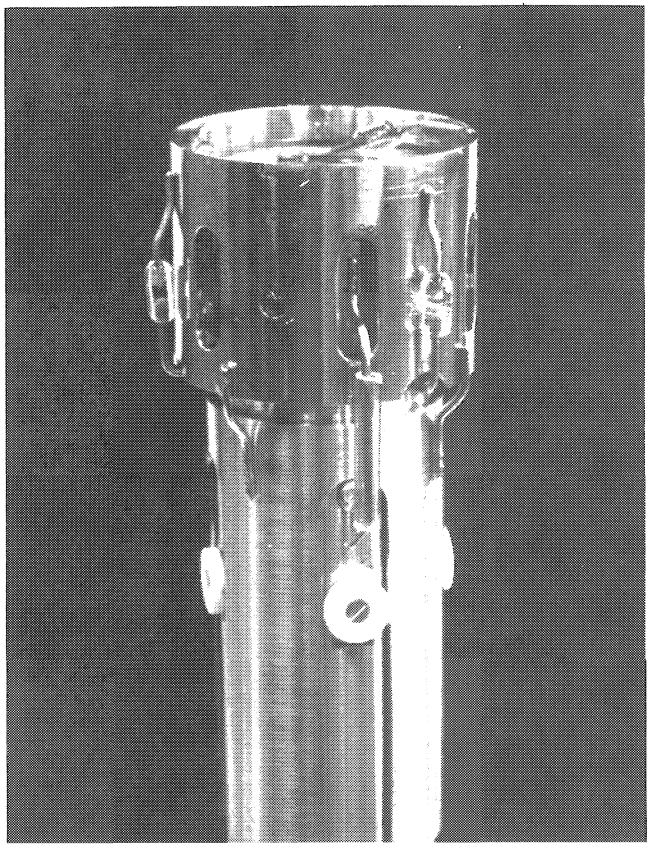

(b) Close-up of CCIS

Fig. 7

Two Views of CCIS/Quadrupole

Source electrodes are supported on a stainless steel cylindrical housing maintained at ground potential. Auxiliary cathodes are welded to it directly. The anode is attached and insulated by sapphire spheres. It is not perforated as in the Redhead gauge. Cathodes K_1 and K_2 are supported and insulated by glass studs. This arrangement provides independent electronic access to the anode and each cathode; it likewise provides a guard ring design which, by preventing leakage between electrodes, prevents interference with low level current detection.

The source housing is perforated and attached to the quadrupole with heavy refractory wire and a slotted sleeve; distance between the faces of K_2 and the quadrupole aperture plate was maintained at 2.4 mm (as close as possible without causing arcing between electrodes).

Tungsten mesh screens were used over the K_2 aperture and the quadrupole entrance aperture for the following reasons: (a) to allow testing of the effect of potential differences between these components without causing beam defocusing, (b) to isolate magnetron and quadrupole electric fields and,(c) to flatten the magnetron potential distribution at K_2 which otherwise bulges through the K_2 aperture; this is to reduce ion defocusing and resultant sensitivity losses.

CCIS/Quad Test Procedures And Results

General. - CCIS/Quadrupole performance was investigated as a function of the parameters discussed below, first to determine optimum source operating conditions and second, to note the resultant spectrometer response to mass and pressure variations. During the first part of the investigation, nitrogen was used as the test gas at a pressure of 5.4×10^{-9} Torr. Initially, a 5.0 kV anode potential was used and cathode potentials V_{K1} and V_{K2} were kept at zero volts; thereafter, values were used which successively were shown to give the best resolution and sensitivity.

Performance vs. quadrupole resolution setting. - A family of nitrogen spectra were recorded as a function of quadrupole resolution dial settings. The latter correspond to ratios of dc and rf rod potentials, U and V respectively, in Paul's (ref. 3) equation for quadrupole spectrometer resolution:

$$\frac{M}{\Delta M} = \frac{0.126}{0.16784 - U/V} \qquad (4)$$

where M is the atomic mass and ΔM the peak width at its base. Spectral resolution changes were determined by comparing the full width at half maximum (FWHM) of the nitrogen peaks. Experimental resolution improved as dial settings proceeded toward higher theoretical resolution; sensitivity correspondingly decreased (as predicted by theory) until a setting was reached (4.95) beyond which sensitivity continued to decrease with no further resolution improvement. This setting was then selected as optimum and used in subsequent experiments.

Performance vs. CCIS anode potential. - As with resolution setting experiments, FWHM measurements were made vs. anode potential (V_A) on a family of nitrogen spectra. This was done both on the low and medium mass ranges (1-50 amu and 10-150 amu, respectively). The optimum value of V_A for both ranges was in the vicinity of 2.0 kV (compared with 5.0 kV normally used in magnetron total pressures gauges). Figure 8 illustrates, for the medium mass range, the resolution improvement and accompanying sensitivity reduction existent as a function of V_A. (It is evident that the discharge was unstable at 5.0 kV).

Performance vs. CCIS magnet position. - Using the optimum resolution setting and optimum anode potential discussed above, spectra were recorded against magnet position; first axially and then rotationally. Positions giving optimum resolution, as determined by FWHM, were selected. Unlike spectral variations with resolution setting and with anode potential, no sensitivity loss accompanied the positionally improved resolution. Resolution was found optimum when the magnet's center coincided with the midplane between cathodes K_1 and K_2. A ± 3 mm axial magnet movement caused about a 20% broadening of the peak's FWHM. A 10% FWHM maximum variation occurred with rotational positioning.

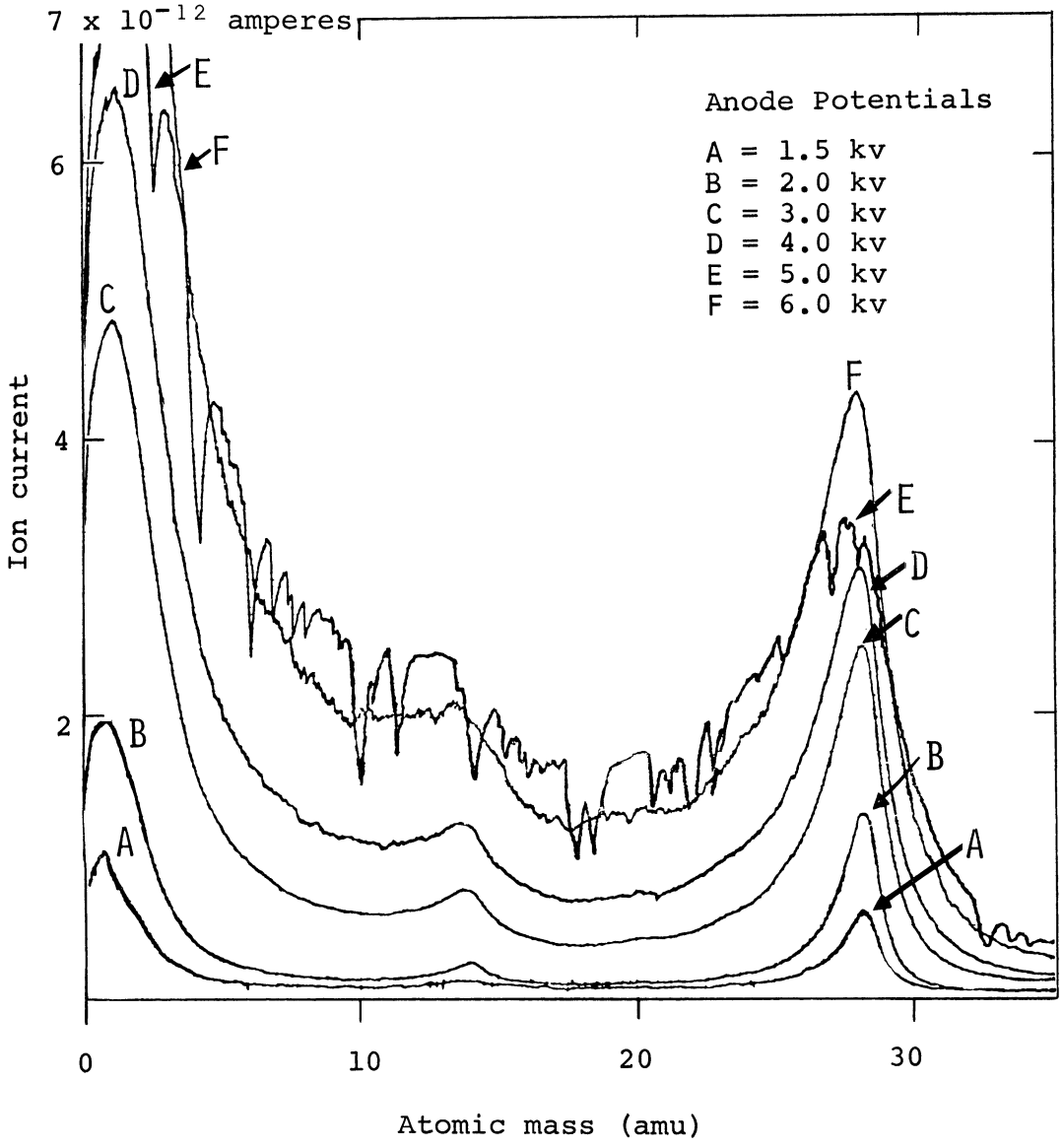

Figure 8.- Resolution and sensitivity vs. anode potential-medium mass range

Performance vs. CCIS ion retarding potential. - Acceleration and retardation of ions prior to their entrance to the quadrupole was effected by equal alteration of cathode potentials V_{K1} and V_{K2} while the quadrupole entrance aperture was maintained grounded. Acceleration was found to degrade quadrupole resolution while retardation improved it. This improvement, coupled with that obtained by lowering the anode potential (discussed above), points to high ion energy as an important resolution limiting factor.

Nitrogen peak narrowing, produced by increasing retardation potentials, is shown in Fig. 9 for some of the values investigated. A 300 volt retardation potential was found optimum, when accompanying a 2.0 kV (later 2.2 kV) anode potential. For this determination the 10% valley criterion* was used, the FWHM criterion being abandoned due to improved resolution.

Performance vs. potential between CCIS cathodes. - When making cathode potential $V_{K1} > V_{K2}$, resolution deteriorated obviously. For $V_{K1} < V_{K2}$, two conditions were tested: (1) with V_{K2} at - 300 volts, resolution remained constant and sensitivity declined, (2) with V_{K2} at zero volts, resolution improved but not to the extent achieved by equal variation of cathode potentials, noted in the previous section. This investigation was, therefore, concluded.

---

*Peak separation which allows a valley less than 10% of the height of either adjacent peak. With one peak, an equivalent criterion was used; the separation between 5% of the peak height on either side of the peak's center line.

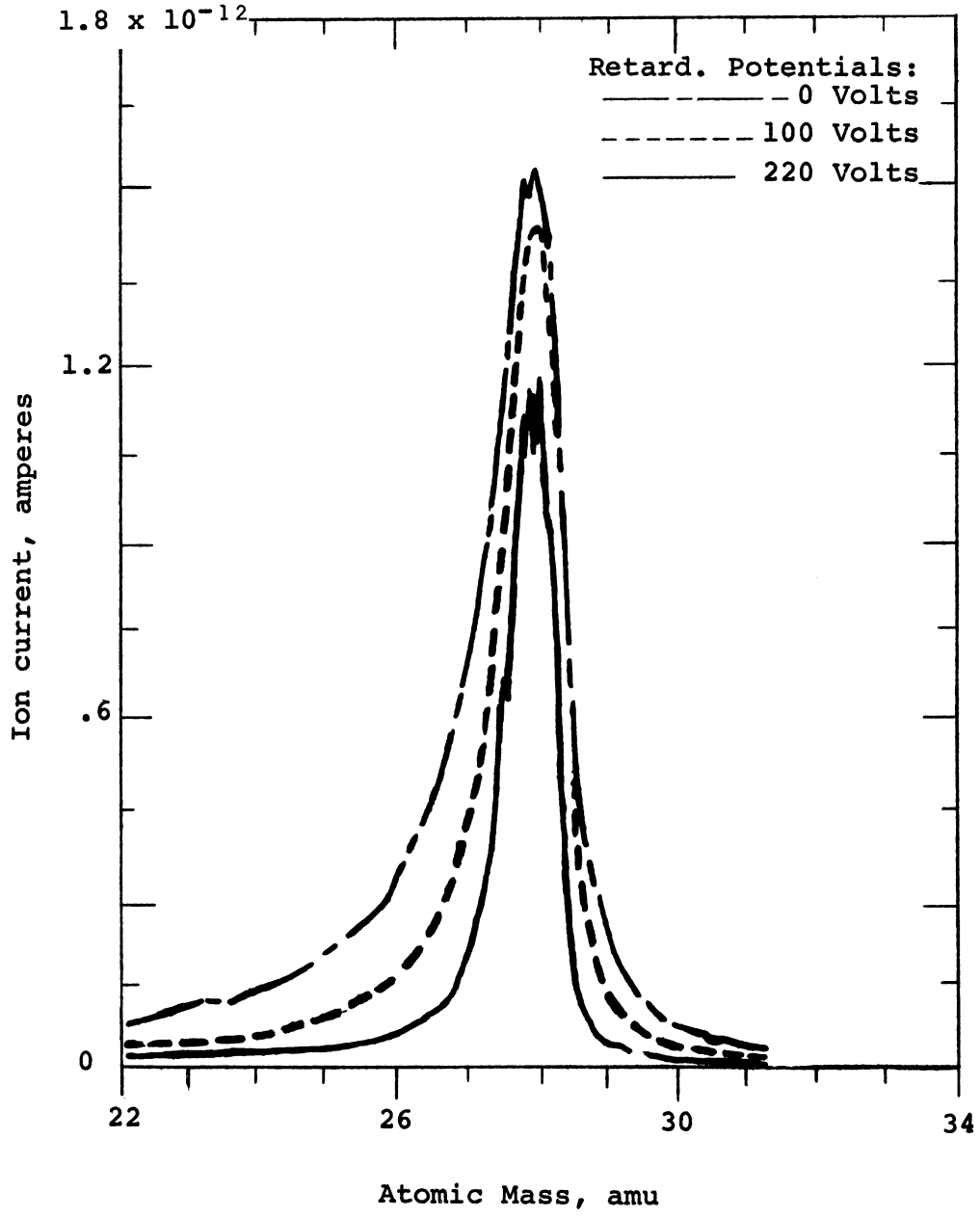

Figure 9.- Effect of retarding potential on resolution and sensitivity of nitrogen peak

Performance vs. quadrupole mass range (frequency). - Figure 10 shows nitrogen spectra obtained on the low and medium mass ranges using optimum conditions, as discussed above. Only a portion of the spectra are shown and scales are normalized to the same mass scale. The superior resolution and sensitivity of the low mass range is obvious. (The noise on the medium mass spectrum is in the X-Y recorder). Resolution at this stage of investigation (using the 10% valley criterion) allowed peak separations of 2.5 amu and 1.5 amu for the medium and low mass ranges, respectively. These values were reproducible. The implications of the spectral differences as a function of mass scanning range will be described in a later section entitled "Discussion of Results".

Performance vs. magnet size. - Experiments heretofore described, were performed with a hollow, cylindrical, ceramic magnet stack with an 11.4 cm o.d., 4.8 cm i.d. and a 5.7 cm length. Most of these experiments were repeated using a smaller magnet stack with an 8.9 cm o.d., 4.8 cm i.d. and 3.8 cm length. Axial magnetic flux densities, in gauss, for the large and small magnets, respectively, were as follows:

(1) on axis at the magnet's center, 1220 and 838.

(2) on axis at the magnet's edge, 397 and 368.

(3) on the inside wall of the magnet at the magnet's center, 1426 and 957.

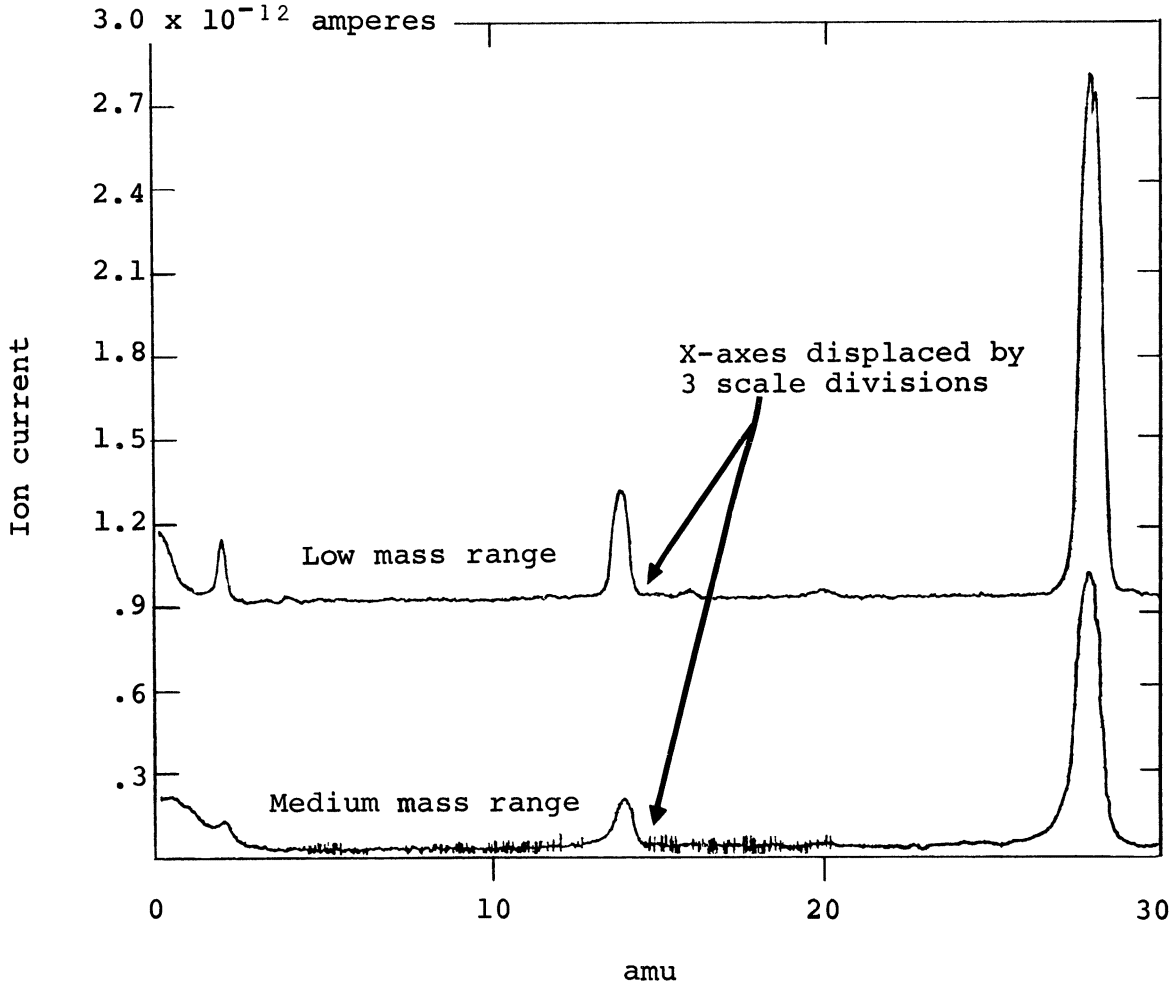

Figure 10.- Performance of CCIS/Quadrupole spectrometer on two mass ranges

The spectra obtained with the small magnet were very similar to those obtained with the large magnet. Resolution at this stage of investigation, allowed peak separations of 3.0 amu and 1.5 amu (using the 10% valley criterion) on the medium and low mass ranges. This compares with 2.5 amu and 1.5 amu, respectively, for the large magnet. Sensitivity was slightly better than half that obtained with the large magnet. Most significantly, the small magnet displayed comparatively large operating mode instabilities; during one mode change, the entire nitrogen peak temporarily disappeared.

Further development might establish reliable operation with little or no loss of resolution or sensitivity, perhaps for still smaller magnets. At present, however, the larger magnet gives a more stable and sensitive performance.

Performance vs. spectrometer cleanliness. - The CCIS/Quadrupole and upper manifold were baked at 425°C for 48 hours prior to the tests to be described next. This was in preparation for testing collector current linearity with pressure and for determining absolute sensitivity.

The baking resulted in an unexpected resolution improvement. Peak separations of 1 amu and .7 amu in the medium and low mass ranges, respectively, were obtained where 2.5 amu and 1.5 amu existed previously. The poorer resolution in the dirtier system is believed produced by increased secondary ion emission, caused by ions or electrons from the source bombarding the quadrupole rods. Secondary ions thus produced part way down the rods would not be fully resolved and could cause the observed resolution deterioration.

As noted in the SUMMARY, one of the objectives of this program is to improve the cleanliness of a quadrupole spectrometer by using a cold-cathode ion source. Accordingly, certain tests were conducted during the program in an attempt to determine, at least qualitatively, the cleanliness of the spectrometer. Since program limitations precluded direct comparison of hot and cold spectrometers, a Modulated Bayard-Alpert gauge was used to simulate a hot filament source. When the gauge is operating, the processes which give rise to the spurious spectra (C^+, O^+, CO^+, CO_2^+, etc.) in hot-filament spectrometers, will also occur in the MBAG. The magnitude of these anomalous peaks will depend on many factors such as filament temperature, electron emission and on initial gauge cleanliness. Therefore, the Bayard-Alpert gauge has had the benefit of a rigorous outgassing procedure and the entire system had been pumped down for approximately 30 days before the first test to be described was begun. Figure 11 shows the results of this test. The test sequence is from the bottom to the top of the figure and the scans are labelled I through V. Scan I shows the background spectra of the system as determined by the CCIS/Quadrupole. The MBAG has been turned off for 18 hours. Scan II shows the spectrum immediately after turn-on of the MBAG. The typical peaks of C^+, O^+, CO^+, and possibly CO_2^+ are seen. Scans III and IV show the CO^+ peak 2 and 3 hours after initial start of the MBAG. It is noteworthy that the CO^+ peak is still present. Scan V shows conditions only five minutes after turning off the Bayard-Alpert gauge. The CO^+ peak has decayed

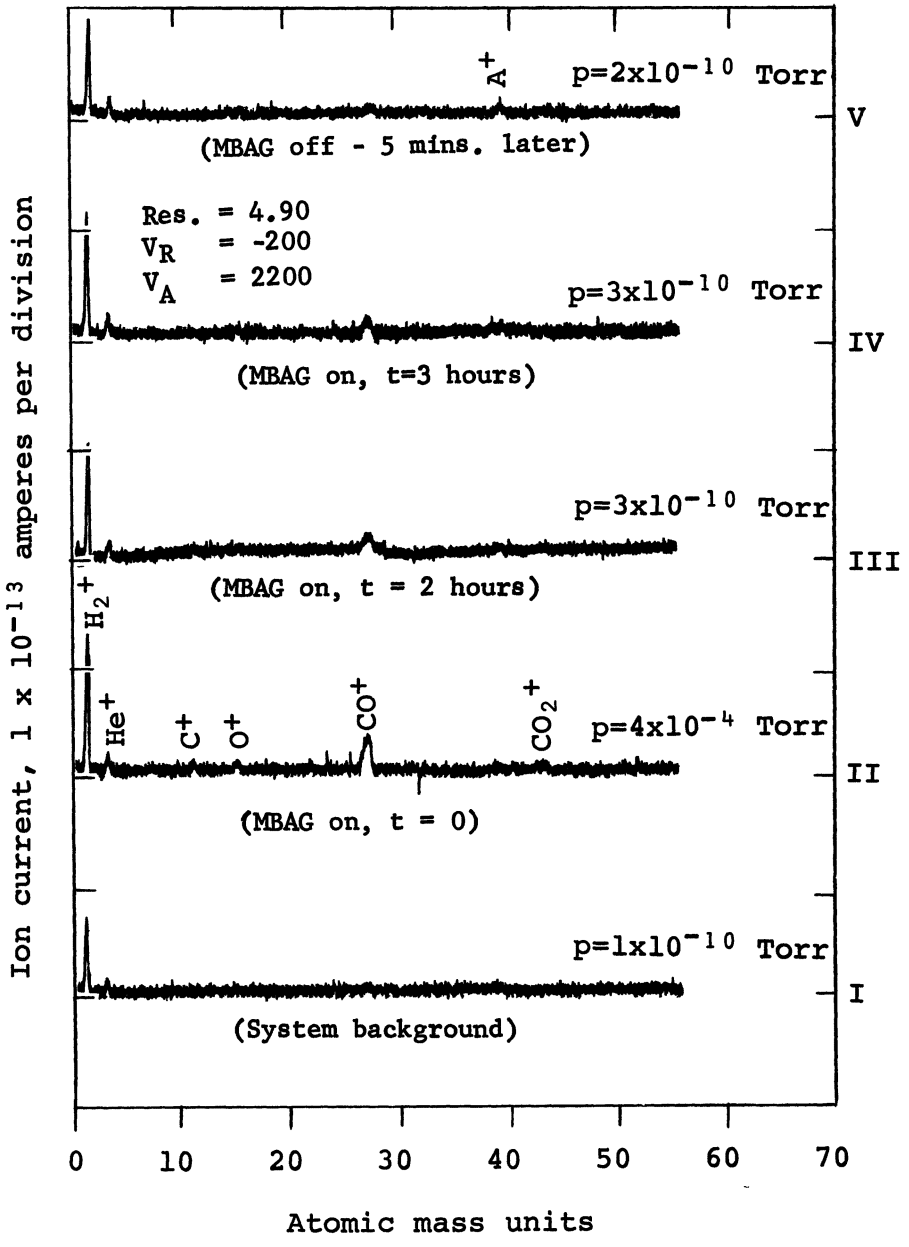

Figure 11.- Background spectra produced by Bayard-Alpert Gauge

more noticeably in the five minute period between IV and V than in the one hour period between scans III and IV. It is obvious that the initiation of the hot-filament gave rise to certain peaks which are not easily removed, despite continuous pumping, as long as the MBAG is operating. The production of these peaks, therefore is not simply a single desorption process, but involves a desorption-adsorption cycle requiring a long time to overcome. A number of such cyclic interchanges are known to exist with hot-filament gauges.

The H_2^+ and He^+ peaks are also noticeable in all the scans. The hydrogen peak (H_2^+) will be discussed shortly. The helium (He^+) peak is probably a remnant from an accidental over-exposure to helium (above 10^{-3} Torr) which occurred weeks before. The system was not baked subsequent to this exposure.

Figure 12 shows a second attempt at defining spectrometer cleanliness. For this test, the UHV valve shown in Fig. 3 between the upper ion pump and upper manifold was removed and placed between the CCIS/ Quadrupole spectrometer and the upper manifold. This configuration is shown in Fig. 5. With this valve intervening the spectrometer and the system it is possible to isolate the spectrometer. Three conditions are shown in this figure. In the first, the spectrum of the entire system is shown. The upper ion pump and

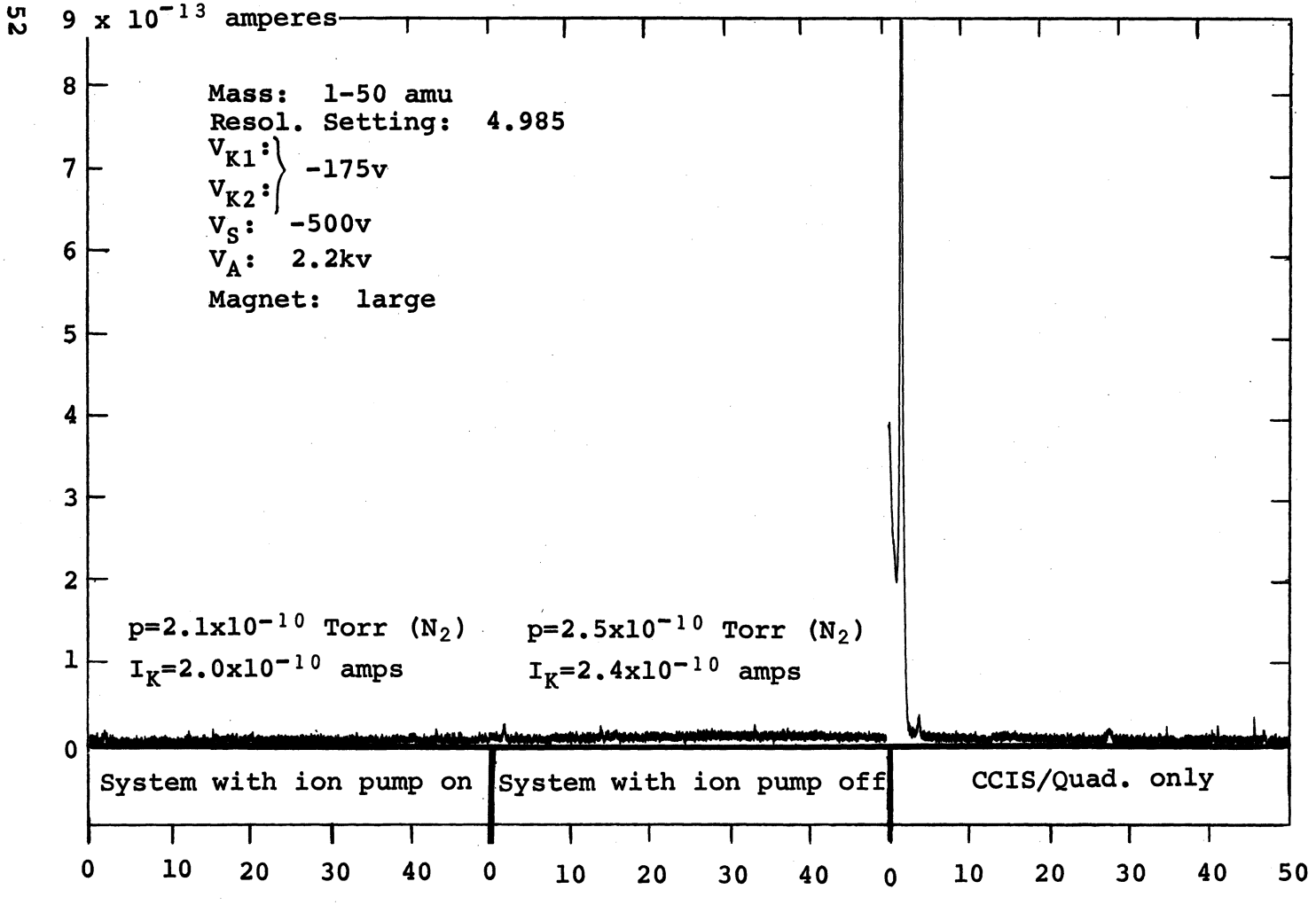

Figure 12.- Background spectra from CCIS/Quadrupole

MBAG are operating and the valve between the spectrometer and the system is open. The middle scan was taken with the ion pump off to determine what gases are being removed by the ion pump. In both the foregoing cases, hydrogen (H_2^+) is the only residual detectable. When the spectrometer is isolated we notice a very large increase in the H_2^+ peak, together with a small helium (He^+) peak. The source of the hydrogen peak is not known. It may be anywhere inside the spectrometer and/or valve configuration. Present speculation is that the stainless steel of the spectrometer housing may be the source. Redhead has experienced similar results using a rigorously cleaned hot-filament spectrometer attached to a stainless steel system. In any event, the familiar C^+, O^+, CO^+ and CO_2^+ spectra were not observed with the spectrometer isolated. The center scan (ion pump off) raises the question as to why so little hydrogen was observed with the ion pump on or off. The answer is that the clean titanium surfaces in the ion pump is an excellent hydrogen getter whether the pump is operating or not.

As noted previously, and as will be noted in a later section, conclusive tests of the CCIS/Quadrupole cleanliness must await a simultaneous comparison with the hot and cold-cathode versions of the instrument under similar conditions. With the exception of hydrogen, only remnants of residual gases have been noted.

Resolution vs. pressure. - Resolution improved slightly with increased pressure, but ion retarding potential had to be reduced to prevent spectral extinction; ion energy apparently decreases with increasing pressure.* In accordance, a retarding potential just under that causing spectral extinction appeared optimum; the values noted at several pressures were as follows: 300 volts at 5.4×10^{-9} Torr, 200 volts at 3.8×10^{-8} Torr, 75 volts at 1.2×10^{-7} Torr, 54 volts at 2.3×10^{-6} Torr.

Figure 13 shows a medium mass range spectrum of an inert gas mixture, obtained at 2.3×10^{-6} Torr subsequent to a 425°C bakeout. It is evident from the Xe^{131} and Xe^{132} peaks that a 1 amu separation has been obtained using the 10% valley criterion. On the low mass range resolution better than .7 amu was obtained. A low mass range methane spectrum at 2.5×10^{-8} Torr is shown in Fig. 14; although not optimum, the same retarding potential was used at 2.3×10^{-6} Torr. A .7 amu peak separation can be deduced at mass 16 using the single peak 10% valley criterion. This resolution is equal to or better than that obtained by the authors using the hot-filament source supplied as standard equipment with this quadrupole; it appears, therefore, that resolution, at this point is limited by the quadrupole itself.

---

*More recent information has been published on the phenomenon showing how the ion energy in a Penning discharge varies with pressure and cell anode voltage. See: Lamont, L. T., Jr., 14th Nat'l. Vac. Symposium, AVS 1967, pp. 149-150.

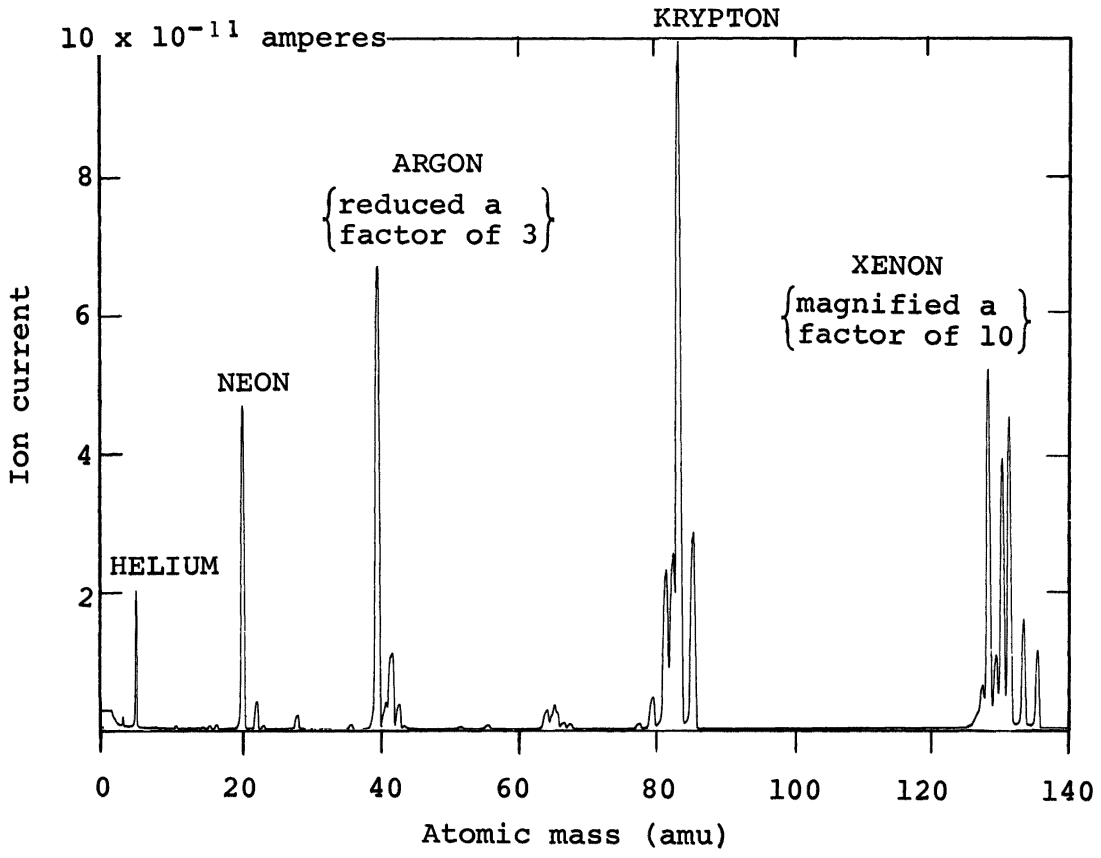

Figure 13.- Performance of CCIS/Quadrupole on medium mass range for inert gas mixture

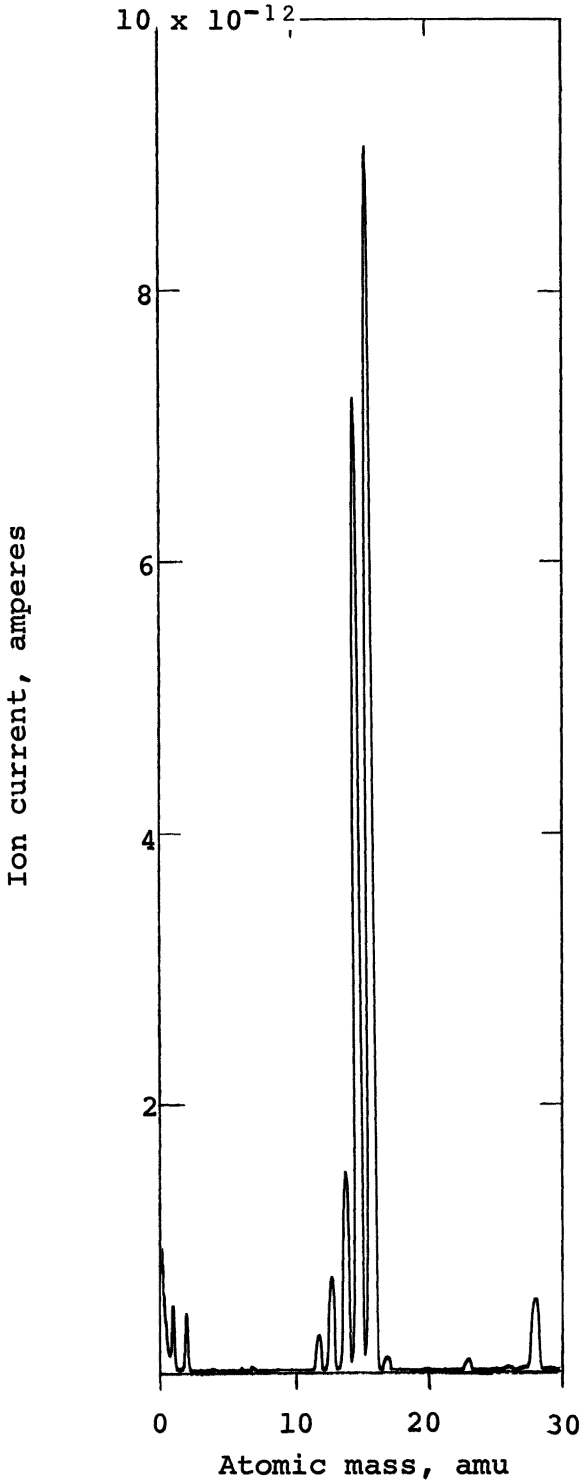

Figure 14.- Performance of CCIS/Quadrupole on low mass range-methane spectra

It is of interest to note the very small peak at mass 17 which is fully resolved, although only one mass unit separates it from the large mass 16 (CH_4^+) peak. Therefore, resolution is greater on the higher mass side of a given peak than on the lower side.

Ion current vs. pressure. - Ion current at the quadrupole collector was investigated as a function of pressure from approximately 3×10^{-9} Torr to 1×10^{-7} Torr for He^4, Ne^{20}, N^{28} and A^{40} on the low mass range and for A^{40} and Kr^{84} on the medium mass range. A constant 100 volt ion retarding potential was used and the following procedure adopted: (a) MBAG emission current was adjusted for each gas, according to relative sensitivities tabulated by Dushman and Young in Dushman (ref. 1), to give a constant pressure sensitivity of .01 amps/Torr, (b) the quadrupole was set on the peak of the mass under investigation, (c) the ion pumps were valved off and the gas under investigation admitted slowly to maintain pressure equilibrium between gauge and ion source, (d) quadrupole collector current was then continuously plotted against Modulated Bayard-Alpert gauge current.

Ion current at the quadrupole collector (i_c) vs. pressure (p) was found to obey the relationship:

$$i_c = kp^n \qquad (5)$$

(where k is a constant) for N_2^{28}, and Kr^{84}, while He^4 and Ne^{20} obeyed equation (5) only in the 10^{-8} Torr range. A decrease in the exponent occurred for the latter gases with decreasing pressure in the 10^{-9} Torr range and was believed due to a leak in the system. The low ionization efficiency of He^4 and Ne^{20} makes them more susceptible to these problems. The exponent n was between 1.15 and 1.20 for nitrogen, argon, and krypton; for neon and helium, it was .927 and .950, respectively.

In a later section of the report, the partial pressure performance of the instrument will be discussed in the realm of 10^{-9} to the 10^{-12} Torr range, for nitrogen, argon, and neon.

Sensitivity vs. atomic mass. - Sensitivity vs. atomic mass for the gases investigated is shown in Table IV. Values are tabulated at 1×10^{-7} Torr and 3×10^{-9} Torr, which are the mean values of the pressure extremes investigated. Sensitivities are derived from representative curves drawn from the data, which follow the relationship given by Eq. (5). The lower pressure values for helium and neon are extrapolated values. Sensitivities obtained at 1×10^{-7} Torr with the hot-filament source operated at a 3 ma emission current are also tabulated for comparison. Resolution for both hot-filament and cold-cathode sources was approximately 1 amu for all values shown. Sensitivities have been corrected for relative abundances and for MBAG sensitivity variation with gas composition. The tabulated sensitivities were obtained with a Faraday cup ion collector and are, therefore, unamplified.

TABLE IV

SPECTROMETER SENSITIVITY VS. ATOMIC MASS FOR HOT FILAMENT AND COLD-CATHODE ION SOURCES.

(L and M Indicate Low and Medium Mass Range Results, Respectively.)

Sensitivity (ma/Torr)

Gas	CCIS		Hot Filament
	3×10^{-9} Torr	1×10^{-7} Torr	1×10^{-7} Torr
He^4	.077[a] (L)	0.064 (L)	.042 (L)
Ne^{20}	.130[a] (L)	0.100 (L)	.068 (L)
N_2^{28}	.400 (L)	0.820 (L)	.250 (L)
A^{40}	.730 (L)	1.200 (L)	.260 (L)
A^{40}	.380 (M)	0.780 (M)	.290 (M)
Kr^{84}	.740 (M)	1.200 (M)	.350 (M)

a = (extrapolated)

It is seen that CCIS sensitivities exceed those of the hot-cathode source over the range of parameters investigated, even though the hot-cathode source was operated at a relatively high emission current. The sensitivity advantage increases with atomic number; under low mass range operating conditions, the CCIS/hot-filament sensitivity ratio increases from 1.5 to 4.6 over the mass range 4 amu to 40 amu.

Absolute sensitivities range from a low of .064 mA/Torr for helium to a high of 1.2 mA/Torr for krypton and argon. The maximum sensitivity variation with pressure for any particular gas is a factor of two over the approximately two decades investigated.

The sensitivity variation with mass is caused by variations both in the ion transmission of the quadrupole and in the ionization efficiency of the source. The quadrupole manufacturer supplied electronic means for adjusting relative mass sensitivities but these controls were not investigated.

Resolution vs. atomic mass. - Some variation in resolution as a function of mass is observable (see Figs. 13 and 14). This is attributed primarily to arbitrary settings of the manufacturer's electronic sensitivity control noted above, since sensitivity can be increased only at the expense of resolution.

Discussion of Results

The above results demonstrate the capability of a quadrupole spectrometer to produce spectra with high sensitivity and resolution when coupled to a CCIS. However, the quadrupole used was selected for its commercial availability and does not represent an optimum design for a CCIS. Optimum designs are discussed in Appendices A and B. A larger rf potential and larger physical dimensions (primarily r_0) are required to accommodate the larger ion energy spread and larger ion beam diameter emergent from the CCIS.

An illustration of the benefits of a larger rf operating potential is the improvement resultant from a switch to the low mass range from the medium mass range. It was noted (see. Fig. 10) that sensitivity increased almost a factor of two and that resolution improved from a 10% valley peak separation of 2.5 amu to 1.5 amu (later 1.0 amu and .7 amu, respectively).

One reason for this improvement can be seen from relationships derived by Paul (ref. 3). The rf potential V, mass M, rf frequency ν, and the radius of the circle inscribed by the quadrupole rods r_o, are related by

$$V = \frac{M\nu^2 r_o^2}{2.3 \times 10^{-20}} \qquad (6)$$

(the constant derives from the use of mks units). Low mass range resolution and sensitivity improvement exists because the quadrupole employs higher frequency (5.3 mHz) on the low mass range than on the medium mass range (3.3 mHz). It can be seen from Eq. (6) that as a result, the rf potential V on the low mass range must be increased to scan the same mass numbers common to both ranges (10-50 amu). However, the larger V required for each mass M increases the transverse ion energy, $U_{T_{max}}$, allowable for 100% transmission, according to

$$U_{T_{max}} = V\Delta M/15M \qquad (7)$$

where ΔM is the peak width at its base. More ions are, therefore acceptable and sensitivity and/or resolution are improved.

Sensitivity and/or resolution improvement can be expected to continue by further increases in the required rf operating potential, until the ions with the largest $U_{T_{max}}$ are accommodated.

Indicative of these higher sensitivity capabilities with larger rf potentials are results obtained with a family of nitrogen spectra recorded as a function of resolution. Here, $\Delta M/M$ was varied, instead of V to reduce the restrictions on $U_{T_{max}}$ according to Eq. (7). Spectra were recorded as previously, but subsequent to achievement of otherwise optimum conditions (except for the 425°C bake). Results for the low mass range are shown in Fig. 15. It can be seen that when resolution is degraded just short of appreciable peak overlap, N_2^{28} sensitivity increased a factor of more than 10. On the medium mass range it increased a factor of 15. The .82 mA/Torr sensitivity for nitrogen at .7 amu peak separation (with 10% valley) therefore might reasonably be expected to approach 10 mA/Torr with equal or better resolution by utilizing higher rf potentials; increasing quadrupole dimensions, primarily r_o, would also assist sensitivity improvement.

Thus, if improved quadrupole design allows enlarging the source exit aperture, a still greater fraction of the source's internal sensitivity can be realized.

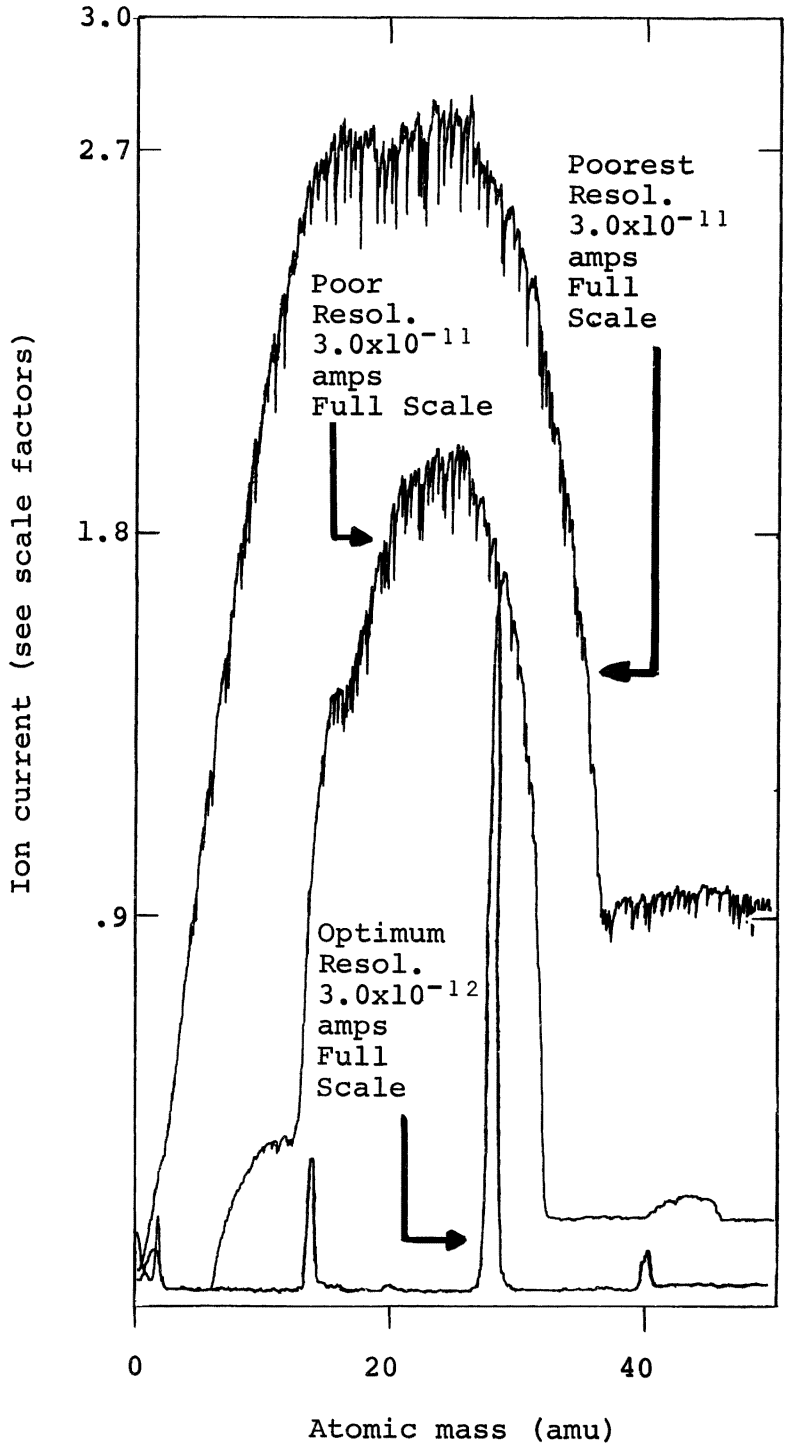

Figure 15.- Sensitivity vs. resolution-
low mass range

Finally, it is noted that two other workers (refs. 4, 5) report the nearly simultaneous development of a CCIS/Quadrupole for use in pressure regions above 10^{-7} Torr. Although their instrument was not intended for UHV use, it is noted that their results parallel these results quite closely.

The next section of this report will discuss the use of ion counting techniques which were applied to the CCIS/Quad in order to improve S/N ratio and to further increase the instrument's ability to detect extremely small partial pressures under UHV conditions.

APPLICATION OF COUNTING TECHNIQUES TO EXTREMELY LOW PRESSURE MEASUREMENTS

Introduction - Program Objectives

This section of the report will describe a previously unreported program conducted under contract NAS1-5347, Task 8. The general objective of this program is to investigate the use of ion counting techniques in the measurement of extremely low pressures. The primary aim of the investigation is to improve the reliability of low pressure measurements by improving the overall signal-to-noise (S/N) ratio of both total and partial pressure measuring devices. A high gain, low noise, electron multiplier is used in conjunction with appropriate ion counting circuitry to discriminate against the undesired noise. The cold-cathode ion source/quadrupole mass filter, developed under the previously described contract (NAS1-2691, Task 8) was employed as a partial and total pressure measuring device in these investigations. The electron multiplier is commercially available as standard equipment of the quadrupole analyzer. The output of the multiplier was readily adapted to a commercial pulse counting instrument (nuclear scaler).

The performance of the spectrometer has been investigated using both dc current and ion counting detectors for comparison and for other experimental purposes to be described later. The work program, which was largely experimental in character, has the following specific objectives:

(1) To evaluate experimentally the ion source-electron multiplier system, by measuring the ion current incident upon the cathode and the pulse arrival rate at the anode and to determine the ion accelerating voltage required to obtain a secondary electron yield of at least one.

(2) To investigate the feasibility of applying pulse height analysis techniques to discriminate between pulses produced by ions and those produced by photons or soft x-rays.

(3) To determine the maximum pressure that may be measured without saturating either the electron multiplier or pulse-counting circuit.

(4) To determine the operating characteristics of the ion source - mass filter - pulse counting system, both as total and partial pressure measuring devices.

(5) To study the performance of the system under extreme high vacuum conditions and to obtain calibration data to as low a pressure as possible.

This program, then, represents the last phase of an overall program to improve the reliability of extremely low pressure measurement devices, particularly partial pressure analyzers. This section of the report will, therefore, stress the elements of improvement that can be made in obtaining more reliable detectors for both total and partial pressure measurement. Although the CCIS/

Quadrupole was specifically investigated, it is anticipated that the results of these investigations are applicable to other instruments and will also serve as guidelines to future improvements, particularly in the selection of electron multipliers and in the design of ion detectors.

Ion Counting Techniques - General Considerations

Advantages. - The basic partial pressure sensitivity of modest resolution ($\frac{M}{\Delta M} \leq 100$) residual gas analyzers (RGA's) lies in the range of 5×10^{-4} to 1×10^{-5} amperes per Torr for nitrogen (mass 28). Without the aid of an electron multiplier, such instruments are limited to an ultimate partial pressure detectability in the realm of 2×10^{-11} to 1×10^{-9} Torr, nitrogen.* The electron multiplier becomes an absolutely essential part of the dc analog ion detector, if improved sensitivity and S/N ratio of the instrument are required.

It is generally recognized that the stability of electron multipliers is inadequate to provide reproducible, quantitative data unless frequent gain measurements are made. Manufacturers of commercial RGA's report that a short-term reduction in multiplier gain of a factor of ten or more is typical initially and they recommend periodic gain measurements for greater reliability. Such instruments are now designed to provide a simple and expedient means of routinely measuring the gain. Special connections are provided

---

*This assumes that the minimum detectable ion current is 1×10^{-14} amperes.

for measuring the ion current at the first dynode and for measuring the electron current output of the multiplier. The gain is readily measured provided that the first dynode current is not below the detectability limits discussed above. If however, the RGA is operating at extremely low pressures, it is impossible to measure the gain of the multiplier and therefore, the sensitivity of the spectrometer cannot be measured directly.

Ion counting techniques offer a possible solution to this problem. All measurements are made at the output of the multiplier, thereby avoiding the difficulties of measuring very small currents at the input. The measurement involves simply the output counting rate (ions/second) and the output dc electron current. Assuming that the detector counts all ions striking the input of the multiplier,* the input current is simply

$$I_{in} = eR \qquad (8)$$

where e = electron charge (1.6×10^{-19} coulombs) and R is the measured ion counting rate in ions/sec. Appropriate correction must be made for multiply-charged species. For singly charged species, the gain for a particular mass becomes

$$G_m = \frac{I_o}{R} \times 6.25 \times 10^{18} \qquad (9)$$

---

*This assumption can be tested as will be discussed later.

where I_o is the output electron current in amperes. This measurement includes the gain-dependancy of the multiplier on the ionic mass since I_o will depend on mass.

Although ion counting techniques offer the important advantage of gain measurement at the output, a number of other advantages may also result therefrom. These will be only briefly described here, but will be fully amplified in later sections.

Depending on certain noise factors largely determined by the spectrometer's ion source, it is possible to discriminate against a substantial portion of undesired noise by means of simple pulse height discrimination. The S/N ratio (compared to dc detectors) can be improved by a factor of 100 or more. The degree of improvement depends on the type of ion source-analyzer and on the detector design and on electron multiplier characteristics.

The present work indicates that with the very high gain/low noise multipliers recently made available, it is possible to circumvent nearly all gain instability in the multiplier (both short and long term). Thus the ion counting detector not only can reduce the uncertainties in detector gain, but shows promise of ultimately completely eliminating gain dependance.

In addition, the use of ion counting techniques eliminates the mass and charge dependancy of the multiplier since the detector response is related only

to the number of events and not the m/e ratio of the ions and to their respective momenta. While this fact does not permit a direct one-to-one correlation between observed counting rate and partial pressure, it does eliminate the detector as a contributor to the spectrometer's partial pressure response characteristics.

Finally, the use of counting techniques provides a direct output for digital data acquisition and analysis using computers, which have proven to be valuable in interpreting complex spectra and in analyzing large amounts of repetitive data.

Disadvantages. - The counting rate method of detecting ions involves the use of complex electronic equipment as the reader has probably surmised. For instance, a preamplifier, a non-overloading amplifier and an amplitude discriminator precede the counting equipment. Automatic mass scanning and data acquisition and recording equipment will obviously be more complex than the corresponding dc equipment. Of course, rate meter circuitry may be used to simplify the essential equipment with some sacrifice in accuracy. For routine qualitative analysis of UHV conditions, the increased complexity and expense of fully automated systems is not justifiable. For quantitative and reliable UHV measurements the relatively simple electronics used during this study may be employed very effectively.

Experimental Apparatus and Methods

Vacuum system. - The vacuum system used in the experimental phase of this program is essentially the same as the system shown previously in Fig. 3. The

system and associated test equipment are shown in Fig. 16. The pumping speed in the UHV section of the system was increased by substituting a 25 liter/second ion pump for the 11 liter/second pump previously used. With the increased pumping speed the ultimate system pressure is approximately 3-4 x 10^{-12} Torr, nitrogen. The bakeable ultra-high vacuum valve shown previously between the upper manifold and the upper ion pump was removed to improve pumping speed. The UHV valve between the upper and lower manifolds was not changed. A portable mechanical pump was substituted for the zeolite roughing pumps, without noticeable change in system performance. The rough pump is used only for short periods during initial system evacuation. Bake-out procedures are as described in the previous contract report.

Cold cathode ion source/quadrupole. - The CCIS/Quad described in a previous section* of this report was modified by the addition of a 14 stage focused dynode (Be-Cu) electron multiplier, purchased from Ultek Corporation, Palo Alto, California. It does not have provisions for measurement of first dynode current and therefore, certain limitations were imposed on experimental methods which will be explained in later sections. The multipliers supplied with later models of the equipment do provide for the first dynode current measurement. This modification is particularly helpful in certain experimental studies.

---

*See section entitled, "Development of the CCIS/Quad Mass Spectrometer".

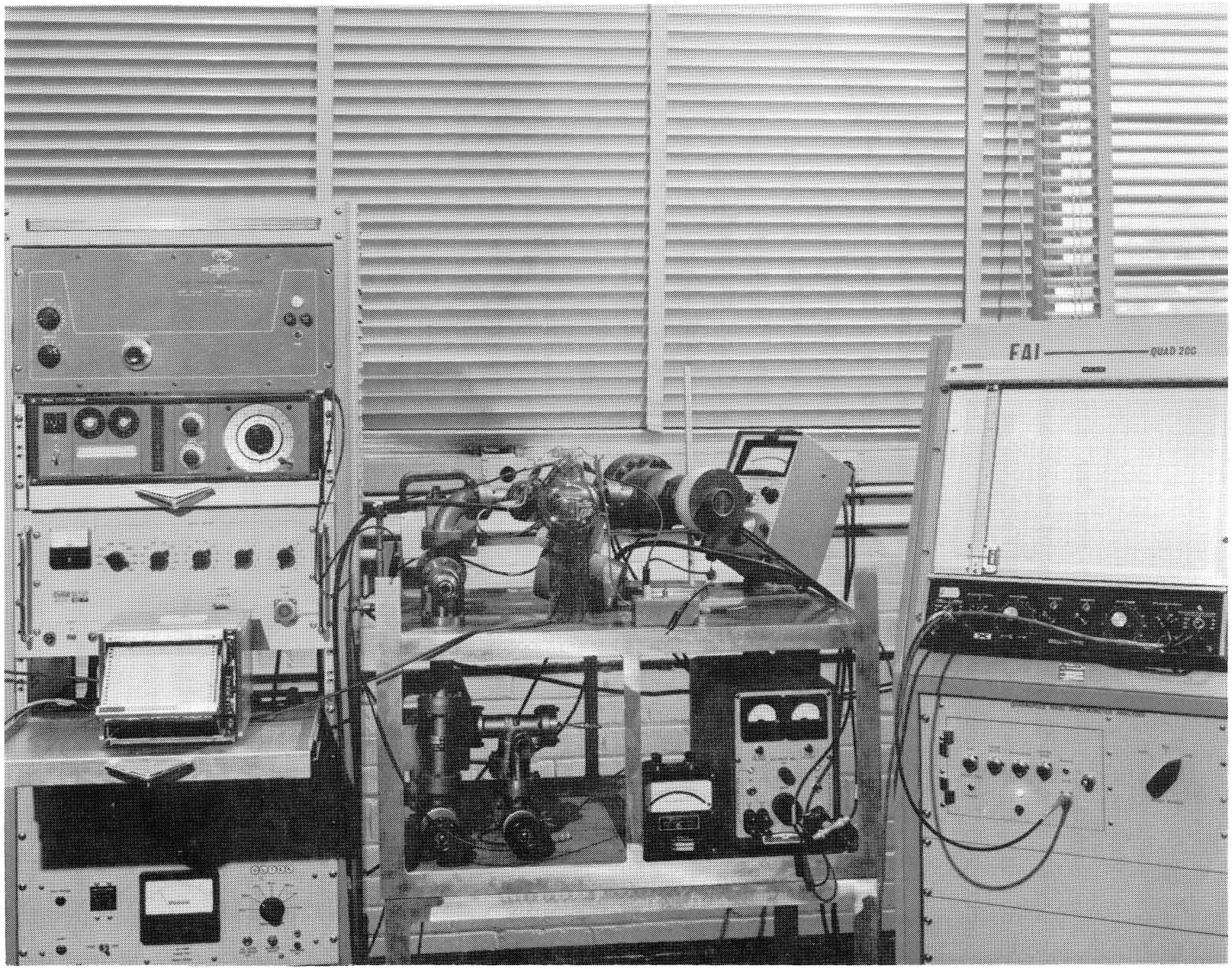

Figure 16.- Photograph of test equipment

The cold cathode ion source/quadrupole is identical in construction to the instrument described in previous sections of this report. The quadrupole analyzer is a modified Ultek Quad 200 as described previously. With the exception of the addition of the electron multiplier, the quadrupole has not been modified. Another section of this report describes in detail, the construction of the cold cathode ion source and its adaptation to the quadrupole.

Electronics for ion counting. - Figure 17 is a block diagram of the equipment used during the ion-counting studies. In general, the equipment is a simple inter-connection of power supplies for operation of the CCIS, together with the quadrupole electronics console. A sweep voltage was derived from the quadrupole electronics to provide the x-axis (mass scale) on the X-Y recorder. An electrometer was employed to detect and record the ion currents at various mass peaks and to measure electron multiplier gain.

Counting data was taken with the simple configuration of standard nuclear scaling equipment shown. The linear pulse height discriminator included in the non-overloading pulse amplifier was used to obtain integral pulse height distribution data for signal and noise and to also discriminate against noise.

The counting equipment used has a relatively low frequency response of 100 kHz. With faster counting equipment the range of counting rates can easily be extended to the order of 10 mHz. The limitation of the present equipment together with other electronic considerations such as resolution loss etc., will be discussed shortly.

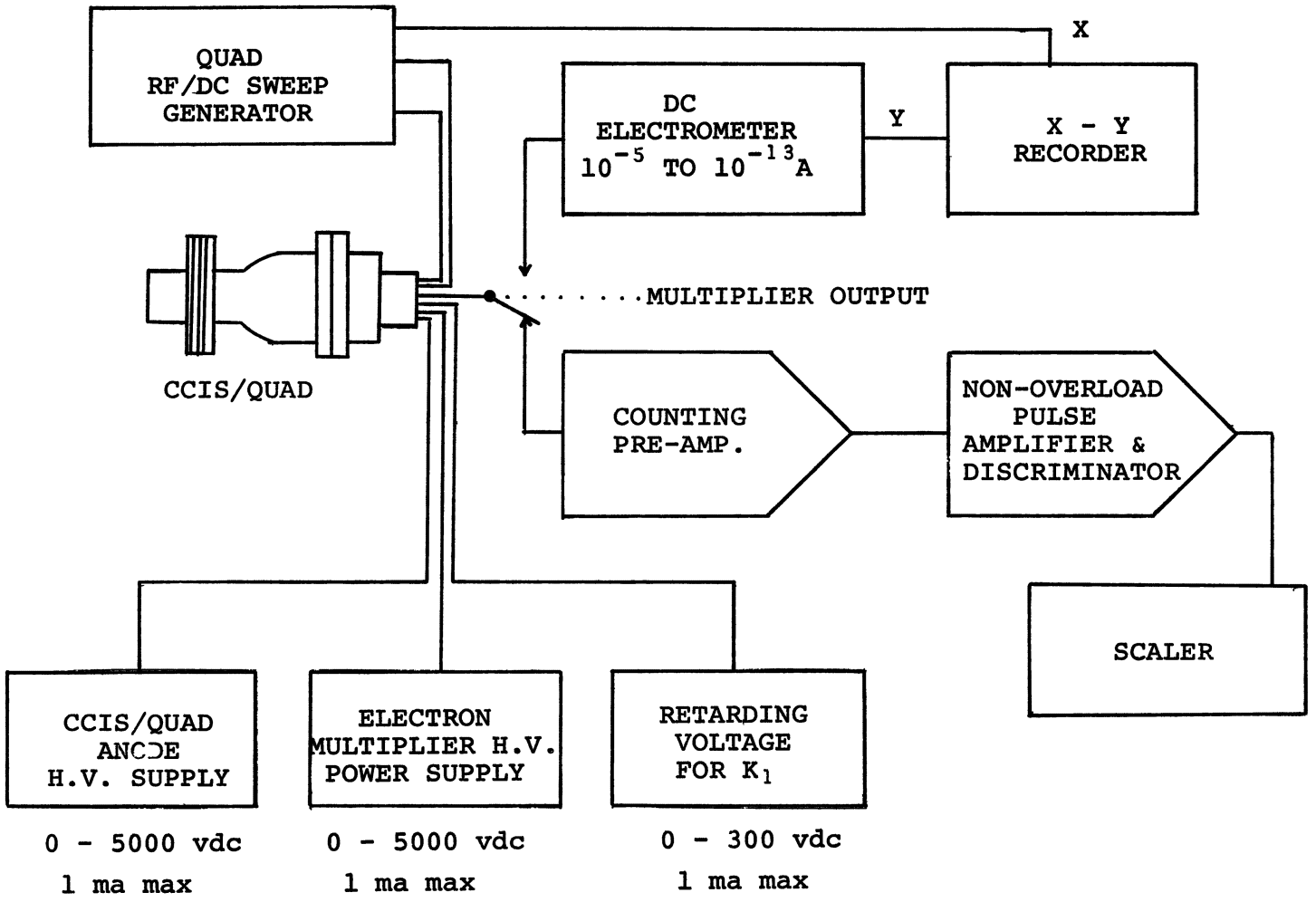

Fig. 17 - Block Diagram of Equipment

While the experimental set-up is quite unsophisticated, it has been found quite adequate in obtaining a wide variety of experimental information relevant to the proper evaluation of ion counting detection methods.

Experimental Results

Preliminary DC S/N ratio studies. - It has been noted in previous sections that the ion detector was a simple Faraday cup. In order to obtain sufficient charge gain for ion counting, a 14-stage electron multiplier was installed at the beginning of the present contract work. Initial studies of S/N ratio were begun on a dc basis, i.e., the output of the electron multiplier was measured by an electrometer.

These early studies uncovered two sources of noise in the output spectrum not previously encountered. At the anode voltage previously found to yield optimum sensitivity and resolution (2200 V), a noticeable dc baseline current between mass peaks was observed. This noise current was approximately 10^{-10} amperes with 2900V on the multiplier. The largest mass peak (mass 28) was 1.5×10^{-9} amperes. The system total pressure was nearly 4×10^{-11} Torr (nitrogen). This baseline current was not independent of mass, but decreased as the sweep increased over the 30 to 55 amu range. Subsequent experiments demonstrated that this decline in baseline with increasing mass was simply due to the rectification of stray quadrupole r-f fields by the electrometer. Accordingly, the shielding of all leads at the connector end of the quadrupole housing was improved and this problem quickly disappeared. The baseline current at low mass numbers remained essentially the same. Further

investigation established that the CCIS was the predominant source of this background noise and the noise current was nearly linearly related to the anode potential of the CCIS. Fig. 18 shows how the signal at mass 28, noise at mass 50 (taken where no peaks were observed), and S/N ratio vary with anode voltage. The S/N appears to be largest at the minimum value of anode voltage investigated.

In an effort to uncover the cause of this noise a number of potential noise sources were considered and investigated. Among these was the strong electron flux which was discovered emerging from the ion source during earlier feasibility studies. Photons are also known to be produced within the discharge (ref. 6). Accordingly, an experiment was performed to define whether or not the noise source was predominantly photons or charged particles.

It will be recalled that the two ion source cathodes (K_1 and K_2) are electrically isolated from the grounded entrance aperture of the quadrupole. This permits the retardation of ions prior to their entrance into the quadrupole. It has been shown in the preceding discussion on the development of the CCIS/Quad, that such retardation is necessary to achieve optimum quadrupole resolution. The effect of the retardation potential on the dc noise background current is shown in Fig. 19.

As the value of the retardation potential (V_R) was increased from zero to 250 volts, the ion current of all mass peaks, including the "on blast" (all ions unresolved at M/e = 0), decreased as anticipated. The baseline noise current however increased. For this

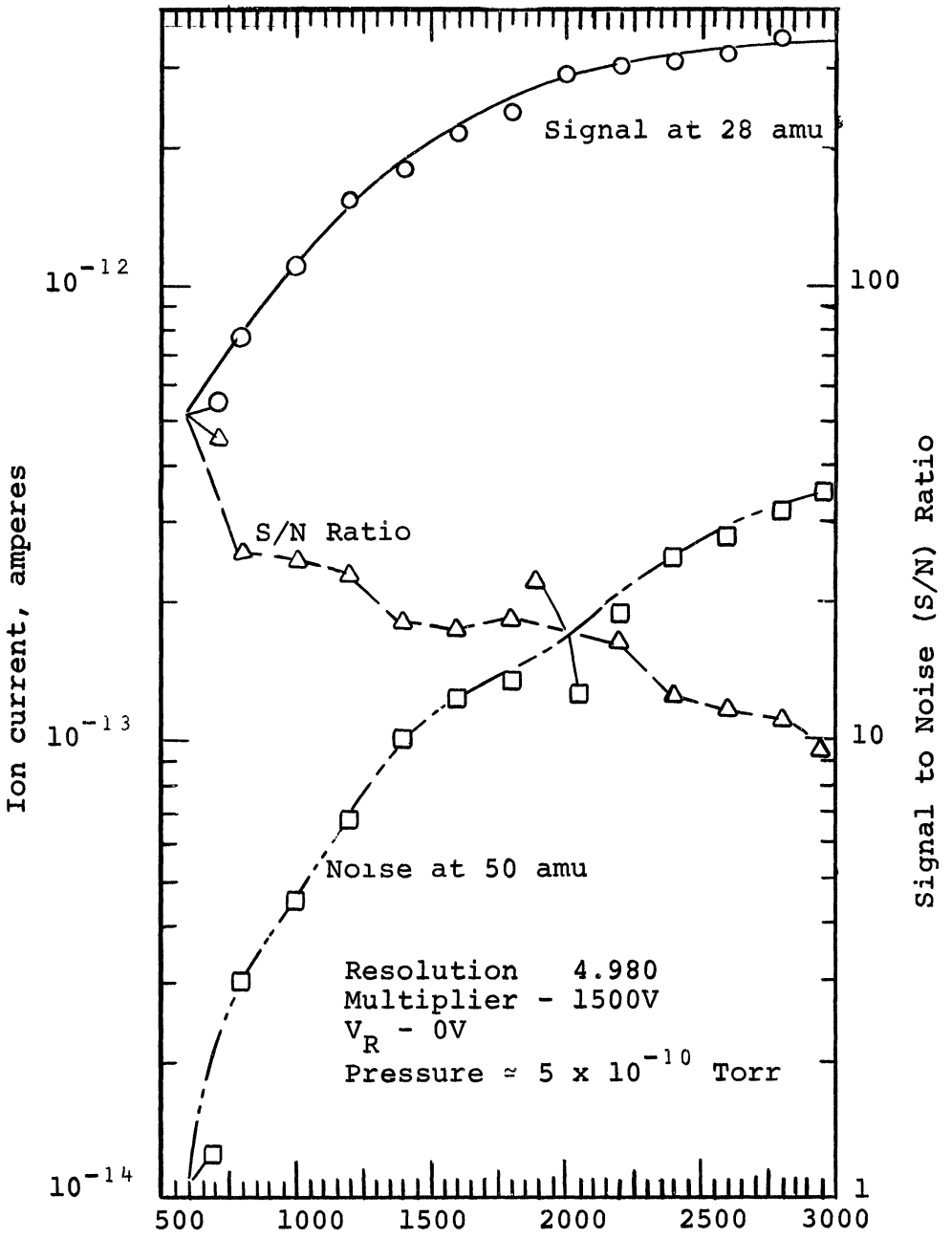

Fig. 18 - DC S/N Ratio vs. Anode Voltage

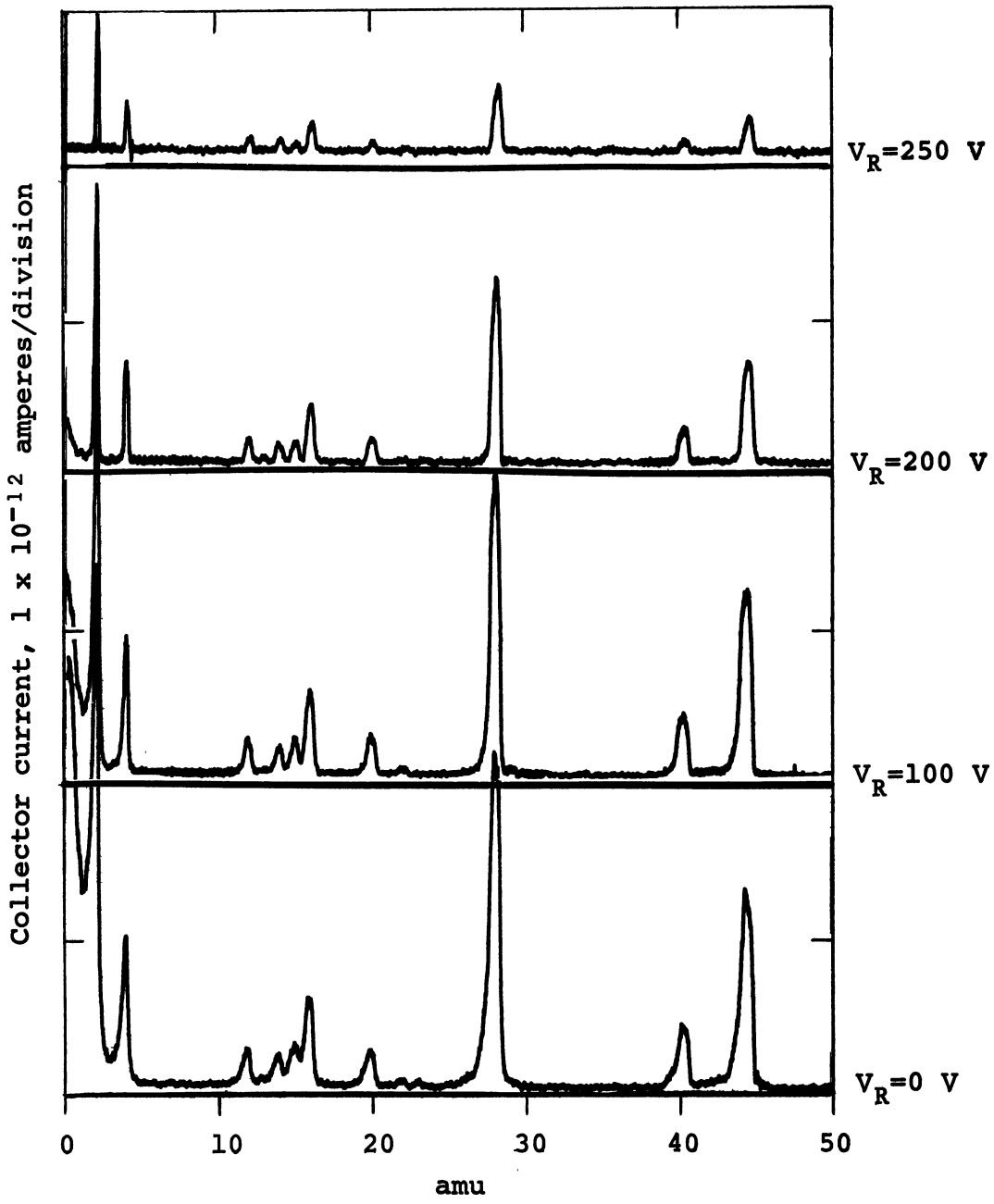

Resolution - 4.985
Pressure - < 5 x 10^{-11} Torr
Gas - Background

Multiplier - 1500 V
B - 865 gauss
Anode - 1400 V

Figure 19.- DC signal and noise vs. retarding potential with solid cathode stub

experiment, a negative retarding voltage was applied simultaneously to the two CCIS cathodes (K_1 and K_2) so that the potential between the exit cathode, K_2 and quadrupole entrance aperture (grounded) is a retarding potential for ions. At the same time, the true anode-to-cathode potential of the CCIS is increased by an amount equal to V_R, and therefore the noise current also increases, as shown in the previous figure. Subsequent experiments were conducted using both positive and negative values of V_R in the range of 0 to 500 volts. The true anode-to-cathode voltage was held constant. In these experiments, no appreciable change in the baseline noise value was observed for either positive or negative values of V_R.

Since the noise level was not observed to change in response to a wide range of external fields which are both retarding and accelerating potentials for charged particles, it is concluded that the noise source is largely photons produced within the ion source proper. These photons then are transmitted along the axis of the quadrupole and subsequently stimulate the first dynode of the multiplier.

An attempt was made to reduce the photon background within the source based upon a very simple assumption. It was postulated that soft x-rays might be produced by energetic electrons within the discharge. These electrons, upon striking the blunt end of the cathode stub, would produce x-ray photons visible from the multiplier end of the analyzer, since the end of the stub fills the major portion of the cathode exit aperture as seen by the multiplier. Consequently,

the stub of K_1 was removed and replaced by a thin-walled tube of the same diamter and length as the stub. In this configuration the multiplier "sees" only the small annulus of the stub area. In the resultant experiment, the operating and vacuum conditions noted in the previous graph were maintained as nearly as possible. The results are shown in Fig. 20. This figure shows the observed baseline current is no longer discernable ($< 1 \times 10^{-14}$ amperes), under conditions similar to those of the solid stub. Moreover, there is no apparent increase in this background as the true anode voltage is increased (V_R increasing). It will be shown later that although the background has been noticeably reduced, it is still observable.

Our present speculation is that the photons are not soft x-rays resulting from electron impacts but are probably identical to the photons observed and photographed by Feakes et al. (ref. 6). Perhaps, by modifying the cathode stub, the visible cathode glow is prevented from establishing itself around the end of the stub and the resultant light surrounds only the outer surface of the tubular stub. Only a small portion of this glow would be visible to the multiplier because the diameter of the tubular stub and ion exit aperture are nearly identical. Despite these present conjectures, the reduction in background dc noise is apparent.

With these investigations the preliminary dc S/N ratio studies were concluded. The unit was then set up for ion counting studies in accordance with the block diagram shown in Fig. 17.

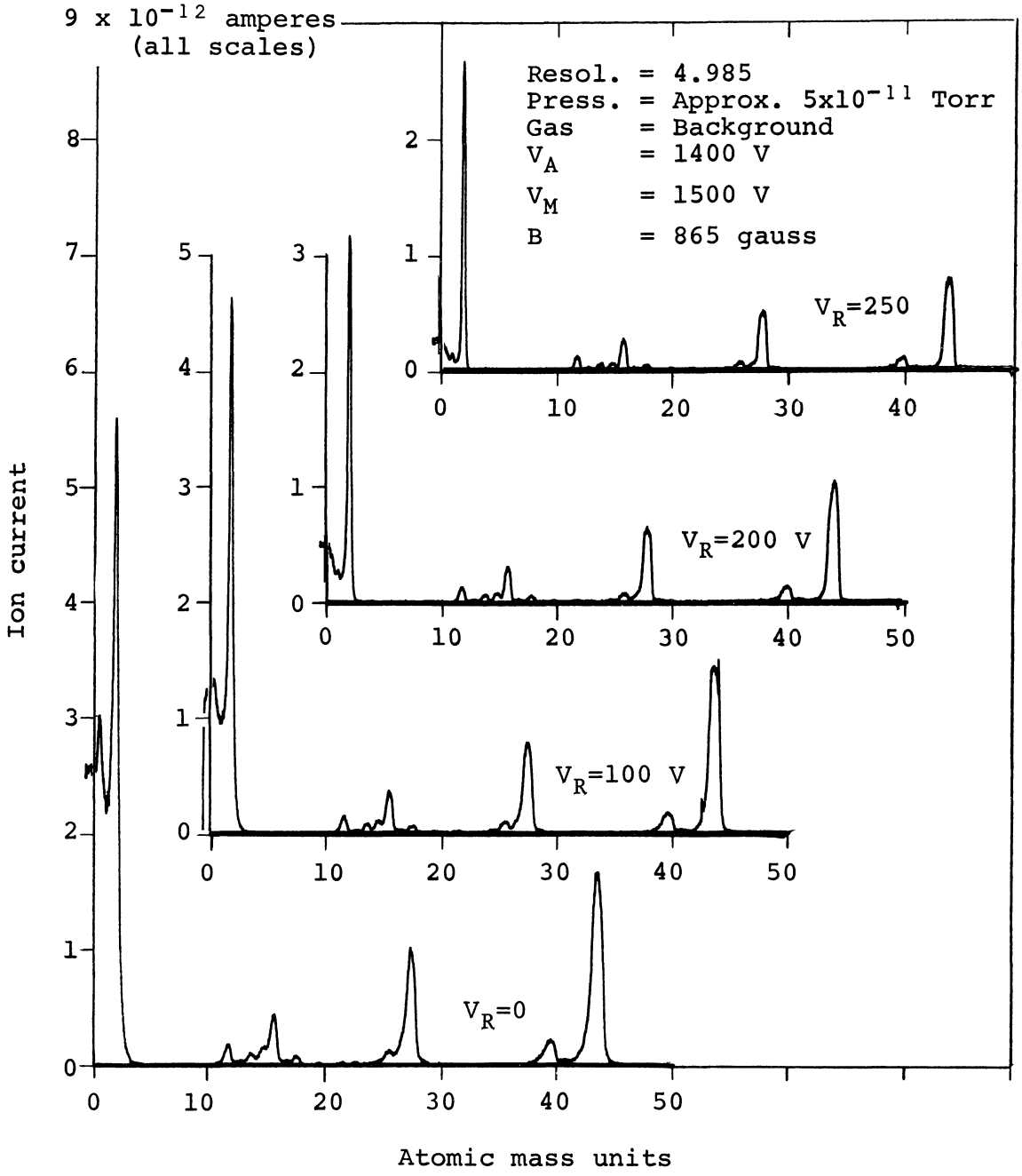

Figure 20.- DC signal and noise vs. retarding potential with tubular cathode stub

Ion Counting Studies - Preliminary Discussions

Before describing the experimental results of the ion counting studies, a more detailed description of the ion counting electronic equipment will be given. These discussions will serve to acquaint the reader with general and specific details of the equipment and methods used in the experimental program. In addition, it is our intent to emphasize how certain data will relate to the overall program goals of improving S/N ratio and increasing the reliability of measurement.

Electron multipliers. - The basic electronic element required for ion counting is the electron multiplier. This device, when combined with a photo-sensitive cathode (photo-multiplier) has seen widespread application in the nuclear instrumentation and in other related photon counting applications (ref. 7). For the present application however, only the electron multiplier section is used. While the problems associated with electron multipliers are many and varied, the general advantages of very large charge gain (10^5 to 10^8) and very wide bandwidth (dc to 100 mHz) make the device particularly attractive for particle detection. The use of multipliers as ion detectors is by no means new (ref. 8), nor is its application to mass spectrometry (refs. 9, 10, 11). More recently the electron multiplier has been utilized in UHV residual gas analyzers as a high-gain, dc ion current detector in commercial vacuum instruments (ref. 12).

Multiplier problems. - For UHV ion-counting techniques, however, two problem areas (common to all multipliers) are most noteworthy. First, the charge gain of the multiplier varies randomly with time for any ion which

produces one or more secondary electrons at the input (first dynode). Accordingly, the short-term burst (nano-seconds) of electrons produced at the ouput for each indident ion, contains a widely variant number of electrons. The small voltage pulse, produced as these electrons charge the output capacity of the multiplier and decay through the output resistance, varies considerably in pulse amplitude. The distribution of these small pulse amplitudes is roughly that of a Poisson distribution (ref. 13). The pulse amplitude of 99% of the pulses extends over approximately two orders of magnitude. For small output capcities of the order of 10^{-11} farads and relatively low-gain multipliers (10^5), the average voltage pulse produces per ion is typically only a few millivolts in amplitude. Further voltage gain is therefore required as with a separate pulse amplifier.

The second most important problem in multipliers is the fact that their average gain varies by large amounts as a function of many uncontrollable factors such as contamination of dynode surfaces by residual gases and debris and by certain fatigue effects in the secondary emission process. Thus, not only are the ion pulse heights widely variable due to statistical problems but they also vary due to environmental conditions. The auxiliary pulse amplifier, therefore must be prepared to amplify a very wide range of small pulses, without over-loading on the largest pulses, and thereby producing spurious counts. At the same time it must also be capable of amplifying the large number of small pulses. Accordingly, the configuration of counting electronics used for ion counting studies must be assembled with some care.

Ion counting electronics. - In the present experimental arrangement, the output of the multiplier is fed into a small emitter-follower preamplifier shown schematically in Fig. 21 to close-couple the non-overloading pulse amplifier/discriminator to the CCIS/Quad. A short length of coaxial cable (3 inches) couples the input of the pre-amplifier to the multiplier in order to minimize cable capacity. The R-C time constant of the preamplifier was chosen to be near 10^{-5} seconds, since the frequency response of the amplifier is approximately 200 KHz. Time constants in excess of 10^{-5} seconds would result in partial integration of the pulses at high counting rates. The RC time constant of the ion pulses measured at the emitter follower preamplifier output is <5 μ secs.

The pulse output of the preamplifier is then fed into a non-overloading amplifier equipped with a single level amplitude discriminator whose selection level may be varied in a linear manner. The ion pulses with amplitude greater than the discriminator level, trigger a Schmidt trigger circuit which presents large pulses of uniform amplitude to the scaler for counting. Although the scaler also includes a discriminator, it was not varied once it was demonstrated that all the Schmidt trigger pulses were large enough to exceed the highest discriminator setting of the scaler. The scaler has a resolving time of approximately 5 μsecs. When the counting rate exceeds approximately 7×10^4 ions/sec., the scaler begins to miss some of the pulses. This phenomenon, known as resolution loss, is predictable for

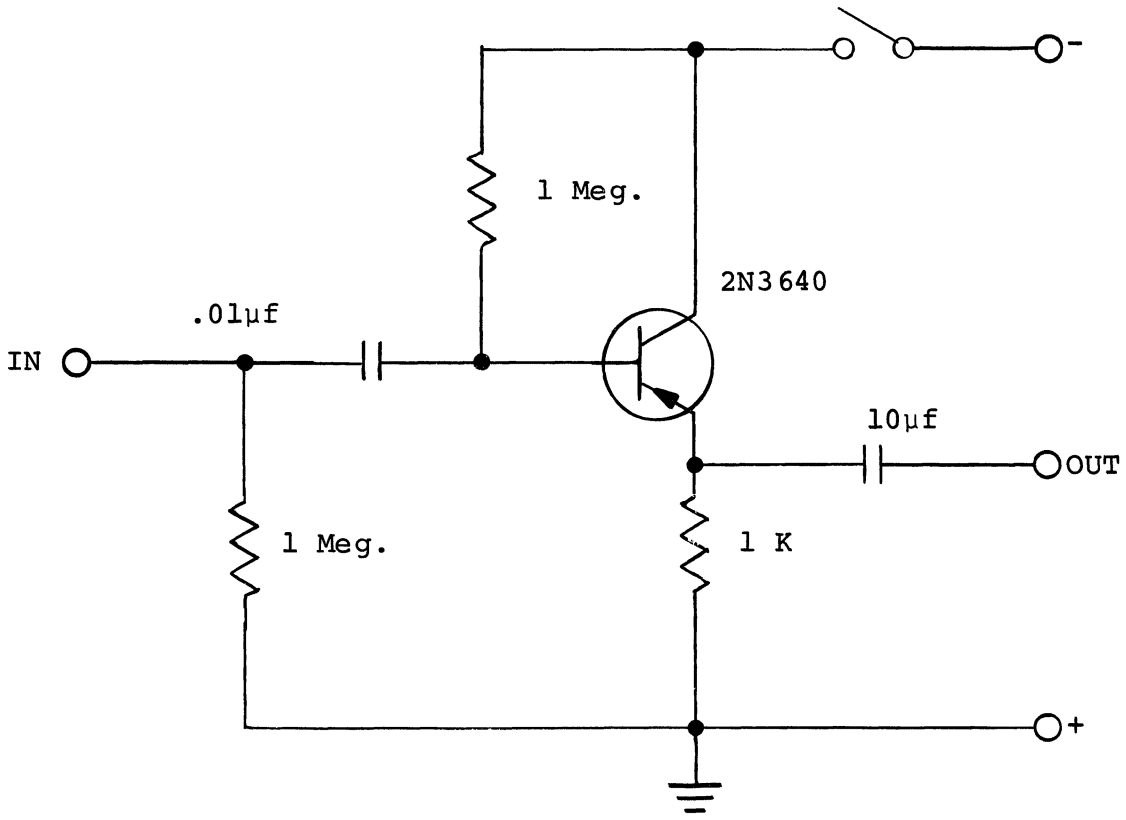

Figure 21. -Preamplifier Circuit Schematic

randomly spaced pulses. The observed and true counting rates are related to the scaler resolving time as shown in the following equation:*

$$R_T = \frac{R_o}{1-R_o\tau} \qquad (10)$$

where R_T is the true counting rate and R_o is the observed rate and τ = resolving time expressed in the same time units as R_o and R_T. In one experiment, the resolution loss was measured by comparing the dc current response and pulse response. It was found that the pulse response was decreasing with respect to the dc current response by an amount predicted by the relation above. Thus it is seen that the counting method is ultimately limited in ability to measure increasingly larger partial pressures by the speed of response of the electronics. With high speed counters, the upper limit of counting rate is estimated to be approximately 7×10^6 ions/sec or 1.1×10^{-12} amperes. It should be recalled that the latter figures represent input current to the multiplier, not output current. Therefore, if the analyzer has the relatively low sensitivity of 1×10^{-5} amps/Torr, the partial pressure (for nitrogen) would be of the order of 10^{-7} Torr at this maximum rate. Thus we see that the counting spectrometer should be able to detect partial pressures well above the UHV region with high speed electronics.

The non-overloading pulse amplifier/discriminator deserves additional mention. The linear pulse height

---

*This relationship applies only to nonparalyzeable counters. See Evans, R.D., "The Atomic Nucleus", McGraw-Hill Book Co., New York, 1955, pp. 786-787.

discriminator built into the non-overloading amplifier was utilized in lieu of a multi-channel pulse height analyzer in certain ion detection efficiency, pulse height analysis and S/N ratio experiments. The data resulting from plotting ion counting rate vs. discriminator setting is in effect a pulse height distribution curve displayed in an integral, rather than differential form. Since the literature (ref. 14) usually presents data in the latter form, a brief introduction will be presented herein, to assist the reader in the interpretation of subsequent data and to show how such data has a direct bearing on basic project goals.

Relation of experimental methods to program goals. - Figure 22 serves to illustrate the form in which pulse height distribution data will subsequently be shown. The spectrometer has been manually set to a typical mass peak and is operating in the ion counting mode. Counting rate data is then taken as a function of the linear pulse height discriminator setting. At each setting, the counter responds to pulses larger than a certain amplitude, set by the discriminator characteristics. If the data is carried to the point where the discriminator finally rejects the largest ion pulse amplitude, the resulting information is essentially* the integral of the pulse

---

*Actually the resulting distribution curve also depends very slightly on the statistics of secondary electron production at the first dynode of the multiplier. In general, however this conversion efficiency dispersion represents a small factor in the distribution of pulse heights, since the number of secondary electrons produced per ion does not vary over two or more orders of magnitude as does the randome gain of multiplier.

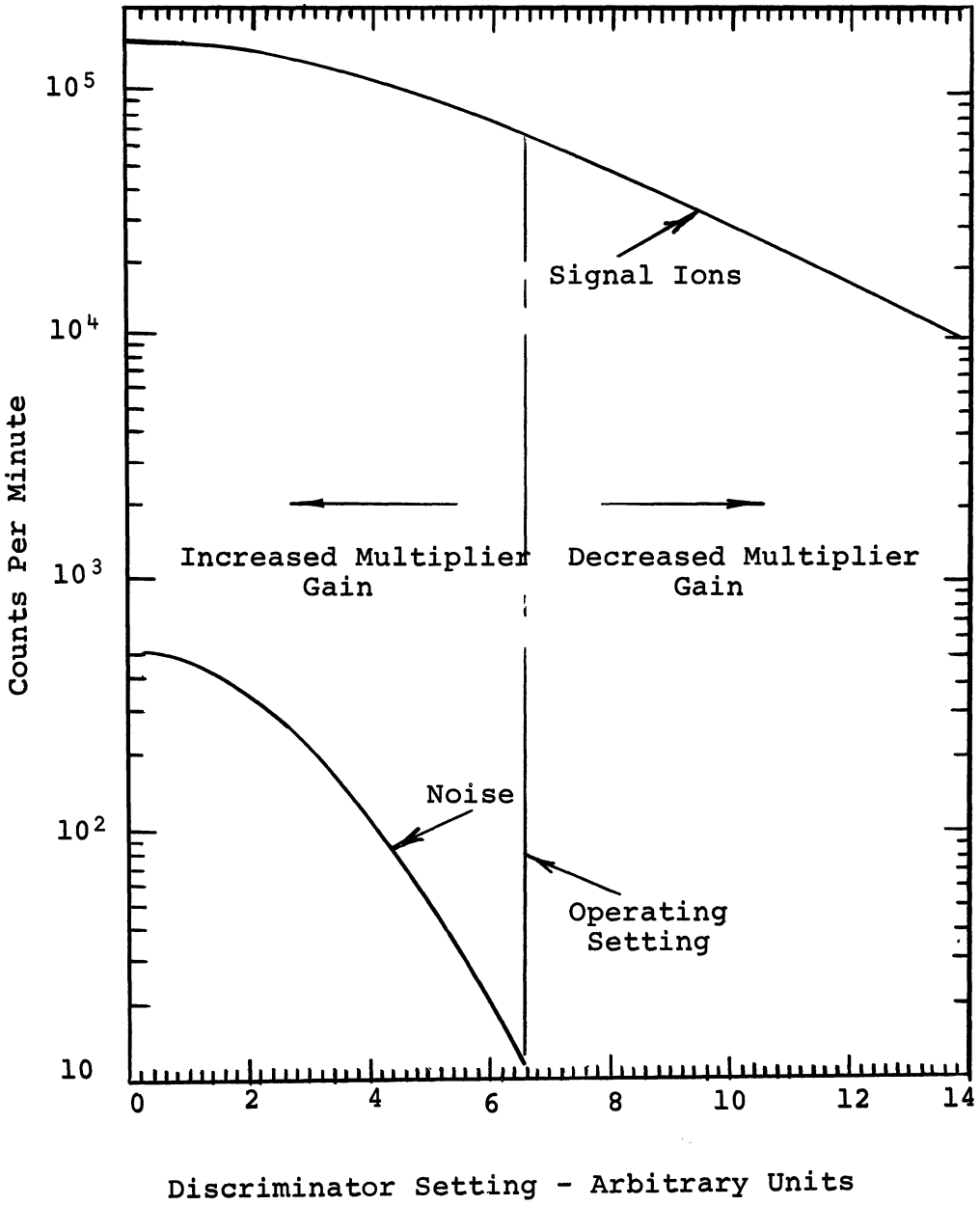

Fig. 22 Illustrative Integral Pulse Height Distribution Curve

height distribution curve of the electron multiplier. In the illustrative example shown in this figure, the integration was stopped when approximately 95% of the ions were less than the discriminator triggering level.

This type of distribution curve has certain analytical advantages over the differential distribution curve. For instance, at "zero" discriminator level, it is obvious that all ion pulses are being counted. Furthermore, the S/N is immediately obtainable at any given noise level. In this example, a S/N ratio of 6500:1 is noted at the 10 cpm noise level. Also, one can immediately determine a "counting efficiency" (observed counting rate/count rate for all ions x 100%) at any given noise level to evaluate the percentage of ions lost by discriminating against noise. In our illustrative example, for instance, the ion counting efficiency at 10 cpm noise level is:

$$\varepsilon_i = \frac{6.5 \times 10^4}{1.5 \times 10^5} \times 100\%$$

$$= 43\% \qquad (11)$$

As noted previously, electron multipliers are inherently unstable devices. As their gain changes, the position of the discriminator level essentially shifts with respect to the pulse height distribution curve as indicated by the arrows on either side of the dotted line marked "operating setting". The sensitivity will, therefore, change in an unknown manner. The integral distribution data, therefore, shows immediately how severe the effect on sensitivity will be of a small amplitude (gain) change. In the illustrative example, this effect is more pronounced at large discriminator levels (lower noise levels). If the system gain (multiplier and amplifier) drops below a

critical value, all ions will not be counted at zero discriminator setting and the integral distribution will not saturate near this zero point. This is the case with regard to the noise distribution curve. Although the illustrative distribution curve does not represent ideal performance, it does serve to illustrate the goals of the proper use of ion counting, which are:

(1) To count all available ions regardless of mass at some prescribed minimum value of overall gain.

(2) To produce the maximum possible amplitude difference between ion and noise pulse height distribution curves.

(3) To reduce the noise background to an absolute minimum.

On the basis of these criteria, we see that the illustrative data represents a rather non-ideal detector in that operation of the discriminator at values > 2 will result in discrimination against ions. This signifies a lack of sufficient gain in the detector (multiplier). In order to count all ions, the discriminator level must be reduced to a point where excessive noise results. Thus, our example, cannot meet the three criteria simultaneously.

Finally, it should be borne in mind that the present work is investigatory in nature and therefore, preliminary in scope. Major improvements in S/N ratio and stability appear probable with better multipliers and detector design. Our conclusions will support this fact.

In summary, we have shown that the integral pulse height distribution data, lends itself to quick analysis and that

project goals of high counting efficiency, minimum dependance on multiplier stability and improved S/N ratio are all readily apparent in this form of data presentation. We shall discuss the ion counting experimental results next.

Ion Counting Experimental Results

Initial investigations. - The initial phase of the ion counting investigations centered on a study of signal and noise pulse height distribution curves of the integral type explained in the previous section. During these experiments, the CCIS anode voltage was maintained at values of 1000 volts or less. It will be recalled that the dc data indicated that the optimum S/N ratio was obtained at very low anode voltages; 500-600 volts. The cathode stub of K_1 was solid, with a rounded tip as noted previously. This was later removed and the tubular stub substituted. A magnet of 850 gauss was used, and the mass spectra of the system residual gases were used for study purposes. Typically, the ultimate system total pressure was in the low 10^{-11} Torr (nitrogen) range, unless indicated otherwise. The predominant residual gases present were H_2, CO, and CO_2 with smaller amounts of He, CH_4 (methance series), neon and argon. No residual constituents were observed above mass 44 (CO_2) and therefore, noise measurements were made at mass 50. The electron multiplier was operated near -2700 volts, a value slightly less than the recommended one of -3000 volts (with respect to ground). The non-overloading amplifier gain controls were set arbitrarily to produce ion counting rates of the order of 10^4 to 10^5 counts per minute for the argon (mass 40) peak.

The major purpose of these early investigations was to learn more of the pulse height distribution characteristics of signal (ion) and noise pulses. If the two distribution curves are essentially the same function with the same average pulse amplitude, discrimination against noise on an amplitude basis would be impossible without incurring a similar discrimination against signal pulses. Briefly then, the S/N ratio would be independent of discriminator setting. On the other hand, if the average signal pulse amplitude is larger than the average noise pulse, some amplitude discrimination is possible. It is assumed in this case that the distribution curves of signal and noise are similar. Finally, if the average pulse heights of signal and noise is significantly different (signal> noise) and the distribution of noise pulse heights is narrower than the signal distribution, the S/N ratio will increase as the discriminator amplitude level is increased.

A secondary purpose of these early investigations was to learn more of the pulse characteristics of noise in the CCIS/Quad and its associated electronics, since the dc investigations indicated that a photon background current, present within the ion source was being detected by the electron multiplier. Accordingly, the signal and noise pulse height distributions were examined as a function of the ion retarding potential, V_R. Figure 23 shows the results of these investigations. The pulse height distribution data is presented in the integral form, as explained in the previous section.

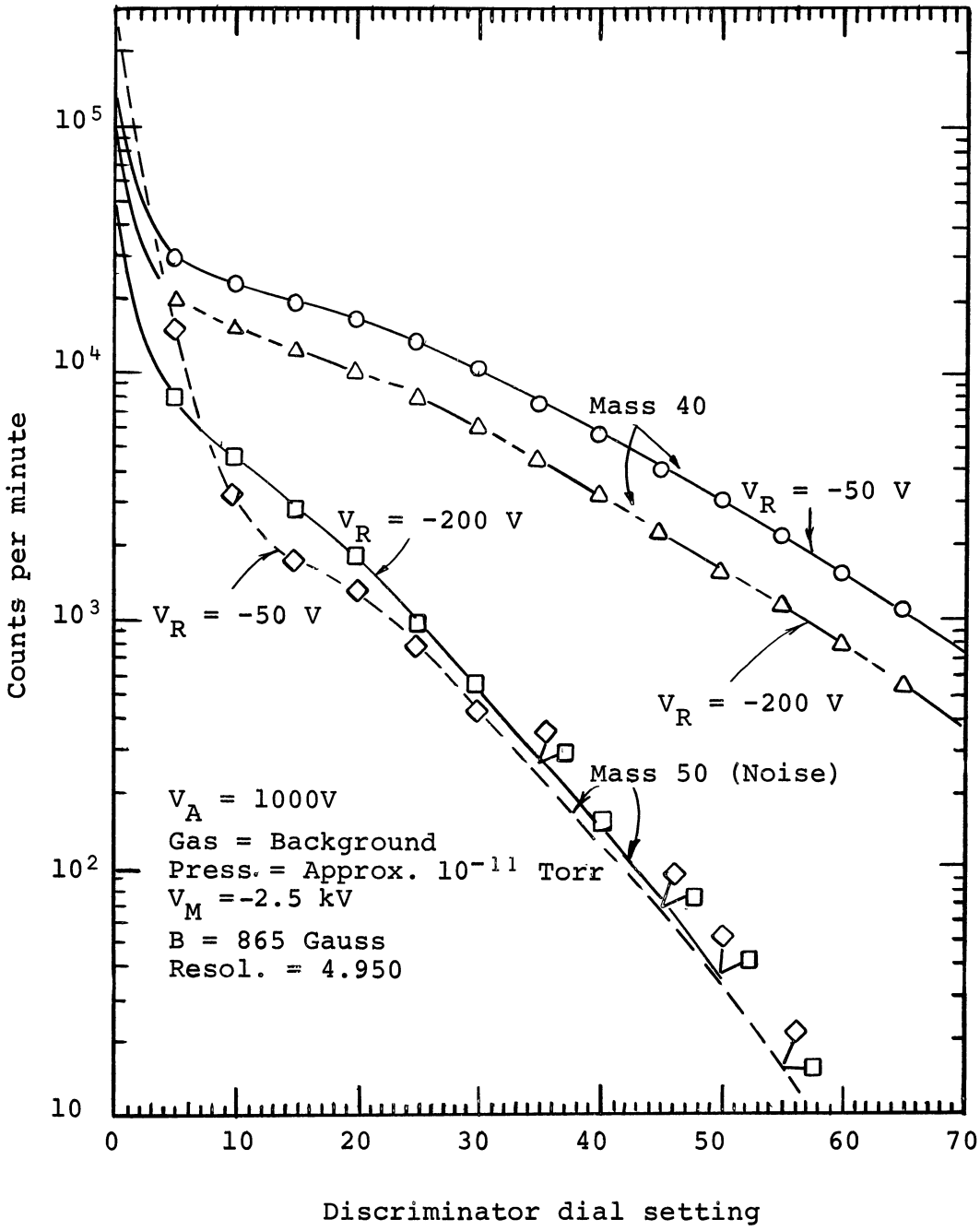

Fig. 23 Signal and Noise Integral Pulse Height Distribution Curve (Argon Ions) vs. Retarding Potential.

Generally speaking, the integral pulse height distribution curves shown in this figure are encouraging. It is noted that as the discriminator is set to trigger the counter on increasingly larger pulses, the S/N ratio steadily increases. At very low discriminator levels, the predominant pulses are noise. Neglecting this very high noise level for the moment, we notice that the distribution of Ar^+ ions extends to pulse amplitudes larger than the corresponding noise pulse amplitudes, although the total number of noise pulses present exceed the number of signal pulses by a significant amount. This then, suggests that the noise pulse hieght distribution is more narrow than the distribution of Ar^+ ions, which is a very necessary conditions for amplitude discrimination against the noise.

The important question that arises is how large is the difference between the average noise pulse height and the average ion pulse height? Unfortunately, this data is not capable of giving us the answer to this question, because the <u>true</u> ion source noise distribution is not actually shown in this figure. It was later discovered that the noise being recorded in the region of the lowest discriminator dial settings was, in reality, stray quadrupole R.F. being fed back to the pulse counting electronics through ac power lines. Since the quadrupole sweep generator was set to detect mass 50, the R.F. potential on the quadrupole was nearly maximum for the chosen mass range (low). The peak value of R.F. was therefore approaching 1000 volts. This situation was later corrected by inserting an R.F. filter into the ac power line supplying the counting equipment. Since the question of the relative differences in signal and noise pulse amplitude is of primary concern it

will be discussed in subsequent sections wherein meaningful data can be presented.

Returning to our discussion of Fig. 23 we see that the retarding voltage V_R has noticeably reduced the ion counting rate as was anticipated, but has had little effect on the noise in the region of the larger noise pulses. Furthermore, the pulse height distribution of ion pulses has not been affected significantly as was anticipated.

Thus it is seen from Fig. 23 that a difference in noise and signal pulse amplitudes exists, although the information is presently only qualitative. Also, the data provides additional evidence that the noise is probably photons within the CCIS. Our next discussions will therefore describe the experiments which were undertaken to determine the effect of the CCIS operating parameters on the S/N ratio and pulse height distribution curves with the aim of maximizing the counting performance of the entire instrument.

Counting S/N vs. CCIS operating parameters. - The CCIS has four operating parameters which affect the instrument S/N ratio. These parameters are:

(1) Ion Retardation Voltage

(2) Anode Voltage

(3) Magnetic Field

(4) Total Pressure within the Ion Source.

The effect of each of these variables on S/N ratio has been studied individually and in combination with one another and the results are described in the following paragraphs. The operation of the multiplier will be considered separately in a later section.

Counting S/N ratio vs. ion retardation voltage: It has been shown that the dc and counting noise level is independent of the ion retardation voltage. The signal is, however, directly dependent thereon.

In a previous section of this report describing the performance of the CCIS/Quad, it was noted that the retarding potential, V_R, has an important bearing on the resolution and sensitivity of the instrument under UHV conditions. For instance, at the anode potential for optimal sensitivity and resolution (V_A = 2200 volts), the value of V_R was specified as -300 volts. The present work indicates that the anode voltage for optimal S/N ratio is nearer to 500 volts. Referring again to Fig. 18, we note that if the anode voltage is reduced from 2200V to 500V, the sensitivity of the instrument will be reduced by a factor of seven. Obviously, the reduction in sensitivity accompanying these low anode potentials must be carefully weighed against the improvement in S/N ratio. It is also to be noted in Fig. 18 that the retardation voltage was zero. If V_R is arbitrarily set to the -300 volt figure specified in the original CCIS/Quad investigations the sensitivity would decrease even further. In fact, as shown by Fig. 24, the sensitivity for Hydrogen (and other masses) will drop to zero for values of $V_R > -100$ volts. Therefore, the selection of optimal values of V_R and V_A will necessarily involve certain trade-offs between sensitivity and S/N ratio. In attempting to make the optimum trade-off, we will first consider the relative effects of V_R and V_A on the sensitivity. Referring again to Fig. 19, we note that

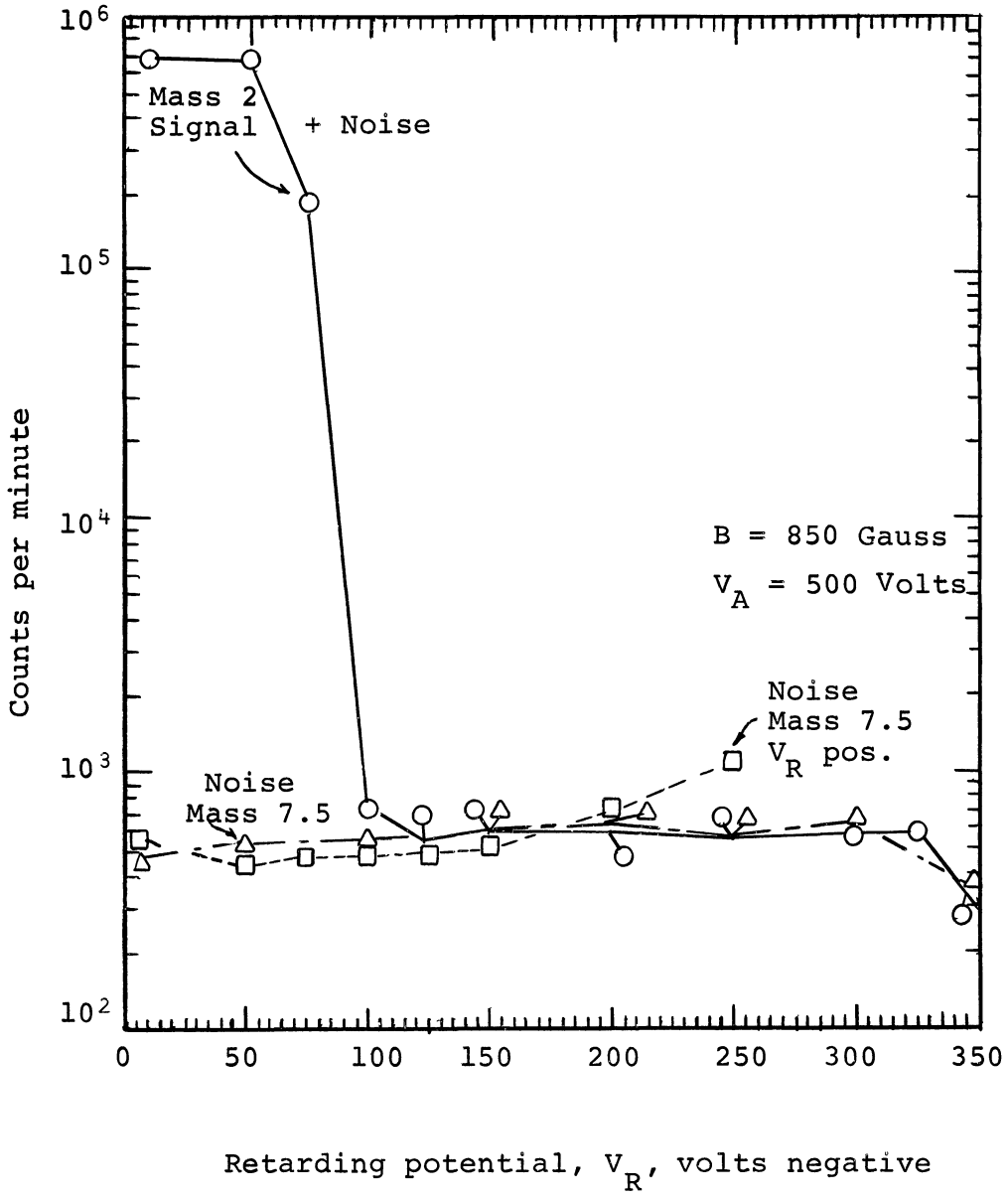

Fig. 24 Signal Plus Noise and Noise vs. Retarding Potential.

S/N ratio and sensitivity have changed only slightly as V_R was increased from 0 to -100 volts; the loss in sensitivity and S/N ratio obviously becomes more pronounced as V_R is increased.

In contrast, the influence of V_R on sensitivity at low anode voltages (500v) is very pronounced for relatively small changes in V_R. Note that in Fig. 24 the ions are cut off for V_R = -100 volts. Therefore for each anode voltage there exists a range of values of V_R which do not alter the sensitivity or S/N ratio appreciably. Conversely, there are values of V_R (not zero) which will make the S/N ratio decrease rapidly with decreasing anode voltage. For example, if V_R = -100 (as in Fig. 24), the ion beam will cut-off when V_A reaches 500 volts. Therefore, the effect of V_R on S/N ratio is also related to the anode voltage which will be discussed next.

Counting S/N ratio vs. anode voltage: Figure 25 shows how the counting S/N ratio varies with anode voltage (V_A) for a non-zero value of V_R (-100 volts). A distinct maximum is observed in the S/N ratio due to the combined effects of V_R and V_A. The signal counting rate and S/N ratio decrease very rapidly for anode voltages < 1000 volts because the chosen value of V_R (-100 volts) accentuates the decline in sensitivity due to the reatarding process. Above 1800 volts, the sensitivity of the source begins to saturate, whereas photon noise is still increasing rapidly. Thus, we see that when the combined effects of both V_R and V_A are examined that the counting S/N ratio appears to be maximum at a considerably higher anode potential and a higher sensitivity than shown in Fig. 18.

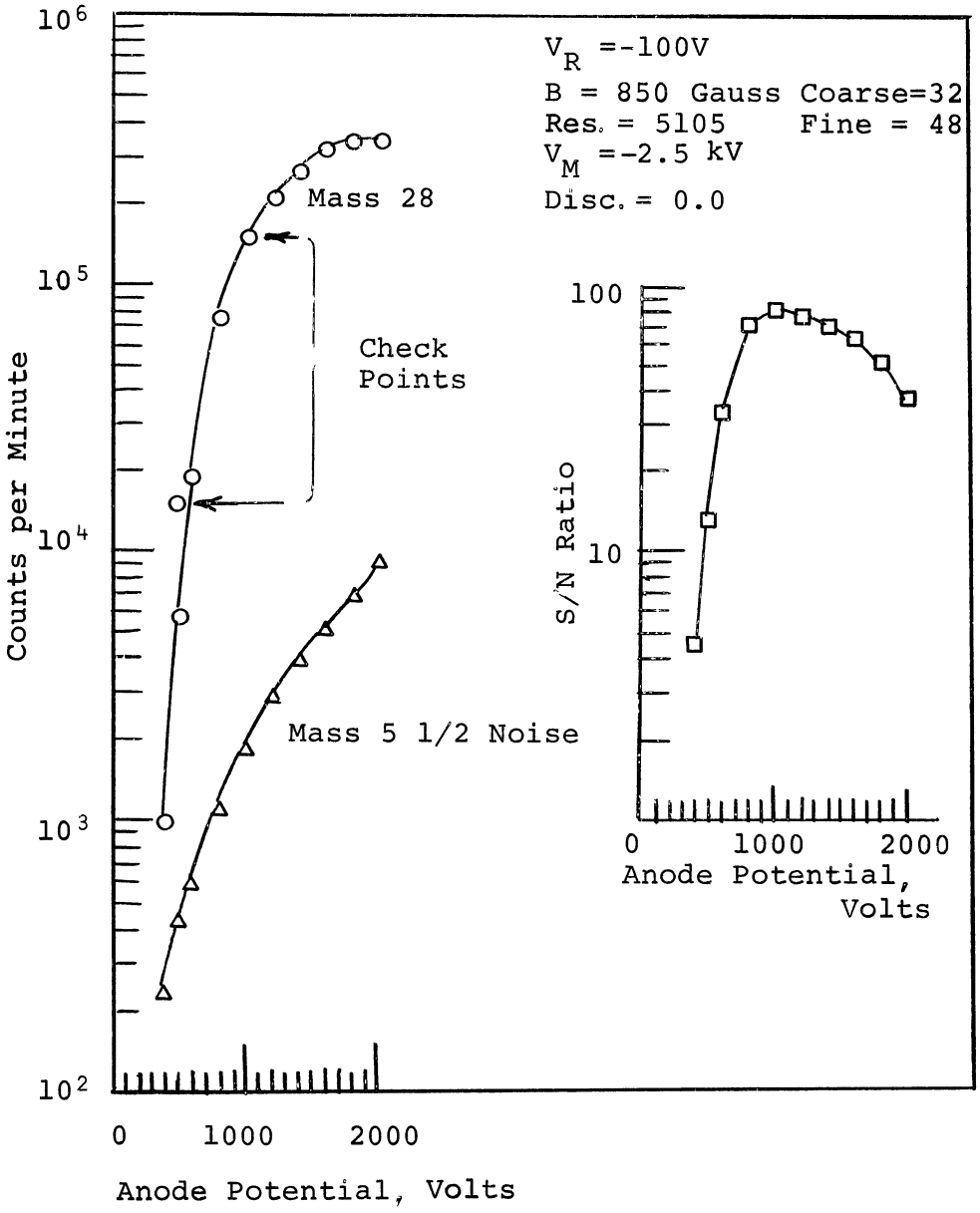

Fig. 25 S/N Ratio vs. Anode Voltage @ Fixed V_R.

Figure 26 shows a spectrum taken with the anode voltage set at 1000 volts and 500 volts. The corresponding retarding voltages are -100 volts and -50 volts, respectively. The latter value was chosen (rather than zero) to suppress the "on-blast" at "zero" mass. This improves the resolution of H^+ and H_2^+ ions.

We also note in Fig. 26 that the dc sensitivity for 1000 volts is approximately a factor of five better than for the 500 volt potential. The counting sensitivity (from Fig. 25) increased ten-fold from 500 to 1000 volts because the -100 volt value of V_R retards more ions at the lower values of anode voltage than does the -50 volt value used in Fig. 26; i.e., the dc sensitivity difference of Fig. 26 would have been larger if the -100 volt retarding voltage had been used in both spectra. Thus, the higher anode voltage (1000 volts) yields a considerably larger sensitivity on both the counting rate and dc basis.

In Fig. 26 the counting rates for the major peaks are noted at the top of each peak. The noise at "mass $5\frac{1}{2}$" is also noted and in this example, the two noise rates were purposely adjusted to the same value by the discriminator. Therefore, the peak counting rates of the major constituents may be compared at the same noise level (about 18 cpm). This comparison shows that the increase in sensitivity at a constant noise level is much more modest (approximately 50% increase at 1000 volts). Again, the retarding voltage is the reason. If

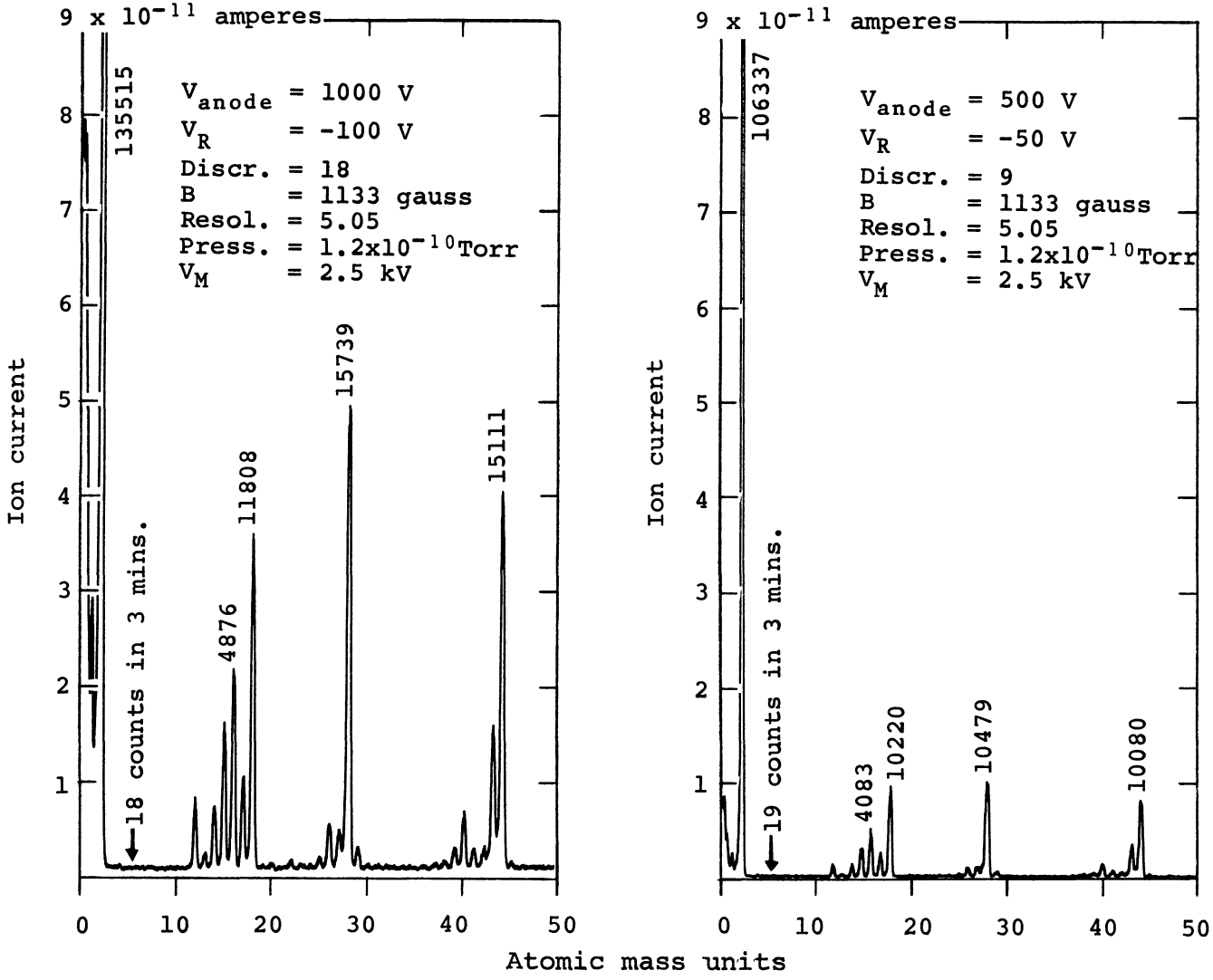

Figure 26.- Background spectra for two anode voltages (at same noise level)

the retarding voltage had been set to -100 volts for both spectra, the S/N ratio and sensitivity differences would be more pronounced.

In brief, the anode voltage for an optimum trade-off of sensitivity and S/N ratio appears to be very nearly 1000 volts. While the S/N ratio may be larger at 500 volts and zero retarding voltage, the sensitivity reduction is not tolerable. The improved sensitivity at 1000 volts is certainly worth the small reduction in S/N ratio.

Counting performance vs. magnetic field: The general performance of the ion counting detector and the spectrometer have been investigated as a function of magnetic field. In this work, two magnets were used which were physically the same but were different in field strength. One magnet was 850 gauss and the other was 1133. The field strength is measured at the center of the magnet's axial hole.

Figure 27 shows how the signal and noise integral pulse height distribution curves differ for both magnets. It is immediately obvious from this data that the stray field from the magnet is effecting electron trajectories within the multiplier. The center of the magnet is approximately 7 inches away from the center of the multiplier and is aligned along the same axis. At this distance, the measured stray field for the 1133 gauss magnet is 33 gauss.

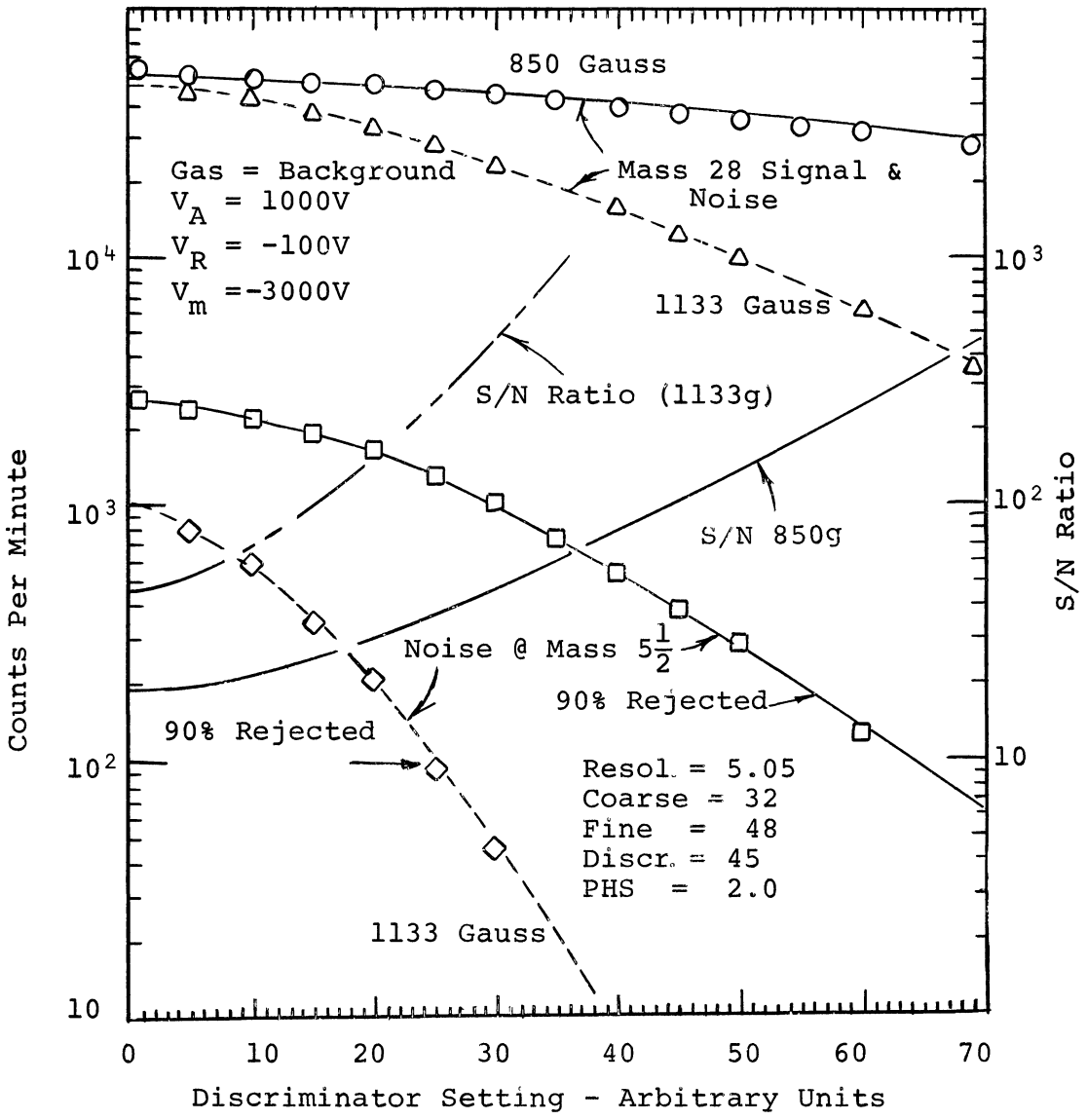

Fig. 27 - Signal & Noise Pulse Height Distribution vs. Magnetic Field

We note first that the pulse height distribution curves for the noise pulses, have been altered with respect to the average pulse height. The 850 gauss magnet clearly increases the average noise pulse height by nearly a factor of two.* We also note that an increase in total noise at zero discriminator level has occurred in the case of the lower magnetic field. For ion pulses, however, the increase in counting rate is only about 10%. It is, therefore, inferred from these observations (increased pulse height and increased noise level) that a corresponding increase in gain has occurred as a consequence of reducing the stray magnetic field at the multiplier. Further examination of the data also shows that a reduced magnetic field results in a noticeable broadening of the distribution curves of both noise and signal. For example, if the 1133 gauss signal and noise distribution were merely displaced by some gain factor G, then shifting these curves to the right (shown by dotted lines) should result in a reasonable matching of the 850 and 1133 gauss curves. Obviously, this will not happen. Therefore, the overall multiplier gain and pulse distribution has been altered and the pulse heights have been increased to include much larger values.

---

*Comparing discriminator settings where 90% of the noise pulses present at the zero discriminator level have been rejected.

If we now examine the data from the standpoint of S/N ratio we find that at zero discrimination level the S/N ratio is 2.5 times better with the 1133 than the 850 gauss magnet. However, at a discriminator value of 70, the 850 gauss S/N ratio is exactly the same value as that of the stronger magnet at a discriminator value of 30. Therefore, discriminator settings can be found in which the S/N ratios are the same for either magnetic field.

Of greater significance, however, is the question of ion counting efficiency and maximum desired noise level. Assume for a moment that the maximum desired noise level is 60 counts per minute (1 count/sec.). We now ask what will be the counting efficiency for each magnetic field at the prescribed noise limit of 60 counts per minute (cpm). We note in the case of the 850 gauss ion distribution curve that at zero discrimination level the slope of the ion distribution curve is very nearly zero. Furthermore, the reduction in stray field has only increase the total number of ions by 10%. For discussion purposes, we assume that the total number of ions available at the first dynode is nearly 53,000 cpm. Later discussion will describe means by which the total number of ions available may be determined. If the number of ions available represents a rate of 5.3×10^4 cpm, then for the 1133 gauss field the counting efficiency is:

$$\varepsilon_i \ (1133) = \frac{2.4 \times 10^4}{5.3 \times 10^4} \times 100\% \text{ at 1 cps noise}$$

$$= 45.4\% \ @ \ 1 \text{ cps noise} \qquad (12)$$

Similiarly, for the 850 gauss field the counting efficiency for 1 cps noise is:

$$\varepsilon_i(850) = \frac{2.8 \times 10^4}{5.3 \times 10^4} \times 100\%$$

$$= 53\% \text{ @ 1 cps noise} \qquad (13)$$

Therefore, we see that the lower stray magnetic field associated with the weaker magnet has the overall effect of (1) improving the counting efficiency and (2) improving the S/N (slightly) at the same background noise count. While these improvements are not significant in the present example, we cannot infer what the results would be as the stray field approaches zero. Obviously, future designs of the CCIS/Quad should seek to reduce these stray fields to the lowest possible values through the appropriate use of magnetic shields and pole pieces within the ion source.

Figure 28 shows the effect of the two magnetic fields on the dc spectrum over the mass range 1-50 amu. We note that the 850 gauss magnet appears more favorable from the standpoint of sensitivity. The numbers shown on the predominant peaks and also at mass 5 $\frac{1}{2}$ are the peak counting rates in counts per minute for signal and background respectively. It is not immediately obvious from these spectra whether or not the dc S/N ratio has been affected by the change in magnetic field. The ratio of the two mass 28 peak heights is approximately 2.3:1 and the noise current between peaks appears to be in the same ratio.

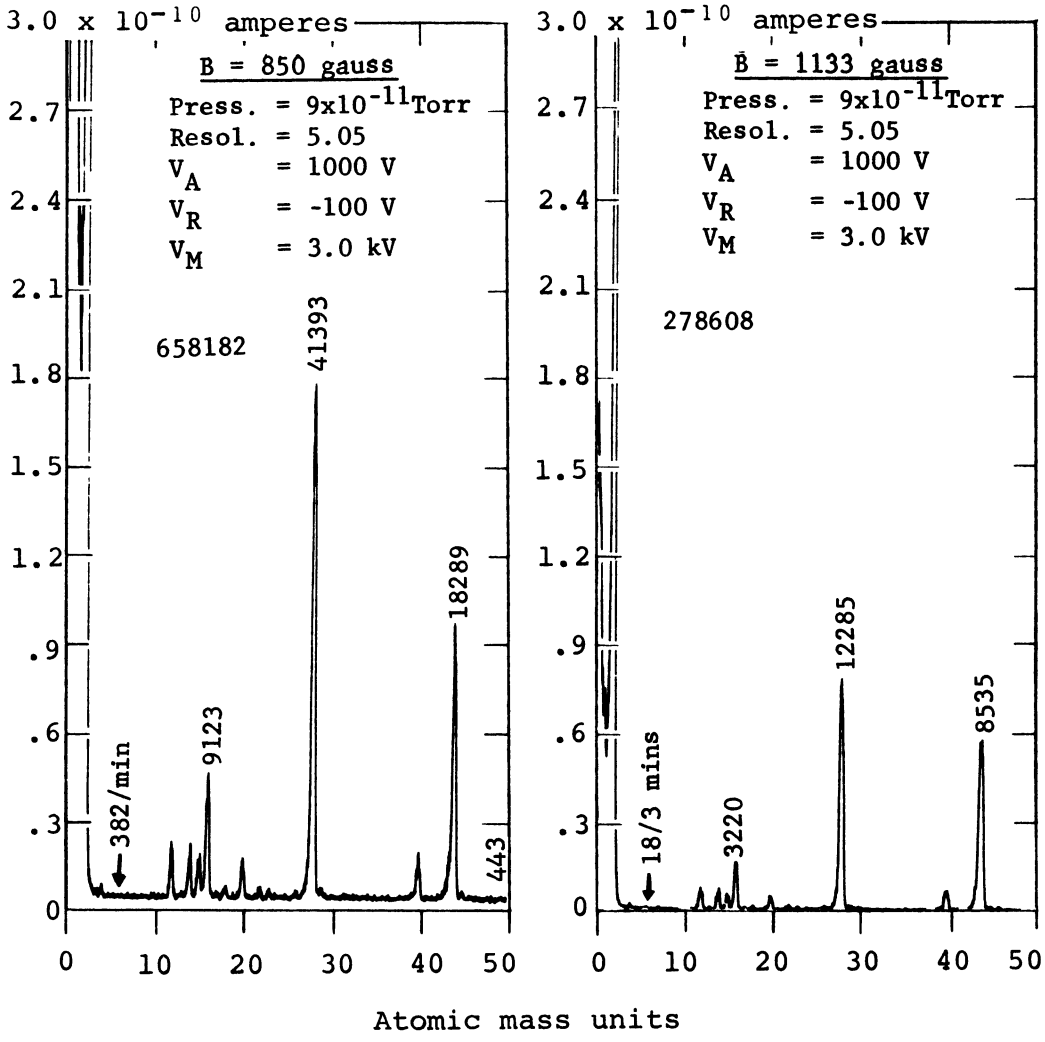

Figure 28.- D. C. and counting performance vs. magnetic field

As noted previously, it is possible to determine the gain of the multiplier from measurements at the output. Figures 27 and 28 display the information required and the criteria to be met. Referring again to equation (9) we note that the only two pieces of experimental information required are (1) the output current measured at the multiplier electron collector and (2) the total counting rate (R) for all ions of the selected mass arriving at the input to the multiplier. The output current (I_o) is the current displayed for any mass peak in Fig. 28. The input ion arrival rate R, is the zero discriminator level counting rate assuming, of course, it has been shown for each mass that R includes all ions of the desired mass. In Fig. 27 the pulse height distribution curve for mass 28 is seen to saturate at the zero discriminator setting. If we assume that this condition signifies the collection of all ions* we may now calculate the multiplier gain for mass 28 from the combined data in Figs. 27 and 28. From Fig. 28 (850 gauss spectrum), the peak current I_o at mass 28 - $5.8 \times 3 \times 10^{-11}$ amperes or 1.74×10^{-10} amperes. The input rate of all mass 28 ions from Fig. 27 (at zero discrimination) - $5.37 \times 10^4/60$ or 8.95×10^2 ions per second. The gain of the multiplier is therefore, from Eq. 9,

---

*This is not entirely correct as will be explained during subsequent discussions.

$$G_m = \frac{1.74 \times 10^{-10}}{8.95 \times 10^{2}} \times 6.25 \times 10^{18} \qquad (14)$$

$$= 1.22 \times 10^{6} \text{ for Mass 28 with 850 gauss}$$

Similarly, the gain for any mass peak may be calculated if it can be shown that all ions of the given mass are being counted. The method of proving this will be discussed shortly.

Although these discussions have shown that the stray magnetic field associated with the stronger magnet does affect multiplier gain, the S/N ratio for the same value of noise (1 cps) and the counting efficiency are not significantly changed. Therefore, the stronger magnet was used during all subsequent investigations, for reasons which will be explained in connection with the calibration of the instrument.

Counting performance vs. total pressure: The last remaining source parameter to influence ion counting performance is the pressure of gas within the ion source. This discussion will be confined to such factors as S/N ratio vs. pressure, ultimate counting rate, maximum S/N, etc. Discussions relating to the instrument calibration for various gases will be described in another section entitled "UHV Calibration of CCIS/Quad".

It has already been noted that the background photon noise in the ion source is dependant on the total "pressure"* within the ion source. Actually, the in-

---

*The word "pressure" is used at this point to simplify the discussions to follow.

tensity of the photon emission is related to the total ionization occurring within the discharge. This, in turn, is related to the number density of each species present and to the ionization efficiency of each species. It is particularly important to recall these facts in the case of our present discussions, because if the relative abundance of the species change as the total pressure changes, the effect on the noise level will be two-fold; the noise will be dependant on both total pressure and on the species. To investigate the relationship between photon noise rate and source pressure, an experiment was planned which would relate the noise rate to the ion current measured at cathode K_1 (I_{K_1}). This current is related to the ion production rate within the discharge. However, difficulties were encountered in the form of an excessive leakage current at the K_1 terminal. This current was larger than the corresponding I_{K_1} currents at the lowest pressures used in the investigation (3×10^{-12} Torr). As the pressure was increased within the ion source, I_{K_1} gradually became large enough to measure but at this point, the photon counting rate became too large to measure on the counting equipment.

Figure 29 shows how the signal (mass 28) and noise counting rates vary in the UHV region as a function of pressure. The pressure readings were observed on the MBAG since I_{K_1} was not measureable as explained above.

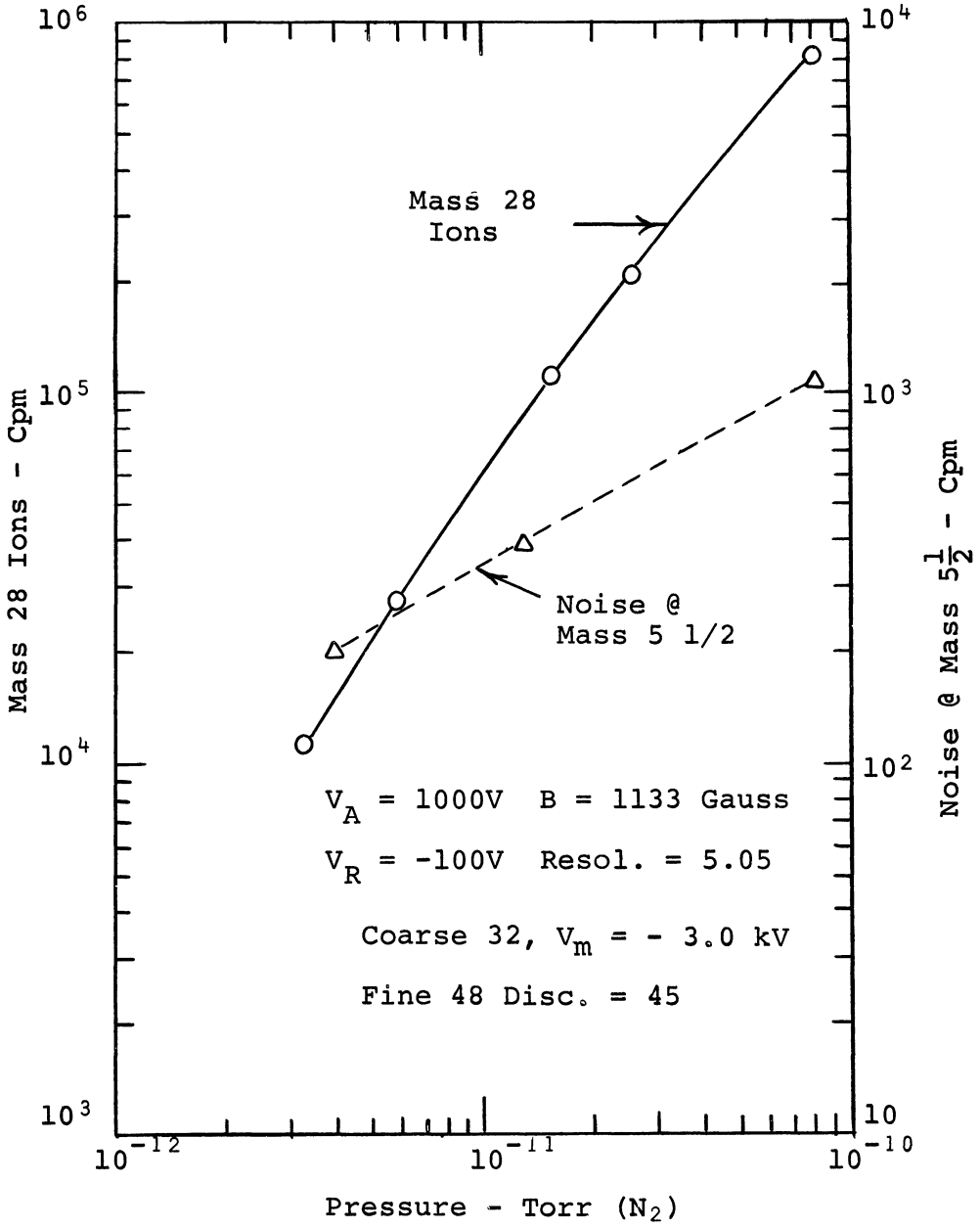

Fig. 29 Signal & Noise vs. Pressure.

Actually this information is of limited value because of the experimental problems noted above. The noise counting rate is seen to increase as the total pressure increases but not at the direct rate anticipated. The information is shown simply to demonstrate that the noise rate is pressure dependant.

Another question arises regarding the effect of pressure on S/N ratio. Assuming that only one gas constituent was present within the ionizer, what would be the effect on S/N ratio? Under these circumstances the S/N ratio should be a maximum, since no other peaks would be present to contribute to the noise.

Figure 30 displays an attempt to answer the question. Although mass 2 (H_2) and a few small peaks are observed, the predominate peaks are mass 28 (N_2^+) and mass 14 (N^+). The observed counting rates for these peaks are shown together with the observed noise at mass 5 $\frac{1}{2}$. The counting rate at mass 28 is noted for two different discriminator settings. The figure outside the parenthesis is for the normal discriminator setting while the number within the parenthesis is the counting rate observed at zero discriminator setting. The latter value corresponds to a counting efficiency of 100%, hence the ratio of these numbers will yield the counting efficiency at the discriminator level used during the test.

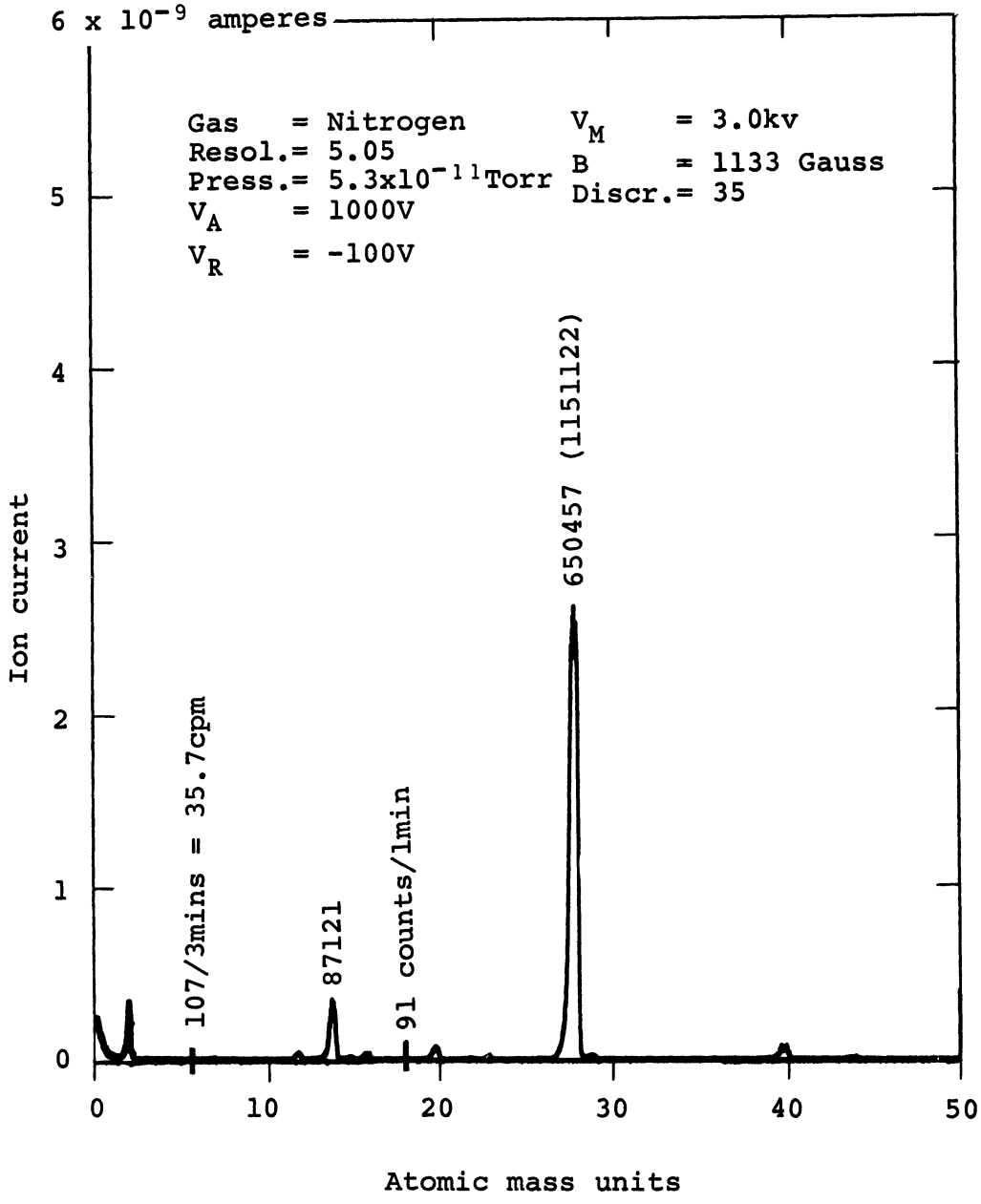

Figure 30.- Spectrum of "Single" species - nitrogen

The observed noise rate at mass $5\frac{1}{2}$ is 35.7 cpm. The background counting rate with the CCIS turned off is 4 cpm. Therefore, the ion source noise rate is approximately 32 cpm. The mass 28 peak shows 6.5×10^5 cpm for the ion counting rate at a nitrogen true pressure of 5.3×10^{-11} Torr. The observed S/N for this "single" (neglecting smaller peaks) species condition is therefore,

$$S/N = \frac{6.5 \times 10^5}{3.2 \times 10}$$

$$= 2.03 \times 10^4 \qquad (15)$$

The counting efficiency for the mass 28 peak is,

$$\varepsilon_i = \frac{6.5 \times 10^5}{1.15 \times 10^6} \times 100\%$$

$$= 56.5\% \qquad (16)$$

The sensitivity for the mass 28 peak (at this pressure) is,

$$S_{28} = \frac{6.5 \times 10^5}{5.33 \times 10^{-11}}$$

$$= 1.22 \times 10^{16} \text{ cpm/Torr, } N_2 \qquad (17)$$

The gain of the multiplier may also be computed:

$$\text{Gain} = \frac{2.5 \times 10^{-9}}{1.15 \times 10^6/60} \times 6.25\ 10^{18} \qquad (18)$$

$$= 8.15 \times 10^5 \text{ (with 1133 gauss magnet).}$$

Finally, it is worthwhile noting that the spectrum shown in this figure displays only trace amounts of C^+, the CH_4^+ series, and CO_2^+, etc., which often characterize spectra taken with hot-filament instruments in the UHV region. The true pressure of N_2 is 5.3×10^{-11} Torr as measured by the MBAG using the modulation technique*. In evaluating the relative cleanliness of this spectrum, it should be recalled that the ion source is not operating in a high pumping speed system. Furthermore, the conductance from the ion source to the small ion pump is relatively low compared to operating the source in a nude configuration inside a high pumping speed system. Despite these rather unfavorable conditions, the source displays relatively few extraneous peaks.

These remarks conclude discussions of the influence of CCIS operating parameters on S/N ratio. The ion detector (electron multiplier) and methods of optimizing S/N at the detector end of the system will be considered next.

Maximizing detector S/N. - The operating conditions of the electron multiplier also influence the overall S/N ratio achieved by the instrument. This section will, therefore, consider and discuss the optimization of S/N at the ion detector. Of equal importance is the collection efficiency of the detector since this effects the sensitivity of the instrument.

---

*The use of the modulation method, together with other necessary information required to determine true pressure will be discussed in connection with the calibration results.

As the ions emerge from the quadrupole, their energy is typically of the order of 100 eV. At this energy the number of secondary electrons created at the first dynode of a typical multiplier per incident ion (secondary emission ratio, γ) will be <1.0, i.e., the average ion will not yield a secondary electron. Therefore, a substantial number of ions will not be counted because at least one electron is required per incident ion to initiate the multiplying process and to produce a pulse at the multiplier output.

Accordingly, the ions must be accelerated before striking the first dynode. The energy required to produce a secondary emission ratio, γ of at least one, is a function of the dynode material (and surface conditions), ionic mass and molecular structure. The necessary information is available in the literature. For instance, Higatsberger et al. (ref. 15) give data on the value of γ vs. ion energy for a number of dynode materials and for all of the inert gases. Their data shows that for the Be Cu dynode (type used in this work), the value of γ for argon is nearly unity in the vicinity of 1000 eV.

The electron multiplier used herein is provided with a grid in front of the first dynode to accelerate the ions as they enter the multiplier. This grid is physically and electrically connected to the first dynode in such a way that isolation of the grid is impossible without damaging the multplier. As a

result, it is not possible to vary the ion acceleration potential without simultaneously varying the voltage on the electron multiplier dynode chain. Accordingly, as the ion accelerating voltage is increased to increase γ, the gain of the multiplier also increases. While this situation hampered certain investigations, it did not render them impossible.

In the discussions to follow, we will be primarily concerned with maximizing the detector S/N ratio by obtaining the largest possible values of γ. As a result, we will be concerned with the counting efficiency of the detector and also with its collection efficiency. The latter term is related to the geometry of ions emerging from the quadrupole and the fraction thereof that strike the first dynode of the multiplier. We will also be concerned to a lesser degree with the noise level of the detector although this noise is much less than the photon noise from the ion source*.

In order to obtain some information on γ, we make use of the techniques previously described in the determination of multiplier gain. That is we will combine counting rate with dc information in the evaluation of γ. We will also depend on the fact that the photon noise is unaffected by the ion acceleration potential on the grid of the multiplier. Therefore, for photons, a

---

*Typically the thermionic emission from the early dynodes is only of the order of 1-2 cpm at 300 vdc and room temperature.

variation in multiplier voltage will result only in a change in multiplier gain. Figure 31 is used to explain this point. This figure shows how the dc output current from the multiplier varies as the multiplier (and ion accelerator) voltages are varied. The photon curve was taken with a large value of retarding voltage, V_R, to purposely prevent ions from entering the quadrupole and, hence, the multplier. Essentially then the two curves are the familiar gain curves for an electron multiplier, with one curve for ions and the other for photons.

Since the photons are not accelerated by the potential on the multiplier grid, the noise curve represents the true gain curve of the multiplier. Assuming a constant photon flux during the measurement period, a constant number of secondary electrons will be emitted from the first dynode per unit time. As the multiplier voltage is increased, the output current also increases in accordance with the gain characteristic of the multiplier.

For ions, however, the output current will depend on the multiplier gain and on the secondary emission efficiency γ of the first dynode. We note that the mass 28 ion curve rises more rapidly for ions than for noise. In fact, over the range of the multplier voltages shown in the figure, the increase in ion current is approximately a factor of three more than the photon current increase. It remains to be shown however, that

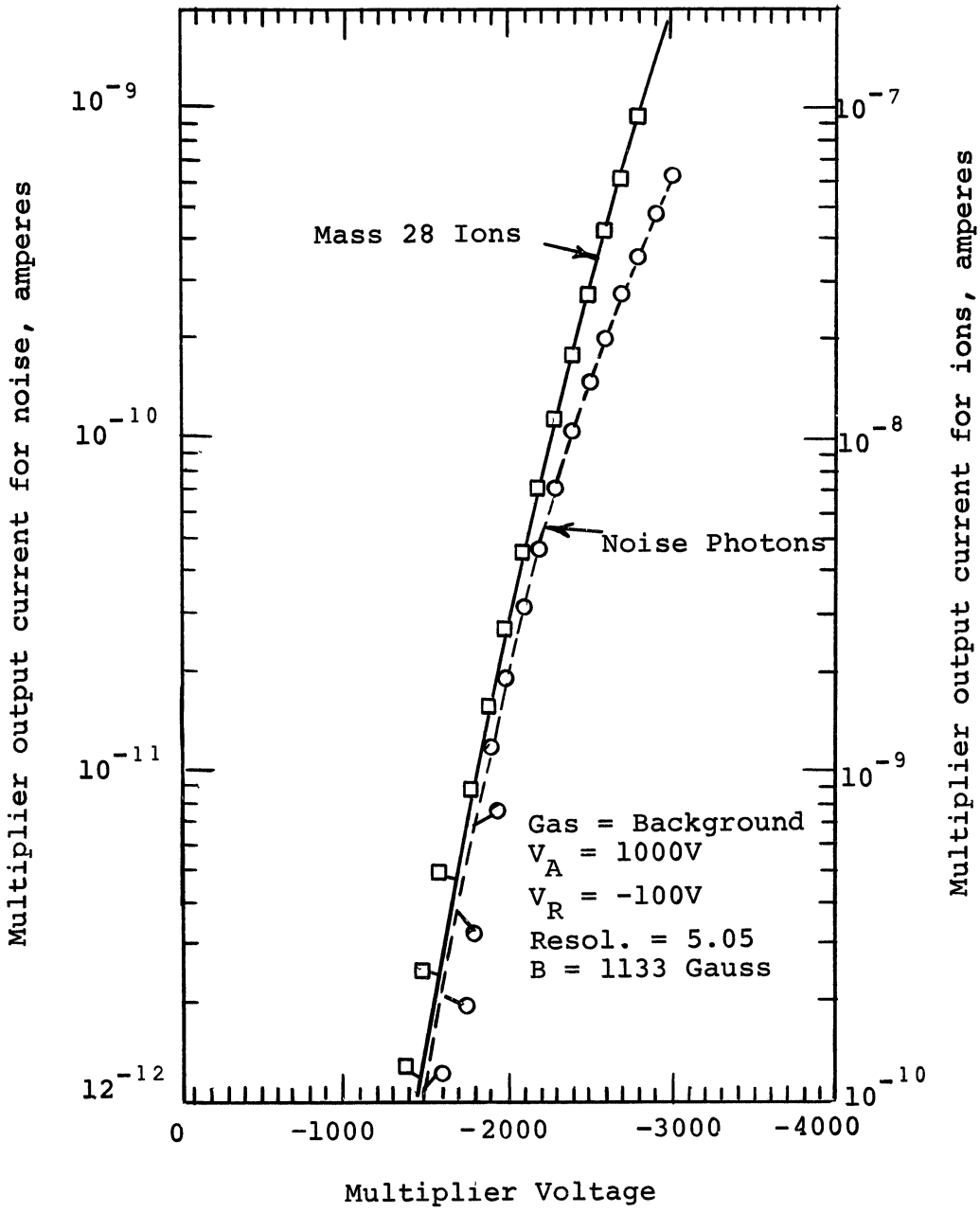

Fig. 31 Ion & Noise Current vs. Multiplier Voltage.

the increase in ion current is not simply an increase in the number of ions being collected by the electron multiplier as a result of an improved ion collection efficiency at the higher acceleration voltages. Briefly, the increase may be due to an increase in the ion counting rate rather than an increase in γ. In general, however, it is obvious that the higher S/N ratio will be obtained at the highest multiplier voltage shown (3000 volts).

Figure 32 shows how the counting rate of the mass 28 peak varies as a function of multiplier (and ion acceleration) voltage. The region of greatest interest lies between 3000 and 3500 volts. Here we see that the ion counting rate has attained a nearly fixed rate of approximately 6×10^4 cpm. The previous figure, however, shows the ion current is continually increasing. The data of Fig. 31, therefore, shows that γ is the quantity which is increasing relative to the normal gain curve of the multiplier. Figure 32 also shows that in the region of 3500 volts both the counting and collection efficiency of the detector is approaching 100%. Data was also taken (integral pulse height distribution) which demonstrates that the ion counting rate is almost completely independent of the discriminator level in the region of low discriminator settings. This fact indicates that all ions produce sufficient pulse amplitudes to be counted, or that the counting efficiency is 100%.

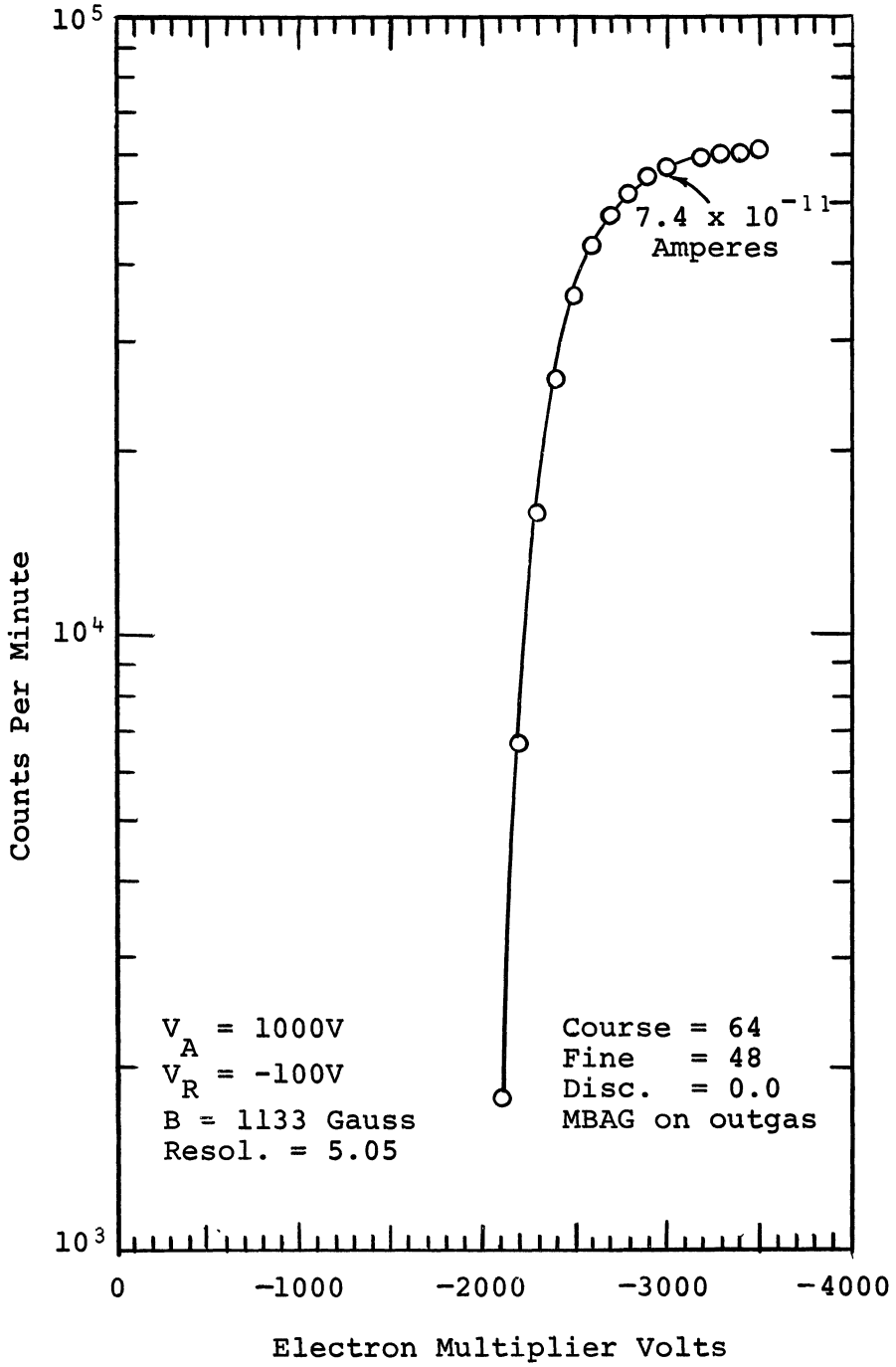

Fig. 32 Mass 28 Counting Rate vs. Multiplier Voltage

An attempt was made to measure γ for comparison with literature values. This is theoretically possible through the use of equation (9). The gain equation for noise electrons may be written:

$$G_n = \frac{I_n}{R_n} \times 6.25 \times 10^{18} \qquad (19)$$

where G_n is the gain of multiplier for noise, I_n is the output noise current (amperes) and R_n is the output noise counting rate in counts/sec. R_n represents the number of secondary electrons/sec. which are released under a constant flux of photons. In order to be counted, each photon must release at least one electron from the first dynode. In making our measurement of G_n, we must, therefore, count individual electrons leaving the first dynode. We would expect that the noise counting rate would saturate at some finite counting rate (as a function of the multiplier voltage) as did the ion rate in Fig. 32. This finite rate, R_n would be used in equation (19), together with a straightforward dc current measurement (I_n) to determine the gain for a single electron leaving the first dynode. The value of G_n thus derived would represent the true gain of the multiplier for single electrons. The observed gain for ions derived, from equation (9) is actually,

$$G_m = \gamma G_n \qquad (20)$$

Simultaneous measurements of G_m and G_n would yield a value for γ. The noise counting rate did not saturate at high multiplier voltages (3600v) and it was discovered that the noise level within the multiplier (ion source source off) was contributing substantially to the overall noise counting rate. It was not possible to determine the true photon noise rate, R_n with sufficiency accuracy under these conditions and the effort to measure γ was therefore abandoned. The best information obtained from the experimental data of Fig. 31 is that γ is approximately 3 at 3000 volts. This is largely based on the literature values for γ published by Higatsberger (ref. 15) for ions of 1000 eV energy.

In order to increase the detector S/N ratio beyond present values, two steps must be taken. First, γ should be made as large as possible by increasing the accelerating voltage and secondly, the detector should be made "blind" to the photon noise. Each of these will involve certain considerations which will be discussed next.

Increasing γ effectively makes the average signal pulse height larger in comparison to the noise. A practical limit exists to the accelerating potential which may be applied to the detector as a result of certain electronic considerations. The output of the quadrupole is essentially at ground potential and the ions emerge with 100 eV energy with respect to ground. To accelerate the ions, a large negative voltage is applied to the accelerating grid and thereafter the ions strike the first dynode without further acceleration or deceleration. If the operating voltage of the multiplier is less than the desired

acceleration potential, the output collector of the multiplier must be operated at a negative potential which is the difference between the acceleration and the multiplier voltages. For example, if an acceleration voltage of 7000 volts is applied to an isolated accelerator, and the multiplier is operated at 3000 volts, the collector of the multiplier will be 4000 volts below ground potential. For a dc detector, this configuration would be quite troublesome since the electrometer must be well insulated from ground (and power lines). For pulse counting, the situation is more tenable because a blocking capacitor may be used to isolate the large dc offset of the collector. The breakdown noise across and/or through the capacitance will eventually limit the acceleration voltage since noise pulses of the order of 1 mv or less occurring within the capacitor will be recorded by the counter. A practical limit for these reasons appears to be around 5000 volts for a multiplier operating at 3000 volts. According to Higatsberger, the resulting increase in γ for argon will be a factor of 1.47 for 5000 eV argon ions compared to 3000 eV ions. Woodward and Crawford (ref. 16) discuss further electronic considerations in the use of ion counting techniques and of the operation of electron multipliers in the "off ground" configuration.

The second improvement that should be made in detector design is to prevent the ion source photons from striking the multiplier first dynode. For the quadrupole analyzer, the problem of separating the ions and photons must be approached more carefully than for magnetic sector instruments. To separate the ions, an electrostatic deflector is used to deflect and accelerate the ions leaving the quadrupole. The entrance to the multiplier is then located so that it is off-axis to the photon beam. The ions leaving the quadrupole exit aperture are widely spread in their angular distribution about the quadrupole axis. The exit angle of a particular ion is a function of many parameters (ref. 17) and careful consideration must be given to focusing the widely dispersed beam into the entrance aperture of the first dynode. Bültemann and Delgmann (ref. 18) have arranged the multiplier of the AMP3* so that the axis of the multiplier is inclined at an angle of 60° to the quadrupole axis. They have studied the collection efficiency of the detector which they report as "almost 100%" for all ions in a wide mass range. Thus, no mass discrimination effects were observed in the collection system due to improper focusing of the various masses. They do not report however, the factor by which the photon background has been reduced. In another configuration reported by Bennewitz

---

*Made by, Atlas Mess und Analysentechnik GmbH, Bremen, Germany.

and Wedemeyer (ref. 19), it is stated that the photon background reduction factor is about 50:1 compared to an on-axis configuration. The ion collection efficiency was not specifically measured but is believed to be 80 - 90%, according to the authors. Mass discrimination due to variations in collection efficiency with mass are not given.

Thus, as evidenced in the literature, further improvements can be made in the counting S/N ratio by locating the multiplier off-axis to avoid the photon background. The magnitude of the improvement will be determined by the configuration chosen. In addition to improving the S/N ratio at the detector, further improvements may be possible within the ion source along the lines previously discussed in connection with the tubular cathode stub.

In concluding our remarks on the ion detector, it is important to recognize that a noticeable improvement in detector stability has been made using counting techniques. Referring again to Fig. 32 we note that only a small change (6.5%) in counting rate occurs if the voltage on the multiplier is reduced from 3500 to 3000 volts. Referring next to Fig. 31, and extrapolating the data to the 3500 volt point for the noise photons, the drop in gain for the multiplier between 3500 and 3000 volts would be at least a factor of two and more likely would be a factor of three. This is certainly a worthwhile improvement.

In summary, the following observations have been made regarding maximizing the ion detector S/N ratio:

(1) The secondary emission ratio, γ is important in determining S/N ratio, but the limitations on improvement by increasing γ are predominantly electronic in nature.

(2) The most important increase in S/N ratio should be the result of locating the multiplier off-axis so that it is "blind" to photons. Careful design is important in order to achieve high ion collection efficiency for all masses.

(3) The sensitivity of the detector to random gain changes in the multiplier is much reduced by the use of counting techniques.

The final section of our report will deal with sensitivity and calibration of the instrument at very low partial pressures.

Ultra-High Vacuum Calibration of CCIS/Quad

General. - It is well known (refs. 20, 21, 22) that the response characteristics (output current vs. pressure) of the Redhead magnetron gauge are of the form

$$I^+ = kP^n \qquad n \cong 1.0 \text{ above } 10^{-10} \text{ Torr}$$

$$n > 1.0 \text{ below } 10^{-10} \text{ Torr} \qquad (21)$$

Where I^+ is the cathode ion current in amperes, P is the pressure in Torr and k is a sensitivity constant for a given species of gas expressed in amperes/Torr. The value of n is dependent on the magnetic field in the region below approximately 10^{-10} Torr. Typically, n has a value of 1.4 or 1.5 for magnetic fields of the order of 1000 gauss. For magnetic fields less than this value, n increases to approximately 1.9 at 900 gauss. Thus, some care must be exercised in measuring and handling the CCIS magnets to prevent unexpected changes in instrument calibration.

It has also been established that the point at which the CCIS becomes non-linear is related to the total cathode current rather than the gas pressure. For example, the work of Feakes and Torney cited above (ref. 22) shows that the non-linear response begins at a point where the total cathode current is nearly 2×10^{-9} amperes for both helium and nitrogen. This point is for an anode voltage of 4500 volts, not the 1000 volts presently recommended.

The best information presently available indicates that n is probably independent of species (at least for helium and nitrogen) in both the linear and non-linear regions. If this is true, then the calibration of the spectrometer is straightforward in that only k need be measured for each gas. For example, if we assume that the sensitivity equation for any species is of the form

$$i_j^+ = k_j p_j^n \qquad (22)$$

then the total cathode current will be

$$I_{K_1} + I_{K_2} = I_t = \Sigma k_j p_j^n \qquad (23)$$

where I_t is the total cathode current. When $I_t \geq 2 \times 10^{-9}$ amperes, n = 1.0 and when $I_t < 2 \times 10^{-9}$ amperes, n = 1.45 (for 1020 gauss). Once k_j is determined for a given species* and n is determined for one gas, then the translation of peak height (current) data into partial pressure information is straightforward.

Accordingly, one of the purposes of the experimental program is to attempt to verify the above assumptions for a limited number of gases. Argon and neon were selected, in addition to the primary calibration gas, nitrogen. Before discussing the results, a brief description of test methods will be given.

Test methods. - The basic pressure standard used is the modulated Bayard-Alpert gauge (MBAG) originated by Redhead (ref. 23). The two modulation currents I_1 (modulator at grid potential) and I_2 (modulator at ground) are used to determine the true pressure P_T, using the relationship

$$P_T = \frac{1}{KI^-} \left(\frac{I_1 - I_2}{1 - \alpha} \right) \qquad (24)$$

---

*Note that k_j can be determined in the linear region of the response characteristics.

where α is the modulation coefficient as defined by Redhead, K is the gauge constant ($Torr^{-1}$) and I^- is the electron emission current in amperes. The MBAG used has been the subject of considerable study in order to verify that certain anomalies in MBAG behavior described by Redhead (ref. 24) and later by Hobson (ref. 25) do not effect the present measurements. For instance, the x-ray limit of the gauge (2.5×10^{-11} Torr) has been carefully measured and was found to be in agreement with the value determined using the modulation techniques at pressures of the order of 3×10^{-12} Torr.

The calibration procedure consists of comparing the CCIS/Quad output (dc or counting rate) to a pressure reading of the MBAG derived from equation 24. The emission current for the given species is derived from Dushman, as explained previously. DC current data was taken primarily to extend the range of measurement to higher pressures, where the ion counting rate exceeds the capability of the counting equipment.

Discussion of calibration results. - Figure 33 shows both the dc current and counting rate response for nitrogen in the range 1×10^{-9} Torr to 3×10^{-12} Torr true pressure. In general the data agrees remarkably well with data taken in 1963 by Torney and Feakes (ref. 21). The

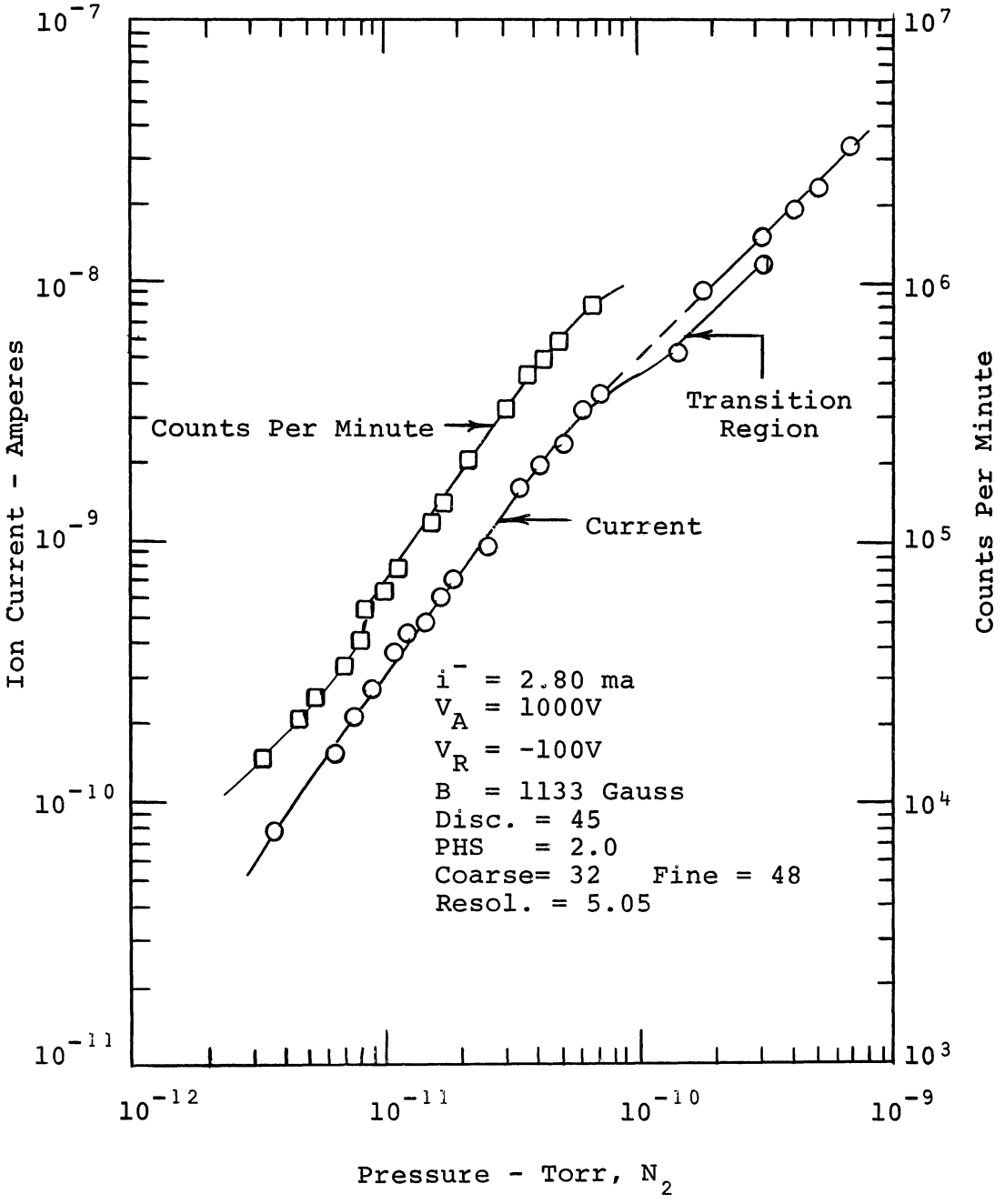

Fig. 33 DC & Counting Rate Calibration for Nitrogen

slope is 1.45 in the non-linear region and the characteristic is reasonably linear above this value. Note that a small resolution loss of 8% is observed in the counting data at a rate of 10^6 cpm. Within the linear region, the counting sensitivity for nitrogen is

$$K_n = \frac{5.4 \times 10^5 \text{ cpm}}{4.0 \times 10^{-11} \text{ Torr}}$$

$$= 1.35 \times 10^{16} \text{ cpm/Torr, } N_2 \quad (25)$$

The measured counting efficiency is approximately 35% for this data. The background due to the instrument alone (line noise subtracted) is 1.7 counts per minute at the lowest pressure measured (2.7×10^{-12} Torr).

The magnet used in the present work is the stronger of the two magnets described previously. Its field strength was 1133 gauss. This magnet was used in order to obtain a response characteristic whose slope in the non-linear region was as nearly unity as possible.

An attempt was made to measure total cathode current I_{K_1} & I_{K_2} to determine the break point in the characteristics. This current defines* where the value of n changes the response from a linear to an exponential form. Again, due to leakage currents in the cathode insulators, the determination could not be made.

---

*See Eq. 23.

A comparison calibration was also made with argon. The data is shown in Fig. 34. Again, both dc and counting rate responses were taken. In general, the argon results are disappointing in that they do not appear to confirm the above theoretical discussions. The value of n is obviously larger for argon than for nitrogen. Also the slopes (for $n > 1$) of argon counting and dc data do not appear to be the same, whereas for nitrogen good agreement is evident. The dc sensitivity for argon in the linear region is approximately 22 amperes/Torr, and for nitrogen, the corresponding sensitivity is 45 amperes/Torr. The ratio of counting sensitivities (N_2/A_r) is also in the ratio of 2:1. These figures are in sharp contrast with previous data taken without the electron multiplier (Table IV). The gain of the electron multiplier was measured for both argon and nitrogen on a number of occasions. The results obtained were in all cases about 20% lower than for nitrogen. This fact is anticipated because the secondary emission ratio is approximately inversely proportional to the square root of the mass of the gases. However, the reduction in sensitivity for argon due to the mass dependency of the multiplier should be more than offset by the increased sensitivity of the ion source for argon which is evident in Table IV. Here, the argon sensitivity is 1.8 times larger (low pressure figure) than nitrogen. The anticipated net result would be that the ratio of argon/nitrogen sensitivities should be approximately 1.45:1 instead of the observed ratio of 0.5:1. At the present time, the reasons underlying these results are not known and therefore, speculative discussions are omitted.

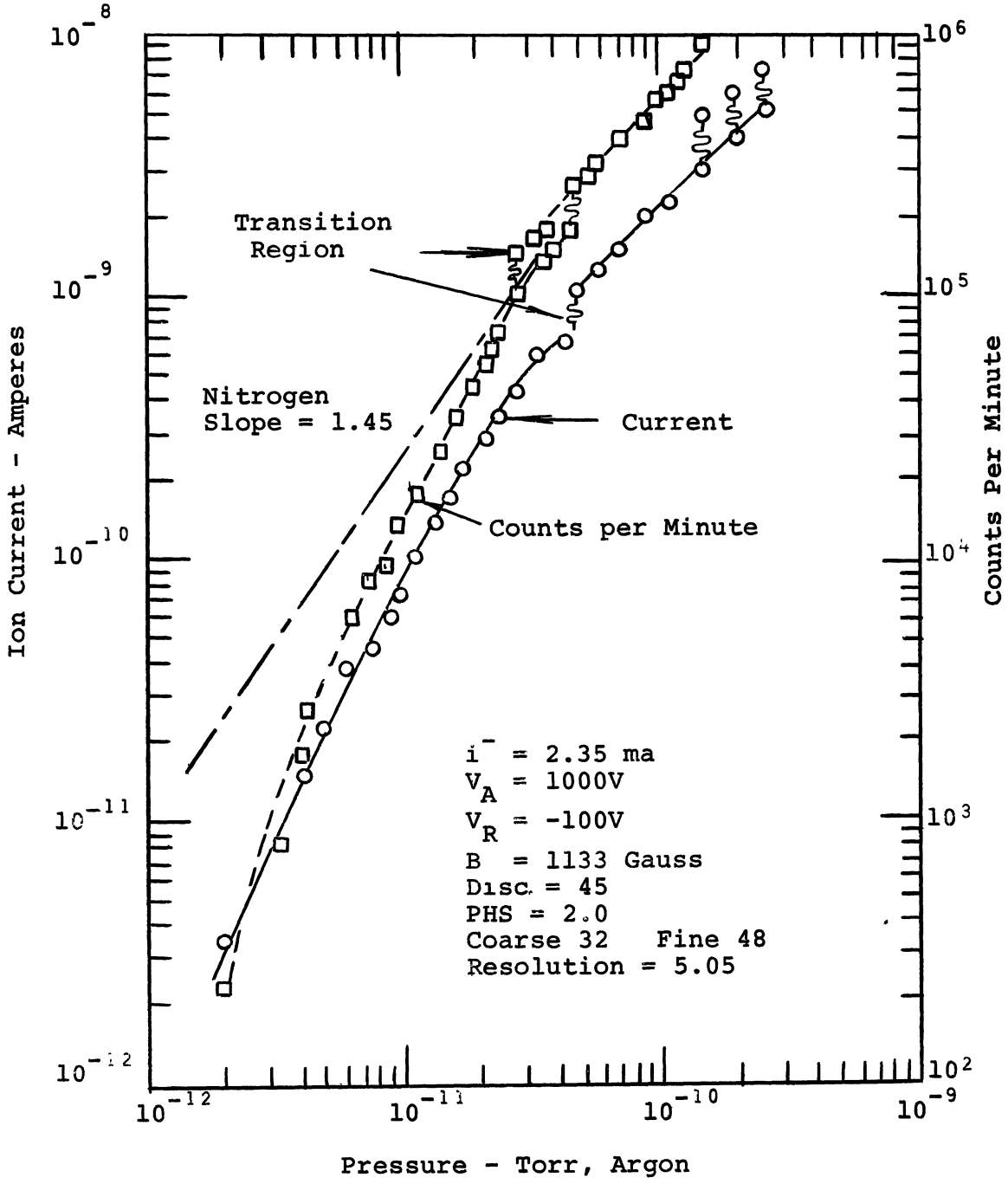

Fig. 34 Dc & Counting Rate Calibration for Argon

Extending the comparison between the nitrogen and argon data, we note that the argon and nitrogen response characteristics exhibit the familiar "transition region" which signals the onset of a change from a power to a linear function as the pressure increases from very low values. In the nitrogen data, the beginning of the transition region is near 6×10^{-11} Torr. For argon, the change begins at a lower value (about 3×10^{-11} Torr, argon). As noted earlier, it is anticipated that the change in slope will occur at a critical value of cathode current, regardless of the species. The pressure at which the change will occur will be a function of the ion source sensitivity for the given species. For a gas with a high ionization cross-section, the so-called "break point" will occur at lower pressures and for a low ionization cross-section, the break point will occur at higher pressures. This appears to be the case with helium and nitrogen. In our present data, however, the break point is lower for argon than nitrogen. In our present data, however, the break point is lower for argon than nitrogen by approximately a factor of two; suggesting that the <u>total</u> discharge current (I_{K_1} and I_{K_2}) is larger for argon than for nitrogen. This would be in much better agreement with the Table IV sensitivity data. Without meaningful data on the total cathode currents, the true reasons for the present uncertainties are not apparent.

It will also be noted that there is a pronounced curvature of the very low pressure section of the argon response characterisitc which is not observed in the case of nitrogen. A background spectrum taken before

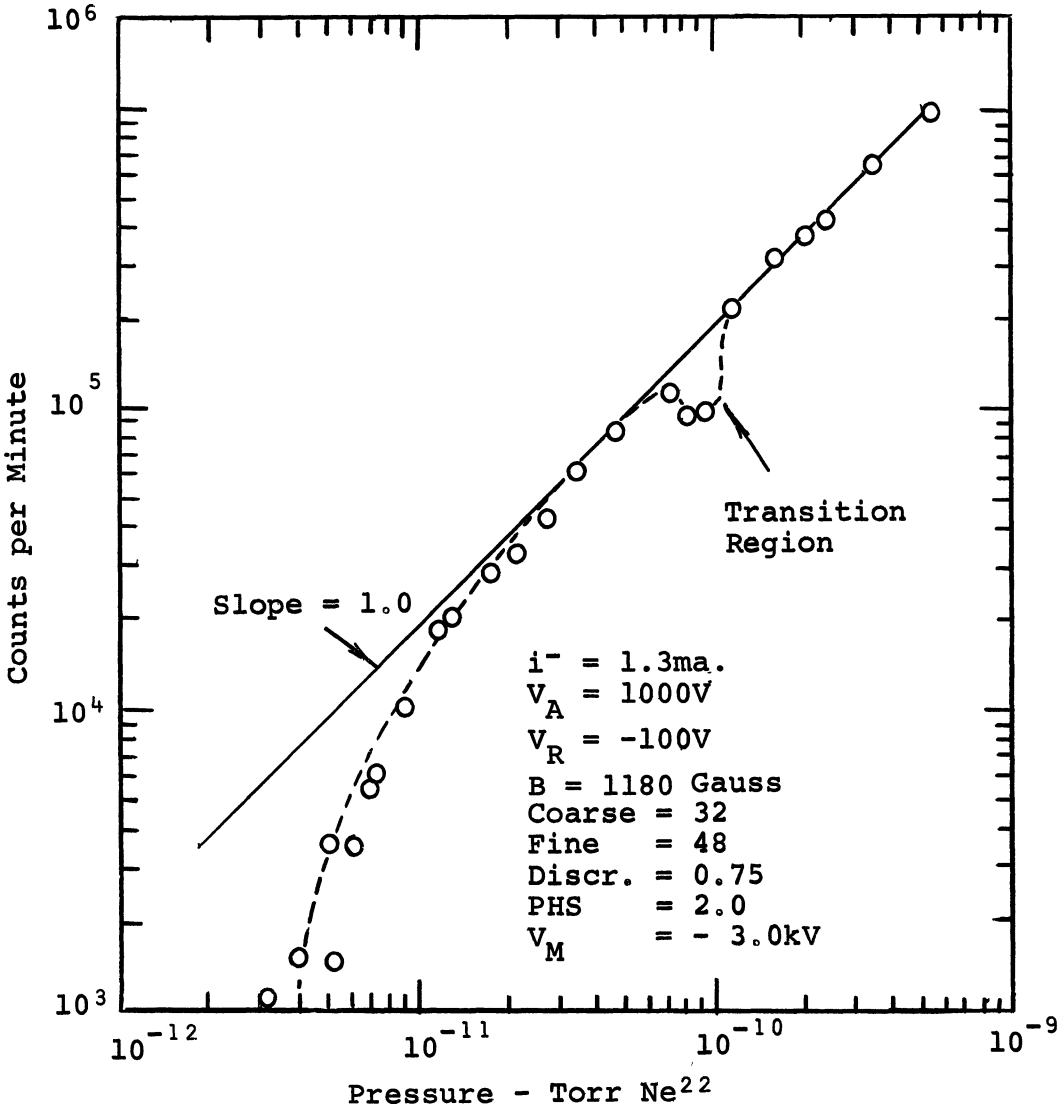

Fig. 35 Counting rate vs. Pressure Ne^{20} & Ne^{22}.

the argon run shows trace amount of masses 2 and 28 which undoubtedly contaminated the calibration gas in each gauge to an unknown extent. Therefore, the argon data below approximately 10^{-11} Torr is probably not valid.

The counting rate response of neon was also investigated in the UHV region. The neon^{22} isotope peak was used and the MBAG data converted to direct partial pressure of this isotope. This natural isotope has an abundance of 9.2% of normal neon. The data of Fig. 35 is, therefore, easily converted to neon data by multiplying the counting rate and pressure coordinates by a factor ten. The sensitivity for either Neon^{20} or Neon^{22} is, of course, the same.

In the case of neon, the response did not show the typical two-slope characteristic found for argon, nitrogen and helium. This is believed to be due to contaminant residual gases existing at very low pressures which originate from desorption effects in the ion pump. The sensitivity for neon can be measured from the data in the linear region. The value shown in this figure is nearly 2×10^{15} cpm/Torr neon.

Table V summarizes the calibration for the three gases used during these tests.

TABLE V

Gas	Counts/Min. Per Torr	Amps/Torr	n @ 1133 gauss
Nitrogen	1.35×10^{16}	45	1.45
Argon	6.0×10^{15}	22	1.80
Neon (20 & 22)	2.0×10^{15}	--	Not determined

Ion source noise level = approximately 5 counts/min. at 4×10^{-12} Torr N_2.

In summary, the UHV counting calibration data has substantiated previous data in the case of nitrogen. For argon, the results in the non-linear region are probably not correct at the lowest pressures because of contaminants affecting the MBAG. The excessive leakage current encountered in the measurement of the total discharge current seriously hampered the experiments and the interpretation of results. Despite these problems, it can be seen that the CCIS/Quad has a capability of measuring true partial pressures into the 10^{-13} Torr range with a relatively large S/N ratio.

Conclusions

The use of counting techniques promises major improvements in S/N ratio, detector stability and measurement accuracy of UHV total and partial pressure measuring instruments. Although the present arrangement is not optimum, it has been shown that a detector can be operated with counting and collection efficiencies approaching 100%. These efficiencies have been achieved

using an in-line quadrupole analyzer-detector system which represents a non-ideal situation for photon noise background rejection. For a magnetic sector analyzer with its excellent noise and signal geometrical separation, the technique may be applied immediately to improve stability and S/N ratio. For axial-aligned r-f analyzers such as time of flight and quadrupoles instruments, the photon background should be reduced by using an electrostatic deflector together with an off-axis multiplier to divert and deflect the ions. These techniques have already been applied to dc current detectors.

Finally, ion counting techniques may also be employed to continuously monitor the gain of the electron multiplier in conventional dc ion detectors if the latter type of detector is preferable for routine analysis.

CONSTRUCTION AND OPERATION OF THE COLD CATHODE ION SOURCE

The ion source for this project was designed to be fitted to an Ultek/EAI model 200 quadrupole analyzer. The cold cathode source replaces the hot filament source which is part of the original assembly. This operation should be performed under clean room conditions and with white gloves to avoid contamination of the internal parts.

Construction of Cold Cathode Ion Source

Manufacturing details. - The assembly, detail drawings and parts list for the construction of the CCIS are shown in Figs. 36 through 53*. As indicated on the drawings, all of the internal parts must be polished smooth with no sharp edges or corners. This is required to prevent field emission in the source.

The anode is first assembled in the retainer with three sapphire balls. This is most easily accomplished using two strips of masking tape on the inside of the anode to hold two of the balls in place. Then tilt the anode to expose the third hold and snap in the third ball with a wood tongue depressor. A 20 gauge nickel wire lead is then spot welded to the anode through one of the slots in the retainer. (See Fig. 37.)

---

*These figures are located at the end of this section of the Report.

The two auxiliary cathodes are spot welded to the retainer, spaced approximately .040" from the anode. Although this dimension is not critical, it should not be much smaller or field emission might become a problem.

The cathode rod is spot welded in the hole of the cathode #1 (K_1) disc and this assembly is held in place by three kovar-glass insulators spot welded to the retainer and the lip of the cathode disc. The spacing again is approximately .040" but is not critical.

The cathode #2 (K_2) disc is mounted with the other three kovar-glass insulators. These are welded on the outside of the retainer with the lower leads bent through the notches in the retainer and welded to the cathode disc at the notches in it.

The source assembly is then welded to the mounting sleeve with three 20 gauge nickel wires bent in the form shown in Fig. 37. The axial symmetry should be retained as closely as possible. When this is completed the assembly should resemble the photograph of Fig. 39.

At this point the assembly should be thoroughly cleaned with a good detergent, preferably in an ultrasonic cleaner, and rinsed with alcohol. After cleaning, it should only be handled with white gloves.

Assembly to the quadrupole. - The CCIS assembly is designed to slip over the end of the quadrupole support cylinder in place of the hot cathode source. First the wiring to the original source must be removed and then the source will slip off the end when the four screws in the quadrupole tube are loosened. A new entrance aperture is added, Fig. 46, to replace the aperture which is part of the original source. This piece slips into the quadrupole tube down to the shoulder and is held in place by two nickel wires spot welded to the outside rim of the aperture and then bent around two of the loosened screws, which are then tightened (see Fig. 37). The CCIS slotted sleeve slides over the quadrupole. The second cathode should be spaced from the entrance aperture about 0.090 in. The sleeve is held in place by the other two screws with #8 flat washers (stainless steel) to clamp the sides of the slot.

The three leads to the CCIS - one to each cathode and one to the anode - are shielded. Pyrex glass tubing is bent to the shapes shown in Fig. 47 and a bifilar winding of #26 or #28 bare OFHC copper wire is wound over the tubing to form the shielding. The leads (nickel) are spot welded to the elements and to the feedthru terminals. The shielding is grounded at the base plate.

The connector plate, (Item 6, EAI Drawing 4054E00244) mounted on the outside of the baseplate is removed and the new plate Fig. 53 with three additional coaxial connectors is installed.

Operation

Equipment required. - Figure 17 is a block diagram of the equipment required for ion counting studies and for dc analog recording of mass spectra. The operating electronics is an Ultek/EAI Model 200 Quadrupole system. The RF/DC generator and associated power supplies were not modified except to derive a sweep voltage proportioned to mass for driving the X-axis of the X-Y recorder. In the case of the Ultek/EAI quadrupole this is obtained at a test-point labelled, "TP-3" on the RF/DC generator sweep circuit diagram. The mass scan voltage supplied to the X-Y recorder is the same whether the quadrupole sweep generator is operated in the manual or automatic mode.

The power supplies required to operate the CCIS (anode and retarding voltages) and the electron multiplier are commercial units. The appropriate voltage and current ratings are noted simply as guide lines for selection of suitable equipment. Well regulated supplies should be used, particularly for the CCIS anode voltage to minimize random noise in the cold-cathode discharge.

The dc analog electrometer should be capable of measuring currents of the order of 1×10^{-14} amperes. Although not absolutely necessary, a variable time-constant is a generally desirable feature to have in the instrument. A linear electrometer is also preferable to a logarithmic instrument because of its greater accuracy of reading.

The pulse counting equipment used is also somewhat flexible. In general, the counting equipment must be able to record a wide range of pulse amplitudes from < 1 to 25 millivolts, depending on multiplier gain. A unit voltage gain pre-amplifier is essential to couple the output of the multiplier to the counting equipment. A very short (low capacity) coaxial cable should be used to couple the multiplier output to the pre-amplifier. This is necessary to preserve output pulse amplitude, which is, of course, dependent on the output capacity seen by the multiplier. The output of the pre-amplifier then can drive the longer cable to the counting equipment without loss of pulse amplitude.

The counting equipment may be as simple or complex as desired. In our experiments, a simple combination of typical nuclear counting equipment was employed; a non-overloading pulse amplifier/discriminator was used to amplify the millivolt pulses to an amplitude sufficient to trigger the scaler-counter. The linear pulse amplitude discriminator (built into the amplifier) was used to discriminate against undesired noise and to study pulse height distributions of signal and noise. While much more sophisticated equipment (pulse height analyzers and counters equipped with digital print-out) may be used if available, the simpler equipment will yield the main body of experimental information required in the study and use of ion-counting techniques as applied to UHV RGAS.

Start up procedure. - When the unit has been pumped down to a pressure below 10^{-6} Torr, the source may be started and the other voltages applied. The stack of magnets is slid on over the narrow end of the housing (about 1 in. beyond the end) and 2000 volts applied to the anode. In order to protect the source and power supply it is prudent to install a large 100 megohm resistor in series with the anode lead and increase the voltage slowly. If an arc does occur, no damage will result. A picoammeter can be wired to the first cathode circuit as a pressure indicator, but this is not necessary. If the pressure is very low (10^{-10} Torr or less), the anode voltage may be increased to 4 - 5000 volts for easier starting.

When ion current appears on the picoammeter or in the quadrupole output at zero mass, the manual peak selector is tuned to a peak. The magnet position is adjusted for maximum peak height. At very low pressures this process can be troublesome because the discharge may extinguish itself occasionally when the magnet is moved. If possible, it is easier to perform this adjustment at higher pressures.

Operating parameters. - Although higher sensitivity is obtained at higher anode voltages, the best signal-to-noise ratio is obtained at approximately 1000 volts (see previous discussion). At very low pressures where electron multiplier and picoammeter noise are high it may be advantageous to increase the anode voltage and reduce the gain at the detector. There are also points

in the operating pressure range, particularly about 10^{-10} Torr where the discharge in the source will oscillate, causing noise in the output. The point of oscillation can be altered by changing the anode voltage. The cathode or retarding voltage is not critical and may be adjusted for the best resolution and sensitivity. The operational characteristics of this parameter are explained in the earlier sections of this report.

The recommended operating voltage for the multiplier will depend on the use requirements and on the condition of the multiplier. For a new multiplier, the operating voltage should be as low as possible to establish adequate dc current sensitivity for the anticipated pressure range. For pulse counting, the voltage should be limited to the value required to count all ions at the minimum discrimination level of the counting equipment. If this 100% counting efficiency cannot be obtained without exceeding the maximum recommended voltage on a new multiplier, additional gain should be obtained in the counting equipment. Preamplifiers are commercially available with additional gain factors of 10 and 100. As the multiplier ages and the gain declines the voltage may be increased to counteract the loss in gain. When operating at high pressures, care must be taken to prevent the multiplier current from exceeding approximately 10^{-7} amperes. If this precaution is not observed a permanent gain loss may occur. For most purposes, a voltage between 2600 and 3000 volts will suffice (new multiplier) for both counting and dc measurements.

Operation of the quadrupole electronics is discussed in the EAI manual. The dial settings which were generally used are as follows: Resolution 4.95; Center Mass (for automatic operation) 4.07; Sweep width 10.00; Coarse Sweep-slow, fine sweep 0.10, and Mass range-low. When the picoammeter is operating at maximum gain the fine sweep control will have to be reduced in order to compensate for the slow speed of response of the picoammeter.

Bake out. - The quadrupole with the CCIS is capable of withstanding bake out temperatures up to 400°C. To obtain extremely low pressures, bake out of the complete system for periods of 8 hours and longer is necessary. At intermediate pressures some systems will reach the required pressure without bake out. However, bake out of the spectrometer will insure cleanliness of the instrument so that measurements will reflect the gas in the system rather than gas emanating from the walls of the spectrometer.

For bake out it is necessary to remove the connector plate (Fig. 53) because the insulation in the BNC connectors will not withstand the temperature. The magnet should also be removed.

The unit as described above has operated with excellent results at pressures down to 10^{-12} Torr. Little trouble should be experienced in duplicating this adaptation if good ultrahigh vacuum practices are followed.

PARTS LIST FOR COLD CATHODE ION SOURCE

	Item	Reg.	Figure #
(1)	Cathode rod	1	41
(2)	Anode	1	42
(3)	Anode Retainer	1	43
(4)	Kovar to glass insulator	6	44
(5)	Sleeve	1	45
(6)	Aperture plate	1	46
(7)	Shielded insulation	1 set	47
(8)	Auxiliary cathode	2	48
(9)	Cathode #1	1	49
(10)	Cathode #2	1	50
(11)	Housing	1	51
(12)	Modification to Quadrupole housing	1	52
(13)	Modification to Quadrupole lead plate	1	53
(14)	Sapphire balls	3	5/32 diam. Adolf Meller Co., Providence, Rhode Island
(15)	Magnets	5	Indiana General Corp., #F5916 magnetized axially in one stack. Valpariso, Indiana.
(16)	Dage 3651-2 connectors	3	

Figure 36 - Parts List

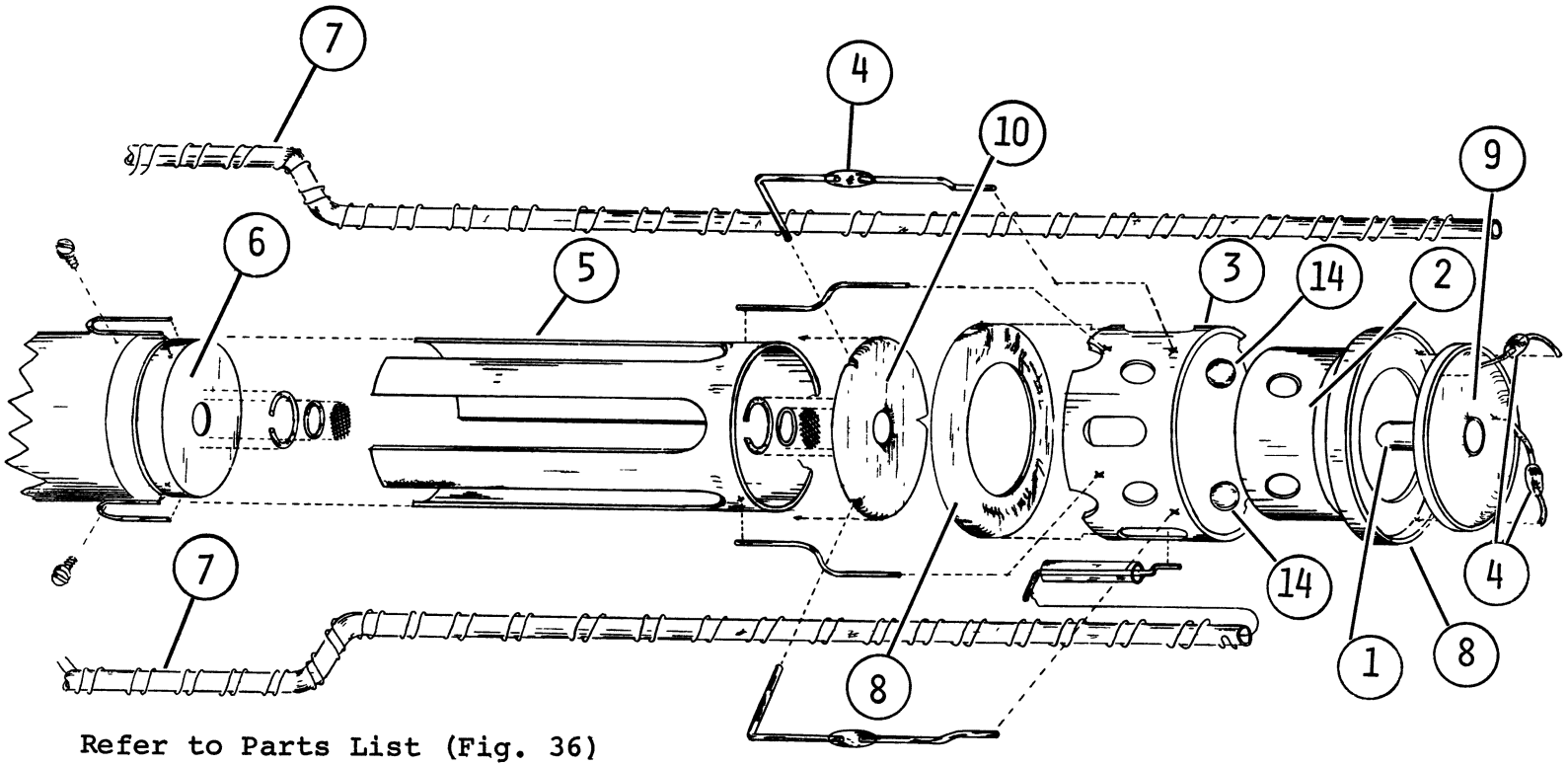

Refer to Parts List (Fig. 36)

Figure 37.- Exploded view of CCIS/Quadrupole

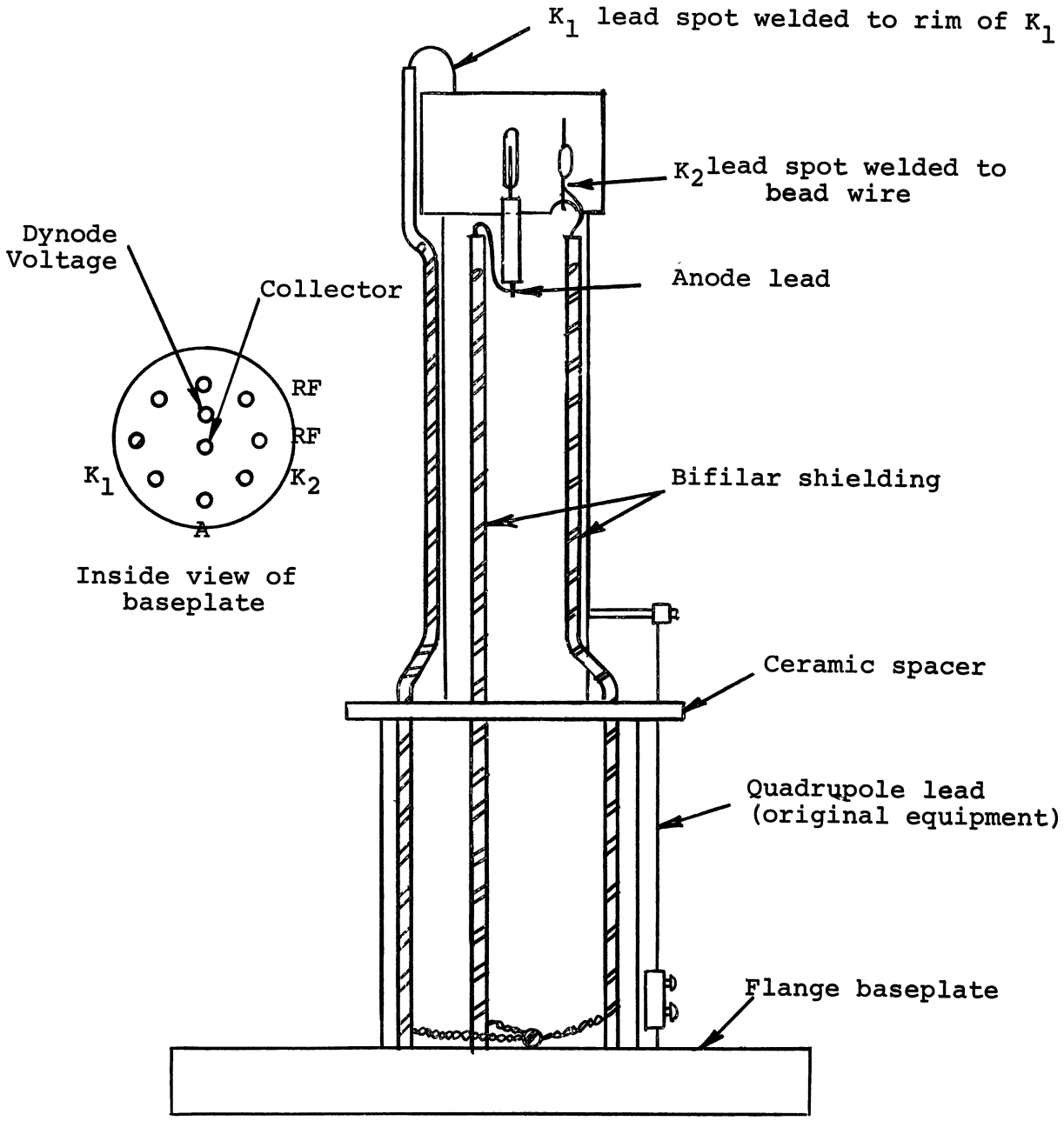

Figure 38 - Lead Assembly

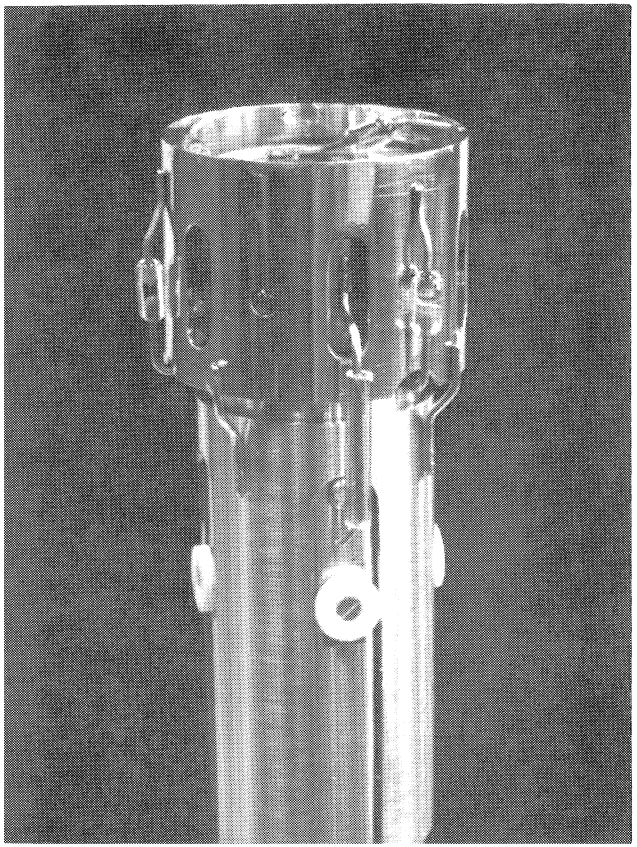

Fig. 39
Assembly CCIS Quadrupole

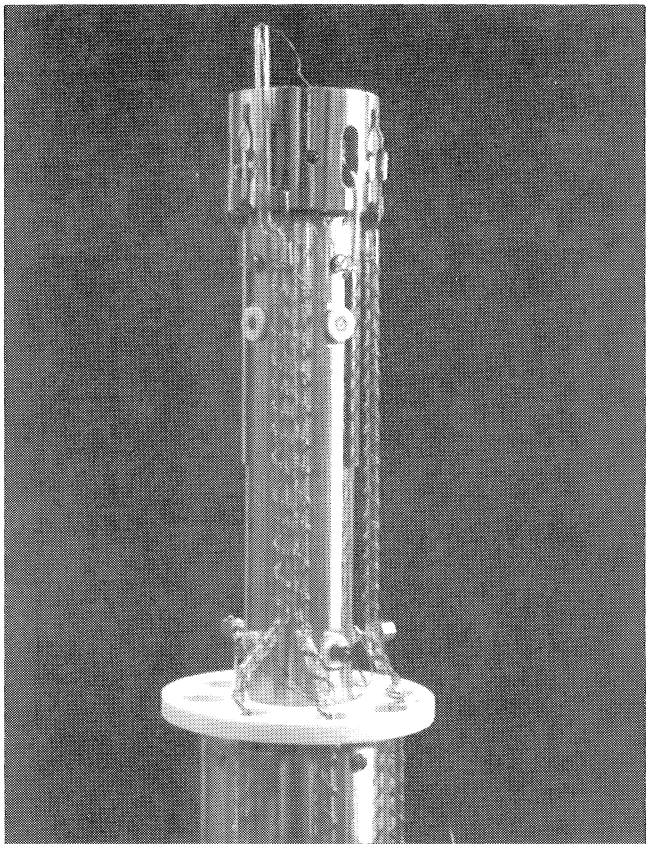

Fig. 40
Lead Assembly CCIS Quadrupole

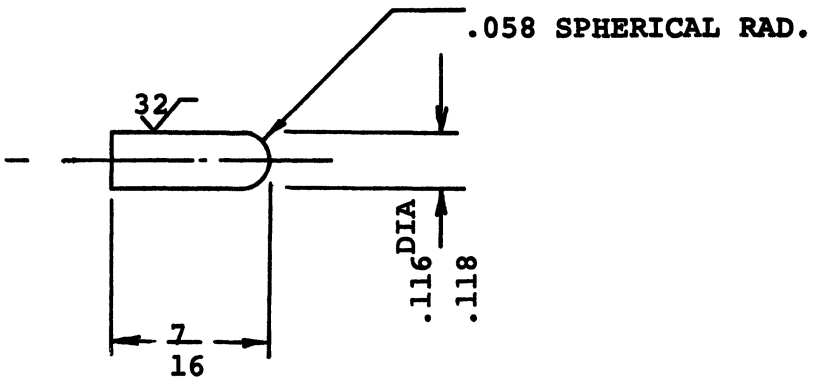

MAT'L - 304 SS

POLISH ALL SURFACES FREE OF MACHINE MARKS AND OTHER IMPERFECTIONS

Fig. 41 Cathode Rod

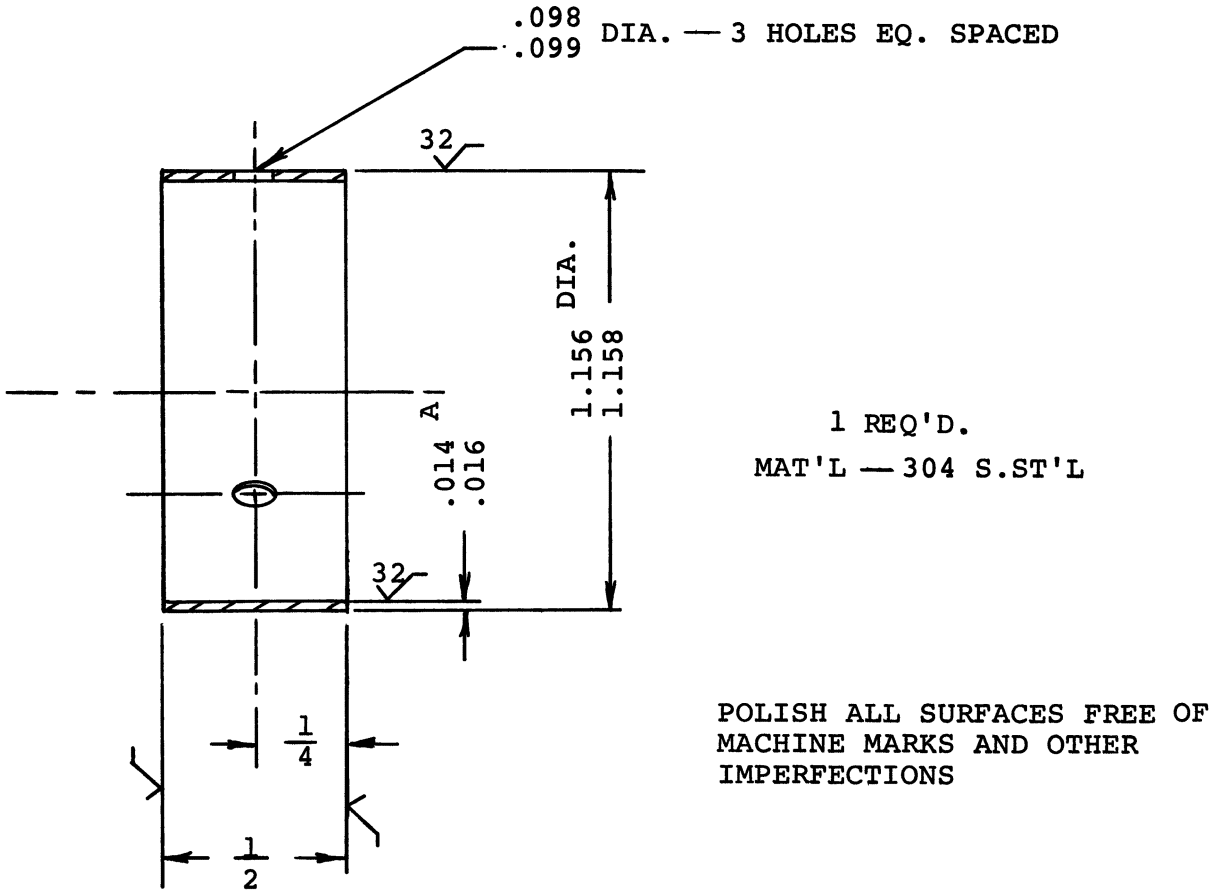
.098
.099 DIA. — 3 HOLES EQ. SPACED
32
DIA.
1.156
1.158
A
.014
.016
32
1 REQ'D.
MAT'L — 304 S.ST'L
1/4
1/2
POLISH ALL SURFACES FREE OF
MACHINE MARKS AND OTHER
IMPERFECTIONS

Fig. 42 Anode

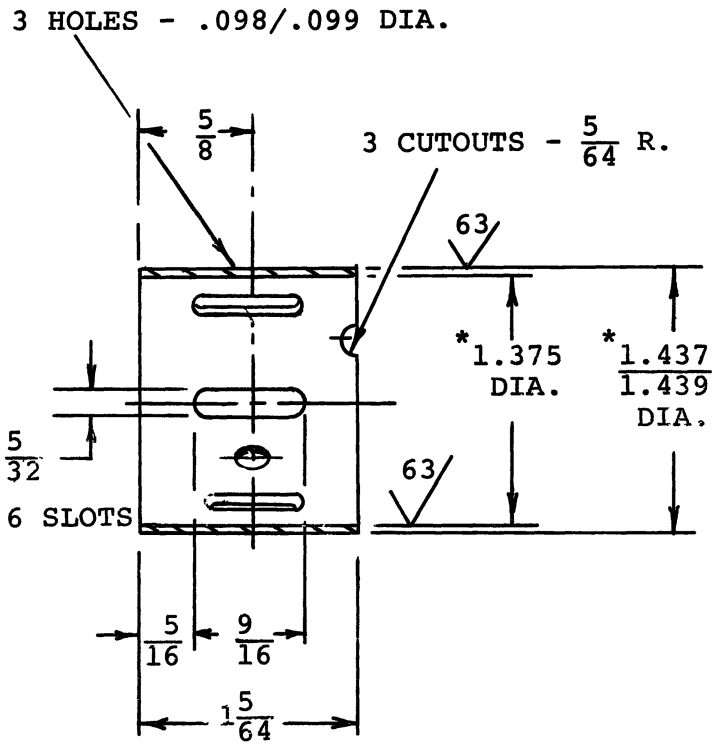

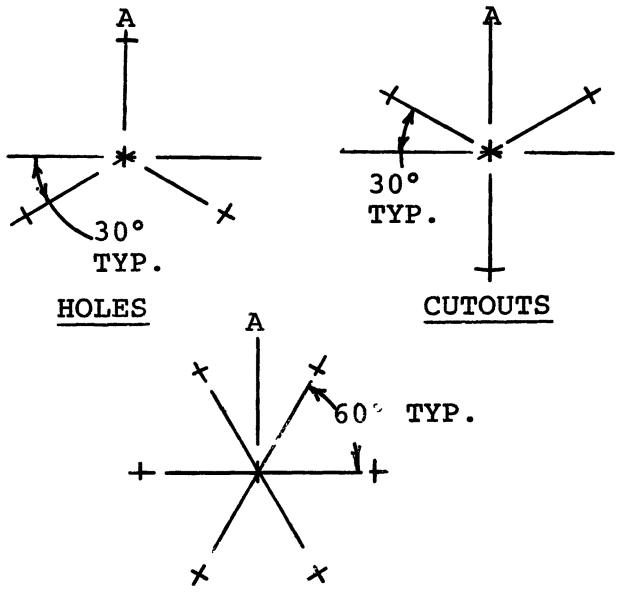

ORIENTATION DIAGRAMS

NOTES -

*THESE DIA'S. TO BE CONCENTRIC WITHIN .001 TIR

POLISH ALL SURFACES FREE OF MACHINE MARKS AND OTHER IMPERFECTIONS

MATL. - 304 SS

Fig. 43- Anode Retaining Cylinder

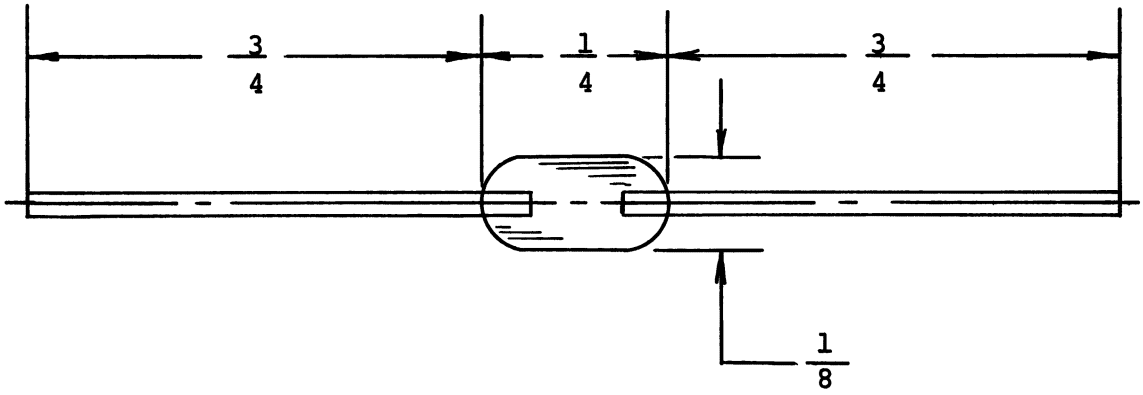

6 Req'd.

NOTES

1. .028 = #22 GA. KOVAR WIRE

2. GLASS TO METAL SEALS MUST BE BUBBLE FREE TO PREVENT VIRTUAL LEAKS (GAS TRAPS)

Fig. 44 Kovar to Glass Insulator

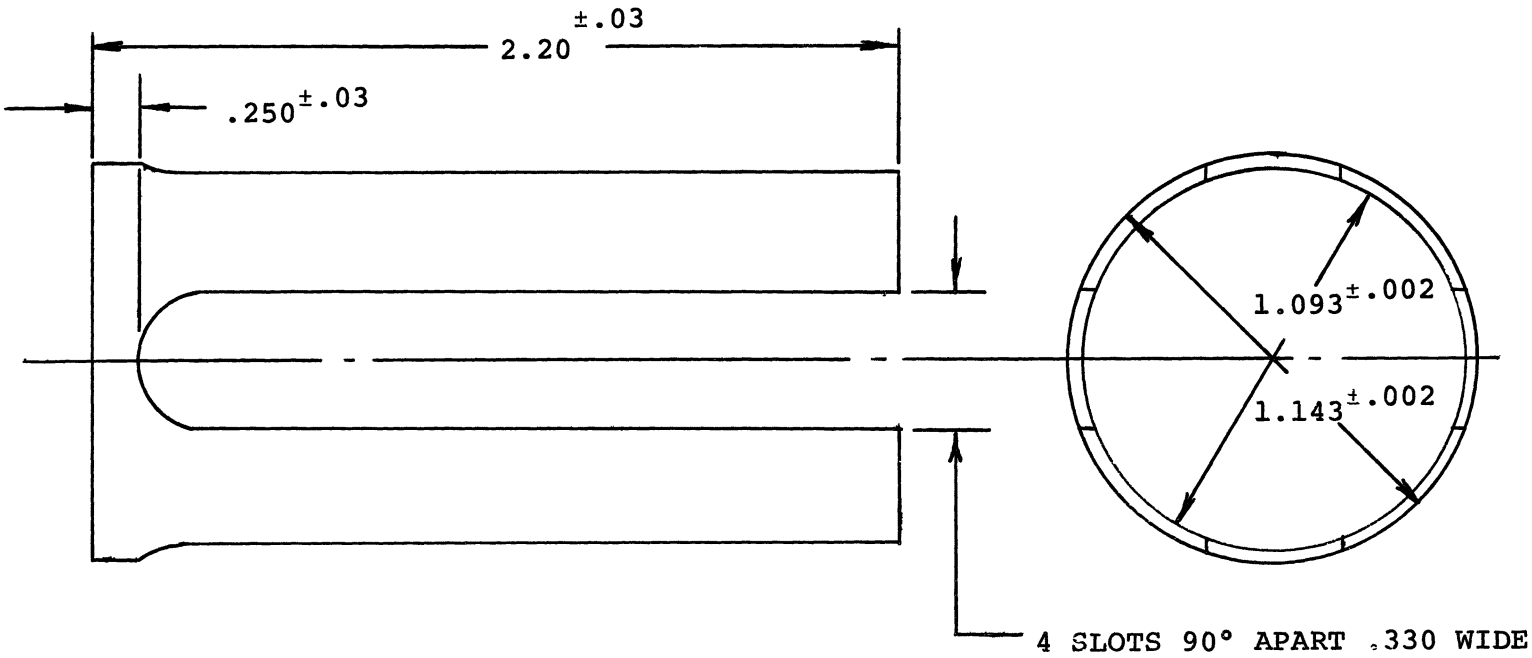

NOTES

1. ALL MACH SURFACES TO HAVE FINISH √32 OR BETTER
2. POLISHED SURFACE TO BE APPLIED BY NRC TECHNICIAN

MATERIAL: 304 S.S.
1 REQUIRED

Fig. 45 Sleeve

Ⓑ METEX ELECTRONICS CORP.
TUNGSTEN WIRE MESH
#.001R130W 5 1/2

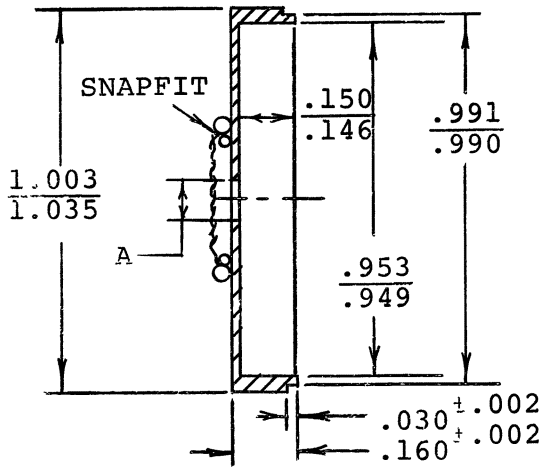

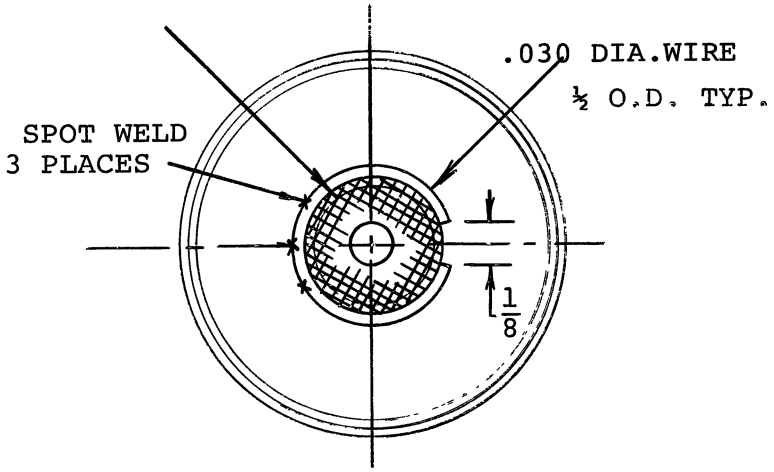

MAT'L - 304 SS

NOTES

1. OVERALL MACH. FINISH TO BE 32 OR BETTER.
2. DO NOT RADIUS EDGES, BREAK ALL SHARP EDGES WITH STONE.
3. POLISH SURFACE TO BE APPLIED BY NRC TECHNICIAN.
4. 1 REQ. "DIM.A" PLATE #1 .100±.002
5. SPOT WELD WIRE MESH (ALL STRANDS) TO INNER RING OF #20 (.031) PURE NICKEL WIRE. INNER RING TO SNAP INSIDE OUTER RING

Fig. 46 Aperture Plate

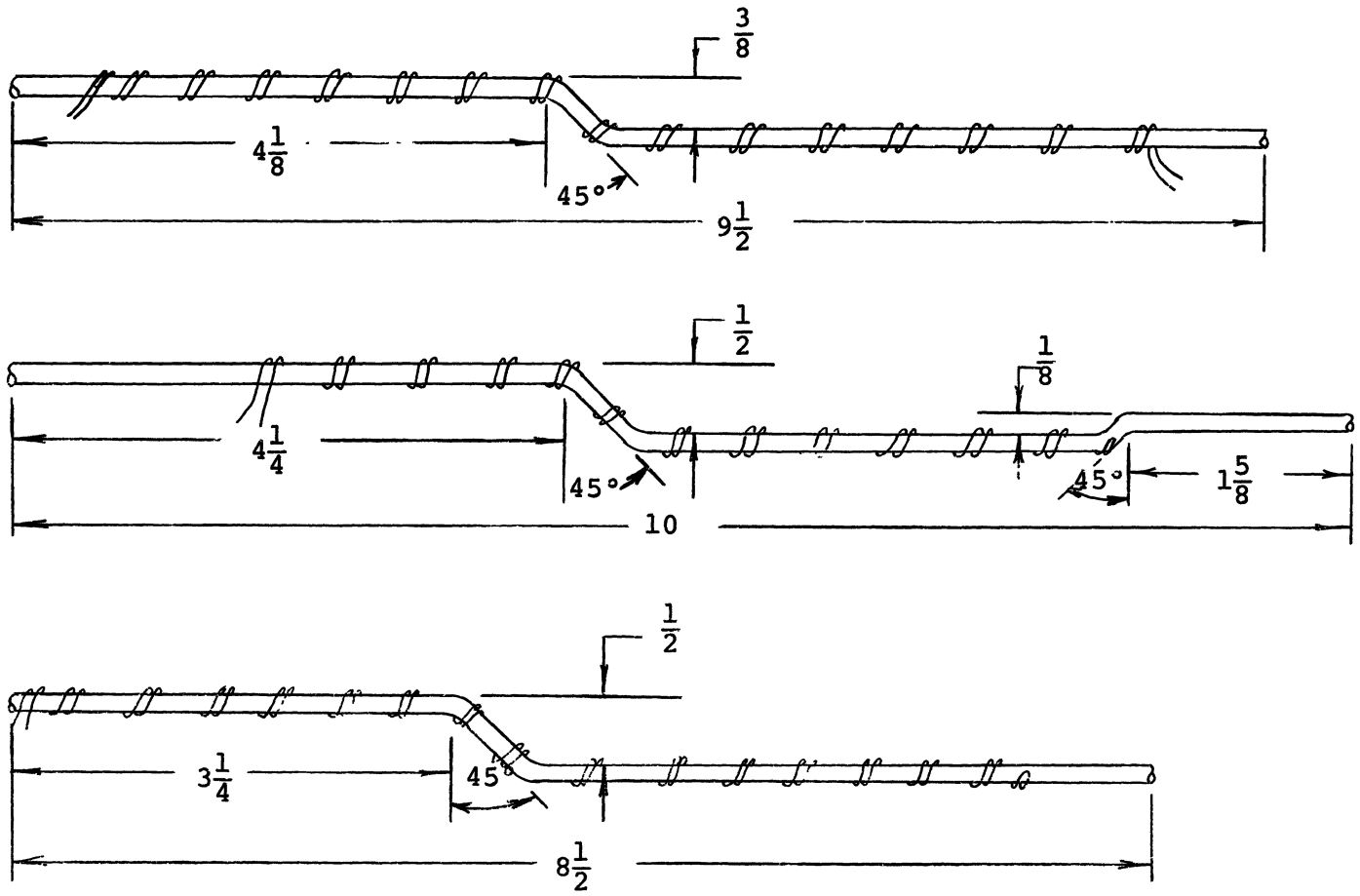

MAT'L

1. PYREX TUBING - 3 MM OD
2. #24 GA. BARE CU WIRE - ALLOW 1½" EXTRA FOR GROUNDING

3 CENTER CONDUCTOR .016" DIAMETER NICKEL WIRE

OPEN ENDS

Fig. 47 Shielded Insulation for Leads

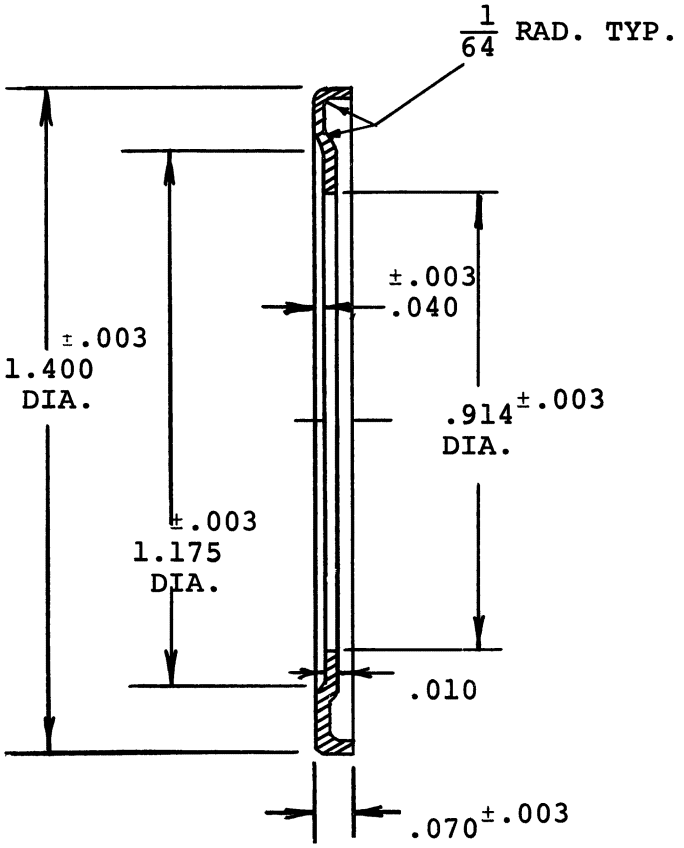

NOTE

DE-BURR ALL EDGES VERY CAREFULLY
ELECTRO-POLISH ENTIRE PIECE

MAT'L - NICHROME V SHEET, .010" THICK

Fig. 48 Auxiliary Cathode

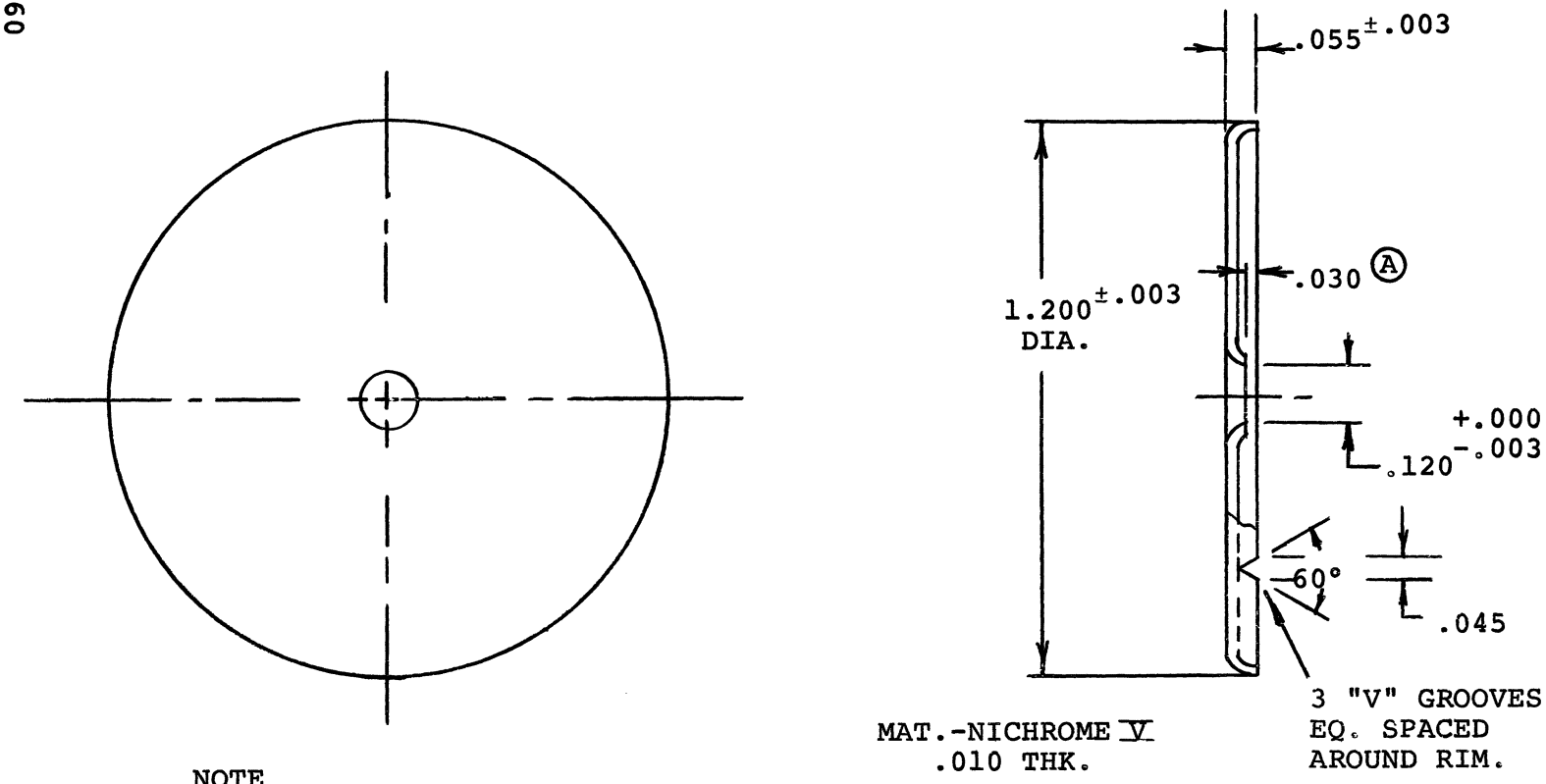

NOTE

DE-BURR ALL EDGES VERY CAREFULLY

ELECTROPOLISH ENTIRE PIECE

Fig. 49 Cathode End Plate

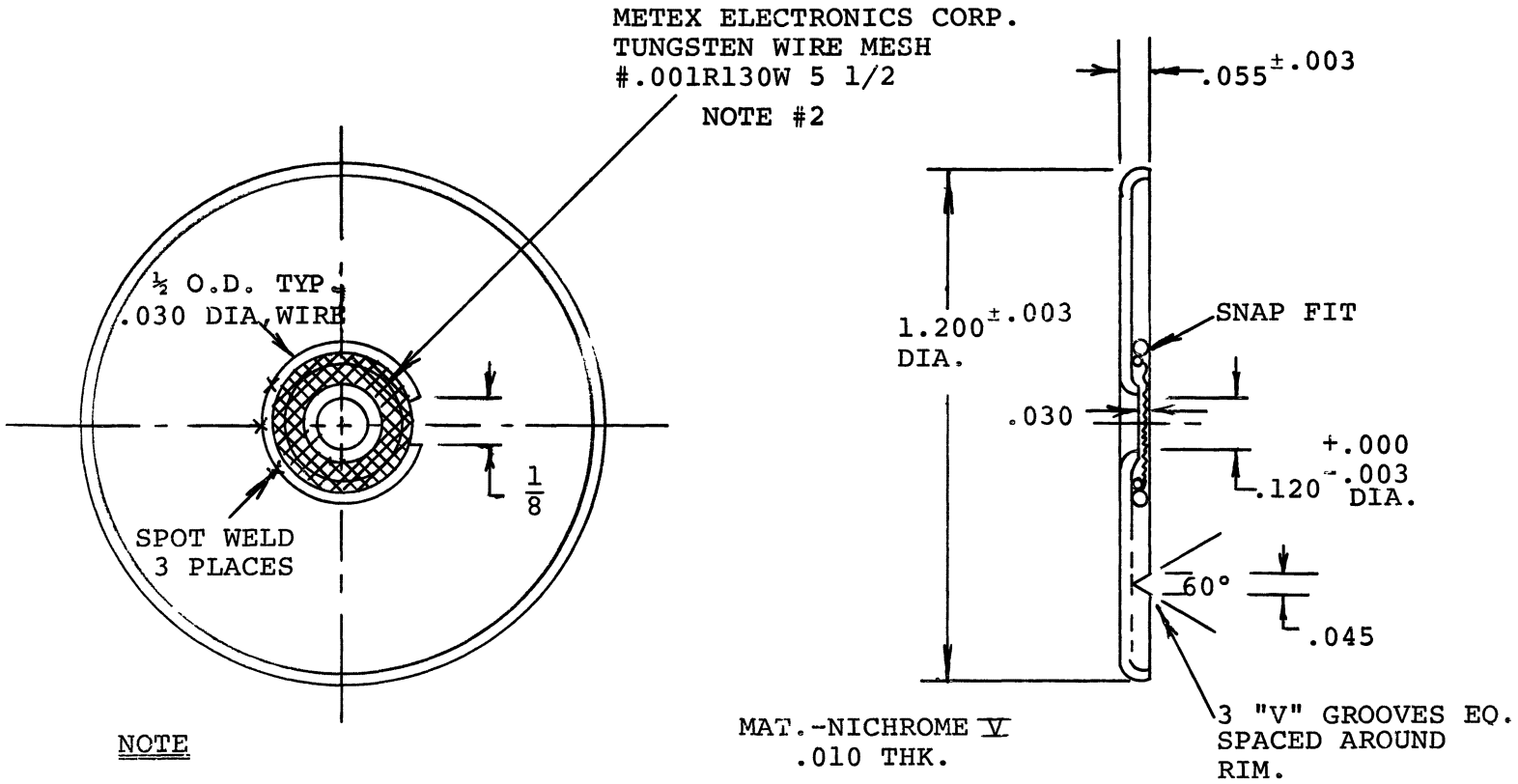

NOTE

1. DE-BURR ALL EDGES VERY CAREFULLY ELECTROPOLISH ENTIRE PIECE
2. SPOT WELD MESH TO INNER RING OF 0.031 NICKEL WIRE

Fig. 50 Cathode End Plate

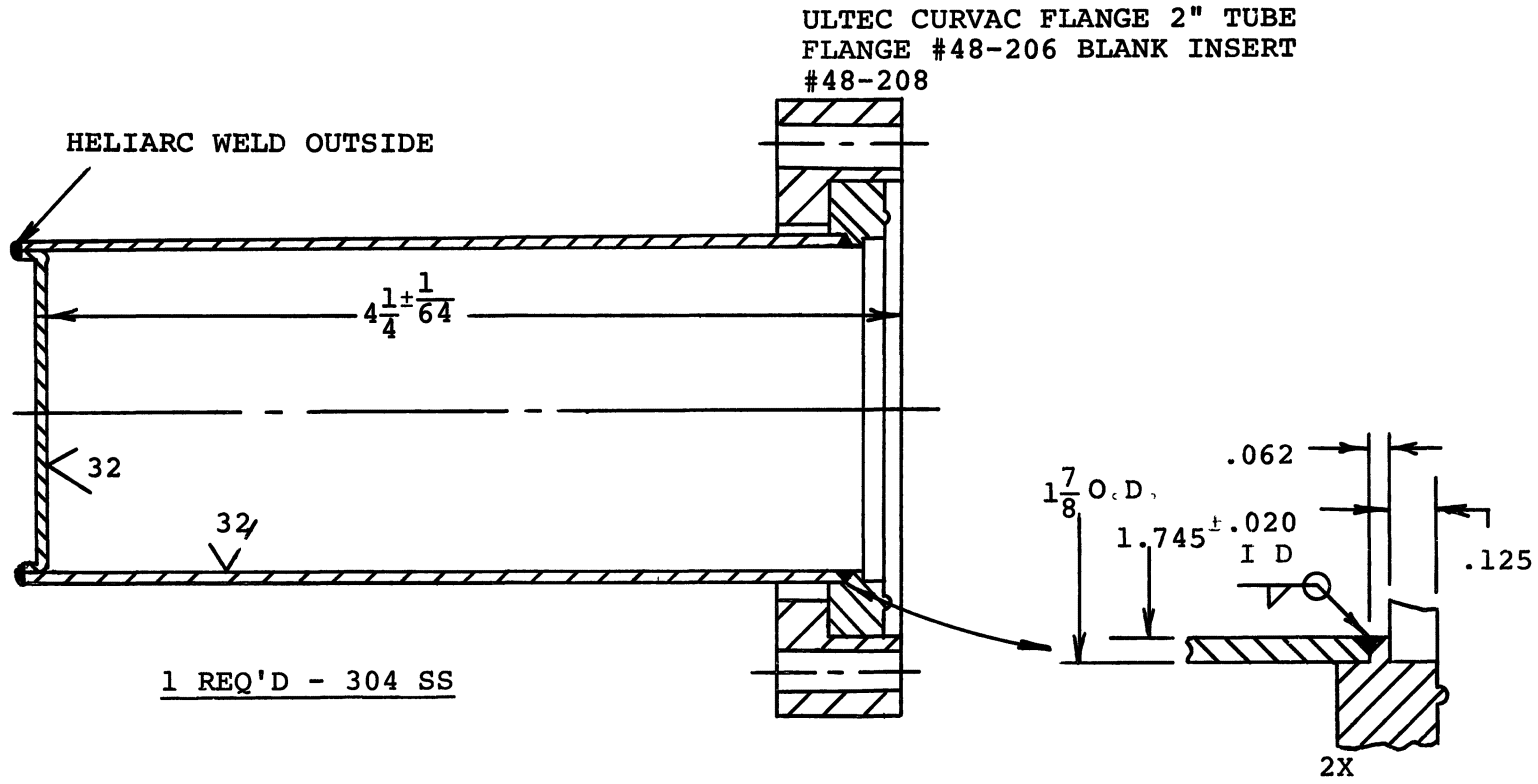

Fig. 51 CCIS Housing

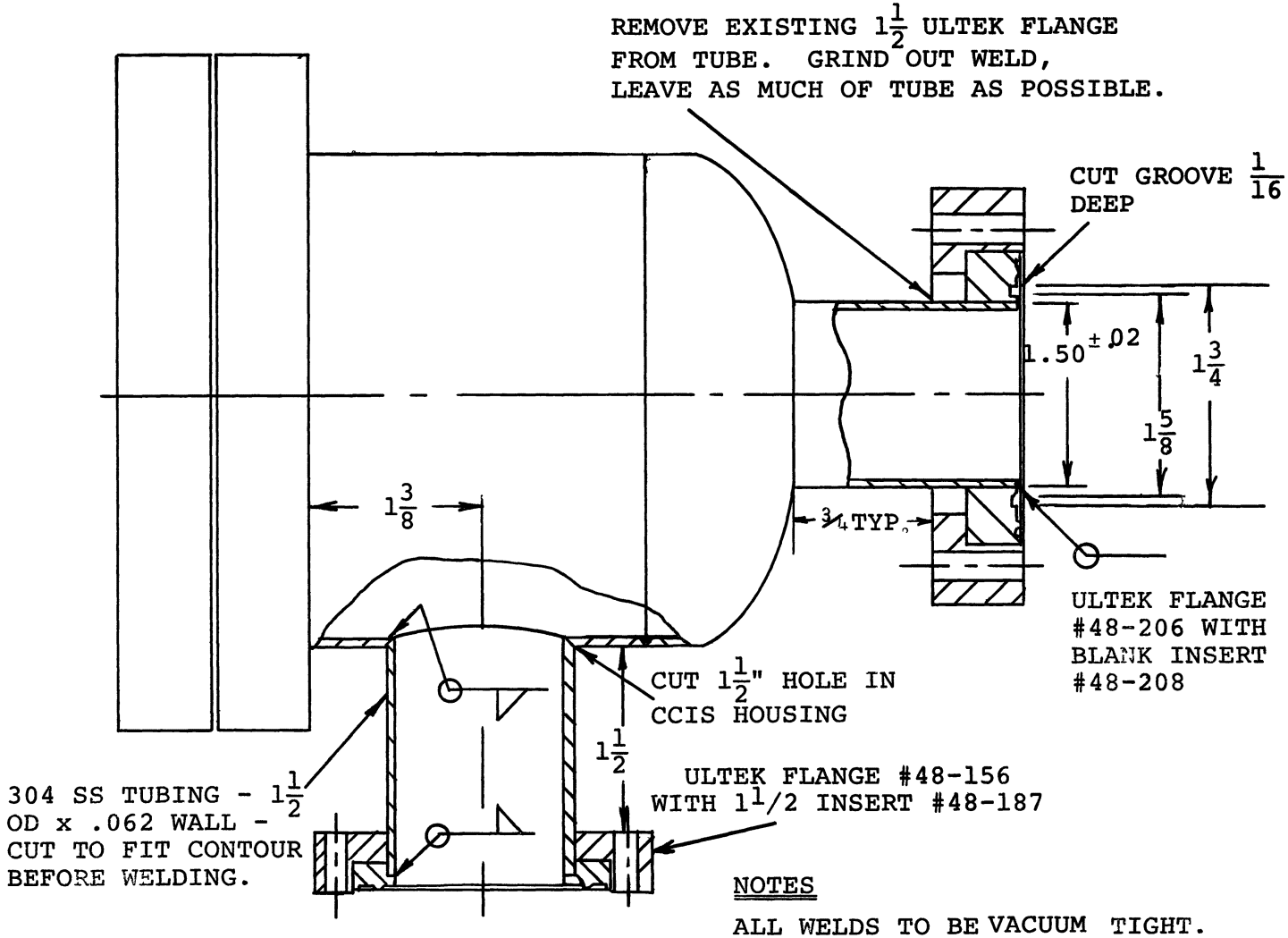

Fig. 52 - CCIS Housing Modification

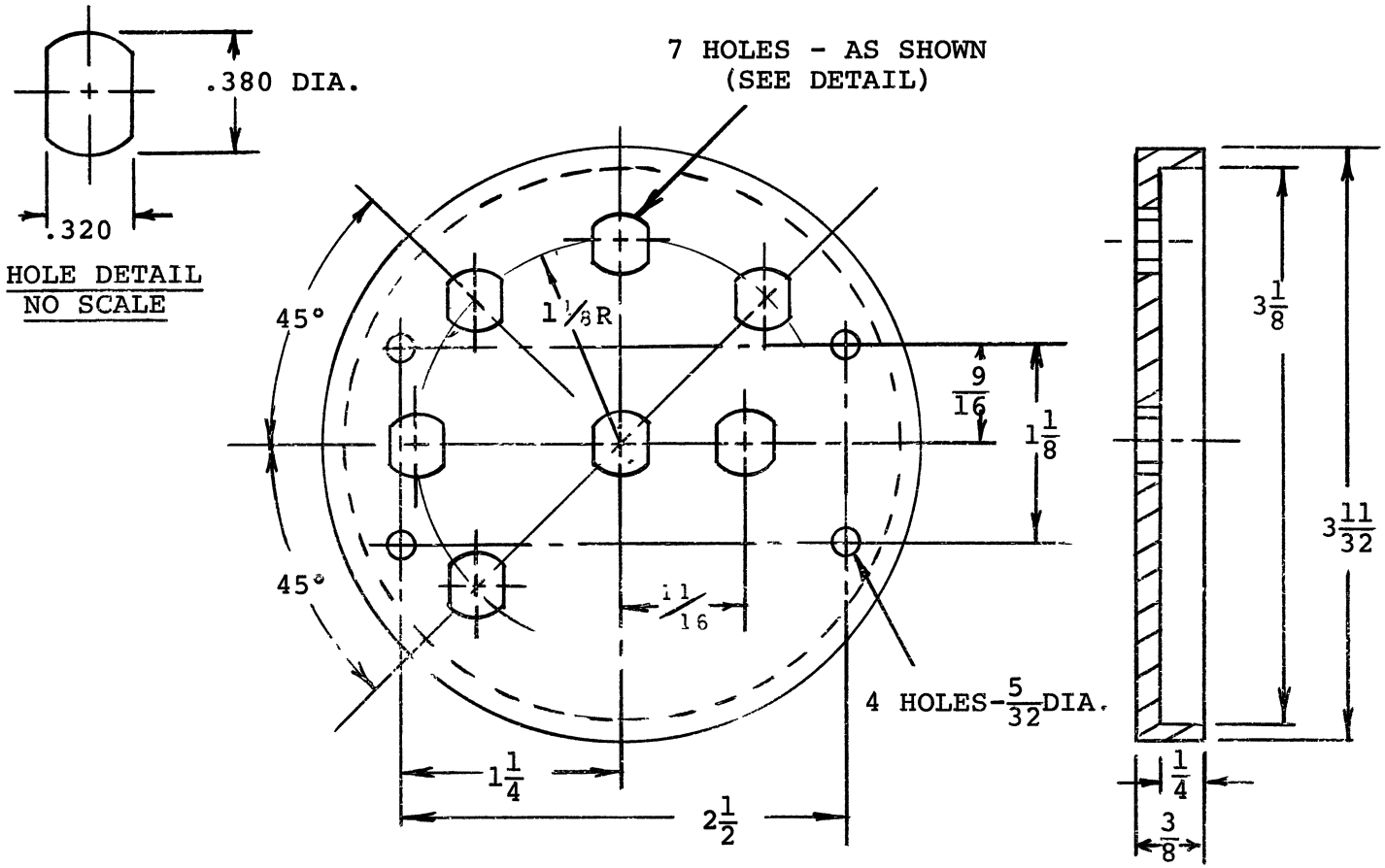

MATERIAL ALUM 2024-T3

Fig. 53 Lead Plate

CONCLUSIONS

The cold-cathode ion source/quadrupole mass spectrometer is a practical laboratory instrument for the analysis of residual gases in UHV systems. It is characterized by a large inherent sensitivity and by its relative spectral cleanliness under very high vacuum conditions.

The cold-cathode ion source employed has been shown to be capable of producing relatively intense beams of low energy ions suitable for analysis by larger quadrupole instruments. In the present work, the achieveable sensitivity and resolution are somewhat limited by the dimensions and operating parameters of the specific quadrupole used.

The investigation of ion counting techniques in conjunction with the CCIS/Quad has demonstrated that improved ion detectors can be designed and built with greater inherent stability and S/N ratio. These techniques can be readily adapted to magnetic deflection analyzers. In the case of in-line analyzers such as time of flight and quadrupole instruments, electrostatic deflection of the analyzed ion beam is recommended to reduce photon stimulation of the electron-multiplier.

Finally, the UHV performance of the instrument has shown that the partial pressure response characteristics of the instrument are in agreement with previously published data for nitrogen. Further work is recommended to define the partial pressure sensitivity for other gases in the UHV region. In this regard, the use of molecular beam calibration techniques may prove more appropriate in defining the partial pressure response for other gases.

REFERENCES

1. Dushman, Saul; and Lafferty, J. M. (Ed.): Scientific Foundations of Vacuum Technique. Second ed., John Wiley & Sons, Inc., 1962, p. 324.

2. Redhead, P. A.: The Magnetron Gauge: A Cold-Cathode Vacuum Gauge. Can J. Phys., vol. 37, no. 11, November 1959, pp. 1260-1271.

3. Paul, W.; Reinhard, H. P.; and von Zahn, U.: The Electric Mass Filter as Mass Spectrometer and Isotope Separator (in German). Z Physik, vol. 152, no. 2, 1958, pp. 143-182.

4. Böhm, H.; and Günther, K. G.: Eine Penning-Ionenquelle für Massenspektrometer. Zeitsch. f. angew, Physik, Bd. XVII, Heft 7, 1964, pp. 553-557.

5. Böhm, H.; and Günther, K. G.: Eine Penning-Ionenquelle für Massenspektrometer. Vakuum-Technik, 14 Jhrg., Heft 7, October, 1965, pp. 192-193.

6. Feakes, F.; Muly, E. C.; and Brock, F. J.: Extension of Gauge Calibration Studies in Extreme High Vacuum. NASA CR-904, Oct. 1967, pp. 118-129.

7. Morton, G. A.: Photon Counting. J. Appl. Optics, vol. 7, Jan. 1968, pg. 1.

8. Allen, J. S.: The Detection of Single Positive Ions, Electrons, and Photons by a Secondary Electron Multiplier, Phys. Rev., vol. 55, 1959, p. 966.

9. Inghram, M. G.; Hayden, R. J.; and Hess: Mass Spectrometry in Physical Research. Nat'l Bur. of Stnds. Circ. no. 522, 1951.

10. Inghram, M. G.; and Hayden, R. J.: Report No. 14, Nuclear Science Series, National Research Council, 1954.

11. Koyama, K.; and Connolly, R. E.: Use of a Commercial Electron Multiplier for Positive Ion Counting in Mass Spectrometry. Rev. Sci. Instr., vol. 28, 1957, p. 853.

12. Davis, W. D.; and Vanderslice, T. A.: A Sensitive High Speed Mass Spectrometer for Ultra-High Vacuum Work. Vacuum Symposium Transactions, A.V.S., Oct. 1960, p. 417.

13. Morton, G. A.: op. cit.

14. Marchand, P.; Paquet, C.; and Marmet, P.: Near 100% Efficiency Ion Detectors for Use with Quadrupole Mass Filter. Rev. Sci. Instr., vol. 37, 1966, p. 1702.

15. Higatsberger, M. J.; Demorest, H. L.; and Nier, A. O.: Secondary Emission from Nichrome V, CuBe, and AgMg Alloy Targets Due to Positive Ion Bombardment. J. Appl. Phys., vol. 25, 1954, pp. 883-886.

16. Woodward, C. E.; and Crawford, C. K.: Development of a Quadrupole Mass Spectrometer. AFML-TR-64-400, M.I.T. Lab. for Insul. Research, Report #194, December, 1964.

17. Brubaker, W. M.: The Quadrupole Mass Filter. Colloquium Spectroscopicum Internationale, IX, Lyon, France, June, 1961.

18. Bultemann, H. J.; and Delgmann, L: Multiplier System of Mass Filter AMP 3. Vacuum, vol. 15, no. 6, pp. 301-306.

19. Bennewitz, H. G.; and Wedemeyer, R.: A Molecular Beam Detector with Electron Collision Ionization and Quadrupole Mass Filter (Trans.). Z. fur Physik, vol. 172, 1963, pp. 1-18. (Available from Defense Doc. Center, Alexandria, Va., AD-457317.)

20. Redhead, P. A.: op.cit.

21. Torney, F. L., Jr.; and Feakes, F.: Pressure Measurements Below 10^{-10} Torr with Bayard-Alpert and Magnetron Gauges. Rev. Sci. Instr., vol. 34, no. 9, Sept. 1963, pp. 1041-1043.

22. Feakes, F.; Torney, F. L., Jr.; and Brock, F. J.: Gauge Calibration Study in Extreme High Vacuum. NASA Cr-167, Feb., 1965, p. 23.

23. Redhead, P. A.: Modulated Bayard-Alpert Gauge. Rev. Sci. Instr., vol. 31, no. 3, March 1960, pp. 343-344.

24. Redhead, P. A.: The Effects of Adsorbed Oxygen on Measurements with Ionization Gauges. Vacuum, vol. 13, 1963, p. 253.

25. Hobson, J. P.: Measurements with a Modulated Bayard-Alpert Gauge in Aluminosilicate Glass at Pressures Below 10^{-13} Torr. J. Vac. Sci. & Technol., vol. 1, 1964, p. 1.

APPENDIX A

FEASIBILITY STUDY ON THE DESIGN AND DEVELOPMENT OF A COLD-CATHODE ION SOURCE

APPENDIX A

FEASIBILITY STUDY ON THE DESIGN AND DEVELOPMENT OF A COLD-CATHODE ION SOURCE

By F. L. Torney, Jr. and P. Fowler
Norton Research Corporation

SUMMARY

An experimental cold-cathode ion source of the magnetron type has been designed, built and tested. The source has been operated at a sensitivity approximately 1500 times larger than conventional hot-filament mass spectrometer ion sources. The total spread in ion energies appears to be perfectly compatible with the requirements of a quadrupole mass analyzer. Further improvements in sensitivity are anticipated. The ion current appears to be a linear function of pressures over the range 10^{-9} to 10^{-6} Torr. Some difficulty has been encountered with an internally trapped gas source of unknown origin.

It has also been found that the ions are readily extracted from the cold cathode discharge by providing a relatively weak accelerating electric field at the exit cathode. The electron component of the extracted beam can be minimized by proper choice of this accelerating potential.

The ion beam emerging from this cold-cathode ion source is characterized by a relatively large spread in ion energy, angular separation and cross sectional area. Because of its unique tolerance for these characteristics, the quadrupole mass filter has been chosen as the most suitable analyzer for use with this type of source.

Various modes of mass scanning may be chosen in operating the quadrupole analyzer. The mode of constant line width scan has been chosen most desirable. A thorough study of the theory of operation of the quadrupole has resulted in a tentative design of quadrupole with the following characteristics:

(1) Mass range: 2 to 100 amu

(2) Resolution over mass range: 1 amu

(3) Transmission efficiency over mass range: 100%

(4) Entrance ion beam diameter: 1.8 mm

(5) Radius, r_o of circle inscribed inside rods: 2 cm $\pm$ 1/4%

(6) Rod radius: 2.32 cm $\pm$ 1/4%

(7) Rod length: 25 cm

(8) Frequency: 1.1 megahertz $\pm$ 1/4% stability

(9) Rf voltage: 3500 volts (max.)

(10) Rf power: 56 watts

(11) Axial spread in beam energy: 31.5 eV

(12) Maximum entrance angle of beam: 15° max.

The problem of focusing the ion beam into the quadrupole has also been studied. Various lens designs have been considered which will focus the beam without increasing its energy. Coupling the output of the source to the input of the analyzer has also been studied, since the effects of transitional electric fields between the source and analyzer are noticeable.

The ion detector located at the output of the analyzer section has also been studied. For partial pressures to 10^{-16} Torr, a normal electron multiplier or a vibrating reed electrometer

have sufficient sensitivity. The minimum detectable partial pressure may be decreased by recourse to a pulse-counting technique using an electron multiplier. However a more satisfactory detector may be the resistance strip magnetic electron multiplier which should allow one to measure partial pressures to 10^{-19} Torr, using continuous current techniques.

INTRODUCTION

The measurement of residual gases in ultra high vacuum (UHV) is rapidly becoming a problem of sizable importance in vacuum instrumentation for space research. While some improvements have been made recently in partial pressure measuring instruments (mass spectrometers), two fundamental problems still have not been adequately solved for present and future requirements. First, these mass spectrometers employ inherently low sensitivity ionization sources of the hot-filament type. Sensitivity improvements are herein only possible at the output of the analyzer. Second, these sources produce undesired spectra of the gases residual to the spectrometer rather than to the system under study. This undesirable characteristic further reduces the effective sensitivity of the measurement.

Cold-cathode ionization sources, on the other hand, have a much higher sensitivity and at the same time are less likely to generate disturbing amounts of spurious gases during operation. Cold-cathode ionization sources, therefore, offer promise of improvement in UHV mass spectrometry.

The overall performance of an UHV mass spectrometer depends on the individual characteristics of its three basic components: the ion source, the mass analyzer, and the ion detector. The

First section of this report discusses the development of a high sensitivity, cold-cathode ion source. The next section discusses the selection and design criteria of the most suitable analyzer for use with this source. The last section discusses the choice of an ion detector to be used with the source and analyzer.

APPENDIX "A" SYMBOLS AND ABBREVIATIONS

A_1	first aperture
A_2	second aperture
A_{K_1}	first auxiliary cathode
A_{K_2}	second auxiliary cathode
C	total capacitance (farad)
d_{max}	maximum allowable ion beam size (meter)
I_c	collector current (amperes)
I_{A_2}	second aperture current (amperes)
I_{K_1}	first cathode current (amperes)
K_1	cathode #1
K_2	cathode #2
L	length of quadrupole rods (meter)
P	pressure (Torr)
P	power dissipated in the quadrupole output tank circuit (watts)
Q	figure of merit for rf tank circuit
r_o	radius of circle inscribed within rod structure (meter)
$U_{a_{max}}$	maximum allowable axial ion energy (eV)
$U_{T_{max}}$	maximum allowable transverse ion energy (eV)

V	peak rf voltage (volts)
$V_{A_{max}}$	maximum allowable axial velocity (m/sec)
V_{K_1}	first cathode potential (pusher potential, volts)
V_{K_2}	second cathode potential (extractor potential, volts)
$V_{T_{max}}$	maximum allowable transverse velocity (m/sec)
Θ	maximum allowable ion entrance angle (rad)
ν	rf frequency (Hz)

COLD-CATHODE ION SOURCES

Cold-Cathode Discharges - General

The relatively high sensitivity of the cold-cathode discharge vacuum gauge is due to two important physical characteristics. First, the ionizing electrons are efficiently trapped in crossed electric and magnetic fields. This trapping prevents electron escape until ionization has occurred. Secondly, the discharge process produces an abundant supply of secondary electrons which are primarily responsible for the ionization. Both mechanisms therefore produce a relatively large ionization current, without the aid of thermionic electron emitters.

As a result of the expanding interests in cold-cathode discharge devices for the production of high vacuum and its measurement, a number of different types of discharge configurations have been devised. These generally can be grouped in four categories, according to the mechanical arrangement of their electrode structures, as follows:

(1) Magnetron type (ref. A1) - Central cathode, coaxial anode, auxiliary cathodes. Magnetic field axial to anode cylinder. Magnetic and electric fields perpendicular.

(2) Inverted magnetron type (ref. A2) - Central anode, coaxial cathode and auxiliary cathodes. Magnetic field axial to cathode cylinder. Magnetic and electric fields perpendicular.

(3) Penning discharge (refs. A3-A9) - Similar to type 1 but without auxiliary cathodes. Magnetic and electric fields perpendicular.

(4) Philips gauge - Central anode loop, two cathode plates either side of anode. Magnetic and electric fields roughly perpendicular. A simplified version of the Penning discharge.

The choice of the best discharge configuration for the mass spectrometer application was not entirely clear-cut. The Philips gauge type was rejected because of its poor electron trapping and because of its poor "starting" characteristics. The output of the Penning discharge is known to be a non-linear function of pressure (refs. A10, A11, A20). Relatively large discontinuities have also been observed in its response characteristics. For these reasons, it was also rejected. The inverted magnetron is inherently less sensitive than the magnetron gauge and it is also non-linear over all of its operating region so far investigated (refs. A2, A13). It also requires a much larger magnetic field to operate satisfactorily. The magnetron type has the highest sensitivity, but it also displays a marked change in its response characteristics below 2×10^{-10} Torr (nitrogen) (refs. A12, A13). It also displays small discontinuities in its pressure/current characteristic. Therefore the choice between the inverted and normal magnetron configuration is a close one.

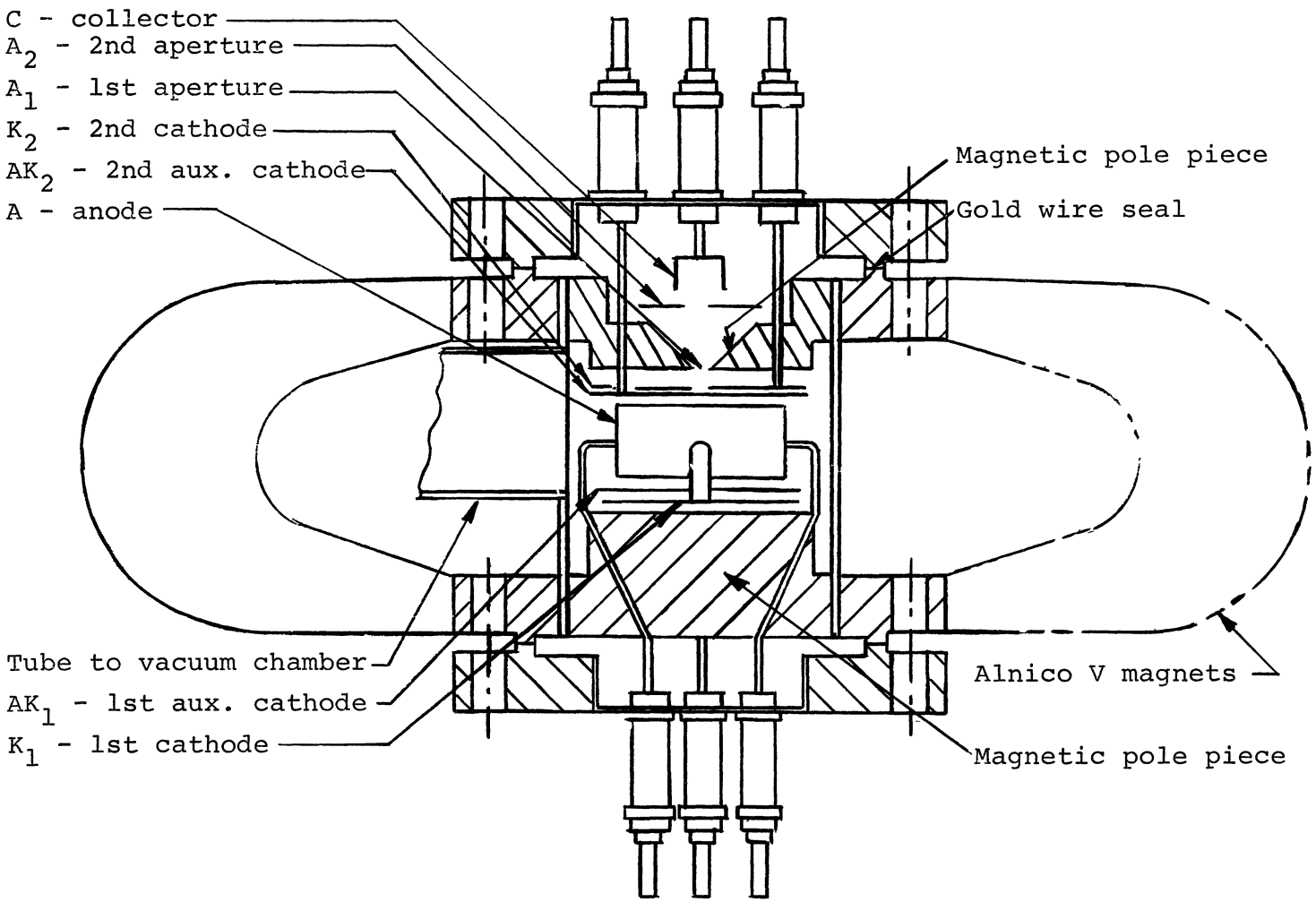

Figure A-1.- Normal Magnetron Cold Cathode Ion Source

It is well known that ions may be extracted from cold-cathode discharges either from the anode or from the cathode (refs. A14-A21). A preliminary decision, therefore, was required on this problem before design of an experimental source could be started.

It was decided to construct an experimental source which would permit a relatively simple conversion to either of the following: (1) normal magnetron - ion extraction from one cathode or (2) inverted magnetron - ion extraction from the anode. It was also decided to investigate configuration (1) first. This decision was based largely on previous experience with ion sources and gauges of this type.

The complex nature of cold-cathode discharges in crossed electric and magnetic fields has stimulated some investigators to formulate simplified theories useful in predicting certain characteristics of these discharges. However, no theoretical treatment has yet been published which may be used to predict completely the discharge characteristics important to this effort. Therefore, construction of an experimental ion source is presently the only practical method of determining the feasibility of the approach.

Experimental Ion Source Design

The mechanical construction of the experimental ion source is shown in Fig. A-1. Figures A-2 and A-3 show detailed views of the source and its parts.

This design incorporates a number of features which are not readily apparent in these figures:

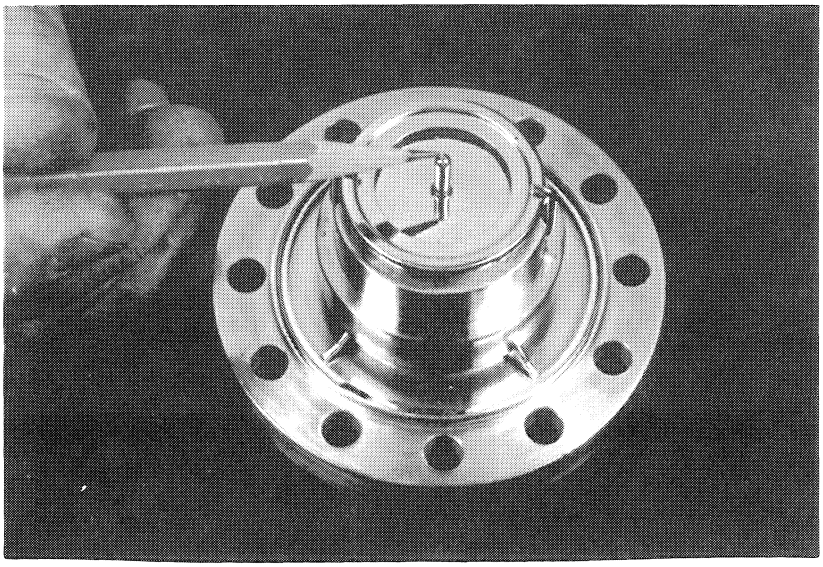

View of Anode End of Source - 1st Cathode (K_1)

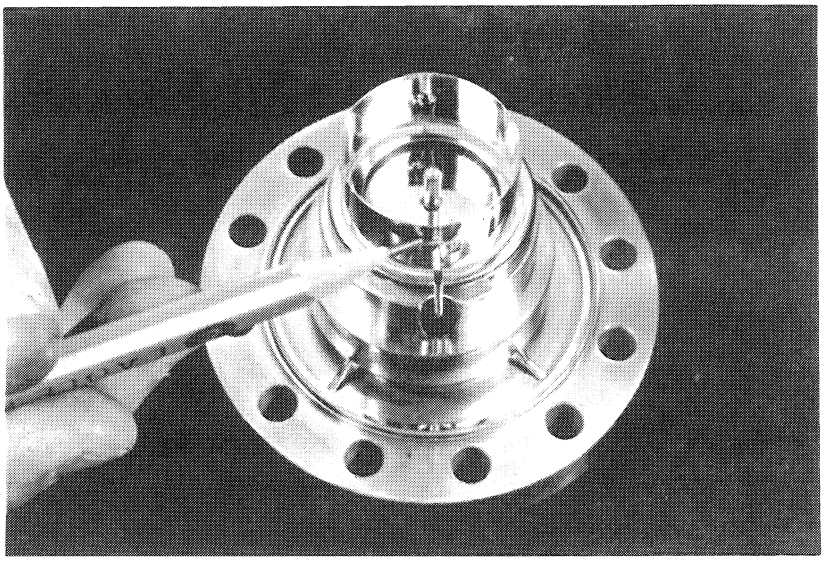

View of Anode End oı Source - Anode (A)

Figure A-2

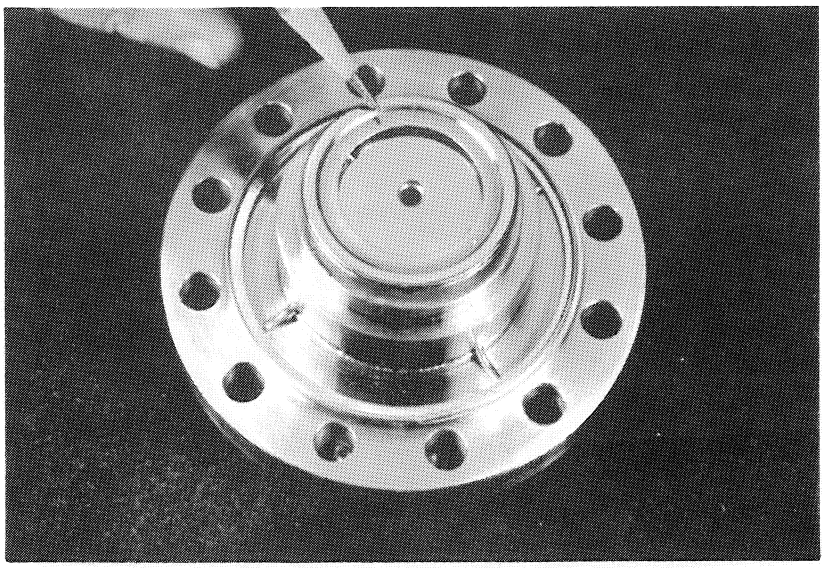

View of Extractor End of Source (AK_2, K_2, A_1)

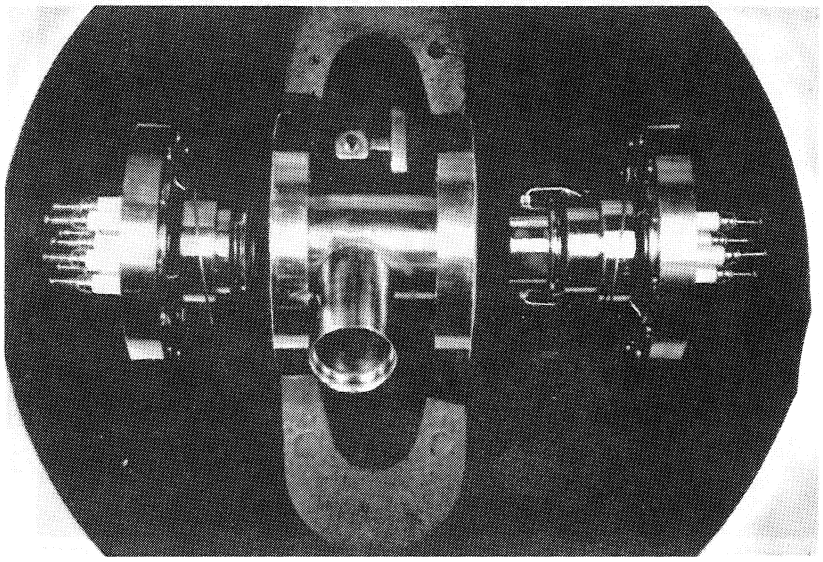

Exploded View - Ion Source and Magnets

Figure A-3

(1) The ion source is designed to be baked at temperatures of 600°C. Gold wire seals and high temperature insulators are used to insure the seal integrity at these high temperatures.

(2) The magnetic circuit is designed to provide magnetic fields up to 2000 gauss. To obtain this large field strength with small magnets, the gap is reduced by locating the poles inside the source and decreasing the gap as much as possible.

(3) Careful attention has been paid to the elimination of all gas traps (virtual leaks).

(4) Guard-ring techniques have been employed in mounting all source elements to minimize electrical leakage currents.

(5) The second cathode (K_2) serves a double purpose. It is a combined cathode and ion extractor.

(6) The ion exit hole in K_2 is purposely made small to extract only the lower energy ions from the discharge.

(7) All materials have been carefully chosen to be compatible with UHV practice. This is particularly true of the moly-permalloy magnet pole pieces.

Theoretical Considerations

Knauer has shown (ref. A16) that two broad spectra of ion energies exist simultaneously within a discharge of the Penning type. These ions are readily extracted through an exit hole on the axis of the discharge. The more energetic ions emerge from

the discharge at relatively large angles with respect to the discharge axis. Ions of lower energy emerge at much smaller angles (nearly along the axis).

These results are of particular importance to any consideration of the use of a cold-cathode ion source for mass spectrometry. Mass analyzers (magnetic, in particular) are intolerant of ion beams with a large spread in ion energy and entrance angle. Due consideration must be given to both these characteristics of the ion beam emerging from a cold-cathode source.

The higher order ion energies noted by Knauer would accentuate the problem of focusing and collimating the ion beam before analysis. Therefore, the experimental ion source shown in Fig. A-1 has been designed to accept only the on-axis, low energy components of the discharge.

Since the energy and entrance angle of ions leaving the source are of great importance to the analyzer, particular attention must also be given to the method of extracting these ions. Any method which produces a pronounced increase in the energy of the beam will complicate the focusing and collimation of the beam. The resulting beam (after collimation) may be too energetic for a reasonably sized analyzer to analyze properly. In this case retardation of the beam is necessary before analysis would be feasible.

The extraction method employed in this experimental source is simple and direct. The voltage on the exit cathode (K_2) is made slightly negative with respect to the opposite cathode and a small potential gradient is therefore provided which accelerates the ions slightly toward the exit hole. The remaining electrodes are maintained at a positive potential with respect to K_2 so that further acceleration is impossible. The success of this method is described later in this report.

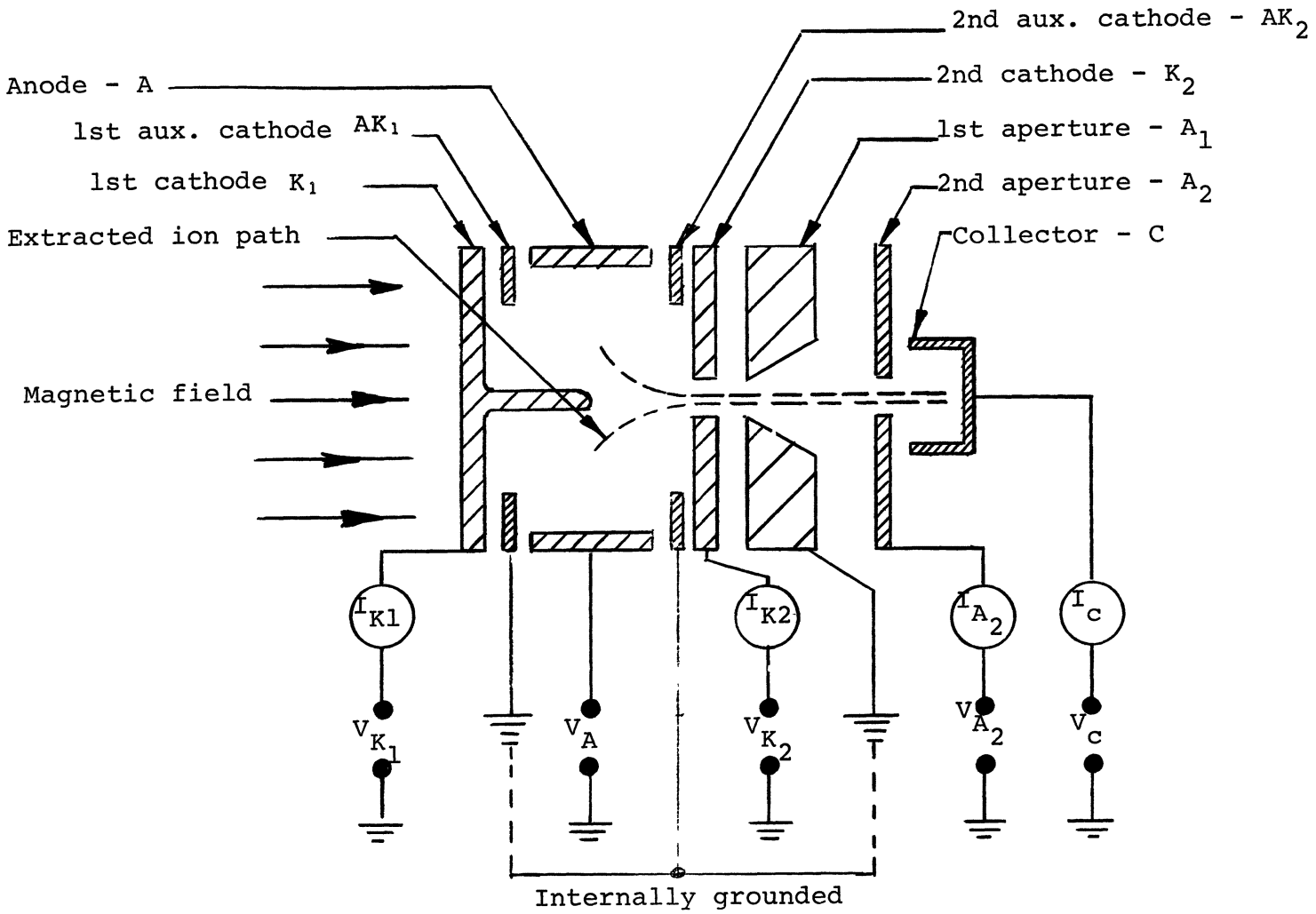

Figure A-4.- Cold cathode ion source schematic

Another desirable feature of this design is the electrical independence of the two cathodes (K_1 and K_2). The fraction of the total discharge ion current collected by the first cathode (K_1) may be measured to indicate <u>total</u> pressure at the same time the extracted ion beam is being analyzed to measure partial pressures.

Experimental Results and Interpretations

The ion source shown in Figs. A-1 to A-3 was assembled and installed on an ultra high vacuum system for experimental study. Electrometers were connected to measure the currents in the various electrodes. These currents were measured before the magnets were attached to determine the magnitudes of leakage, field emission and other noise currents. With 6000 V on the anode, these currents were negligibly small at each electrode. Careful polishing of the high voltage (anode) supports and other critical elements is credited with the prevention of these undesirable currents.

Six magnets were installed on the ion source and the study of ion extraction was undertaken. Figure A-4 shows an electrical schematic of the source and the nomenclature to be employed in this report. The first auxiliary cathode (AK_1) and first aperture (A_1) are internally connected to ground. All potentials are measured with respect to ground, unless otherwise noted.

Figures A-5 and A-6 show the two measurable components* (I_{A_2} and I_C) of the extracted ion beam as a function of extraction potential ($-V_{K_2}$) and anode voltage (V_A). The sensitivity (amperes per Torr) for nitrogen is calculated for each anode potential at an extraction potential of -40 volts.

*Current I_{A_1} is not measurable because aperture A_1 is grounded internally.

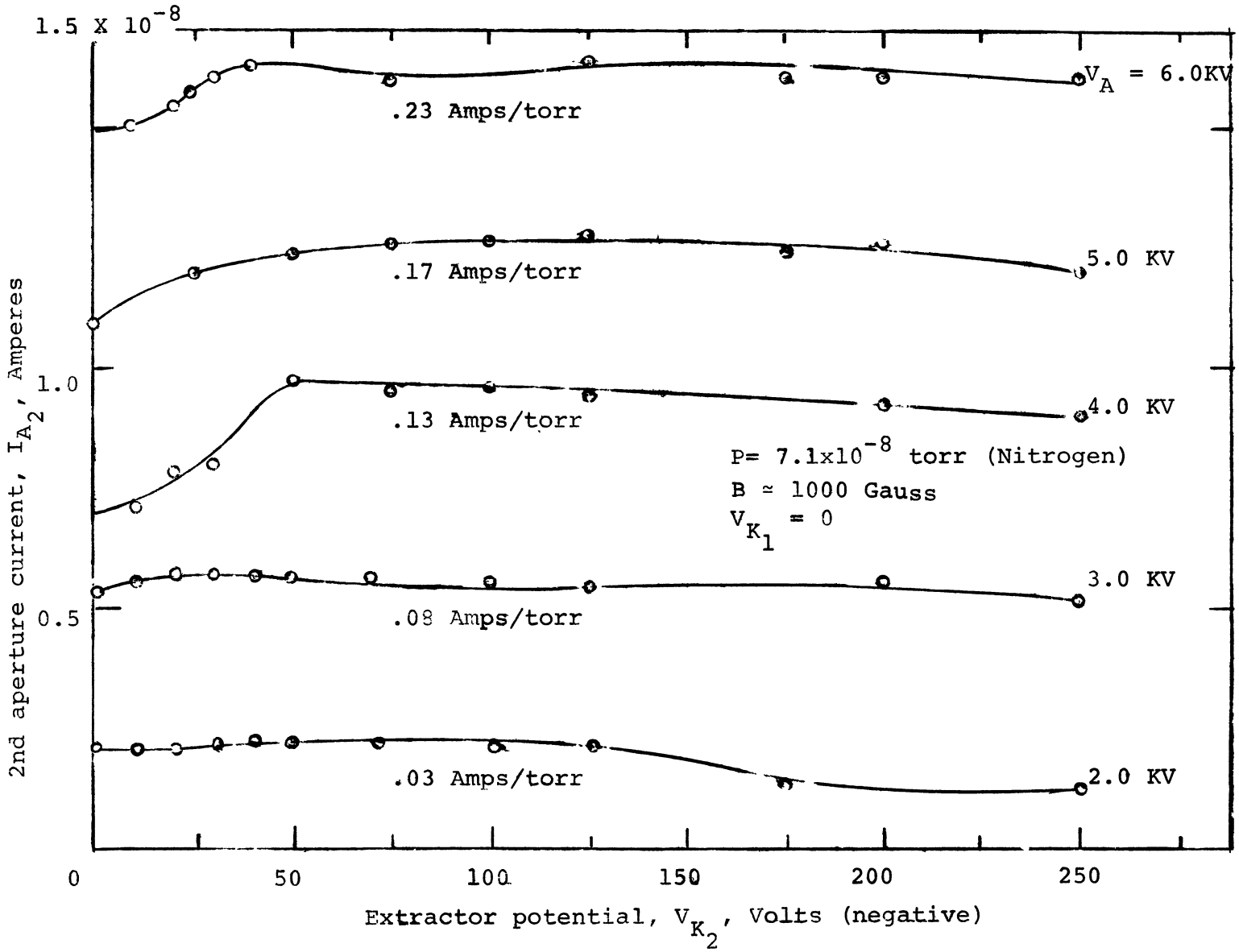

Figure A-5.- 2nd aperture current vs. negative extractor potential.

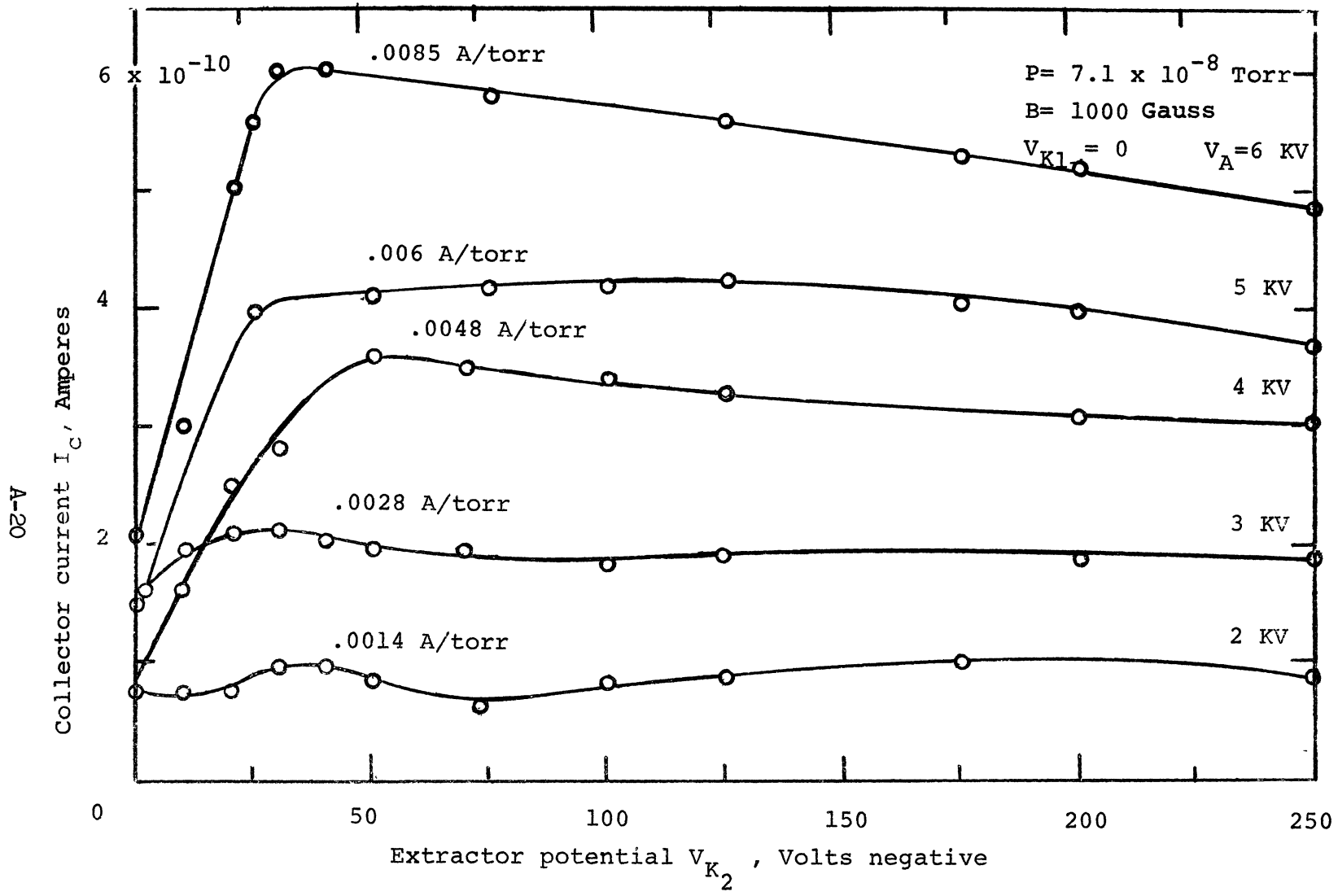

Figure A-6.- Collector current vs. negative extractor potential

It is apparent from these data that a relatively large number of ions have been successfully extracted from the discharge by the application of small negative potentials to K_2. Figure A 7 shows how the extracted ion currents I_{A_2} and I_C are affected by both positive and negative voltage on K_2. The ion current collected by the first cathode (I_{K_1}) is also shown. The collector ion current drops noticeably as V_{K_2} is varied from -30 volts to +30 volts. The corresponding change in I_{A_2} is less marked. At the same time the extracted ion current ($I_{A_2} + I_C$) decreases, the current in the first cathode, I_{K_1} increases.

These effects may be explained qualitatively in the following manner. As the extraction voltage, V_{K_2} is made more negative, ions are removed from the discharge which normally would be collected by K_1, hence the rise in extracted ion currents is accompanied by a reduction in the number of ions collected by the first cathode. However, the rise in extracted ion current reaches a plateau with further increase in V_{K_2} (negative) potential as does the attendant decrease in I_{K_1}. The fractional decline in I_{K_1} is accompanied by almost exactly the same fractional increase in collector current.

The fact that the collector current I_C, and first cathode current I_{K_1}, quickly reach maximum and minimum values as V_{K_2} is made more negative than 30 volts, is probably related to the geometry of the aperture holes. The arrangement of the three apertures, A_2, A_1 and the exit hole in K_2, permits the collector to view only a small effective volume of the discharge region When a certain fraction of the ions in this small volume have been extracted, the extracted currents cease to increase.

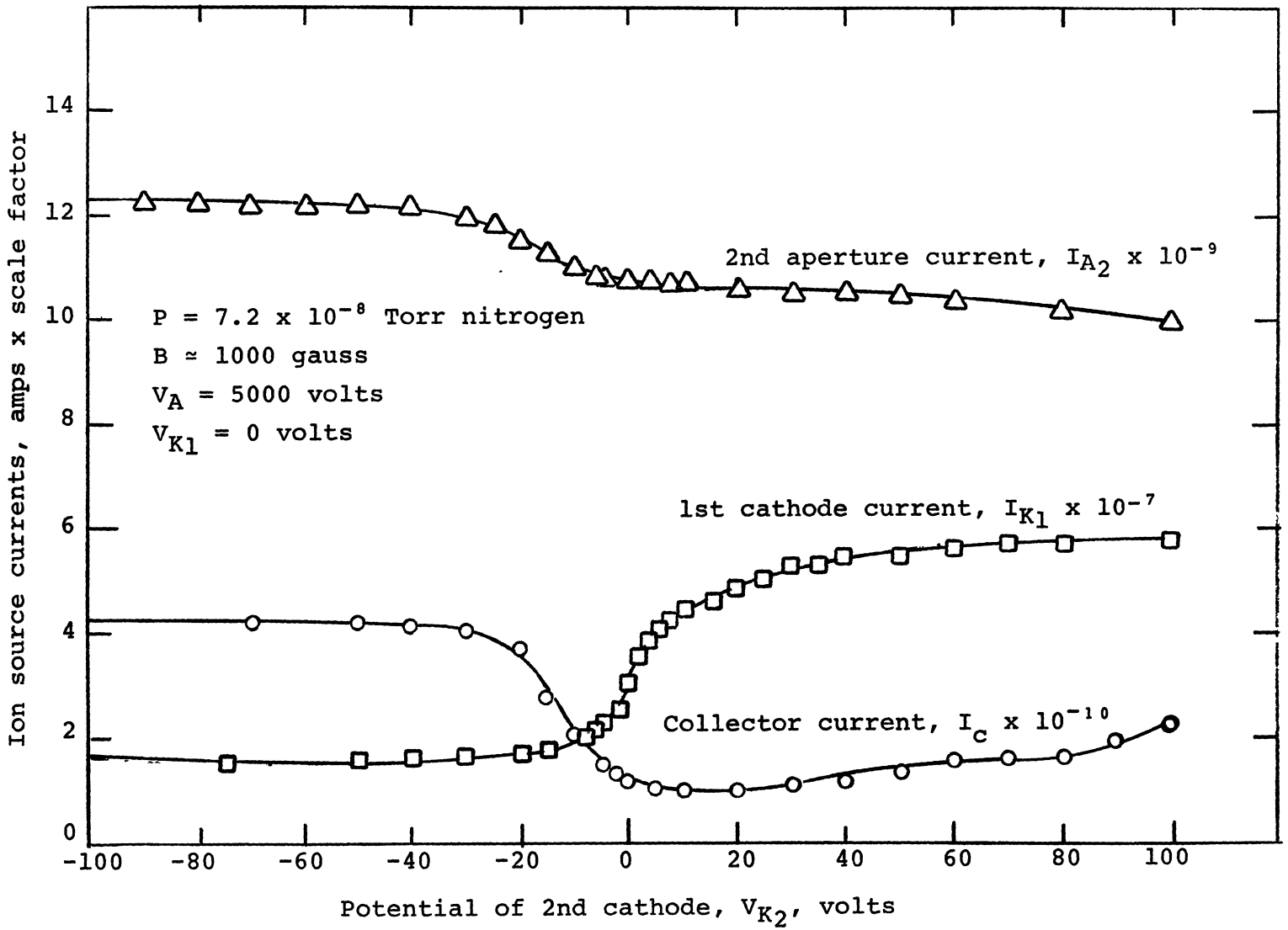

Figure A-7. - Ion extraction data - Method I - V_{K_2} negative

Figure A-8 shows that ions may be extracted from the discharge by applying ion repelling (positive) voltages to K_1. This plot also points out some noticeable differences between the two methods. The collector current becomes negative for negative values of V_{K_1}, suggesting the extraction of electrons from the discharge. The presence of electrons in the beam would also explain the more noticeable change in I_{A_2} (compared with Fig. A-7) with cathode potential. It would also explain why I_C saturates more slowly with cathode potential changes when this extraction method is employed.

Both methods yield nearly (within 15%) the same number of extracted ions per unit of pressure. However, other factors must also be considered in selecting the most desirable method of extraction. These factors are:

(1) Extraction Voltages - Method I (V_{K_2} negative) produces a maximum extracted ion current with 40 volts applied to K_2. Method II (V_{K_1} positive) requires slightly higher voltages to reach maximum.

(2) Beam Currents - Method II (V_{K_1} positive) produces evidence of an electron current component in the beam. Although electrons in the beam will not influence the mass analyzer, they do make the determination of correct source sensitivity more difficult.

(3) Energy Distribution - Method II requires larger potentials to extract the ions and therefore the emergent ion beam is likely to be of higher energy. Method I actually applies weak retarding fields (A_1 and A_2) with a subsequent reduction in energy of the beam.

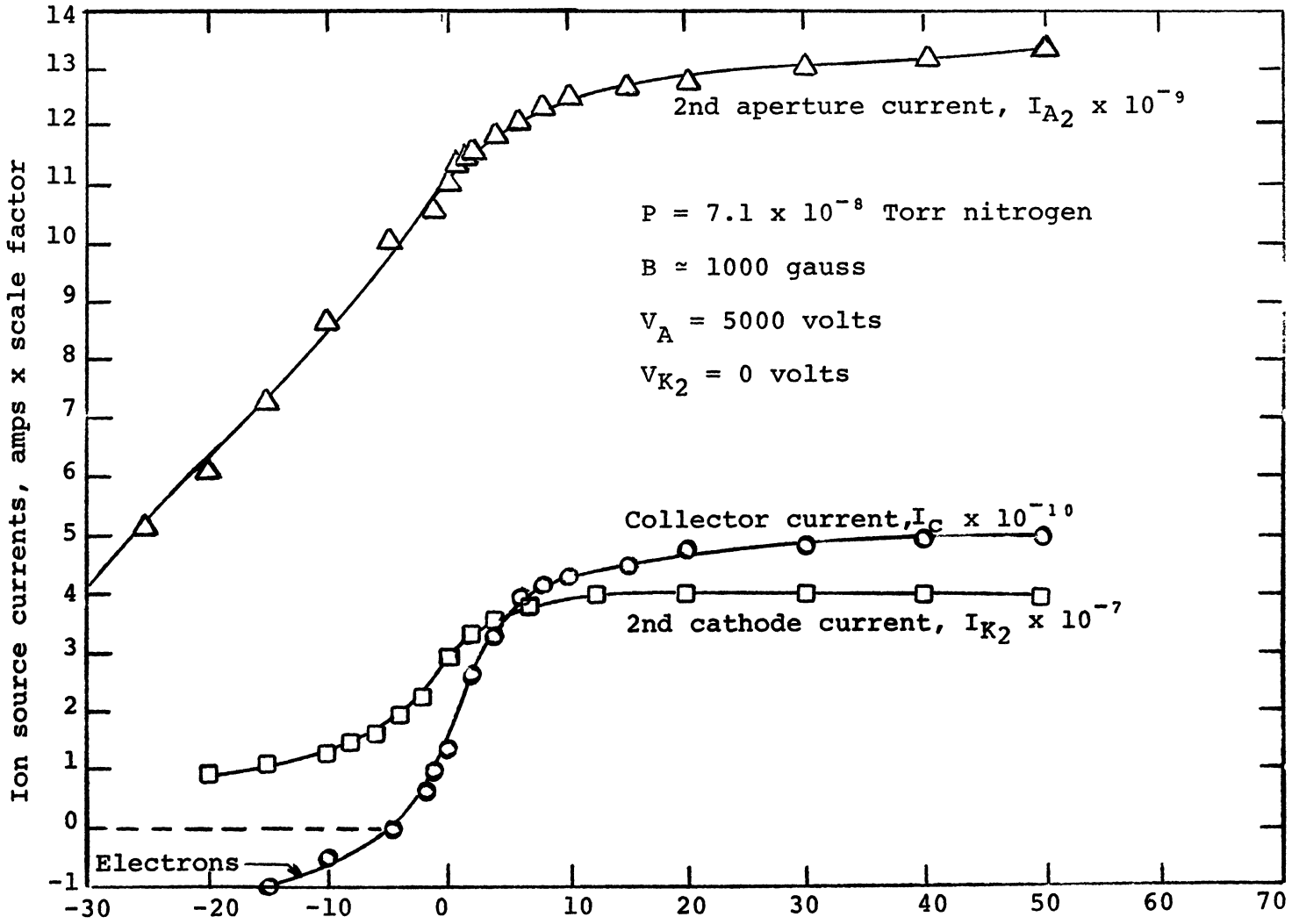

Figure A-8.-Ion extraction data - Method II - V_{K_1} positive

(4) Electronic Considerations - The ion current in K_1 produces a means of measuring total pressure within the future spectrometer. This measurement is most conveniently made with K_1 at ground potential.

After considering the above factors, it was concluded that Method I extraction was more desirable. This method was then used to study the ion source performance in more detail as described next.

Figure A-9 shows the energy distribution of an unfocused beam of ions striking the collector. These measurements were made using positive (retarding) potential at the collector to repel ions entering the collector box. This retarding field is a measure of the ion energy. These measurements have been made for a family of values of negative V_{K_2} potentials. It will be noted that the ordinate displays both positive (ion) current and negative (electron) current values. It will also be noted that the predominant charge carrier is the electron if V_{K_2} is zero or slightly negative. As V_{K_2} is made more negative, the predominant charge carriers become low energy ions.

Figure A-10 is a replot of the V_{K_2} = -40V data (Fig. A-9). This plot shows the distribution of ion energies in the beam in better perspective. This figure also shows that 97% of the collected ions have energies compatible with the quadrupole analyzer design to be discussed in the next section of this report. It therefore appears that the majority of ions extracted from this ion source will have a sufficiently small spread in energies to be analyzed by a practical design of quadrupole analyzer.

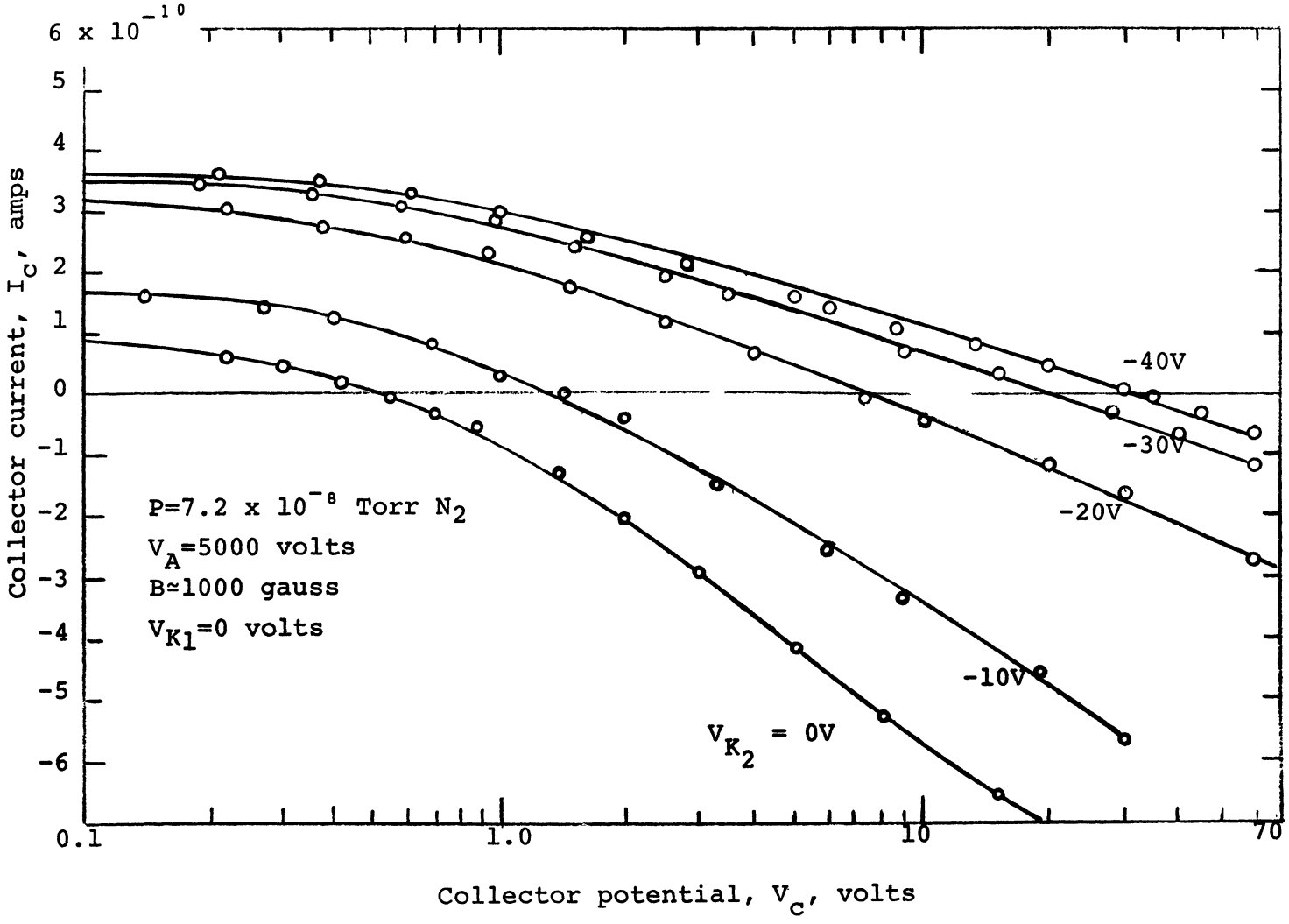

Figure A-9.- Collector current vs. collector potential
Unfocused beam - not corrected for contact potentials

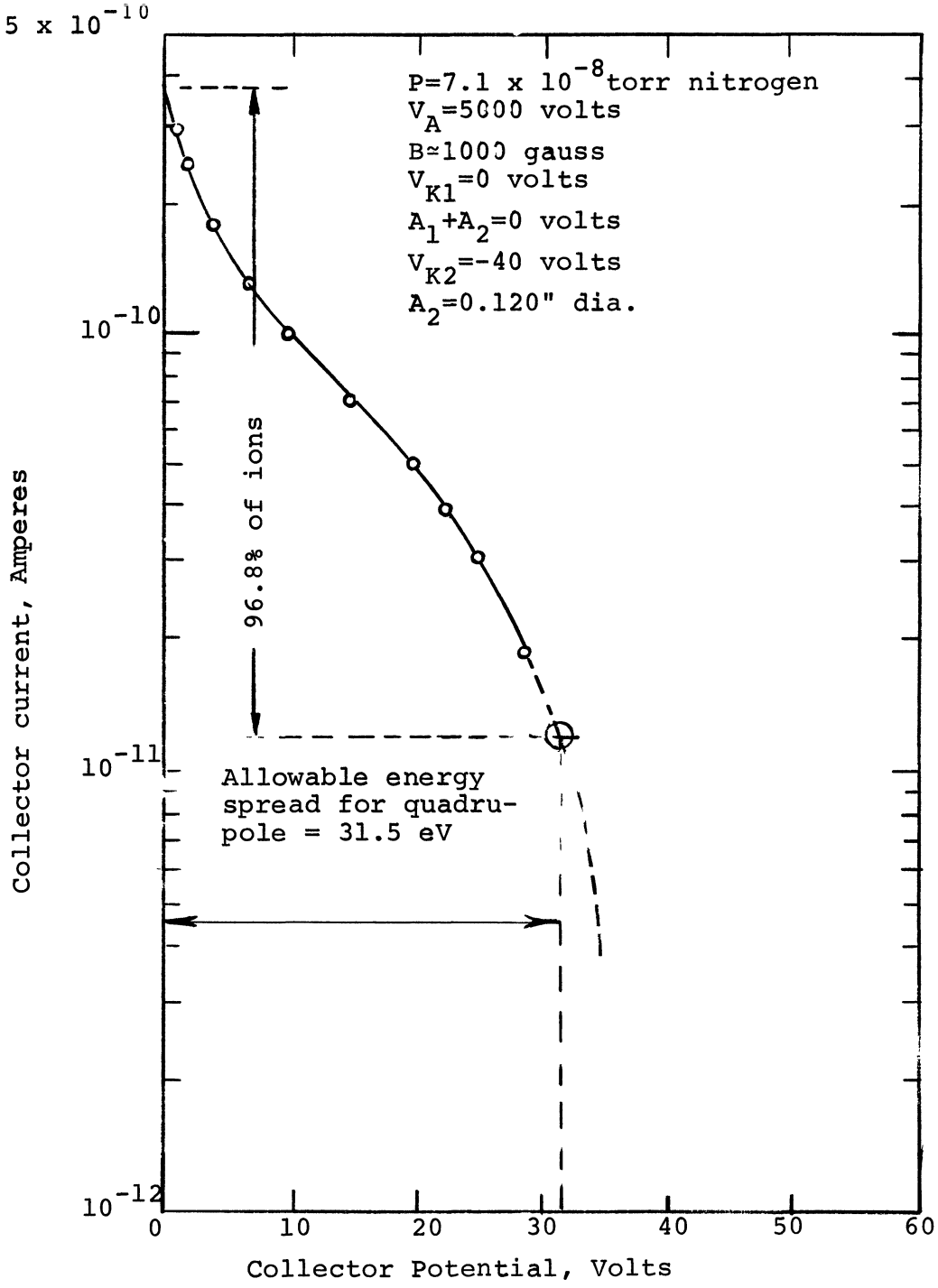

Figure A-10.— Unfocused ion energy distribution at ion collector

The very low energy ions encountered in the source were not confidently anticipated. The literature references accompanying this report do not parallel this experience. Previous experiences with a cold-cathode source yielded much larger ion energies (hundreds of electron volts). The reason may lie in the method of ion extraction wherein large accelerating fields were applied to the emerging ion beam. At the present time, the energy distribution of the ion beam appears perfectly matched to the requirements of the quadrupole mass analyzer.

Figure A-11 shows how the extracted ion currents and the discharge current respond to changes in pressure (nitrogen) from less then 10^{-9} Torr to 10^{-6} Torr. The ion source was baked at 400°C for approximately 18 hours prior to taking these data.

These data show that the total extracted ion current (in the linear region) is quite large. The sensitivity values noted on this graph were determined at a pressure of 10^{-7} Torr (nitrogen). The highest sensitivity for extracted ions was measured at the second aperture plate, A_2 and has a value of 0.16 amps/Torr. The collector sensitivity is 0.005 amps/Torr. This value is about one-half the value anticipated, but is 500 times the sensitivity of some hot-filament ion sources used in contemporary mass spectrometers. Attempts were made to focus more ions into the collector by applying suitable potentials to A_2. This resulted in an increase in collector sensitivity from 5 ma/Torr to 15 ma/Torr. It was evident, however, that better focusing means must be provided in future designs.

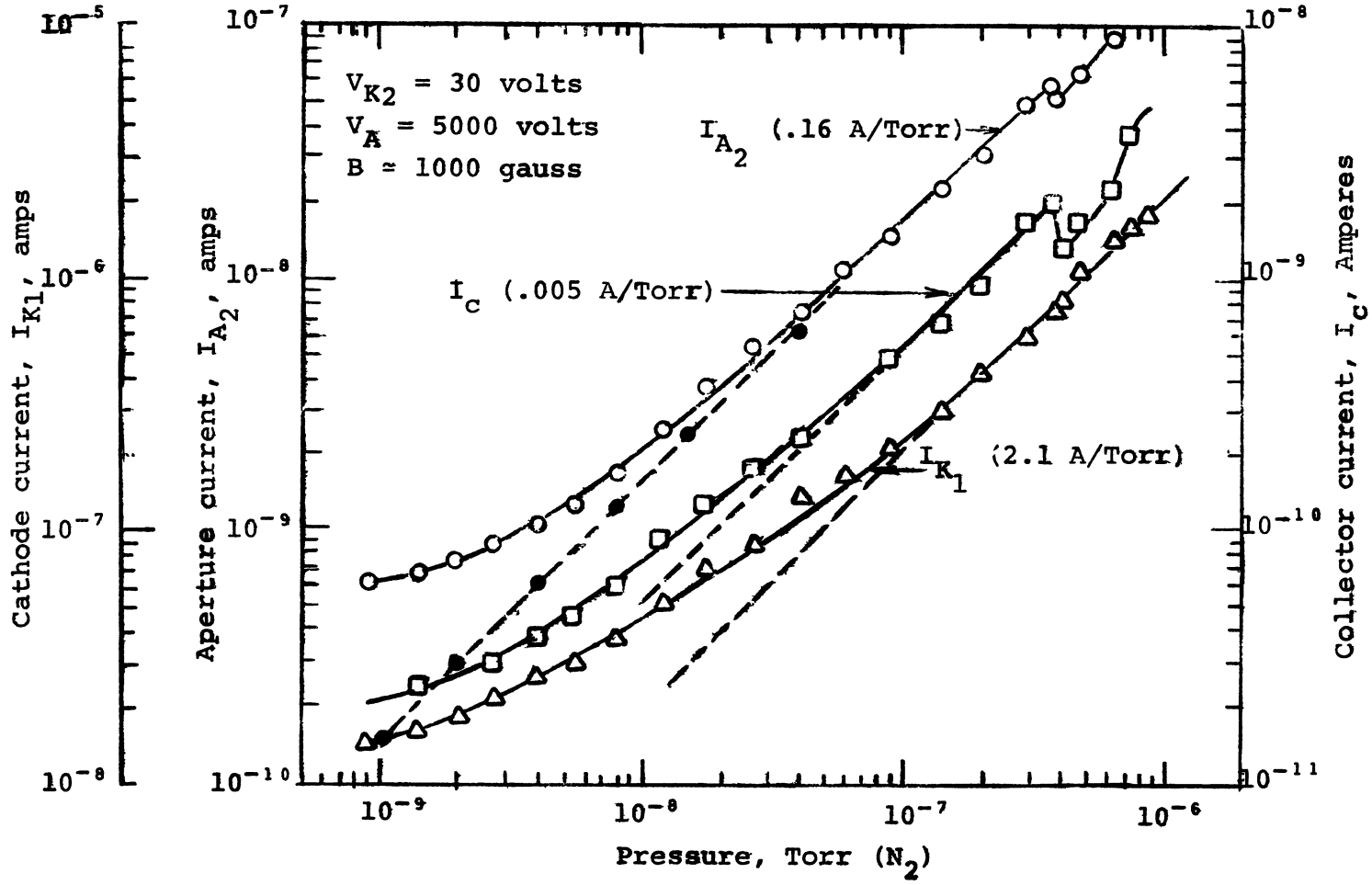

Figure A-11.- Ion currents vs. pressure

The non-linear response of the ion source below the mid 10^{-8} Torr range was not anticipated. Efforts were made to discover the cause of this problem but conclusive results are not yet available. It appears that the discharge itself was not producing any noticeable outgassing and there were no external leaks found in the source enclosure. It was theorized that a virtual leak existed in the source structure. The source was disassembled and it was noticed that the first collimator-pole piece (A_1) was wedged tightly in the source housing. This could lead to a noticeable virtual leak and hence to the non-linear responses shown by Fig. A-11. This problem can be easily corrected in the future.

If a virtual leak did exist in the source during this experiment, then by simply subtracting the current equivalent of this background pressure, the true response of the gauge would be linear. This has been done in the case of the I_{A_2} current curve and the results indicate this response curve is the sum of a constant (pressure independent) term and a linear function of pressure. It should also be mentioned that no "background" currents (in the absence of a magnetic field) were observed which were large enough to cause this effect.

SELECTION OF MASS ANALYZER

Mass Analyzers - General

Prominent characteristics of the beam extracted from a cold-cathode ion source are: (1) the relatively large beam cross section utilized in order to obtain high sensitivity, and

(2) the large spread in kinetic energy of the ions comprising the beam. In general, these are undesirable characteristics of an ion source for use with most mass spectrometers.

Several spectrometers are tolerant of an ion beam with a large spread in kinetic energy (ref. A22). Some of these utilize both magnetic and electrostatic fields such as the double focusing (ref. A23) or the cycloidal (ref. A24) mass spectrometers. However, in order to obtain high resolution with a large injected ion beam size, the spectrometer becomes large and costly. The presence of the large magnet required in these spectrometers is undesirable, not only because of their bulk and weight but also because of the unavoidable fringing field which is detrimental to the operation of the ion source.

Quadrupole Mass Filter

A mass analyzer that provides high resolving power for an ion beam of large size and energy spread is the electric quadrupole mass filter (ref. A25). It is small, light in weight and relatively simple in construction. There is no magnet with the associated fringing field problem and the electric fringing field may be shielded from the ion source. The mass filter may be constructed entirely of materials that are bakeable to temperatures required for attainment of UHV. It has been shown by Brubaker (refs. A26, A27) to be well suited for use in satellites as a mass analyzer. Scanning of the complete mass range under consideration may be rapidly carried out by varying voltage or frequency. The disturbing effect of contact potentials which occur in some spectrometers are minimized due to the high potentials applied to the mass filter electrodes.

The quadrupole mass filter consists of four parallel cylindrical rods equally spaced on a circle of radius r_o, about equal to the rod diameter. Opposite pairs of rods are electrically connected together. An electrostatic potential, U, and an rf potential, V, of frequency, ν, are applied to the rods as shown in Fig. A-12. The equations of motion for an ion of mass M and charge e in the field of these rods are,

$$M\ddot{x} + e(U + V \cos 2\pi \nu t) \frac{x}{r_o^2} = 0$$

$$M\ddot{y} - e(U + V \cos 2\pi \nu t) \frac{y}{r_o^2} = 0 \qquad \text{(A1)}$$

Paul et al. (refs. A25, A28-A30) and Fischer (ref. A31) show these equations to be forms of the Matthieu equation. The solutions to that equation correspond to stable (bounded) and unstable (unbounded) trajectories of the ions. Whether the motion of an ion is bounded or unbounded depends on the mass and charge of the ion and the voltages applied to the rods. Of all the ions injected with finite momenta into a quadrupole mass filter, those that are unstable and those stable ions whose maximum amplitude is $\geq r_o$ will be captured by the rods after a sufficient number of cycles of the rf field. In this manner only a small band of masses manage to travel the length of the quadrupole, where these ions are collected and detected.

General Design Criteria

Paul et al. have provided criteria for the design and the capabilities of the quadrupole mass filter. They show that the mass filter provides a stable trajectory for ions of mass,

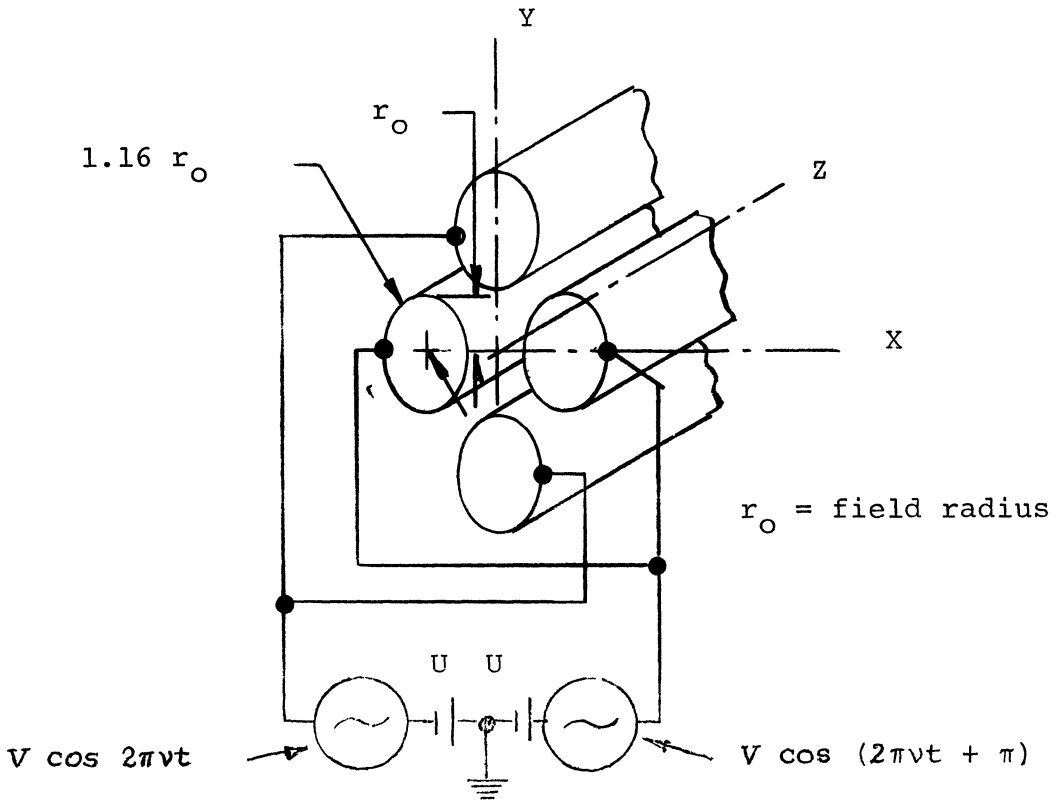

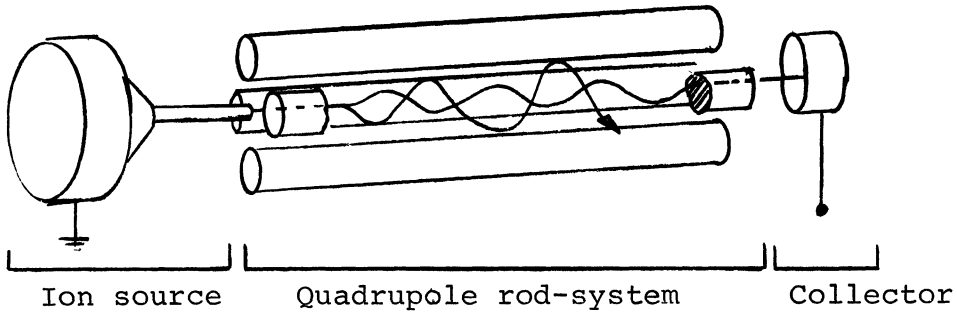

Figure A-12.— Schematic view of quadrupole mass filter

$$M = 2.30 \times 10^{-20} \frac{V}{\nu^2 r_o^2} \qquad \text{(A2)}$$

The mks system will be used throughout unless otherwise noted. Equation (A2) is plotted for various ν and r_o in Fig. A-13.

The resolution of the mass filter is defined as the mass of the ion divided by the width of the mass peak at its base.

$$\text{Resolution} = \frac{M}{\Delta M} = \frac{0.126}{0.16784 - \frac{U}{V}} \qquad \text{(A3)}$$

Design criteria to obtain a given resolution with 100% transmission of the stable ions are:

$$\left.\begin{array}{l} \text{Required voltage stability,} \\ \qquad = \frac{1}{2}\left(\frac{\Delta M}{M}\right) \\ \text{Required frequency stability and dimensional accuracy,} \\ \qquad = \frac{1}{4}\left(\frac{\Delta M}{M}\right) \end{array}\right\} \qquad \text{(A4)}$$

Maximum allowable transverse energy of ions injected on axis,

$$= U_{T_{max}} = \frac{V}{15}\left(\frac{\Delta M}{M}\right) \qquad \text{eV} \qquad \text{(A5)}$$

Maximum allowable axial energy of ions for ion selection to occur,

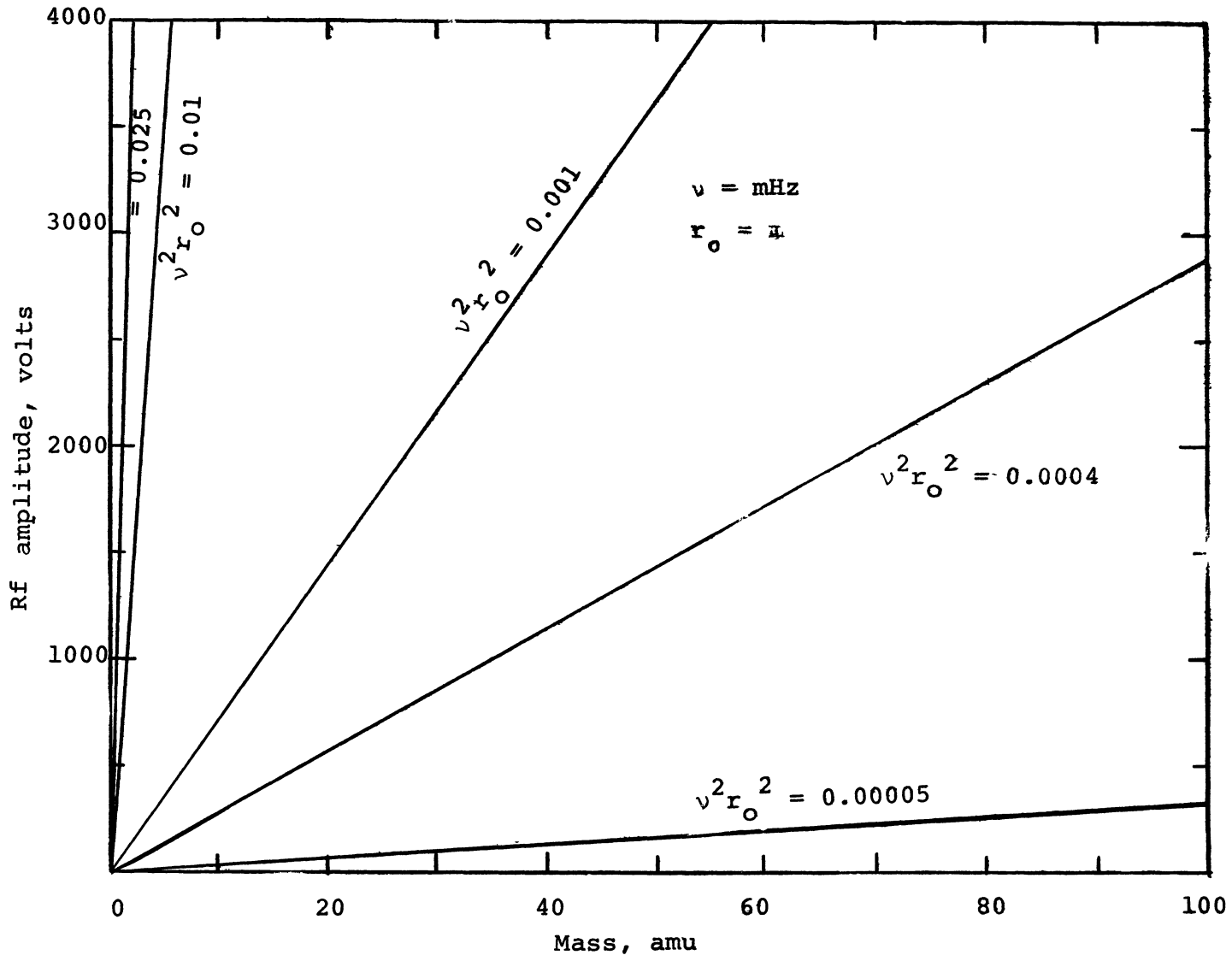

Figure A-13.- Rf amplitude vs. mass of ion

$$= U_{A_{max}} = 5.82 \times 10^{-3} \frac{L^2 V}{r_o^2} \frac{\Delta M}{M} \quad \text{eV} \tag{A6}$$

where L is the length of the quadrupole rods.

Maximum allowable ion beam size for axially directed ions,

$$= d_{max} = r_o \left(\frac{\Delta M}{M}\right)^{\frac{1}{2}} \tag{A7}$$

The power dissipated in the device is

$$P = 2.36 \times 10^{40} \frac{C M^2 \nu^5 r_o^4}{Q} \tag{A8}$$

where C is the total capacitance and Q is the figure of merit for the final tank circuit of the rf generator. This power dissipation is plotted versus ν^5 in Fig. A-14 for various rod radii assuming C=100 pf. and Q=300. Also included are curves of equal rf voltages for ions of mass 100 amu. Ions of smaller mass are represented by similar curves nearer the abscissa.

Using the above criteria it has been shown (ref. A29) that a mass filter can be designed to provide variable resolution with a maximum resolution sufficient to separate adjacent ions of atomic mass 100 and less. At the same time, the filter can be made to yield 100% transmission for the stable ions. This is desirable not only for high sensitivity but, what is more important for mass spectrometry, relative ion abundances may be directly compared.

It should be mentioned here that the monopole mass filter, first described by von Zahn (ref. A32) has most of the desirable characteristics of the quadrupole, and is simpler to construct.

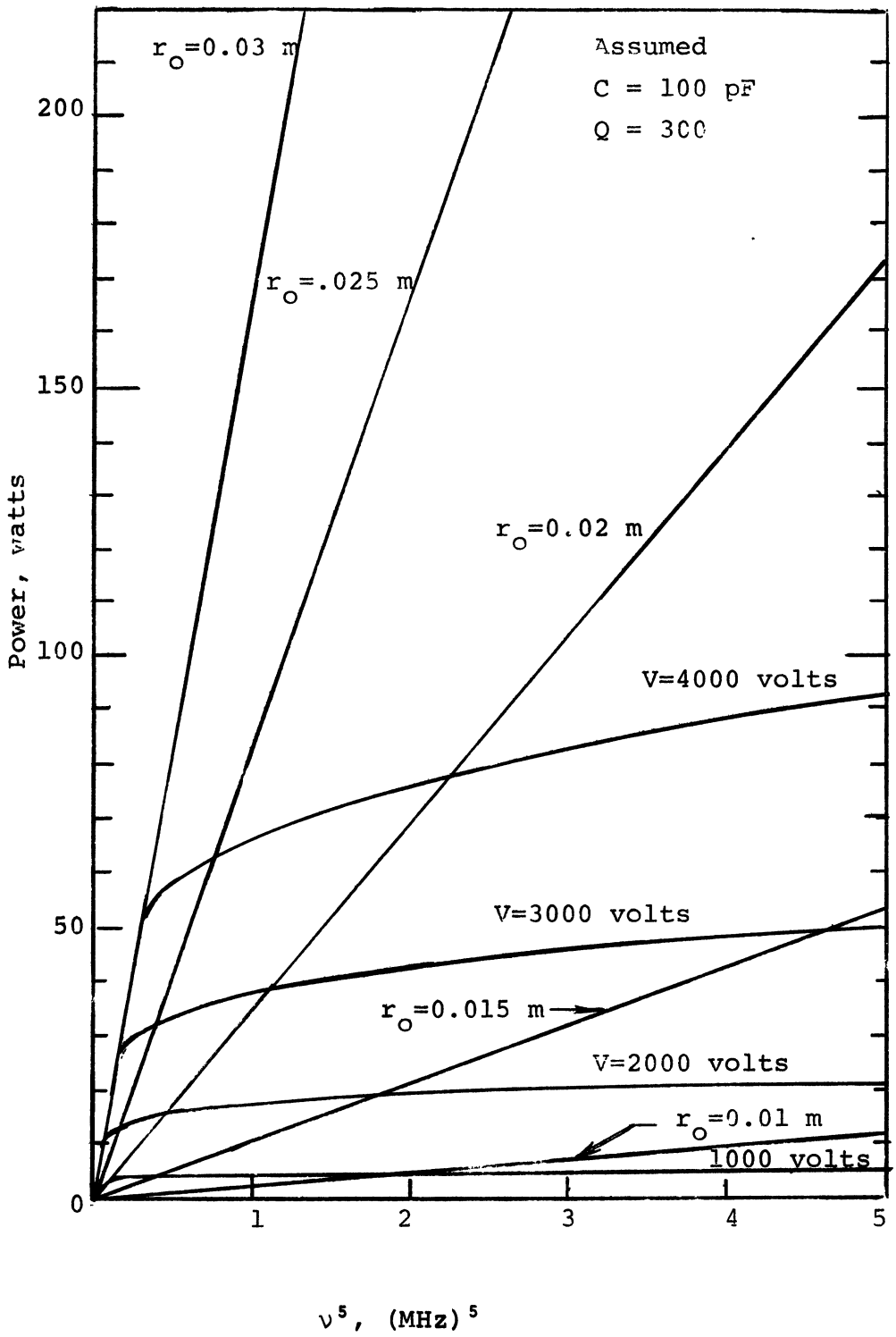

Figure A-14.- Maximum power Required for mass 100 a.m.u. ions vs. fifth power of frequency

However, due to its inherently lower transmission as compared to the quadrupole, it was not considered further for use as the analyzer.

Mass Scanning Modes

In considering the above criteria, the three principal modes of scanning the mass spectrum were examined. As seen from Eq. (A2), mass scanning may be accomplished by varying either the frequency or the voltages. The three modes considered have been previously reported in the literature and are listed below.

Mode 1 U and V varied such that $\frac{U}{V}$ = constant, ν = constant (Paul et al. (ref. A28)). Resolution is constant for the entire mass spectrum.

Mode 2 U = aV-b, ν = constant, where a and b are constants (C. E. Woodward and C. K. Crawford, (ref. A33)). Line width is constant for the entire mass spectrum.

Mode 3 $\frac{U}{V}$ = constant, ν varying (von Zahn, (ref. A32)). Resolution is constant for the entire mass spectrum.

We choose the mass range of interest to be M = 2 to 100 amu. Thus, in order to separate ions of adjacent mass, we must have for Mode 2, ΔM = 1 amu, and for Modes 1 and 3, $\frac{M}{\Delta M}$ = 100. For Modes 1 and 3, Eq. (A3) yields

$$\frac{U}{V} \text{ (Modes 1,3)} = 0.16658 \qquad \text{(A9)}$$

In the case of Mode 2, we substitute U = aV-b into Eq. (A3) and obtain,

$$\Delta M = 7.94(0.16784 - a)M + \frac{bM}{0.126V} \qquad \text{(A10)}$$

Substituting Eq. (A2) into the last term in Eq. (A10) we have,

$$\Delta M = 7.94(0.16784 - a)M + \frac{1.825 \times 10^{-19} b}{\nu^2 r_o^2} \qquad \text{(A11)}$$

Thus from Eq. (A11), we see that if a is chosen to be 0.16784, the line width is independent of mass. Assuming for Mode 2 that ΔM = 1 amu, we may solve Eq. (A11) for b and obtain the relation between scanning voltages for Mode 2,

$$U(\text{Mode 2}) = 0.16784V - 9.10 \times 10^{-9} \nu^2 r_o^2 \qquad \text{(A12)}$$

Comparison of Scanning Modes

In order to compare operation of the mass filter in the three modes, we consider the allowable energy spread of the ions and the maximum tolerable spread of the ion beam.

Allowable transverse momenta of ions. - Substituting Eq. (A2) into Eq. (A5), we have

$$U_{T_{max}} = 2.9 \times 10^{18} \nu^2 r_o^2 \Delta M \qquad \text{eV} \qquad \text{(A13)}$$

Therefore, $U_{T_{max}}$ is independent of mass for Mode 2. Assuming reasonable values of ν = 1.10 mHz , , and r_o = 0.02 m, in

order to be consistent with reasonable values of rf voltage (3500 volts) and power dissipation (56 watts), we have

$$U_{T_{max}} \text{ (Mode 2)} = 2.32 \qquad \text{eV}$$

Comparing this with operation in Mode 1, where $\frac{M}{\Delta M} = 100$, we see from Eq. (A13) that

$$\frac{U_{T_{max}}\text{(Mode 1)}}{U_{T_{max}}\text{(Mode 2)}} = \frac{M^*}{100}$$

where M* is the ionic mass in amu. Thus, for mass 100 amu ions, Modes 1 and 2 have comparable transverse energy tolerance, but for smaller masses, Mode 1 can tolerate less, being only 2% that of Mode 2 for hydrogen ions.

Equation (A5) shows that Mode 3 with the value of V given above can tolerate,

$$U_{T_{max}}\text{(Mode 3)} = 2.32 \qquad \text{eV}$$

so that Mode 3 tolerates the same constant value over the mass spectrum as does Mode 2.

$U_{T_{max}}$ is plotted in Fig. A-15 as a function of r_o^2 for various values of ν in Mode 2 operation.

Allowable axial momenta of ions. - In order that selection of the stable ions occur, it is necessary that the initial kinetic energy be less than that given by Eq. (A6). Substituting Eq. (A2) into Eq. (A6), we have

$$U_{A_{max}} = 2.53 \times 10^{17} L^2 \nu^2 \Delta M \qquad \text{eV} \qquad \text{(A14)}$$

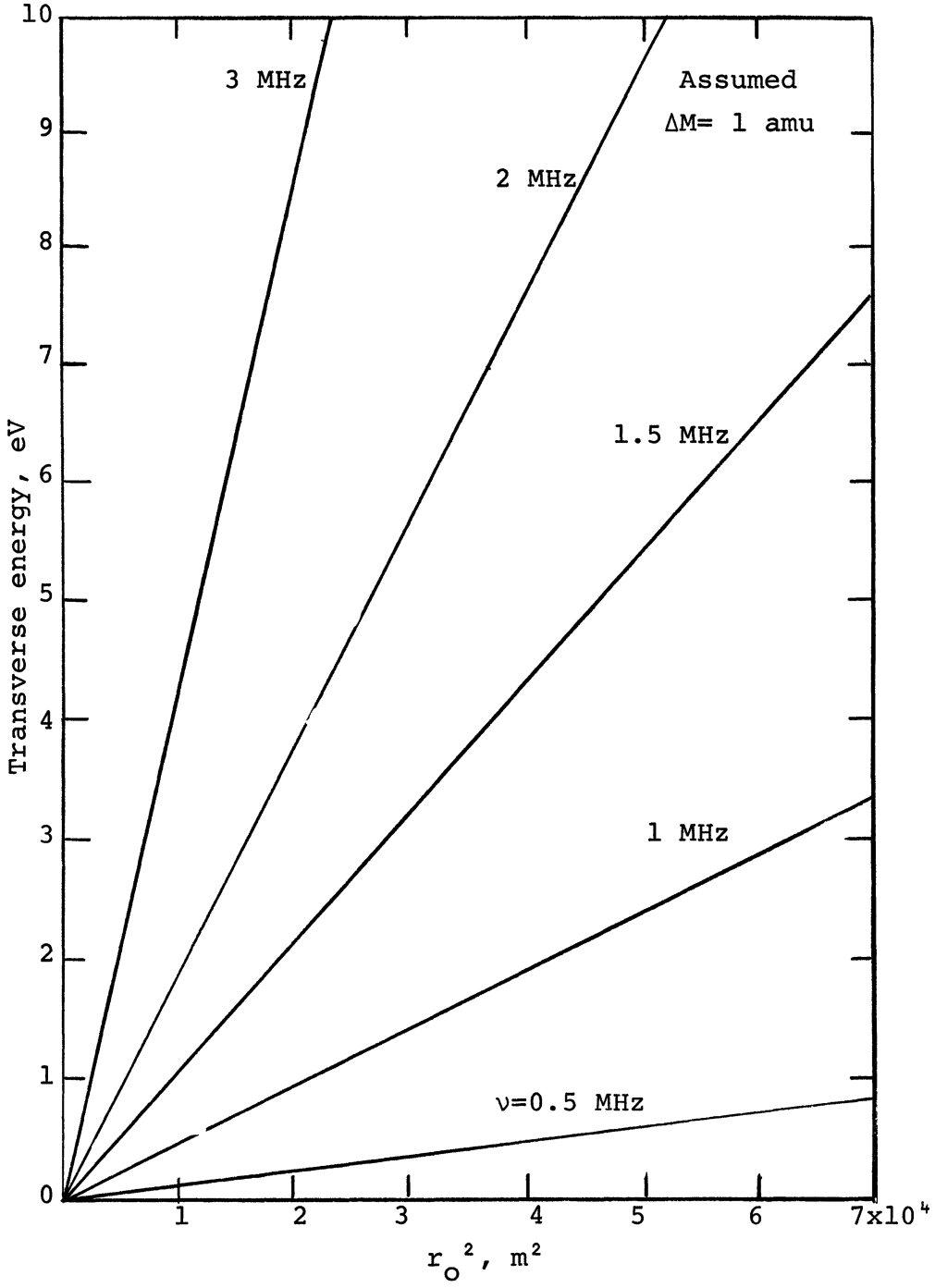

Figure A-15.— Maximum transverse voltage for unity transmission vs. field radius squared

Although we see that $U_{A_{max}}$ increases with the square of the guadrupole length, in the interest of keeping the spectrometer small, we shall assume L = 0.25 m. Thus for the values assumed in the previous subsection above, we see that Mode 2 can tolerate for ions of all masses, a constant axial energy equal to

$$U_{A_{max}} = 31.5 \qquad \text{eV}$$

For Mode 1, we see as before,

$$\frac{U_{A_{max}} \text{ (Mode 1)}}{U_{A_{max}} \text{ (Mode 2)}} = \frac{M^*}{100}$$

so that Mode 1 tolerates less axial ionic energy than does Mode 2 for ions of $M^*<100$ amu.

For Mode 3, we refer to Eq. (A6) and for an rf voltage of 3500 volts, we have

$$U_A \text{ (Mode 3)} = 31.5 \qquad \text{eV}$$

so that Modes 2 and 3 tolerate equal constant ion energies over the whole mass spectra.

$U_{A_{max}}$ is plotted in Fig. A-16 as a function of rod length, L for various values of ν in Mode 2 operation.

Maximum allowable ion beam diameter. - The maximum diameter of an axially directed ion beam which has unity transmission through the mass filter, is approximately

$$d_{max} = r_o \left(\frac{\Delta M}{M}\right)^{\frac{1}{2}} \qquad \text{(A7)}$$

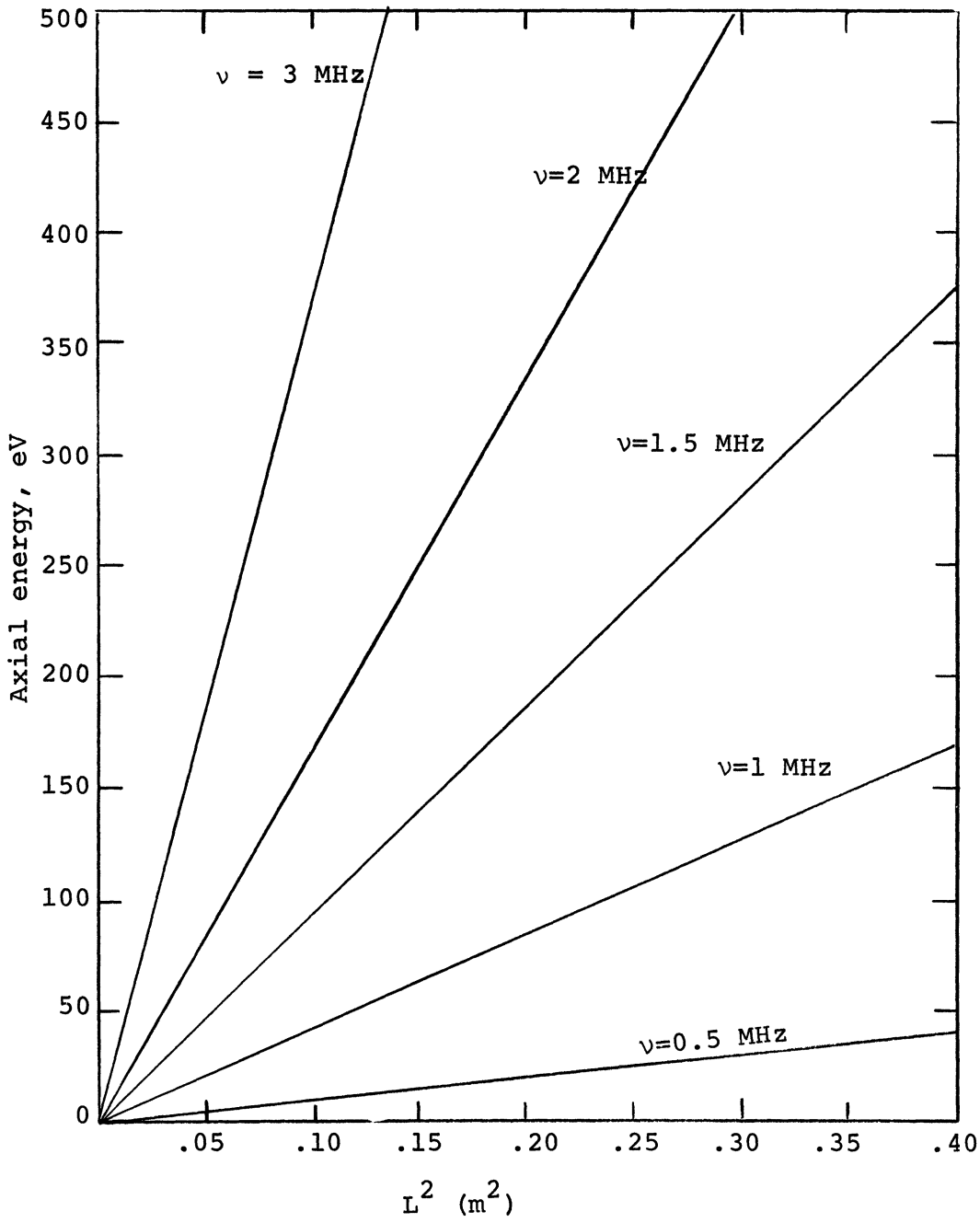

Assume ΔM = 1 amu

Figure A-16.— Maximum tolerable axial ion energy for selection to occur vs. rod length squared
Assumed ΔM = 1 amu

Thus, for Modes 1 and 3,

$$d_{max}\ (\text{Modes } 1,3) = \frac{r_o}{10}$$

However, for Mode 2 with M = 1 amu,

$$d_{max}\ (\text{Mode } 2) = \frac{r_o}{M^{*\frac{1}{2}}} \tag{A15}$$

Therefore, the beam diameter that the mass filter can transmit is always larger for Mode 2 for masses less than 100 amu.

We now assume that the beam diameter is larger than given by Eq. (A7) and calculate the transmission of the beam assuming the ions are uniformly distributed across the beam with density $\sigma(kg/m^2)$. Thus, if the beam diameter is $d>d_{max}$ we have, approximately, for the transmission,

$$T = \frac{\sigma\pi\frac{d_{max}^2}{4}}{\sigma\pi\frac{d^2}{4}} = \frac{r_o^2\,\frac{\Delta M}{M}}{d^2} = \frac{r_o^2}{d^2}\,\frac{\Delta M}{M} \tag{A16}$$

This is plotted in Fig. A-17 as a function of mass for Mode 2.

Frequency and voltage stability. - From Eq. (A4) we see that the frequency and voltage stability required are inversely proportional to the resolution, $M/\Delta M$. Thus, these requirements are the same in all modes for ions of mass 100 amu, but ions of smaller mass have less stringent requirements in Mode 2, due to its decrease in resolution with ionic mass.

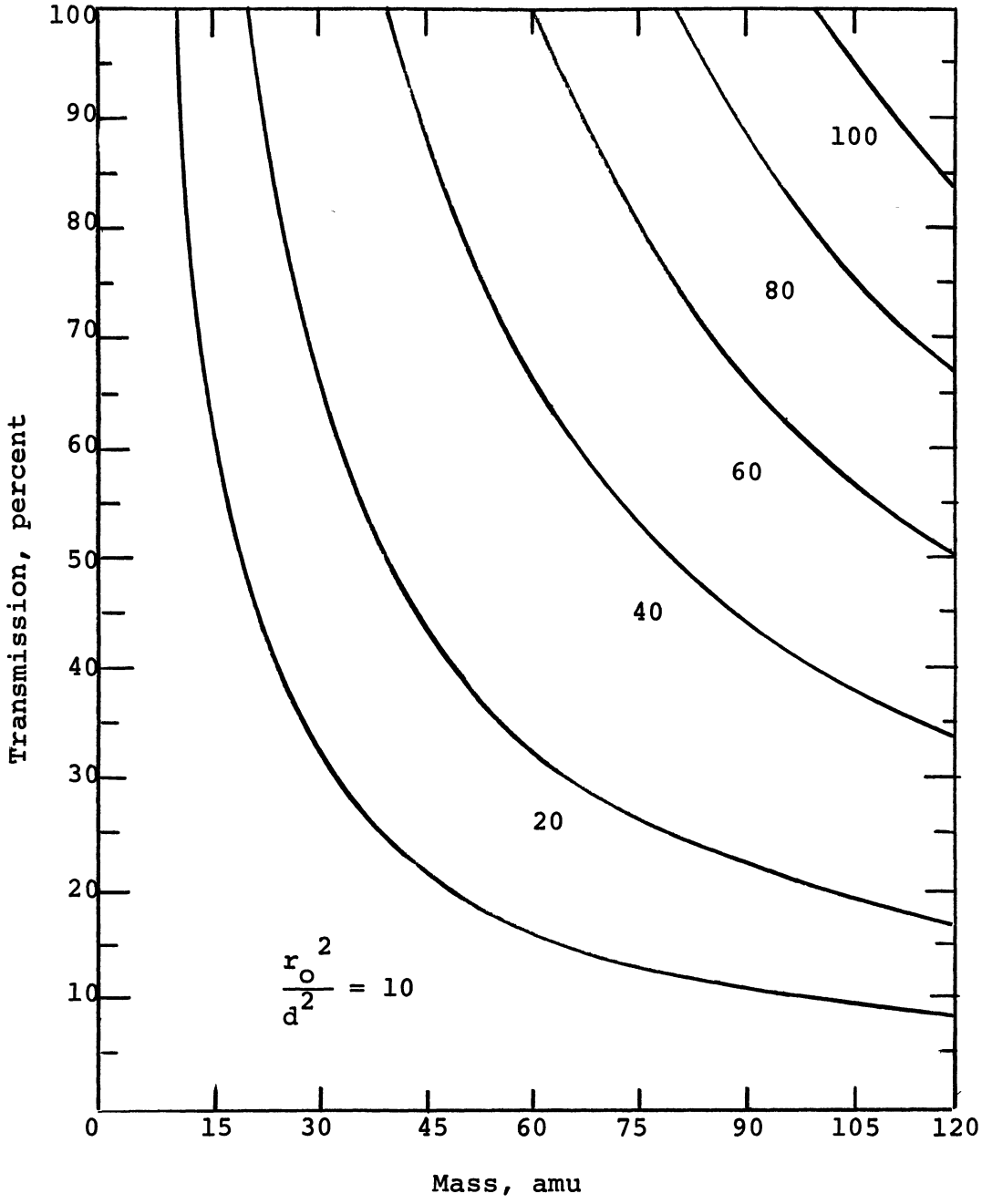

Figure A-17.- Transmission of mass filter vs. mass of ion

Assumed ΔM = 1 amu

Choice of Mass Scanning Mode

From the preceding discussions of scanning modes, we see that operation in Mode 1 is inferior in all respects to operation in Mode 2 for ionic masses less than 100 amu. The frequency varying Mode 3 is seen to tolerate the same initial ion energies as does Mode 2, but the latter tolerates a larger ion beam size and requires less frequency and voltage stability than the former for masses less than 100 amu. If, however, the beam is kept small and if the power supply is stabilized well enough for transmission of mass 100 amu, then Mode 2 has no advantage over Mode 3 on the basis of the above criteria.

The choice of Mode 2 over Mode 3 is made on the basis of engineering considerations. Frequency scanning from 2-100 amu is seen from Eq. (A2) to require a frequency span of 7:1. Circuit design requires this be done in 3 or 4 separate tuning ranges. Each range requires a different value of V. Thus, some scan ranges would have less than the maximum value of 3500 volts assumed above. Equations (A5) and (A6) show that this would decrease the tolerable initial ion energy below that of Mode 2. In addition, there are many practical problems involved in designing a 350 $\pm$ 0.5% volt rf generator which is tunable and stabilized over a wide frequency range.

On the other hand, a workable quadrupole mass filter operating in Mode 1 has been built by Shoulders (ref. A34). Whightman, of the National Research Council, who has successfully used Shoulders' design, points out that conversion of the electronics for operation in Mode 2 would be a simple and straightforward procedure.

It is concluded that the mass filter should be operated in Mode 2.

Entrance Conditions

The equations of motion, (A1), for the ions in the mass filter have implicitly within them that the rod length, L, is infinite. In other words, it is assumed that there is no fringing field to disturb entering ions. Paul et al. (ref. A25) first suggested the possibility that the fringing field is responsible for attainment of smaller transmission than theoretically expected. Brubaker (ref. A26) suggested that loss in transmission noted by him at higher frequencies and at lower energies is due to the fringing field.

In their mass filter, Paul et al. used a cylindrical canal which was maintained at zero potential, the potential of the quadrupole axis. If their reported loss in transmission is due to entrance fringing field, it is obvious that extending the canal farther into the quadrupole field should serve to minimize the effect of this field.

The effect of the perturbation of the quadrupole field by the canal was studied. Using Eq. (A15) to define the minimum canal needed and assuming a 0.05 cm thick wall for the canal, we find the perturbation of the quadrupole potential at the circumference of the canal to be less than 0.6%. Since the stability required of the voltages is seen from Eq. (A4) to be 0.5% for a resolution of 100, the effect of the canal extending into the mass filter well beyond the fringing field region is negligible.

In order to minimize the effect of the fringing field, Redhead's group at the National Research Council, Ottawa, following Shoulders' work, has used the wide mass range focusing

properties of an rf quadrupole lens. This lens is capacitively coupled to the mass filter rods and positioned so as to surround the electron optical elements coupling ion source to mass filter. Such a lens minimizes the defocusing action of the transition field region.

A problem which must be considered when using a magnetron ion source is the high energy of the extracted ions. The results presented in the COLD-CATHODE ION SOURCE section suggest that no such problem exists with the present ion source design since the majority of the ions have energies small enough to be handled by the mass filter suggested here. However, focusing of the beam into the entrance canal is required. If the focusing is accomplished with cylindrical or aperture lenses the ions will be accelerated and thus will be too energetic to be selected by the mass filter. A solution to this would be to electrically separate source and analyzer and interpose a retarding field. A more attractive solution would be the use of a unipotential lens (ref. A35) system which introduces no net change in energy of the focused ions.

In designing the electron optical system an important consideration is the maximum angle which entering ions can make with the axis. The tangent of this angle is given by:

$$\tan \theta = \frac{\text{Max. tolerable transverse velocity}}{\text{Max. tolerable axial velocity}} = \frac{v_{T_{max}}}{v_{A_{max}}} \qquad \text{(A17)}$$

Now since

$$U_{T_{max}} = 1/2M(v_{T_{max}})^2$$

and

$$U_{A_{max}} = 1/2M(v_{A_{max}})^2 \qquad \text{(A18)}$$

Therefore, combining Eqs. (A5), (A6), (A17), and (A18) we have

$$\tan \theta = 3.38 \frac{r_o}{L} \qquad \text{(A19)}$$

ION COLLECTION AND DETECTION

The ions emerging from a mass filter tend to make large angles with the axis of the filter. As a result of this, the area of the collector must be large. A Faraday cup of area equal to the exit area of the mass filter would be admirably suited to serve as the collector. With a vibrating reed electrometer having a limit of detectability of 2×10^{-17} amperes arranged so as to read the ion input to the Faraday cup, we could measure a partial pressure of 4×10^{-16} Torr if the ion source sensitivity is .05* amps/Torr and the transmission of the mass filter is unity. The use of an electron multiplier as an amplifier to feed into a less sensitive electrometer, leads to approximately the same minimum detectable partial pressure. The reason for this lies in the dark current flowing in the anode circuit of the multiplier in the absence of a

*This sensitivity figure is assumed to apply over the entire pressure range of interest to this discussion.

signal input to the first dynode. The magnitude of this dark current in a well designed electron multiplier tube is about 10^{-10} amperes. For an assumed gain of the multiplier of 10^7 this corresponds to an equivalent input current to the first dynode of 10^{-17} amperes. Thus, we see that with this combination of electron multiplier and electrometer and an ion source sensitivity of .05 amps/Torr, the minimum detectable partial pressure is of the order of 10^{-16} Torr.

It should be stated here, however, that the time constant of the vibrating reed electrometer in measuring currents on the order of 10^{-15} amps or less, is excessively large, being several seconds in the case of the smaller currents. Thus for measuring these small currents, the electron multiplier with microsecond response is a preferable detector.

In order to measure partial pressure less than 10^{-16} Torr, the electron multiplier may be used to count ion pulses. In this case, each ion input will correspond to one standard size output pulse. By integration of these output pulses, the ion current can be measured. Using counting methods, the highest counting rate presently possible is about 10^6 pulses per second. This corresponds to a current of 1.6×10^{-13} amperes. Assuming an ion source sensitivity of 0.05 amps/Torr, we see that pressures higher than 3×10^{-12} Torr cannot be measured using ion counting techniques. If methods become available for pulse counting at higher rates, the multiplier characteristics then determine the highest pressure measurable. The dead time of a multiplier which is the time required for the secondary electrons generated as a result of one ion input to avalanche and reach the anode is on the order of 10 nanoseconds. Thus a maximum in-

put to the first dynode of 10^8 ions per second could be measured. This would correspond to a maximum measurable pressure of 3×10^{-10} Torr.

The lower limit measurable with the counting technique is again determined by the electron multiplier dark current. Now however, we must consider how many standard pulses per second this dark current corresponds to. Some pulses may correspond to electrons originating in dynodes beyond the first, thus, not yielding a standard pulse. The characteristic curve for an electron multiplier delineating the pulse height distribution would be required, therefore, before the counting rate lower limit may be stated with certainty. It is estimated that the minimum detectable counting rate corresponds to a current less than 10^{-17} amperes, and therefore, this could be more sensitive than the other methods discussed above.

As has been stated before, the ions emerging from the mass filter make large angles with the axis, and thus, a large detector area is required. The area of the first dynode in a normal electron multiplier is small, making it unsuitable for our purposes. Several alternatives have been suggested. First is the use of different multiplier structures, such as the tubular (refs. A32, A37) multiplier, or the disc-type multiplier used by Shoulders, or even the Venetian-blind multiplier. Perhaps the most satisfactory alternative would be the use of scintillation crystals, with or without an intermediate dynode. One complication arising in this latter method is the need for ten to twenty thousand eV of ion energy. The shielding of the mass filter from such voltages may prove to be a problem. In whatever method chosen, we must keep in mind the requirement for bakeability. Paul Redhead has noted that ultrahigh vacuum is hard to reach with any multiplier.

It should be pointed out that in the case of the large entrance area multipliers, the entrance angle of the ions is important in determining the multiplication to be expected. One does not have this problem with the scintillation scheme discussed above. In addition, the problem could be minimized using the resistance strip magnetic electron multiplier described by Goodrich and Wiley (ref. A38). This multiplier is reported to have a gain of over 10^7, and dark currents corresponding to less than one-tenth electron per second input to the cathode. The cathode is a large surface perpendicular to the direction of the entering beam of ions. Magnetic fields of only 400 gauss are required. Using the ion source, discussed above, partial pressures as low as 1.7×10^{-19} Torr might be measured, using continuous current methods. This is superior to the normal electron multiplier and to the vibrating reed electrometer. If a satisfactory multiplier of this type is available commercially it is recommended as the detecting scheme for the ions from the mass filter.

CONCLUSIONS

This study effort has shown that the development of an ion source and quadrupole mass analyzer suitable for extreme high vacuum mass spectrometry appears quite feasible. The quadrupole analyzer is shown to be uniquely suited to the mass separation of a beam of low energy ions extracted from the cold-cathode source. It also appears that a suitable lens system can be designed to further improve the sensitivity of the ion source described herein without compromising the performance of the analyzer.

Further work is necessary, however, before a prototype model of such a spectrometer can be constructed.

APPENDIX A

REFERENCES

A1. Redhead, P. A.: The Magnetron Gauge: A Cold-Cathode Vacuum Gauge. Can. J. Phys., vol. 37, 1959, pp. 1260-1271.

A2. Hobson, J. P.; and Redhead, P. A.: Operation of an Inverted Magnetron Gauge in the Pressure Range 10^{-3} to 10^{-12} MM. Hg. Can J. Phys., vol. 36, 1958, pp 271-288.

A3. Penning, F. M.: Ein Neues Manometer Für Niedrige Gasdrucke, Insbesondere Zwischen 10^{-3} und 10^{-15} MM. Physica, 4, no. 2, 1937, pp. 71-75.

A4. Beck, A. H.; and Brisbane, A.D.: A Cylindrical Magnetron-ionization Gauge. Vacuum, vol. 2, 1952, p. 137.

A5. Haefer, R.: Die Zundspanning von Gasentladungen unter dem Einfluss eines transversalen Magnetfelds in Druckbereich von 10^{-1} bis 10^{-8} Torr. Acta Phys. Austriaca, vol. 7, 1953, p. 52.

A6. Haefer, R.: Uber den Mechanismus der Zundung einer elektrischen Gasentladung unter der Einwirkung eines transversalen Magnetfelds in Druckerbeich 10^{-1} bis 10^{-8} Torr. Acta Phys. Austriaca, vol. 7, 1953, p. 251.

A7. Haefer, R.: Die Strom-Apanungascharakteristiken einer selbstandigen Gasentladung im transversalen Magnetfeld. Acta Phys. Austriaca, vol. 8, 1954, p. 213.

A8. Somerville, J. M.: Sparking Potentials in a Transverse Magnetic Field. Proc. Phys. Soc. B, 65, 1952, pp. 620-629.

A9. Kugler, G. A.; Ollemdorff, F.; and Roggendorf, A.: Über die Beweglichkeit elektrischer Ladungsträger unter dem gleichzeitigen Einfluss starker elektrischer und magnetischer Felder. Z. Physik, 81, 1933, pp. 733-744.

A10. Newton, G. P.; Delz, D. T.; Miller, G. E.; Horowitz, R.: Response of Modified Redhead Magnetron and Bayard-Alpert Gauges Aboard Explorer 17. Vacuum Symposium Transaction, A.V.S., vol. 10, 1963, p. 200.

A11. Dushman, S.; Lafferty, J. M.: Scientific Foundations of Vacuum Technique. Second ed., John Wiley & Sons, Inc., 1962, p. 316.

A12. Torney, F. L., Jr.; and Feakes, F.: Pressure Measurements Below 10^{-10} Torr with Bayard-Alpert and Magnetron Gauges. Rev. Sci. Instr., vol. 34, 1963, p. 1041.

A13. Feakes, F.; and Torney, F. L., Jr.: The Performance Characteristics of Three Types of Extreme High Vacuum Gauges. Vacuum Symposium Transactions, A.V.S., vol. 10, 1963, p. 257.

A14. Helmer, J. C.; and Jepsen, R. L.: Electrical Characteristics of a Penning Discharge. Proc. IRE, vol. 49, 1961, p. 1920.

A15. Guthrie, A.; and Wakerling, R. K.: "Vacuum Equipment & Techniques." National Nuclear Energy Series, div. 1, vol. 1, McGraw-Hill Book Co., Inc., 1949, pp. 207-212.

A16. Knauer, W.: Mechanism of the Penning Discharge at Low Pressures. J. App. Phys., Vol. 33, no. 6, 1962, p. 2093.

A17. Keller, R.: Wissenschaftlicher Tiel. Helvetica Phys. Acta, 21, 1948, pp. 170-172.

A18. Lorrain, P.: Une nouvelle source d'électrons et son inversion comme source d'ions. Helvetica Physica Acta, vol. 21, 1948, p. 497.

A19. Mills, C. B.; Barnett, C. F.: High-Intensity Ion Source. Rev. Sci. Instr., vol. 25, no. 12, 1954, p. 1200.

A20. Gunther, K.: A Partial Pressure Vacuum Gauge Working According to the Principle of the Electrical Mass Filter. Vacuum, vol. 10, 1960. pp. 293-309.

A21. Gunther, K.; Hänlein, W.: The Mass Filter Partial-pressure Vacuum Gauge. Transactions Second International Congress on Vacuum Science and Technology, Pergamon Press, Oxford, 1961, pp. 573-580.

A22. Kerwin, L.: Mass Spectroscopy. Advances in Electronics and Electron Physics, VIII, 1956, pp. 187-253.

A23. Dempster, A. J.: New Methods in Mass Spectroscopy. Pro. Amer. Phil. Soc., vol. 75, 1935, pp. 755-767.

A24. Bleakney, W.; and Hipple, J. A.: A new Mass Spectrometer with Improved Focusing Properties. Phys. Rev., vol. 53, 1938, pp. 521-529.

A25. Paul, W.; and Steinwedel, H.: A New Mass Spectrometer with no Magnetic Field (in German). Z. Naturforschung, 8a, 1953, pp. 448-450.

A26. Brubaker, W. N.: Instruments and Measurements. Vol. 1, Academic Press Publishers, New York, 1961, p. 305.

A27. Brubaker, W. N.; and Tuul, J.: The Influence of Ion Entrance Aperture Size and Exitation Frequency on the Performance of a Satellite Quadrupole Mass Filter. Eleventh Annual Conference on Mass Spectometry and Allied Topics, ASTM Committee E-14, May 19-24, 1963, pp. 371-378.

A28. Paul, W.; and Raether, M.: Das elektrische Massenfilter. Z. Physik, Bd. 140, 1955, pp. 262-273.

A29. Paul, W.; Reinhard, H. P.; and von Zahn, U: The Electric Mass Filter as Mass Spectrometer and Isotope Separator (in German). Z. Physik, vol. 152, no. 2, 1958, pp. 143-182.

A30. Paul, W.; Osberghaus, O.; and Fischer, E.: Ein Ionenkäfig. Forsch-Ber. d. Wirtsch. Ministeriums Nordhein-Westfalon Nr. 415, 1958.

A31. Fischer, E: Die dreidimensionale Stabilisierung von Ladungstrügern in einem Vierpolfeld. Zeitschrift für Physik 156, 1959, pp. 1-26.

A32. von Zahn, V.: Monopole Spectrometer, a New Electric Field Mass Spectrometer. Rev. Sci. Instr., vol. 34, no. 1, 1963, p. 1.

A33. Woodward, C. E.; and Crawford, C. K.: Design of a Quadrupole Mass Spectrometer. Laboratory for Insulation Research. MIT Technical Report 176, Jan. 1963.

A34. Hansen, W. W.; et al.: "Final Report No. 13 in Microminiaturized Field Emission Tubes." Stanford Research Institute, contract DA 36-039 SC84526.

A35. Zworykin, V. K.; Morton, G. A.; Ramberg, E. G.; Hillier, J.; and Vance, A. W.: Electron Optics and the Electron Microscope. John Wiley & Sons, Inc., New York, 1945.

A36. Oshchepkov, P. K.; Skvortsov, B. N.; Osanov, B. A.; and Siprikov, I. V.: Applications of Continuous Secondary Electron Multiplier for Amplifying small Currents. Instr. and Exp. Tech., 1960, p. 611.

A37. Goodrich, G. W.; and Wiley, W. C.: Continuous Channel Electron Multiplier. Rev. Sci. Instr., vol. 33, 1962, p. 761.

A38. Goodrich, G. W.; Wiley, W. C.: Resistance Strip Magnetic Electron Multiplier. Rev. Sci. Instr., vol. 32. no. 7, 1961, p. 846.

APPENDIX B

DEVELOPMENT OF A MASS SPECTROMETER DESIGN

APPENDIX B

DEVELOPMENT OF A MASS SPECTROMETER DESIGN

By P. Blum and F. L. Torney, Jr.
Norton Research Corporation

SUMMARY

A new experimental cold-cathode ion source has been designed and constructed. The primary purpose was to investigate methods of increasing the source sensitivity obtained in the feasibility study, compatible with the requirements of a quadrupole mass spectrometer. The source contains a probe for measuring ion energy spectra through a 1 mm simulated quadrupole entrance aperture. The probe's position is adjustable relative to the ion exit aperture. The design includes an electrostatic lens and provision for comparing sensitivities both with and without the lens. Also included is provision for testing for optimum cathode potentials. Modifications have been made in the magnetic geometry used in the feasibility study source; cylindrical ceramic magnets have reduced external bulk considerably; elimination of pole pieces has increased accessibility to the ion exit aperture and reduced internal bulk and gas traps for improved UHV performance.

Methods of optimizing sensitivity without the lens were studied first. As a function of cathode potential, the sensitivity remained constant for positive values and rose appreciably (up to a factor of 7) for negative ones. An

intense electron component accompanied the negative potentials however, making the higher sensitivites suspect; experiments conducted to verify them were judged inconclusive.

A family of ion energy spectra were obtained as a function of distance from the ion exit aperture. The energy distributions over all distances and all cathode potentials (both positive and negative) showed ions predominating at low energies and decreasing continuously with increased energy, a situation beneficial to high quadrupole spectrometer sensitivity. Maximum sensitivity occurred nearest the exit aperature and again at a point more distant.

The highest sensitivity obtained for a positive pusher cathode potential (+40 volts for example) and an ion energy range of 0 - 30 eV (an acceptable energy range for a quadrupole spectrometer) was 5.5 mA/Torr (nitrogen). This was recorded at both 0.14 in. and at 0.88 in. from the exit aperture This sensitivity, obtained through the 1 mm diameter probe aperture compares with a somewhat lower figure obtained with a 3 mm diameter aperture used in the feasibility study. A minimum sensitivity improvement of 10 has therefore been achieved, without the use of a lens

Frequent changes in sensitivity to pressure were observed in the magnetron portion of the source. Cathode current changes up to 35% were observed at constant pressure. Conditions to which this apparent operational mode switch is attributable, or the pressure region to which it is confined, were not investigated (due to leaking feedthrus).

The sensitivity benefits of an electrostatic lens were next investigated. A three aperture einzel lens was designed for this purpose. It has the advantage of focusing without increasing ion energy and enables suitable electronic coupling between source and quadrupole. Analytical investigations conducted to determine optimum design and operation revealed severe lens limitation for the particular conditions and requirements of the cold-cathode ion source. It indicated that the lens would provide no benefit in increasing source sensitivity over placing the quadrupole close to the source, unless an especially favorable beam geometry existed (e.g., a nearly parallel and mono-energetic beam).

Experimental studies were conducted for several positions of lens and probe relative to the ion exit aperture. A large range of lens focusing potentials were applied and energy spectra were obtained for selected values. The effect of differing cathode potentials was also studied. It was concluded for each situation that the lens provided no sensitivity improvement. However, anomalies in lens operation were also observed. These were attributed to the presence of electrons in the beam and their resulting focusing and/or reflection. The results of electron reflection by the lens supported doubts about the validity of higher sensitivities obtained for negative cathode potentials.

A quadrupole mass analyzer design chart has been constructed covering a wide range of possible design values. Their interdependence, which is rather complicated, it thereby made evident. As a result, a set of design parameters have been determined which are optimally matched to

both the experimentally determined characteristics of the cold-cathode ion source and the objectives of an UHV mass spectrometer.

INTRODUCTION

This program has been undertaken to fill the need for a mass spectrometer for measuring partial pressures in the ultrahigh vacuum (UHV) region. Two fundamental problems have limited this capability in the past, both lying with the ion source portion of the spectrometer. One is insufficient source sensitivity. The other pertains to source cleanliness.

Mass spectrometers commonly use an ion source with a hot-filament, the latter supplying electrons in abundance for molecular ionization. While this type of device has much to recommend it, the above stated problems severely restrict its usefulness in ultrahigh vacuum. A primary difficulty is that the heat generated causes both decomposition of gases and their evolution from the source itself, thus causing confusion in both the type and amount of gases to be measured. Cold-cathode ion gauges of the magnetron type (refs. B1, B2) on the other hand have sharply reduced this difficulty while producing the highest sensitivities thus far attained; the sensitivity of these devices results from immensely increased electron path lengths, effected by crossed electric and magnetic fields. This research program has been directed toward adapting a cold-cathode magnetron type discharge for use with a mass analyzer.

The first phase of this program (Contract NAS1-2691, Task 2*), demonstrated the feasibility of this approach by constructing and testing a cold-cathode ion source. In essence, the source consisted of a magnetron configuration modified to allow extraction of the ions from the discharge. The ions are thus accessible for analysis with a mass spectrometer. Studies revealed, among other salient characteristics, an ion beam sensitivity of 5 mA/Torr after passing through an aperture of 3.0 mm in diameter. This is 500 times the sensitivity of conventional hot-filament mass spectrometer ion sources. A companion study showed that a quadrupole mass spectrometer was best suited to the energy and dimensions of this beam and tentative design parameters were specified.

The present phase of the program has been directed toward developing and testing an improved source design. In particular, methods are investigated for improving beam intensity compatible with the energy and dimensional requirements of a quadrupole mass analyzer. A quadrupole design chart has been composed to aid in optimally matching source and quadrupole characteristics.

The new source has been designed to include some improvements while deferring others to allow versatility in determining optimum electronic parameter values, optimum positioning between source and quadrupole and to allow testing the effectiveness of an electrostatic lens. Source and experiments were designed for study of source response to variations in pressure and gas composition subsequent to optimization studies.

---

*See Appendix A.

APPENDIX "B" SYMBOLS AND ABBREVIATIONS

A	anode
C	Faraday cup (ion collector)
i_c	ion collector current (amperes)
I_Q	simulated quadrupole aperture plate current (ampere)
j	current density at object (amperes/unit area)
j´	current density at image (amperes/unit area)
K_1	pusher cathode
K_2	extractor cathode
L_1	lens aperture plate #1
L_2	lens aperture plate #2
L_3	lens aperture plate #3
Q	simulated quadrupole aperture plate (probe)
V	ion energy per unit charge at object (eV/esu)
V´	ion energy per unit charge at image (eV/esu)
V_c	ion collector potential (volts)
V_c	voltage applied to central cathode (volts)
V_o	voltage applied to outer cathode (volts)

V_I	negative electrode potential corresponding to ions initial energy (volts)
V_{K_1}	pusher cathode potential (volts)
θ	angle between ion path and lens axis at object (radians)
θ'	angle between ion path and lens axis at image (radians)

ION SOURCE DESIGN

Overall Electrical and Mechanical Design

Figure B-1 and B-2 illustrate, respectively, the electrical schematic of the source and the more detailed mechanical layout, drawn approximately to scale. Figure B-3 is a photograph of the internal components mounted on the flange. Three sections are shown as follows:

(1) The magnetron portion or source proper. This consists of a pusher cathode (K_1), an extractor cathode (K_2), an anode (A), two auxiliary cathodes and a stack of five cylindrical magnets.

(2) An electrostatic lens. This consists of three aperture plates L_1, L_2, and L_3.

(3) A probe. This consists of a simulated quadrupole aperture plate (Q) and a Faraday cup or ion collector (C). It is used for studying ion beam characteristics and can be made to simulate the dimensional and energy restrictions of a quadrupole mass analyzer.

The source has been designed so that both probe and lens are moveable with respect to the magnetron and each other and so that experiments may be conducted with the lens either in or out of the system. Electronic access has been provided to allow monitoring currents and/or applying potentials to K_1, A, L_2, Q and C.

Each of the three sections are supported on a steel mounting cylinder either by direct spot welding or via

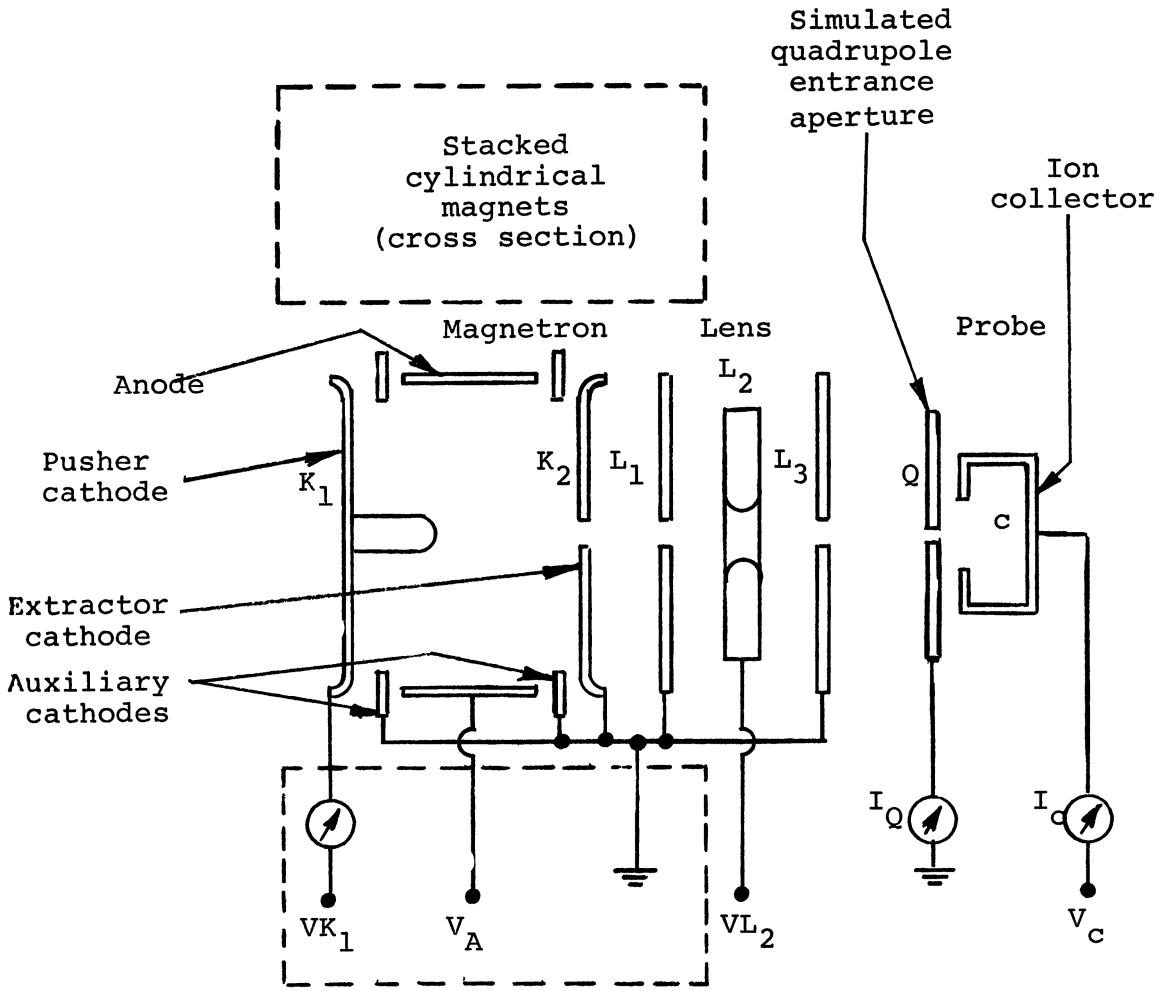

Figure B-1.— Cold cathode ion souce with lens, schematic

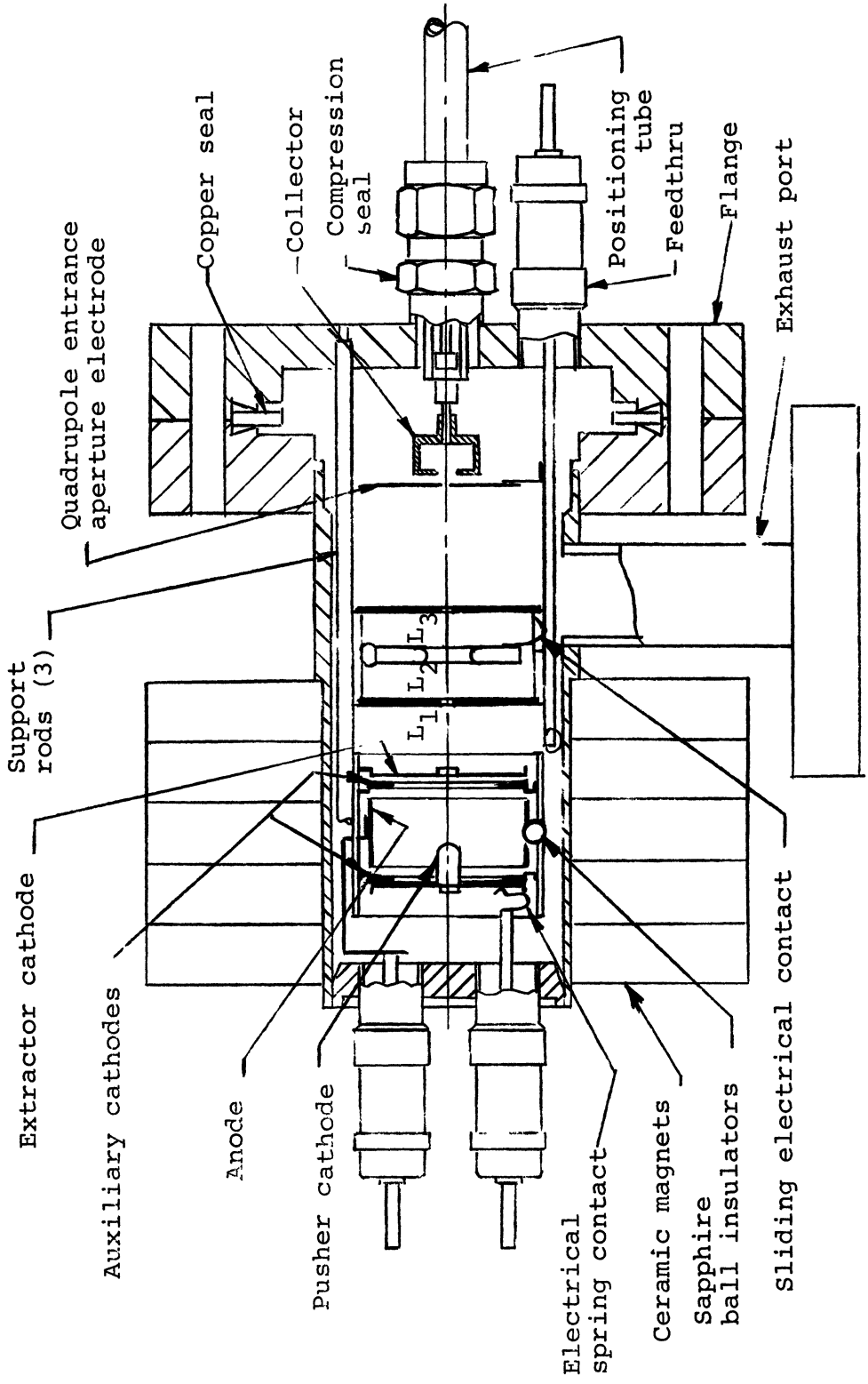

Figure B-2.- Cold cathode ion source

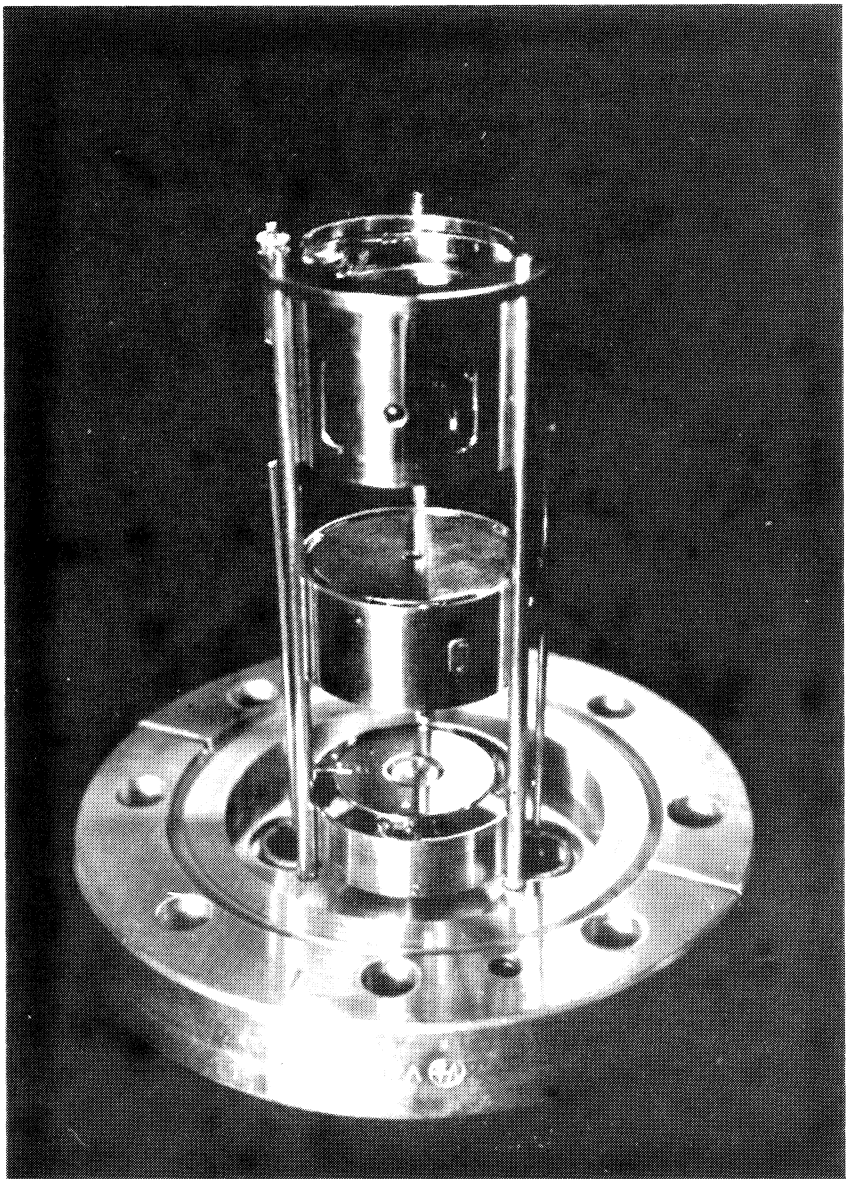

Figure B-3 View of Internal Components of Cold Cathode Ion Source. From Top to Bottom Magnetron, Lens and Probe

insulated spacers (sapphire balls are used for L_2 and the anode, kovar-to-glass studs for the remaining elements). The mounting cylinders are supported on three steel rods which are welded to a flange. Electrically, this design provides a guard-ring arrangement for all elements not operating at ground potential. Mechanically, the design permits alignment and inspection of components when the flange is removed from the housing.

Positioning is accomplished by sliding the lens and/or probe along the three supporting rods. The probe is adjustable with a positioning rod, which passes through a "Swagelok" connector, without opening the flange. The lens assembly is moved forward by pushing with the probe. (The flange must be removed to move the lens backward.) Measurements on the positioning rod outside the source enables determination of distances between the lens, magnetron and probe.

The "Swagelok" connector was designed for use during source sensitivity studies only (both with and without the lens), at pressures in the 10^{-8} Torr range. Since the "Swagelok's" teflon washers are not bakeable at high temperatures, it is essential that they be removed for studies at lower pressures. The plan originally called for replacement of the entire connector with a ceramic feedthru welded into the flange subsequent to the sensitivity studies. For reasons to be discussed in a later section, this plan was not followed.

Feedthrus are made of a high alumina ceramic, 430 stainless steel and a gold alloy seal. Ion source

elements are of Nichrome-V, while the remaining elements and housing are of 303 or 304 stainless steel. All flanges are standard Varian "Conflat" flanges using a copper gasket. The materials used enable the entire unit (with teflon washers removed) to be baked at 450°C. Sealed joints are heli-arc welded. These have been kept internal wherever possible to prevent gas traps.

The Magnetron

The magnetron portion of the cold-cathode ion source, in both the feasibility study and in the present one, is a modification of the magnetron gauge described by Redhead (ref. B1). The reasons underlying its choice over other types of cold-cathode discharges can be found in Appendix A, together with a comprehensive bibliography on the subject. Application of the magnetron gauge as in ion source for spectrometry purposes required that the normal magnetron configuration be modified to allow an extracted ion beam. This was accomplished by separating the single, spool-shaped cathode into two cathodes, one with a remnant stub and one with an aperture. Modification of the horseshoe magnet ordinarily used was also necessary.

In the present source the magnetic arrangement was further modified. Magnetic pole pieces which were in front of cathode K_2 and behind cathode K_1 have been removed (Fig. B-1). In addition, the array of horseshoe Alnico magnets previously used have been replaced by a stack of cylindrical ceramic magnets. Among the benefits of this modification are the following: (1) elimination of pole pieces reduces surface area and gas traps to

allow improved UHV performance, (2) the quadrupole can be brought closer to the ion exit aperture (K_2) for more efficient utilization of extracted ions - whether a lens is used or not, and (3) the cylindrical magnets provide a far more compact design than those previously used.

Provision has been made for monitoring cathode current at K_1 (which indicates total pressure) and for applying a potential between K_1 and K_2 to study the effect of this potential on the extraction of low energy ions. Cathode K_2 has been grounded to keep it at the same potential as Q. Since Q must be grounded for proper operation of the quadrupole, this arrangement prevents undesirable lens action in the intervening space.

The Probe

The probe, shown in Figs. B-1, B-2, and B-3, is a commonly used method of exploring ion energy distributions. It consists of a Faraday cup or ion collector C preceded by an aperture plate Q, which serves as an electrostatic shield.

An ion beam incident on Q and C when both are of ground potential will produce a current at C (I_c). This will be produced by ions of all energies incident. However, if a positive potential is applied to C (V_c), ions with energy less then eV_c, where e is the charge on the ion, will have insufficient energy to overcome the potential barrier and will be turned away. A plot of I_c vs. V_c will therefore provide the ion energy distribution of that portion of the beam passing through Q.

By making the aperture in Q to correspond to the dimensional restrictions of a quadrupole mass spectrometer and the retarding potential V_c to correspond to the energy restrictions, the probe serves to give the useable source sensitivity in amps/Torr referred to a quadrupole entrance. A Q aperture of 1 mm was used in the present study. The probe was designed to be moveable so that beam characteristics could be measured as a function of distance from the source as well as a function of different object and image distances with the lens in use.

In practice the beam emerging from K_2 contains electrons as well as ions. This serves to make I_c negative when V_c exceeds some positive value. When I_c is plotted against V_c, to obtain the ion energy distribution, special problems of interpretation result which will be discussed with the presentation of the EXPERIMENTAL RESULTS section of this report.

The Lens

Analytical approach, lens limitations. - Literature on the optics of charged particles is almost totally concerned with electrons. While the laws governing ion and electron optics are essentially identical, the properties of the present source and the requirements of the present lens pose fundamental differences in the problems of usual concern in electron optics.

The peculiar beam properties of the cold-cathode ion source, which must be anticipated, are large divergence, lack of homocentricity and large ion energy spread, (from an optical view point). The peculiar lens requirement is concentration of the largest number of ions from this beam into a small aperture (1 mm in diameter) while maintaining minimum ion energy (for optimum source sensitivity - discussed in the QUADRUPOLE DESIGN section of this report).

An electrostatic lens was chosen for this work over a magnetic one. Among its relative advantages are small bulk, versatility and a focal length independent of charge to mass ratio (e/M) (ref. B3). As a result of the latter, electron electrostatic lens studies, including experimentally determined focal lengths, are applicable to the present ion lens design.

The approach taken to the lens design was to treat the quadrupole entrance aperture as image and the ion source extractor aperture as object. Since for every object point there must be a conjugate image point, it follows, (discounting aberration effects and aperture limitations) that all ions from the object hole must land in the image hole. This approach eliminates the need for knowing the extracted ions' angular distribution and requires no restrictive assumptions, such as beam homocentricity.

To ascertain optimum lens design and optimum operating parameters, a most pertinent fundamental optical relationship, Abbe's sine law, was enlisted. Derivable from the

principle of least action (ref. B4), it is independent of lens system or type of radiation. Applying it to ion optics, a relationship is obtained between image current intensity (current/unit area) and radial and axial ion energy, namely

$$j' = j\ (V'\sin^2\theta'/V\sin^2\theta) \qquad \text{(B1)}$$

Here j' and j represent ion current intensity at image and object, respectively; θ' and θ represent the angle which arbitrary ion paths make with the lens axis at image and object, respectively; V' and V represent corresponding ion energy per unit charge at the image and object, respectively.

It can be seen that a fundamental limitation is placed upon the maximum attainable image intensity by the ion energy restrictions at the image imposed by a mass analyzer. High image intensity requires large V' and/or large θ, while low axial and radial energy at the image requires small V' and θ'. An optimum compromise between the two goals is therefore necessary.

Abbe's sine law also provides one of the important reasons for choice of an einzel lens design. Here, ions leaving the lens have the same energy as those entering. It therefore has been possible to design a lens (to be discussed in the next section) so that $V' = V$, thus leaving total ion energy intact. This is at the expense of increasing the radial component of the energy. However, the radial component increases only as the square root of the total energy increase which would be required of an accelerating lens to produce the same intensity.

An additional source of intensity limitation arises because source ions are not monoenergetic. Reduced intensity here results because ions of different energy cannot produce an image at the quadrupole entrance aperture for the same lens operating conditions. Since no methods presently exist for the solution of this problem (chromatic aberration) in electron (or ion) optical systems (ref. B5), the only recourse is to image about the energy of greatest intensity.

Finally, intensity is a function of lens electrode aperture size and spacing. If for a particular positioning of object, image and lens the outer apertures of the lens are too large, then the electrostatic field bulging through them is distorted by object of image electrodes (or by interference from the magnetron field bulging through the K_2 aperture) with resulting aberration (refs. B6, B7) and hence, reduced image intensity. On the other hand, if the apertures are too small, only a small fraction of the source ions are intercepted by the lens, again resulting in image intensity reduction. Obviously a compromise must again be effected.

The above indicated lens limitations constitute problems reducible by optimum choice of lens design, positioning and operating parameters. However, it should be indicated that other limitations exist which are not so reducible. For example, a wide beam divergence results in spherical aberration for which there are no known

solutions in electron optics (ref. B5) and little recourse to minimizing in the present situation. Finally, unless the lens is made to affect the field inside the magnetron, it can under the conditions assumed, supply no more than approximately 9 times the intensity available to the Q plate aperture by itself, with the latter placed adjacent to the source exit aperture. (This is the ratio of exit aperture area to Q plate aperture area.) The latter figure actually appears much too high. An intensity increase of 9 requires a magnification of 1/3 and hence an image to object distance ratio of 3. This forces the lens back so that only a fraction of the beam solid angle emerging from the source can be intercepted by it; a maximum of unity magnification appears closer to the truth.

The above pessimistic conclusions are based on a necessarily pessimistic, general approach to the problem which must assume a broad, non-homocentric beam with a broad energy distribution (from an optical viewpoint). A beam more favorable to lens action may actually exist and the latter assumed problems may be minimal, hence the necessity for experimentation.

Design and operation. - Figures B-1, B-2, and B-3 show the lens section, which consists of electrodes L_1, L_2, and L_3. A design employing plane electrodes was chosen over cylindrical ones for compactness, versatility, and for reduction of both spherical aberration and ionic space charge effects. The design chosen is that of an einzel lens which follows the proportions of the lens designed and studied by Zworykin (ref. B8). As previously

discussed, the einzel lens has the advantage of focusing without increasing total ion energy, although the radial and axial components of this energy are changed. Selection of Zworykin's design has the advantage of making utilizable the focusing properties determined and plotted from his experimental data and giving assurance of an aberration-free design.

Lens focusing is accomplished by varying only the potential on L_2. Electrodes K_1, L_1, L_3 and Q are kept at the same potential (ground) to provide a field-free region on each side of the lens (ref. B9). This is essential to aberration-free performance since fields on either side of the lens would act to distort those of the lens itself. This arrangment also fulfills the zero potential requirements of the axis of the quadrupole analyzer.

Lens focal lengths can be determined from a graph published by Zworykin (ref. B10) and shown in Fig. B-4. As normally used for electrons, chart potentials V_C* and V_O correspond to the externally applied electrode potentials. This is because lens potentials (to a good approximation) are solely responsible for the electron's energy (ref. B11), or potential per unit charge (V/e), within the lens. For the cold-cathode ion source, however, ions have an initial spread of energies upon emerging from the source which are independent of lens electrode potentials. Ion energy within the lens is therefore the sum of the ions' initial energy and that resulting from lens potentials.

---

*Not to be mistaken for the collector potential symbol V_C used elsewhere in the text.

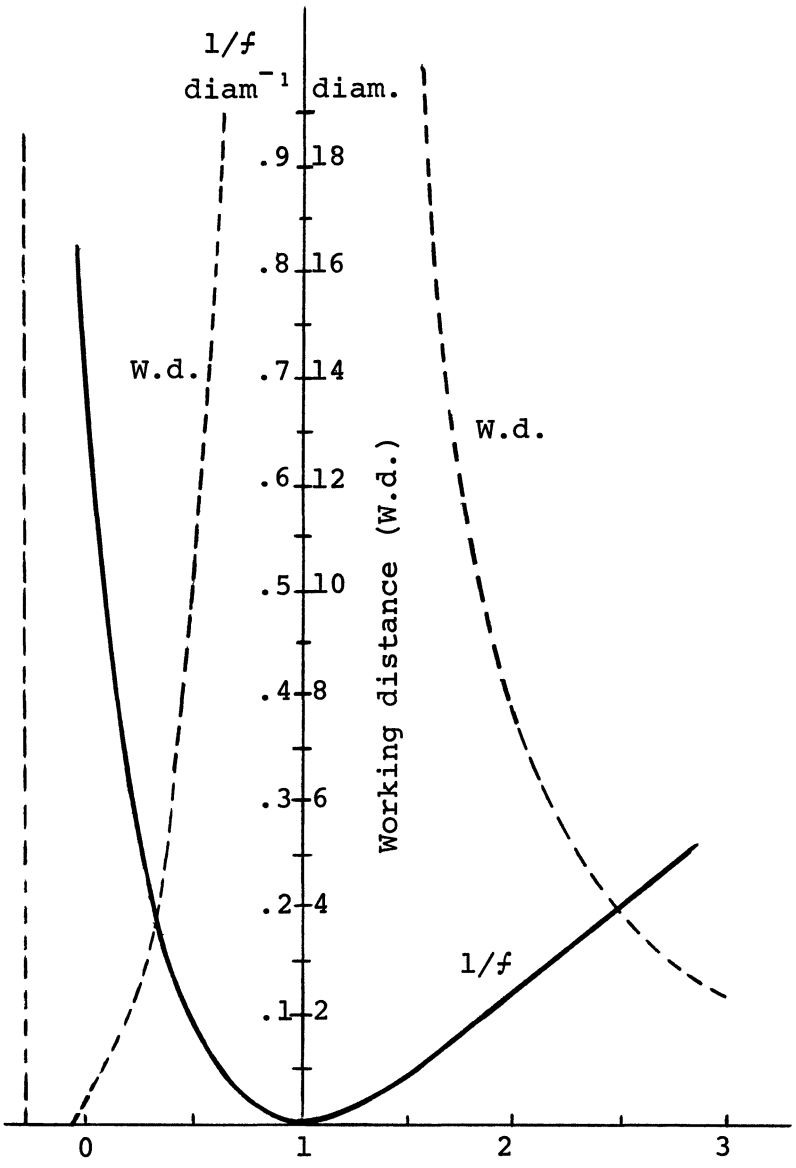

Figure B-4. — Graph for determining focal lengths (from Zworykin ref.B10)

Chart potentials were therefore determined by first assigning a negative electrode potential V_I to correspond to the ion's initial energy (e.g., $V_I = -30$ volts for a 30 eV ion). If V_{L1} and V_{L2} are the externally applied potentials to L_1 and L_2, respectively, then since V_{L1} is kept at zero volts,

$$\frac{V_C}{V_O} = \frac{V_I + V_{L2}}{V_I}$$

Figure B-4 therefore indicates an infinite focal length for V_{L2} at zero volts and there is no lens action. The focal length decreases when V_{L2} is made either increasingly positive or negative. The focal length approaches zero for V_{L2} positive and approximately equal to V_I. However, for negative values of V_{L2}, $f \to 0$ only as $V_{L2} \to \infty$. Thus, Fig. B-4 can be used to determine focal lengths for any combination of V_I and V_{L2}. When $V_C/V_O > 3$, focal lengths can only be estimated.

EXPERIMENTAL PROCEDURES AND AUXILIARY APPARATUS

Experimental source study was arranged into essentially three stages, subsequent to preliminary tests, as follows: (1) measurement without a lens of ion current intensity vs. energy as a function of (a) pusher cathode potential V_{K1} and (b) distance from the ion exit aperture; (2) determination of lens effectiveness in improving sensitivity; and (3) measurement of ion current intensity vs. energy as a function of gas composition and pressure.

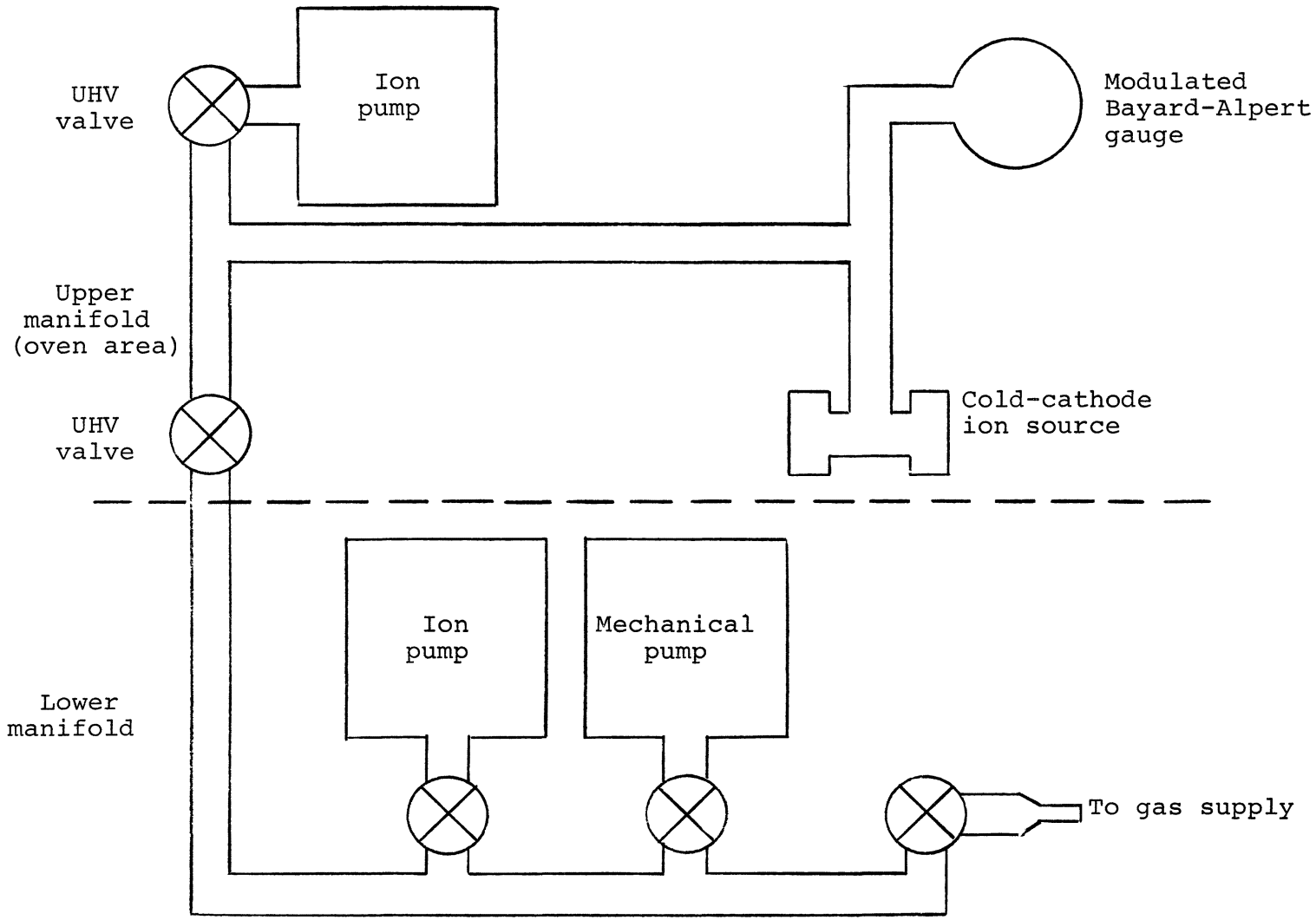

Figure B-5.- Vacuum system schematic

The "Swagelok" fitting was used in stages (1) and (2). It allowed positioning of probe and lens via the positioning rod (Fig. B-2) without opening the flange and allowed each new distance between components to be measured externally. Completion of stages (1) and (2) allowed positioning to be fixed and allowed removal of the "Swagelok" teflon washers, to permit high temperature bakeout of the source in preparation for stage (3).

Preliminary to experimental study, considerable care was exercised in aligning internal source components. This was critical for lens studies, since a narrowly focused beam might miss an off-centered probe aperture, for example. Critical elements of the magnetron and probe were assembled with the aid of alignment jigs. These centered and spaced the elements within their respective mounting cylinders. Lens elements were machine fitted. Subsequent to assembly, the entire source, including the lens, was centered in a lathe and alignment further checked with a cathetometer. Necessary adjustments were made by bending the kovar-to-glass supporting studs.

Prior to assembly, electronic components were polished to prevent high voltage breakdown, undesirable field emission and undesirable electrostatic field perturbations.

The vacuum system employed is shown schematically in Fig. B-5. A top view is shown photographically in Fig. B-6. The overall test set up is shown in Fig. B-7. The vacuum system was divided into upper and lower manifold units. This arrangment allowed the upper portion to be

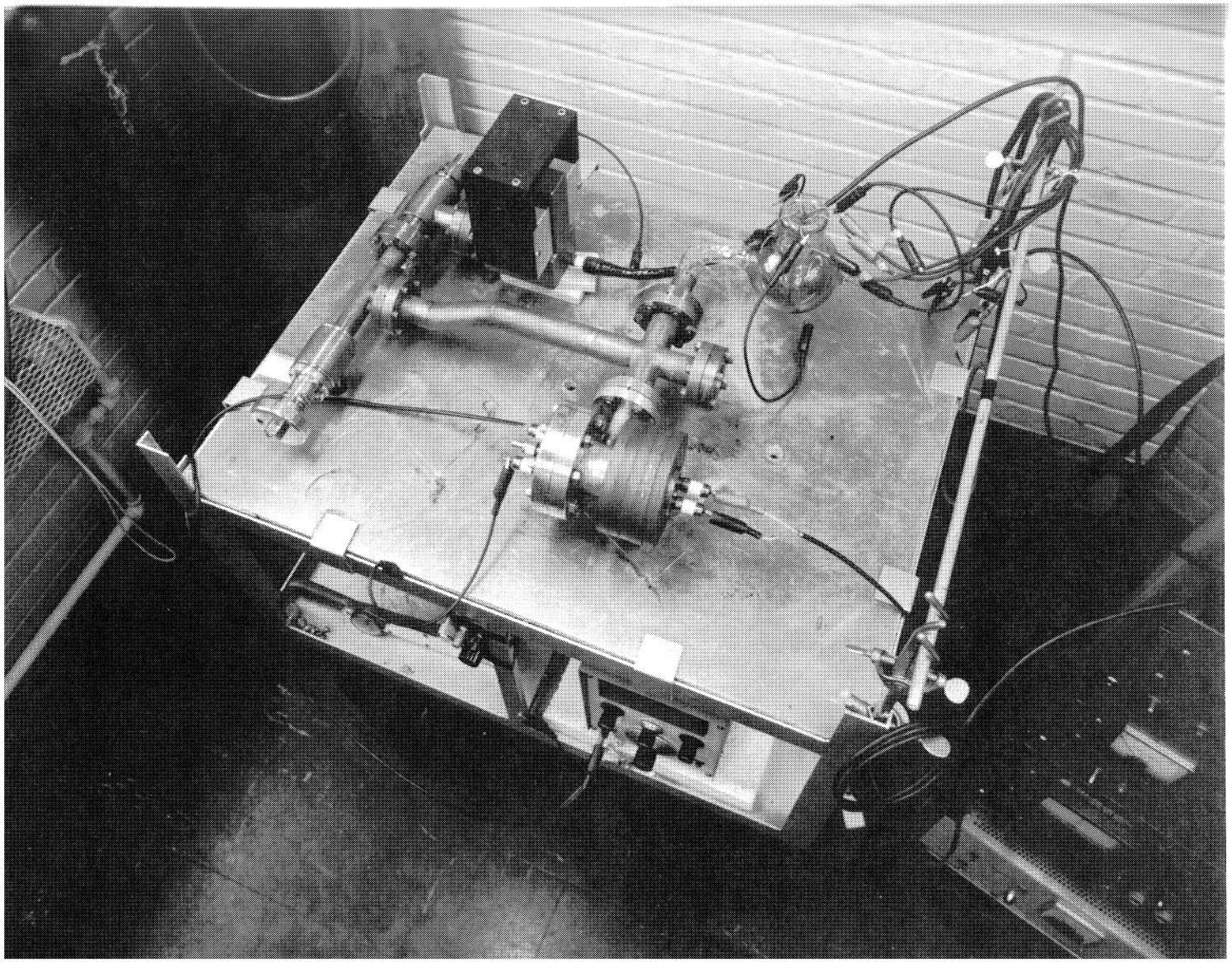

Figure B-6 View of the Upper Manifold Portion of the Vacuum System

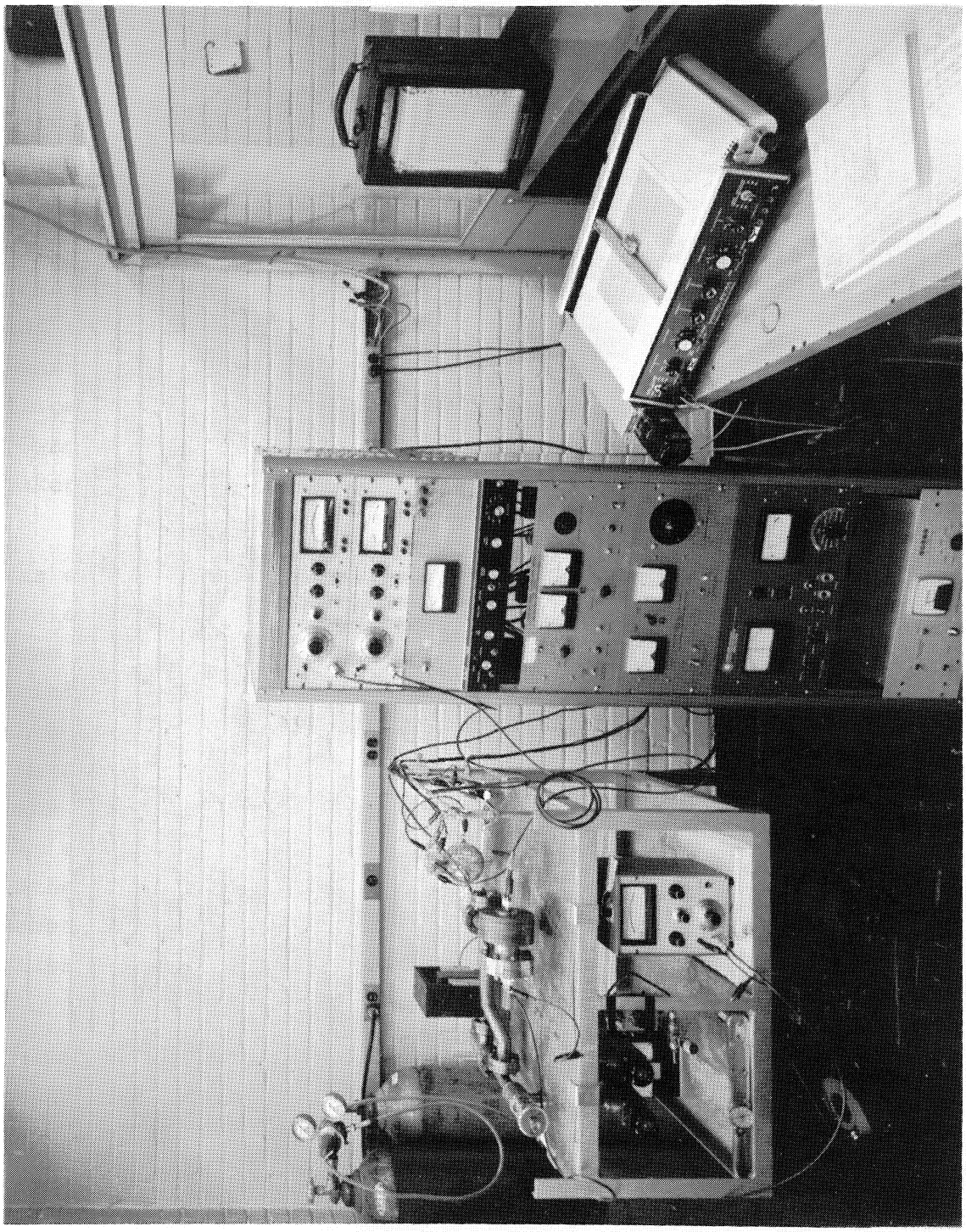

Figure B-7 View of Vacuum System and Associated Electronics

oven baked while being pumped from below. Subsequent to bakeout, the upper manifold, thus cleaned, was valved off from the lower and pumped on itself.

The upper manifold consisted of the cold-cathode ion source, a modulated Bayard-Alpert gauge, an 11 liter per sec. Ultek Model 10-252 ion pump, a Granville-Phillips Type L ultrahigh vacuum valve for valving off the upper manifold from the lower and a Varian valve for closing the ion pump. A Granville-Phillips thermostatically controlled oven was used for baking the upper manifold system.

The lower manifold consisted of a 20 liter/sec Ultek Model 10-354 ion pump, a small mechanical pump, a port for feeding gas to the system and associated Granville-Phillips UHV valves for closing off the three outlets.

Energy spectra were obtained with the aid of a battery-operated Keithley Model 600A electrometer. Measurements of collector current I_c vs. collector potential V_c were made by insulating the electrometer from ground via a styrofoam block and reading currents with the case raised to the selected V_c values. Collector leakage currents, obtained with the anode potential off, were subtracted from collector current readings after each set of readings were obtained.

Keithley Model 610 electrometers monitored the remaining electrode currents I_Q and I_{K_1}. A Moseley (Model 2D-2A) X-Y recorder proved expeditious for recording source characteristics during the lens experiments.

Magnetic field measurements were made prior to source studies and again during lens experiments.

EXPERIMENTAL RESULTS AND CONCLUSIONS

Ion Beam Studies Without the Lens

Ion energy distribution vs. V_{K1}. - Initial experiments were concerned primarily with determining which value of pusher cathode potential V_{K1} would provide the highest ion beam intensity through the Q aperture and with determining the resulting ion (and electron) energy distribution. The results of these experiments are shown in Fig. B-8. Collector current I_c is plotted vs. collector potential V_c for $-110 < V_c < +110$ volts and for $-40 < V_{K1} < +40$ volts.

The K_2 to Q distance chosen was 0.61 in., approximately the same as used in the feasibility study. Anode potential was 5.6 kV and the mean pressure was 5.5×10^{-8} Torr (nitrogen). The axial magnetic field at the center of the magnetron was 1225 gauss.

The curves for positive V_c display steep slopes initially, gradually leveling off as V_c increases. This indicates a predominance of low energy ions for all values of V_{K1}, enabling high quadrupole analyzer sensitivity. Highest sensitivities are indicated for $V_{K1} \leq 0$, since the ratio of differential collector current to differential retarding potential ($\Delta I_c/\Delta V_c$) is then greatest. However, a predominant electron component is also indicated for $V_{K1} \leq 0$. For negative values of V_{K1} reliably to represent a quantitative ion energy distribution, it is therefore essential that the electron current passing through Q remain constant for all positive values of V_c.

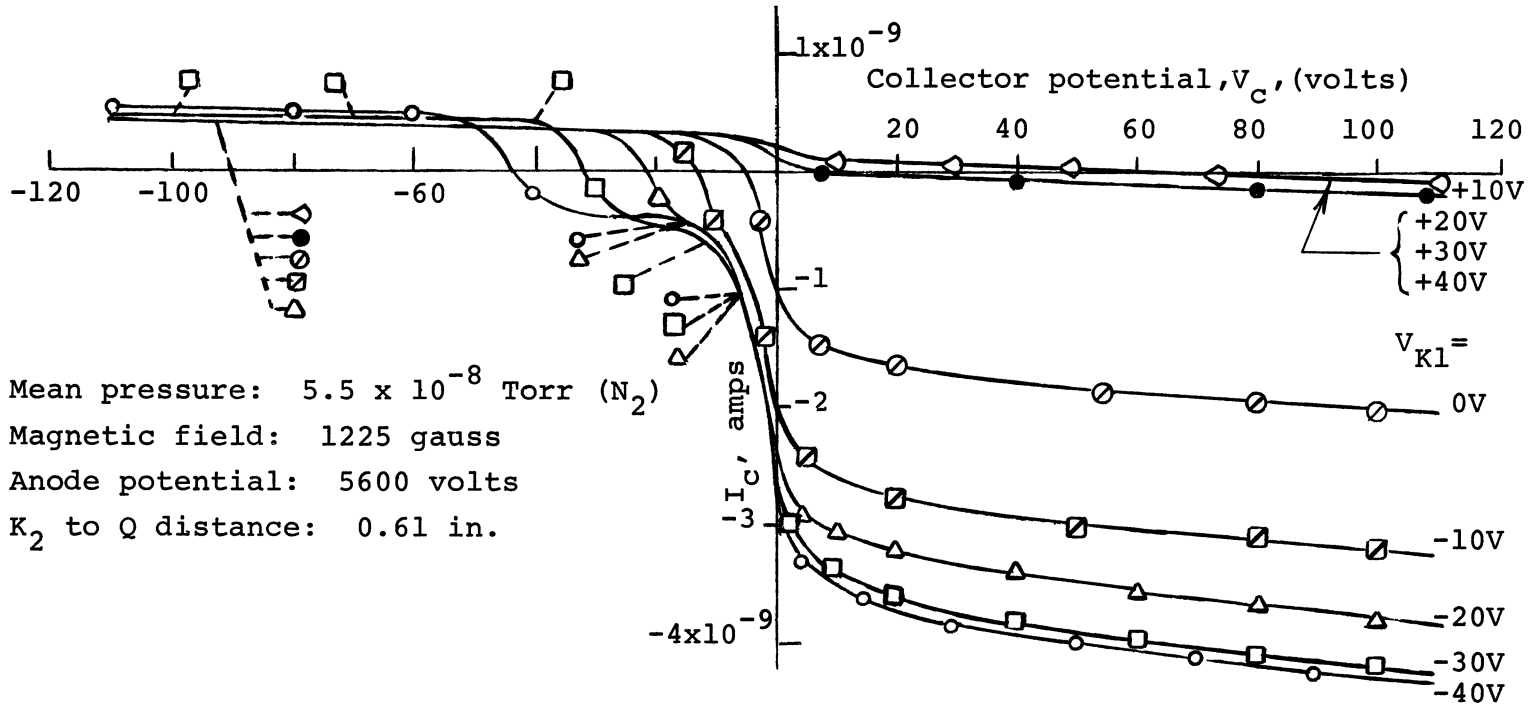

Figure B-8.- Collector current vs. collector potential for selected pusher cathode potentials (V_{K1})

Although Helmer and Jepson (ref. B12) apparently assumed a constant electron current when probing the ion energy distribution of a Penning source having a large electron component, it was considered essential to investigate this situation experimentally. For this purpose, data on I_c vs. negative V_c, shown in Fig. B-8 was taken. The verification sought was based in the following reasoning:

> If the electron component remains constant for positive V_c, then the ion component must remain constant for negative V_c. At some negative value of V_c, when all electrons are retarded, the total ion current will be indicated as the absolute value of I_c. This value must therefore equal or exceed the ion current, ΔI_c, indicated for positive values of V_c, over some range ΔV_c.

Over the negative V_c range investigated, the data of Fig. B-8 fails to give the sought after verification. For $V_c < -50$ volts, collector current is essentially constant and independent of V_{K1}. The data therefore indicates that essentially all electrons have been retarded. Hence a total ion current of approximately 0.5×10^{-9} amps is indicated. This fails to equal or exceed ion currents indicated for positive V_c when $V_{K1-} < 0$. For example, for $V_{K1} = -40$ volts and $\Delta V_c = 100$ volts ($0 < V_c < +100$ volts), $\Delta I_c = 1.8 \times 10^{-9}$ amps.

Two explanations are possible. One is that some electrons have not been retarded due to the presence of a higher energy component, this would mean that the plateau value of I_c does not represent total ion current. The other explanation (possibly in combination with the first) is that the change in I_c with positive V_c is caused by drawing in increasing numbers of electrons through Q as V_c is made increasingly positive. Lens study data, to be discussed shortly, supports the latter explanation. However, a careful extension of the data to values of $\pm V_c$ in the vicinity of anode potential might be required to answer these questions more completely.

In Fig. B-9, differential collector currents, obtained from the data of Fig. B-8, have been plotted against V_{K1} for selected intervals of retarding field potentials. In view of the above discussion, only those currents plotted for positive values of V_{K1} can be considered a valid quantitative representation of ion beam current as a function of energy (only small electron components are indicated for these values in Fig. B-8). The values shown for negative V_{K1} are probably too high, although possible. Very likely, they are of the same order of magnitude as those of positive V_{K1}. Values of I_c are shown to be essentially independent of positive values of V_{K1}. The percentage of the beam made up of particular energy ions is shown to be essentially invariant with V_{K1}, with low energy ions predominating.

Figure B-10 shows a typical integral ion energy spectrum indicated by the data of Fig. B-8. Ion beam sensitivity in amps/Torr is plotted against ion energy for V_{K1} = +40 volts.

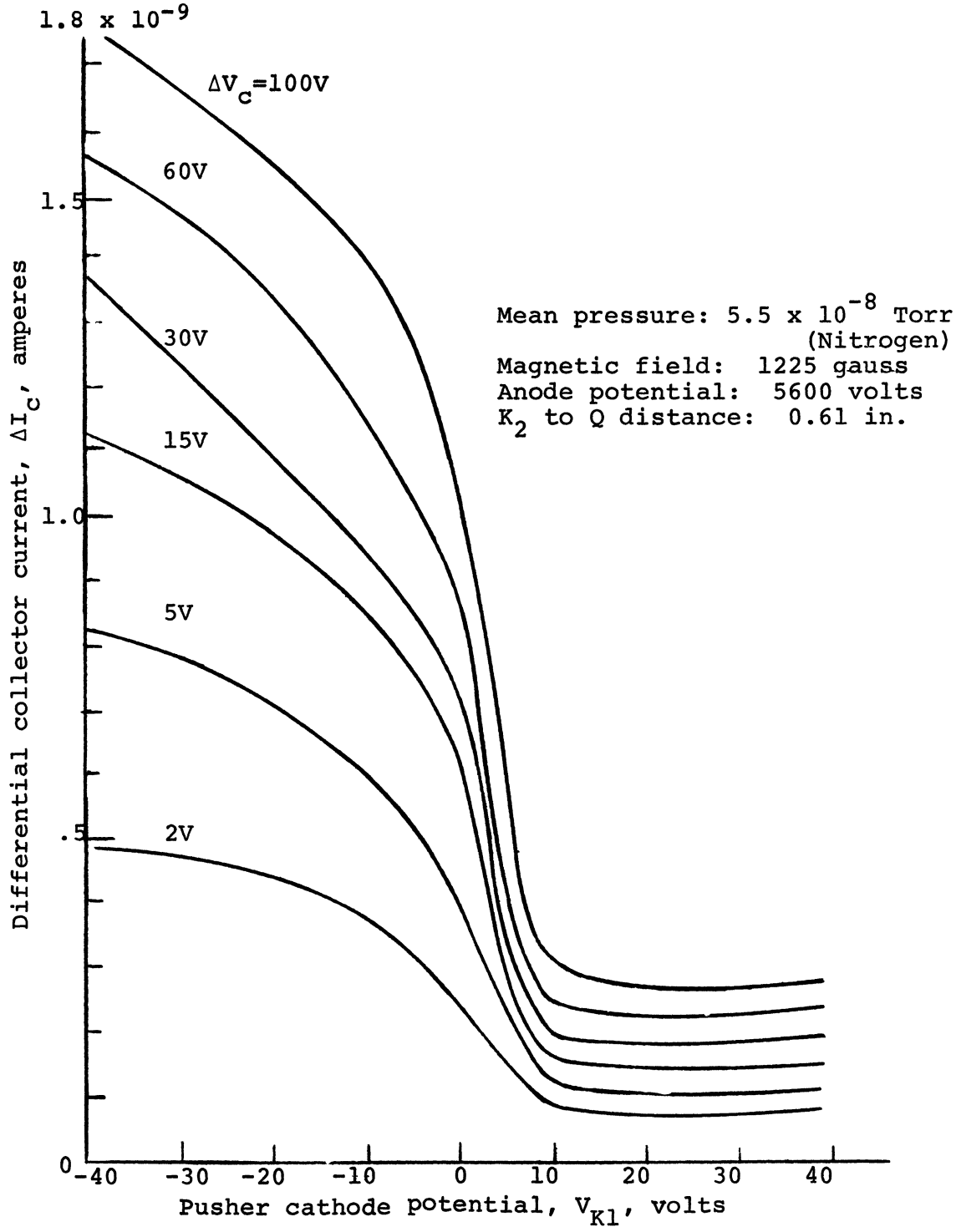

Figure B-9.— Differential collector current vs. pusher cathode potential for selected intervals of collector potential

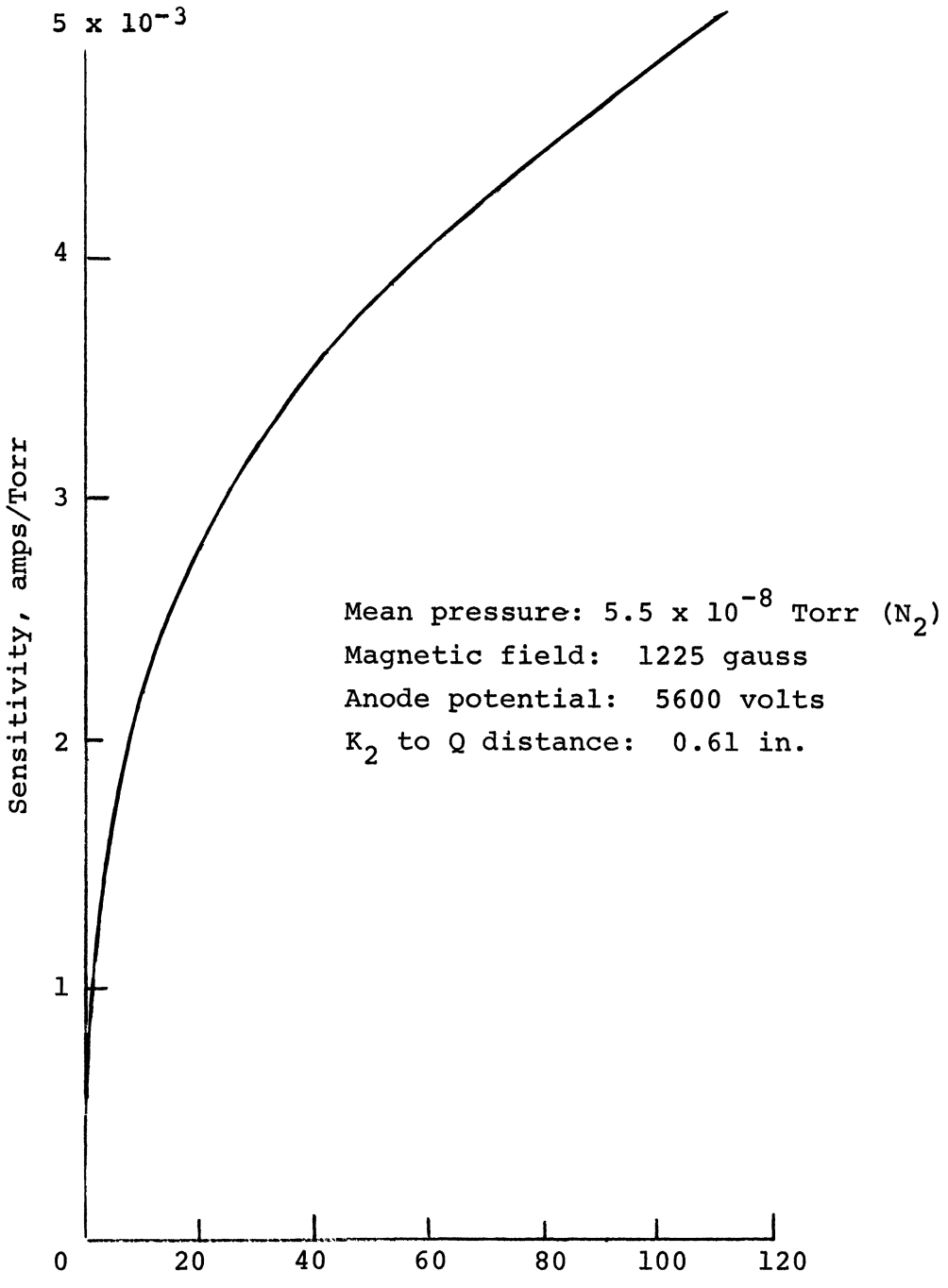

Figure B-10.— Sensitivity vs integral ion energy at 0.61 inches, for V_{K1} at +40 volts

It is seen for example that ions between zero and 30 eV constitute about 2/3 of the ions under 100 eV while ions between zero and 10 eV constitute about half.

Ion energy distribution vs. distance. - In view of the above discussed lack of evidence of a convincing sensitivity advantage of one value of V_{K1} over others, studies of ion energy spectra vs. distance were conducted with V_{K1} = +40 volts, zero and -40 volts. The results of these studies are shown in Figs. B-11, B-12, and B-13 respectively. Differential collector current between zero V_c and selected positive values is shown over a K_2 to Q distance range of 0.14 in. to 1.83 in.

Conditions are essentially the same as in previously discussed data including a mean pressure of 5.5×10^{-8} Torr. However, there is a pressure variation of $\pm 0.3 \times 10^{-8}$ Torr. (The data shown at 0.61 in. is taken from the data of Fig. B-8, already discussed.) Difficulties were encountered with what appeared to be changes in operational mode. As a result, cathode current I_{K1} was observed to change by as much as 35%. While care was taken to preserve the same mode for all data taken, there is doubt about the mode for V_{K1} = +40 volts at 0.88 in. (Fig. B-11). The indicated current therefore may be in error by as much as ±35%.

For all three values of V_{K1} , the highest differential collector current is seen to be obtained nearest the beam exit aperture, (with the exception of values for V_{K1} = +40 at a distance of 0.88 in. for V_c > 30 volts). A current

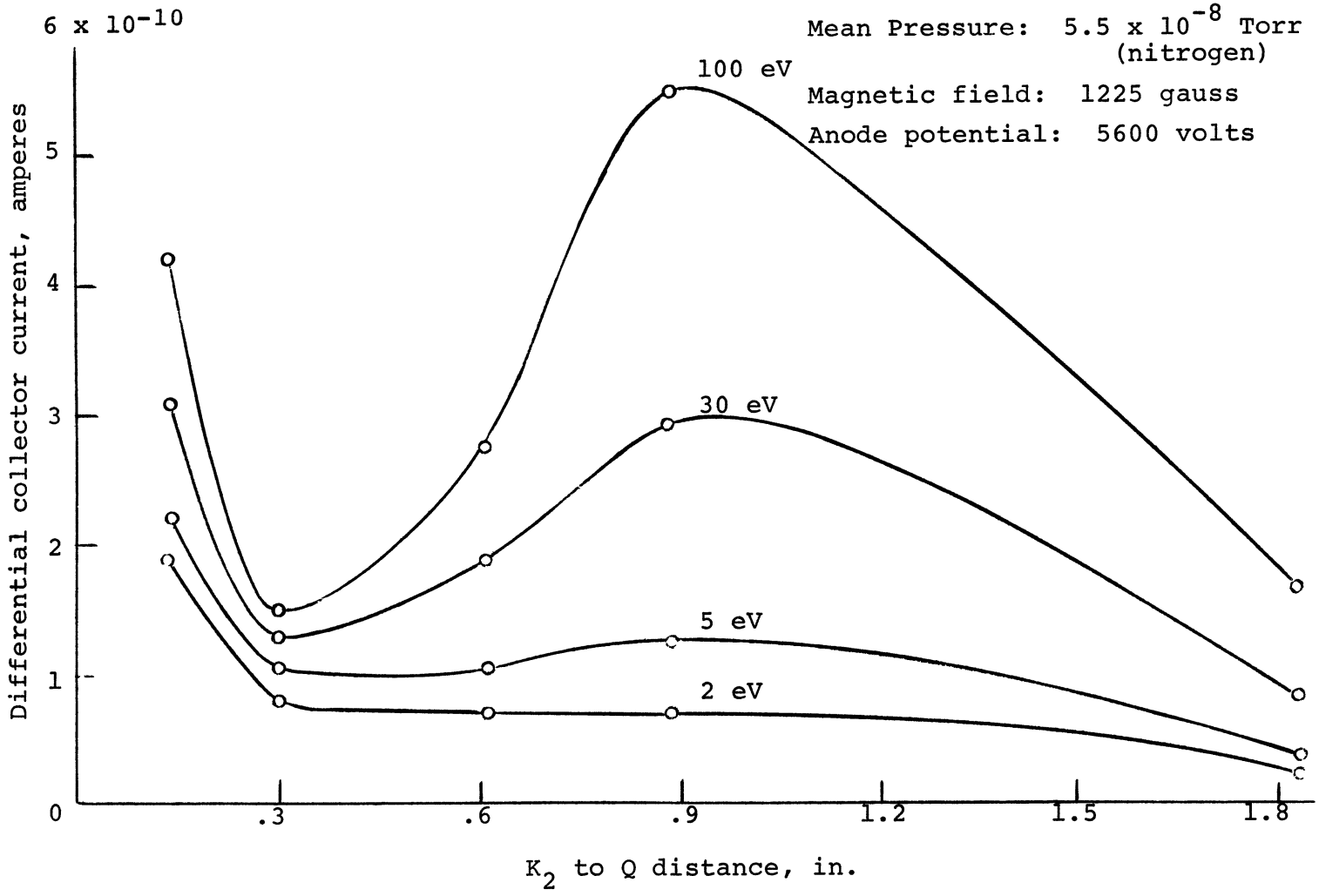

Figure B-11.- Differential collector current vs. distance for selected energy intervals, for V_{K1} = +40 volts

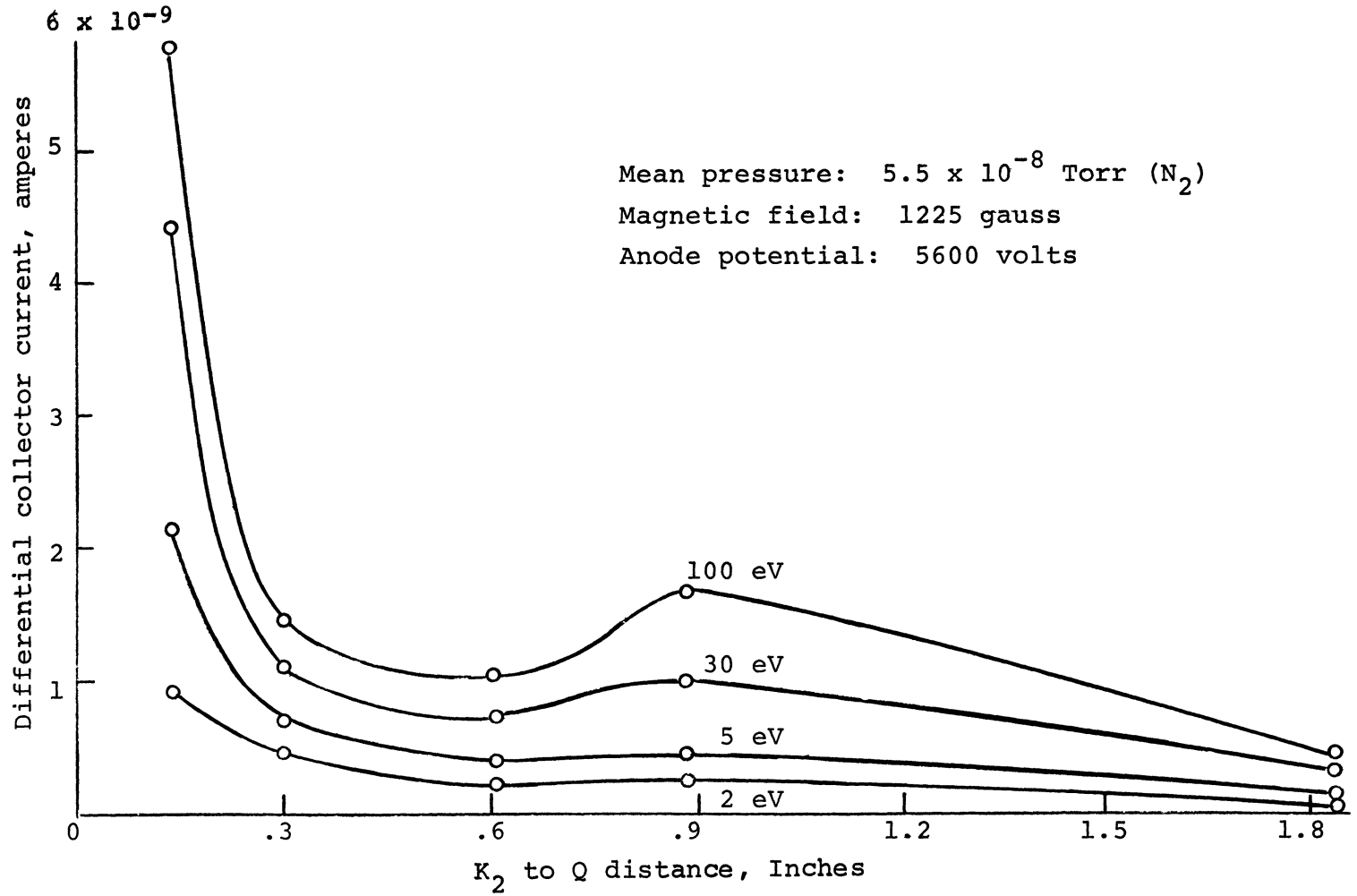

Figure B-12.- Differential collector current vs. distance for selected energy intervals, for V_{K1}= zero volts

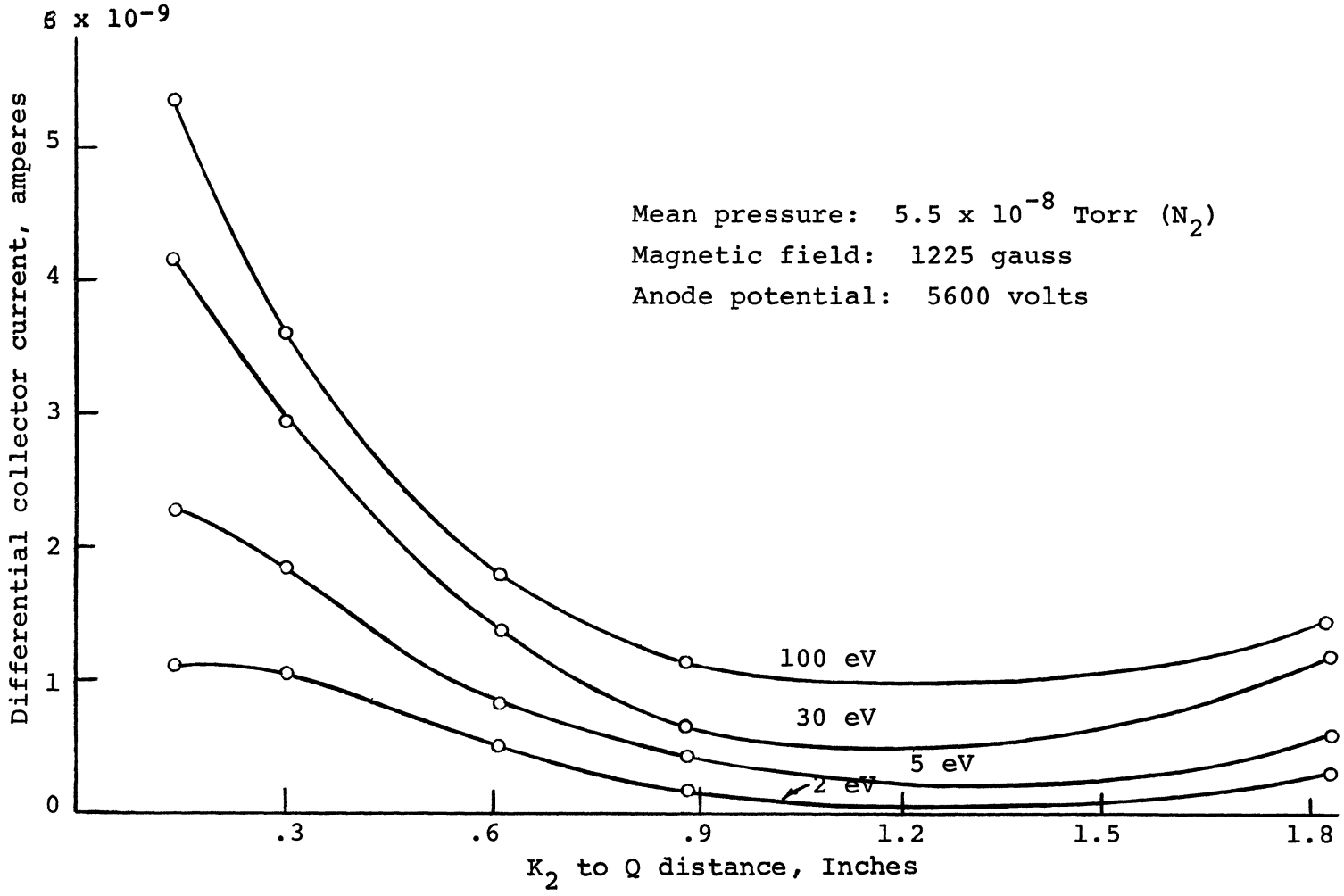

Figure B-13.- Differential collector current vs. distance for selected energy intervals, for V_{K1} = -40 volts

peak also occurs at a point more distant. For V_{K1} = zero volts and +40 volts the second peak is approximately at 0.88 in., while for V_{K1} = -40 volts it is further but less precisely indicated (due to the limited data obtained). The precise energy distribution is seen to vary with both distance and V_{K1}. However, low energy ions are indicated to predominate over all values of V_{K1} and distance in a manner approximating that shown in Fig. B-10.

Considering ions with energy < 30 eV as an example, the highest indicated sensitivities are 5.5 ma/Torr for V_{K1} = +40 volts, at distances of both 0.14 in. and 0.88 in. For V_{K1} = zero volts and -40 volts the indicated sensitivities are 80 mA/Torr and 76 mA/Torr respectively, both at 0.14 in. However, in view of the large electron component present for the latter two V_{K1} values, their sensitivity figures are probably too high, as discussed earlier.

The more conservative figure of 5.5 mA/Torr obtained for V_{K1} = +40 volts at a distance of either 0.14 in. or 0.88 in. compares with 5.1 mA/Torr obtained with the source used in the feasibility study. Since the latter used a Q aperture (then called A-2) nine times the area of the present one, a minimum sensitivity improvement of a factor of 10 is indicated without the use of a lens.

Lens Effectiveness

Three positions of lens and probe were selected for experimentation, as follows:

(1) K_2 to L_2 = 1.38 in. and K_2 to Q = 1.83 in. This constitutes an object distance (K_2 to L_2)

approximately three times the image distance (L_2 to Q) to provide a 1/3 magnification of the K_2 exit aperture at Q. A minimum of one L_3 aperture diameter was left between L_3 and Q to prevent distortion of the lens field and consequent aberration.

(2) K_2 to L_2 = 0.82 in. and K_2 to Q = 1.63 in. This constitutes the closest proximity between K_2, lens and Q for largest beam fraction interception without lens field perturbation, either by the magnetron field or adjacent electrodes. In the event of a nearly parallel beam, nearly all ions would be focused into Q (discounting aberrations) by making Q the focal point.

(3) K_2 to L_2 = 0.46 in. and K_2 to Q = 0.90 in. This constitutes approximately the closest possible distance between K_2, the lens and Q without the three physically touching each other. The largest beam fraction is thereby intercepted by the lens while Q is also closest for maximum demagnification, which in this case is unity. There is no regard for field perturbations by electrode or magnetron field proximity and the importance of such aberrations vs. the importance of intercepting a larger fraction of ion beam is thereby tested. The possibility exists of lens interaction with the field of the magnetron for extraction of a larger number of ions and of focusing a near parallel beam into Q (magnification is then unimportant).

By varying lens potentials over several hundred volts, the requisite focal distances for the indicated positions should be attainable. This is discussed in a previous section entitled "The Lens", together with a fuller discussion of the reasons underlying the choice of the experimental conditions selected and of expected lens performance limitations.

Examples of data obtained at position (1) are shown in Figs. B-14* and B-15 for V_{K1} = zero and +40 volts, respectively. Collector current I_c is shown plotted against lens potential V_{L2} for $-120 < V_{L2} < +120$ volts. This was done for several values of retarding potential V_c, as shown, to note the effect on ions of different energies, since focusing will be energy dependent. Other conditions are essentially the same as for previously discussed experiments without the lens.

It is seen in Fig. B-14 and to a lesser extent in Fig. B-15 that the ratio of differential collector current to differential retarding potential, $\Delta I_c/\Delta V_c$, increases as V_{L2} becomes more positive and decreases as it becomes more negative. Superficially, this appears to indicate ion focusing and ion defocusing, respectively. However, such behavior seems highly unlikely. An important reason is that low energy ions are indicated to be convergent long after V_{L2} is sufficiently positive to retard them; e.g., 10 eV ions (indicated by I_c for $0 < V_c < 10$ volts) are still shown increasing when V_{L2} is +120 volts.

This anomalous behavior can be accounted for by focusing of electrons in the beam. For V_{K1} = 0 (Fig. B-14)

---

*Figures B-14 through B-19 are machine plotted and therefore no data points are shown.

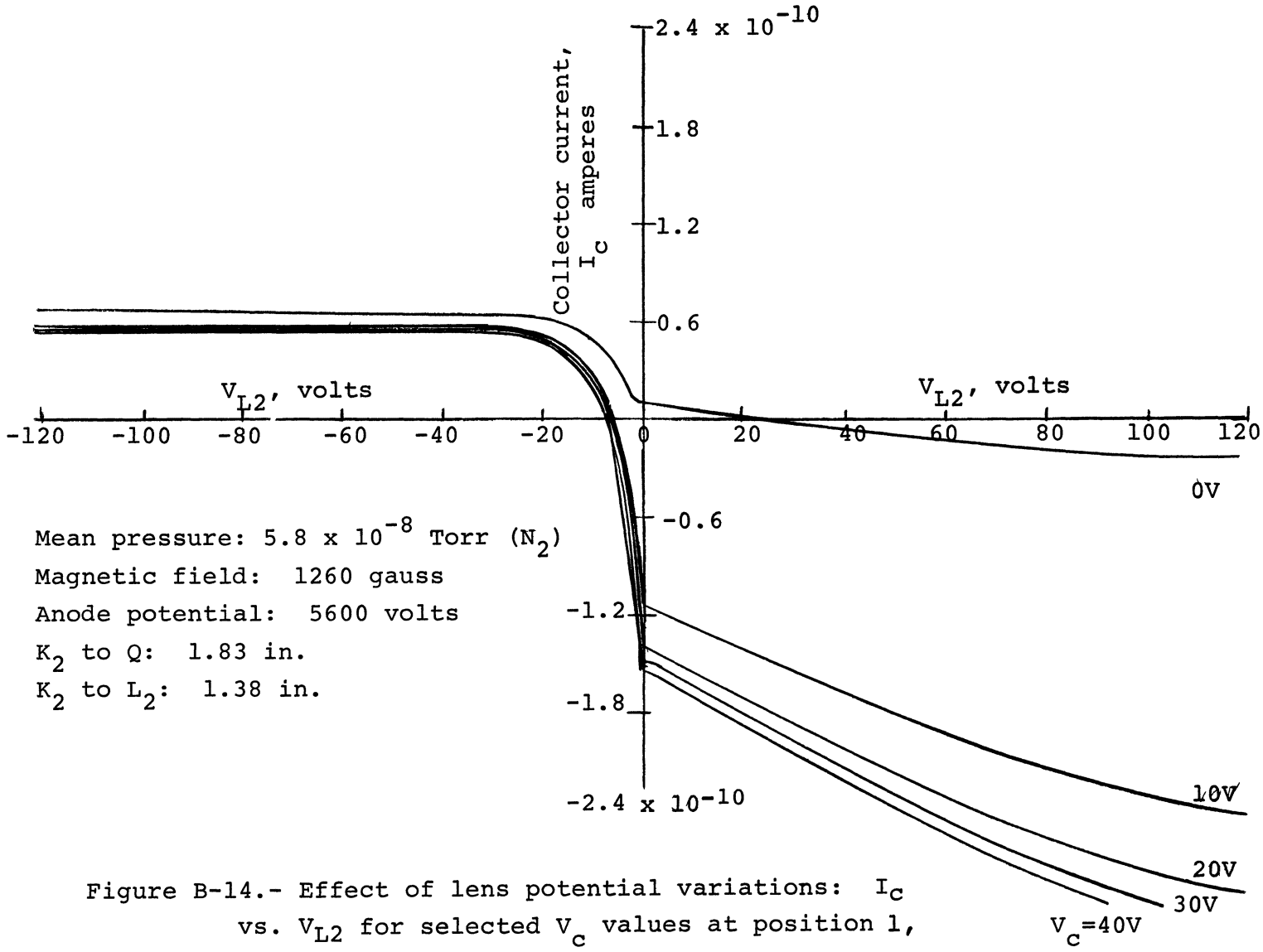

Figure B-14.- Effect of lens potential variations: I_c vs. V_{L2} for selected V_c values at position 1, V_{K1} = zero volts

this effect predominates over ion focusing, over the V_{L2} range shown. Electron focusing is evident because I_c goes negative as V_{L2} goes positive even when $V_c = 0$. However, as indicated by previous data obtained without the lens, electrons also appear to be drawn through Q when V_c is made positive. Therefore, when V_{L2} is made increasingly positive this effect would be enhanced and thus account for the apparent increase in ion current. For $V_{K1} = +40$ (Fig. B-15) this effect is smaller since there are fewer electrons in the beam.

When V_{L2} is made negative, low energy electrons are eventually repelled. Figure B-8 shows that at $V_{K1} = 0$ the electrons (or their low energy component) have a maximum energy of about 20 eV. In Fig. B-14, ΔI_c decreases until V_c is approximately -20 volts. This indicates that only at that point is ΔI_c purely ionic. The latter effect is pronounced for $V_{K1} = 0$ volts because of the predominant electron beam component. This effect also accounts for the increase in I_c at $V_c = 0$, where V_{L2} goes negative. For $V_{K1} = +40$ volts, the effect is negligible due to the very small electron component. Thus, much of the anomalous ion defocusing shown for negative V_{L2} appears accounted for.

The focusing pattern of position (1) was repeated for position (2), as indicated in Fig. B-16.

While a complete understanding of this complicated situation would require perhaps considerably more study, it must be concluded that the lens provides no reliable improvement in ion sensitivity. This possibility was anticipated and a number of reasons for it discussed in "The Lens" section.

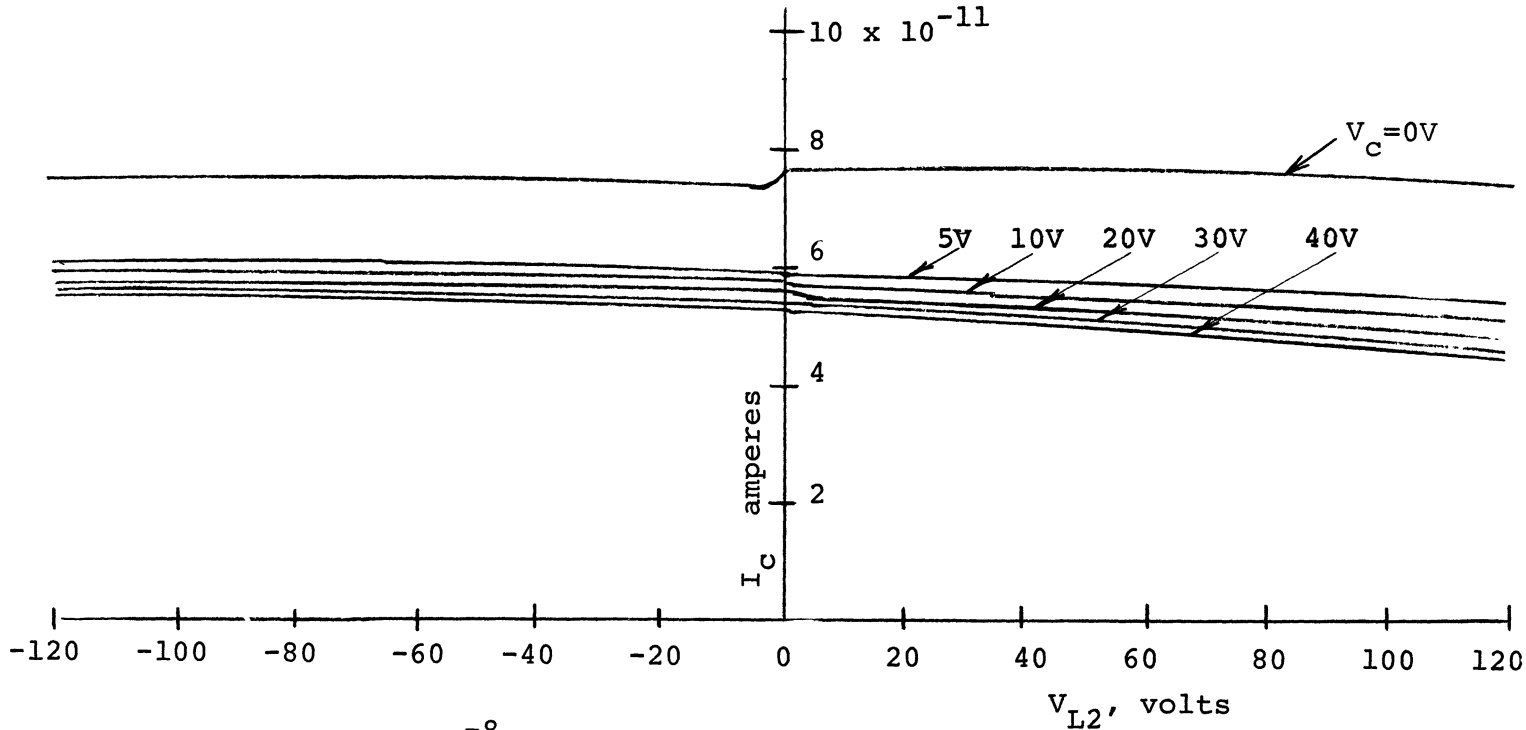

Mean pressure: 5.8×10^{-8} Torr (N_2)
Magnetic field: 1260 gauss
Anode potential: 5600 Volts
K_2 to Q: 1.83 in.
K_2 to L_2: 1.38 in.

Figure B-15.- Effect of lens potential variations: I_c vs. V_{L2} for selected V_c values at position 1, V_{K1} = +40 volts

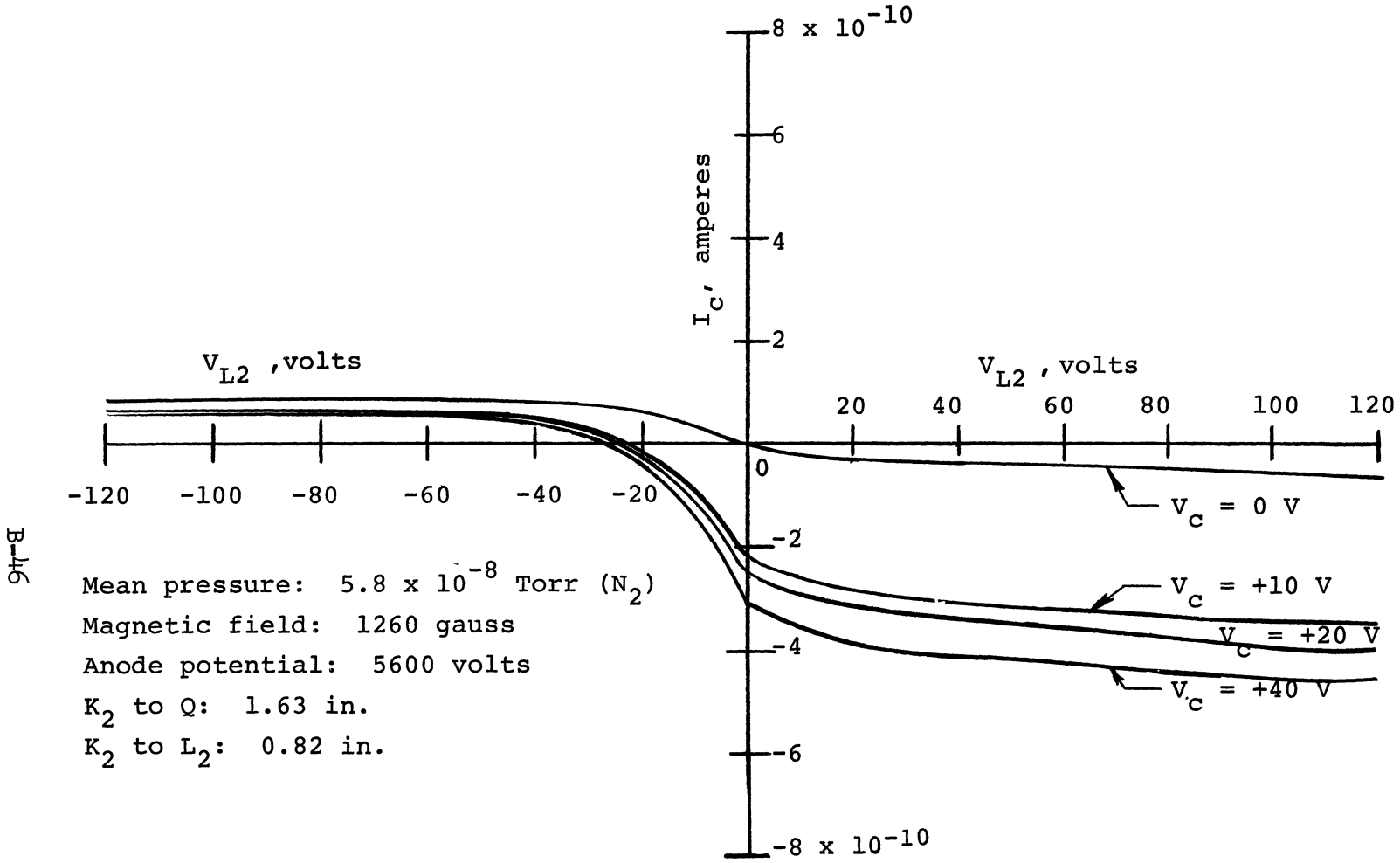

Figure B-16.- Effect of lens potential variations: I_c vs. V_{L2} for selected V_c values at position 2, V_{K1} = zero volts

Focusing was also investigated by plotting collector current I_c against Q aperture current I_Q as a function of V_{L2}.

This was based on the reasoning that when focusing occurs, it must be indicated by both a maximum positive I_c and by a maximum I_c/I_Q ratio. A wider range of lens potentials were used here, in consideration of the possibility that a space charge effect in the lens might be altering its equipotential distributions.

A representative curve obtained for position (2) is shown in Fig. B-17, for V_{K1} = 0 volts. Arrows along the curve indicate the direction taken by the data as V_{L2} was varied from 0 to +540 volts and from 0 to -540 volts. Ion focusing is indicated for both positive and negative values of V_{L2}. The most intense focusing is indicated for positive V_{L2}, with a peak occurring at V_{L2} = +510 volts. However, I_c vs. V_c curves obtained for V_{L2} = +510 volts showed no improved ion current sensitivity in the energy range of interest. The same results were obtained for V_{K1} = +40 volts and -40 volts.

The focusing curve obtained at position (3) is shown in Fig. B-18; it includes data for V_{K1} = 0, -40 and +40 volts. Fig. B-19 shows the associated I_c vs. V_c curves obtained at these focusing potentials, for $-40 < V_c < +40$ volts. As before, no improvement in ion current sensitivity is evident at these low energies. (On the contrary, this approach has led to a decided ion current decrease.)

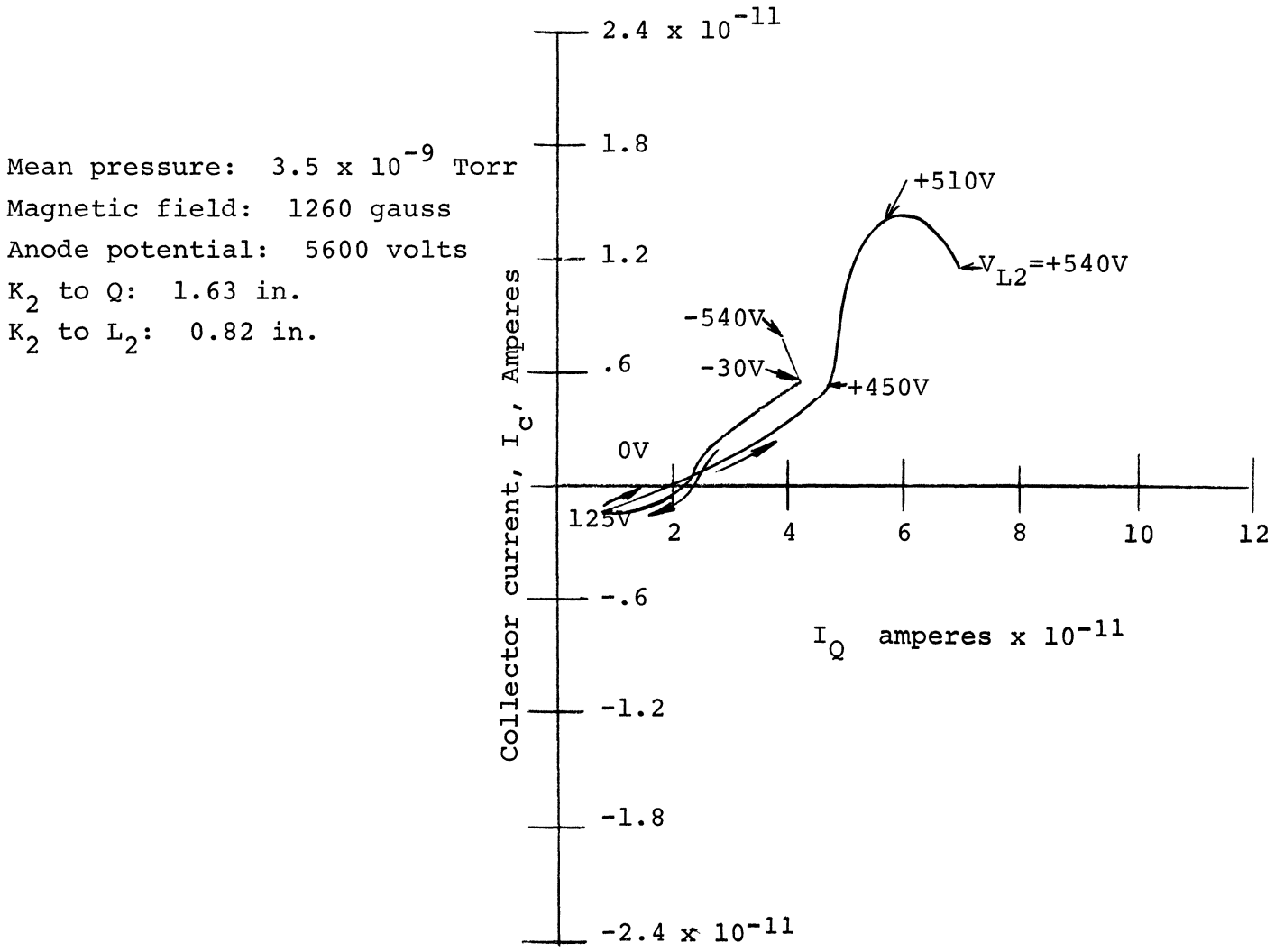

Figure B-17.- Effect of lens potential variations on I_c and I_Q at position 2 for V_{K1} = zero volts

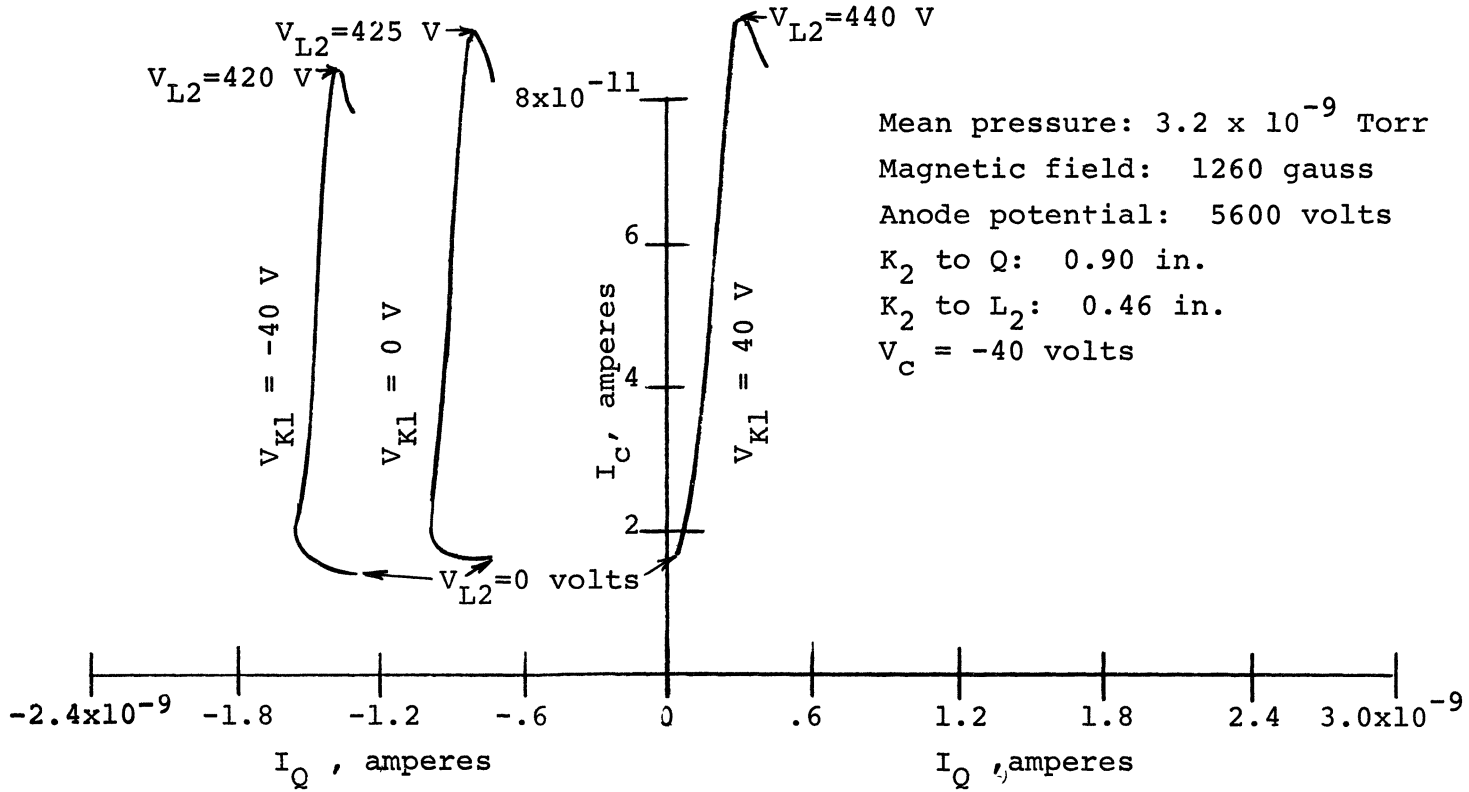

Figure B-18.- Effect of lens potential variations on I_c and I_Q at position 3, for V_{K1} = +40, Zero and -40 volts

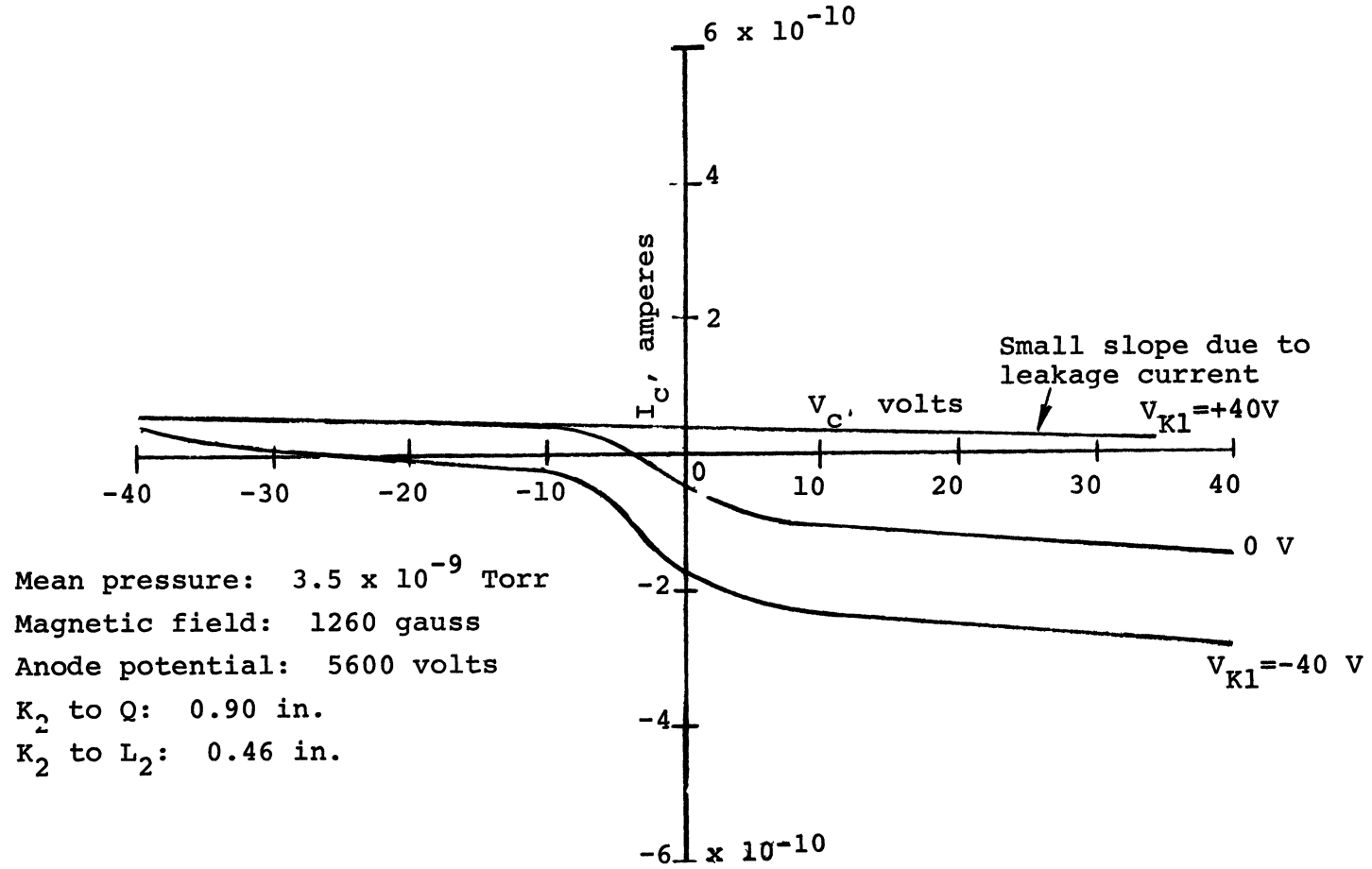

Figure B-19.- Ion and electron energy spectra at focusing potential for position 3: V_{L2} = +420 Volts

Vacuum Performance Characteristics

Subsequent to the above studies, the instrument was prepared for the final stage of experimentation, requiring clean up of the source and system for operation well below 10^{-9} Torr. This phase is primarily concerned with determination of the behavior of ion collector current as a function of pressure and determination of the effects on the ion energy distribution of gas composition.

The design originally called for replacement of the "Swagelok" connector with a ceramic feedthru after sensitivity studies were performed. However, it was decided that dummy "Swagelok" fittings, substituting steel washers for teflon, would enable high temperature bakeout, while lens or Q plate feedthrus could be used for the collector.

Unfortunately, subsequent to high temperature bakeout of the source with the latter arrangement, leaks developed in three of the feedthrus. Repeated attempts at repairing them without hazarding new feedthru welding operations proved unsuccessful. It was therefore impossible to conduct the gas composition and linearity studies under this contract. (Sensitivity of I_C and I_{K_1} vs. pressure was checked and found to be linear between 1×10^{-8} and 5×10^{-8} Torr.

QUADRUPOLE MASS SPECTROMETER DESIGN

Summary of Design Criteria

Reasons for selection of the quadrupole analyzer, discussion of its general design criteria and mass scanning

modes, as well as associated references are contained in the final report for Contract NAS1-2691, Task 2 (Appendix A). The following design equations and mode selection are taken from that report.

The quadrupole mass analyzer is illustrated in Fig. B-20 together with ion source and ion detector; symbols used in the following discussion are also indicated. The analyzer consists of four rods with superimposed steady state and rf potentials on each. The rf potential on one pair of rods is 180° out of phase with the other pair. Operation derives from the motion of ions in the field of these rods. The descriptive equations of their motion, using cartesian coordinate axes, x, y and z, are

$$M\ddot{x} + e\,(U + V\cos 2\pi\nu t)\,x/r_o^2 = 0 \qquad \text{(B2)}$$

$$M\ddot{y} - e\,(U + V\cos 2\pi\nu t)\,y/r_o^2 = 0 \qquad \text{(B3)}$$

where

M = mass of the ion

U = steady state rod potential

V = rf rod potential

ν = frequency of the V potential

e = electronic charge on the ion

r_o = radius of circle inscribed by the four rods

Ion trajectories, determined from the solution of these equations may be either stable or unstable. If unstable, or

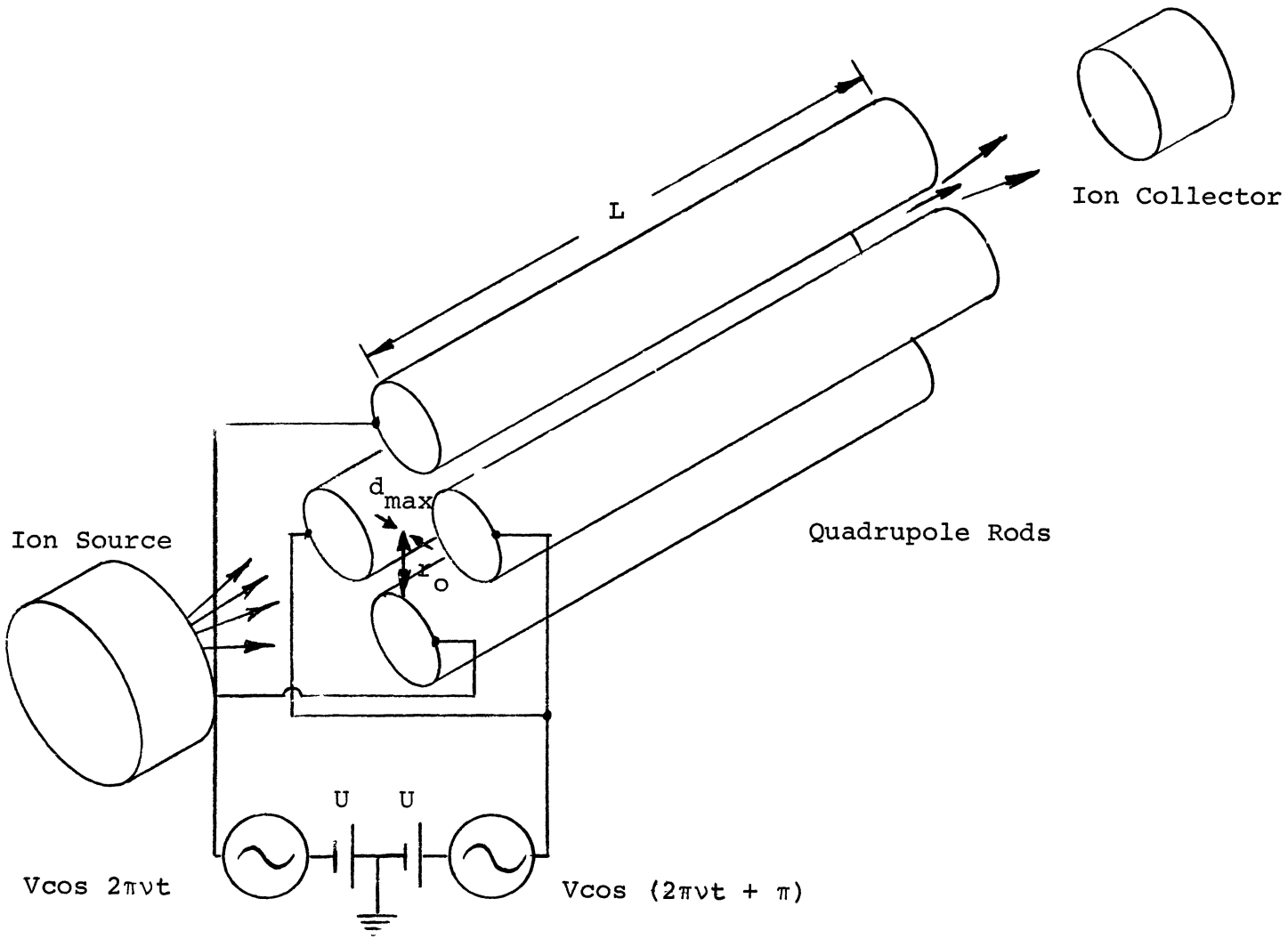

Figure B-20.- Schematic of Quadrupole Mass Analyzer

if stable with amplitude $\geq r_o$, the ions will be captured by the rods after a sufficient number of cycles of the rf field. The filtering process operates by providing stable, bounded paths only for the mass selected. A stable trajectory exists if

$$M = 2.30 \times 10^{-20} \, V/\nu^2 r_o^2. \tag{B4}$$

A mass spectrum is thus scanned by varying V and/or ν. (Mks units are used unless otherwise stated.)

Three scanning modes have been described in the literature. The mode selected requires the mass peak width, ΔM, to remain constant. Since the resolution is determined from

$$\frac{M}{\Delta M} = \frac{0.126}{0.16784 - U/V} \tag{B5}$$

the selected scanning mode and a choice of 1 amu for ΔM requires that

$$U = 0.1678 \, V - 9.10 \times 10^{-9} \, \nu^2 r_o^2 \tag{B6}$$

For a fixed peak width, 100% transmission of stable ions can be obtained by satisfying the following conditions:

$$\text{Potential stability} = \frac{1}{2} \left(\frac{\Delta M}{M}\right) \tag{B7}$$

$$\text{Frequency stability and dimensional accuracy} = \frac{1}{4} \left(\frac{\Delta M}{M}\right) \tag{B8}$$

$$U_{T_{max}} = \frac{V}{15} \left(\frac{\Delta M}{M}\right) \tag{B9}$$

where $U_{T_{max}}$ = maximum transverse energy of ions injected on axis (in electron volts).

$$U_{A_{max}} = 5.82 \times 10^{-3} \frac{L^2 V}{r_o^2} \left(\frac{\Delta M}{M}\right) \tag{B10}$$

where $U_{A_{max}}$ = axial ion energy and L = length of the quadrupole rods.

$$d_{max} = r_o \left(\frac{\Delta M}{M}\right)^{\frac{1}{2}} \tag{B11}$$

where d_{max} = maximum allowable beam diameter for axially directed ions.

The power P required of the device is

$$P = 2.36 \times 10^{40} C M^2 \nu^5 r_o^2 / Q \tag{B12}$$

where C = total capacitance of the quadrupole and Q^* = figure of merit of the final tank circuit of the rf generator.

Design Chart

Construction. - A design chart has been constructed to simplify the otherwise complicated interrelationships of quadrupole design parameters and thus to allow selection of characteristics that will be optimally matched to those of the cold-cathode ion source.

---

*No relation to the Q aperture plate symbol used elsewhere in the text.

For the detection of masses from 2 to 100 amu, selection of a mode where ΔM remains fixed and equal to 1 amu ensures that essentially no adjacent peak overlap will occur. Imposition of the requirements of Eqs. (B7) through (B11) ensures essentially 100% transmission of stable ions. Design flexibility has thus been reduced. However, still unspecified and/or undetermined, are values for V, r_o, $U_{T_{max}}$, d, P, $U_{A_{max}}$, L, ν and U.

To clarify the interdependency of these parameters, the preceding design equations have been rewritten in terms of a minimum number of variables. These are V, r_o and L. (While ΔM, M, C and Q also enter into the equations, they are fixed. ΔM is 1 amu, M has a maximum value of 100 amu and Q and C are made as high and low, respectively, as practicable; reasonable estimates of these values, which were used in the preceding equations are Q = 300 and C = 100 pF.) Constants in the rewritten equations have been calculated for all variables in mks units except for M and ΔM, which are in amu. The following equations remain unchanged:

$$U_{T_{max}} = \frac{V}{15} \left(\frac{\Delta M}{M}\right) \tag{B9}$$

$$U_{A_{max}} = 5.82 \times 10^{-3} \frac{L^2 V}{r_o^{\,2}} \left(\frac{\Delta M}{M}\right) \tag{B10}$$

$$d_{max} = r_o \left(\frac{\Delta M}{M}\right)^{\frac{1}{2}} \tag{B11}$$

Equation (B4) is rewritten to give ν explicitly in the new units

$$\nu = \frac{3710}{r_o} \sqrt{V/M} \ . \qquad \text{(B4a)}$$

Equation (B12) is rewritten by substituting M from Eq. (B4) and ν from Eq. (B4a). This gives

$$P = \frac{1.52 \times 10^{-8} V^{5/2}}{r_o M^{\frac{1}{2}}} \qquad \text{(B12a)}$$

Equation (B6) is rewritten by substituting ν from Eq. (B4a). This gives

$$U = V\ (0.16784 - 0.125/M) \qquad \text{(B6a)}$$

or

$$U_{max} \approx 0.168V \text{ (for M = 100 amu)} \ . \qquad \text{(B6b)}$$

The design chart was constructed from a selected range of values for V, r_o and L using the above equations. It is shown in Fig. B-21.

V, r_o, and L are independent of each other. All other parameters depend on either V, r_o or both and are therefore tabulated to their right. L effects only $U_{A_{max}}$ and therefore heads only the $U_{A_{max}}$ columns. The chart is constructed with M = 100 amu, the largest mass to be analyzed.

Interpretation and selection of values. - Once a design is chosen, r_o, L, ν, and $U_{A_{max}}$ remain fixed. L and r_o remain fixed because they pertain to the physical dimensions of the quadrupole (Fig. B-20). Frequency ν is kept fixed by mode choice. Fixed values of ν and r_o then force the ratio V/M to remain fixed (Eq. B4a). Since M = 1 amu, and

V (volts)	r_o (cm)	$U_{T_{max}}$ (eV)	d_{max} (mm)	ν (MHz)	P (watts)	$U_{A_{max}}$ (eV) L=5cm	L=10cm	L=15cm	L=20cm	L=25cm	V (volts)
500	0.5	0.33	0.5	1.660	1.700	2.890	11.60	25.90	46.40	72.60	84
	0.9	0.33	0.9	1.922	0.950	0.893	3.56	9.00	14.20	22.40	84
	1.3	0.33	1.3	0.639	0.655	0.428	1.71	3.84	6.85	10.70	84
	2.0	0.33	2.0	0.415	0.425	0.181	0.72	1.62	2.89	4.52	84
1000	0.5	0.67	0.5	2.340	9.600	5.750	23.00	51.80	92.10	144.00	167
	0.9	0.67	0.9	1.300	5.250	1.770	7.10	15.90	28.40	44.40	167
	1.3	0.67	1.3	0.900	3.690	0.850	3.40	7.65	13.60	21.30	167
	2.0	0.67	2.0	0.585	2.400	0.361	1.44	3.25	5.78	9.05	167
2000	0.5	1.34	0.5	3.320	54.500	11.600	46.20	104.00	185.00	290.00	334
	0.9	1.34	0.9	1.840	30.200	3.520	14.30	32.00	57.10	88.00	334
	1.3	1.34	1.3	1.280	21.000	1.730	6.90	15.50	24.20	43.10	334
	2.0	1.34	2.0	0.830	13.600	0.725	2.90	6.60	11.60	18.40	334
3000	0.5	2.00	0.5	4.070	150.000	17.400	69.70	157.00	279.00	436.00	501
	0.9	2.00	0.9	2.260	83.000	5.380	21.40	48.60	85.60	129.00	501
	1.3	2.00	1.3	1.560	52.500	2.560	10.20	23.10	41.00	64.10	501
	2.0	2.00	2.0	1.030	38.000	1.110	4.45	10.00	17.80	27.90	501
7500	0.5	5.00	0.5	6.430	1480.000	43.600	174.00	392.00	697.00	1091.00	1250
	0.9	5.00	0.9	3.580	822.000	13.400	54.80	122.00	215.00	337.00	1250
	1.3	5.00	1.3	2.470	568.000	6.400	25.60	57.90	102.00	160.00	1250
	2.0	5.00	2.0	1.600	368.000	2.730	10.90	24.70	43.70	68.40	1250

Figure B-21.- Quadrupole Design Chart

since V/M, L and r_o are fixed $U_{T_{max}}$ and $U_{A_{max}}$ must also remain fixed (Eqs. B9 and B10).

As a consequence of the above fixed values, V, d_{max}, P and U are mass dependent. This is evident by inspection of Eqs. (B4a), (B11), B12a), and (B6a), respectively. Since numerical chart values are calculated for M = 100,amu values of V, P and U shown are the maximum required, while d_{max} is the smallest required.

Selection of the mutually independent parameters V (for mass 100), r_o and L specifies the quadrupole design. Determination of optimum values will not be considered.

It is evident from the chart that the larger V is made, the larger is the resulting analyzer sensitivity, since both $U_{T_{max}}$ and $U_{A_{max}}$ are thereby increased. The value of V has no effect on the maximum allowable beam diameter d_{max} and it poses no design problem on frequency ν or steady state potential U over the ranges tabulated. The upper limit on V is determined by the associated power requirements P. The higher V is made the larger is the resulting P, with resultant increases in size and cost of the rf power supply. The Atlas quadrupole described by Brunnee (ref. B13) uses a power supply whose size appears reasonable. It produces 30 watts of rf power, in addition to other power requirements. This is accomplished in a standard rack mounted chasis with 9 x 19 in. front panel dimensions. This would allow V in the 2000 to 3000 volt range and results in a $U_{T_{max}}$ of about 2.00 eV.

The chart illustrates that increasing r_o has two opposing effects on quadrupole sensitivity: (1) It increases the sensitivity by allowing increased beam diameter (since d_{max} is proportional to r_o (Eq. B11), area and, hence, sensitivity is proportional to r_o^2). (2) It decreases sensitivity by restricting the permissable axial ion energy $U_{A_{max}}$ is inversely proportional to r_o^2 (Eq. B10). Experimental results indicate condition (1) to be overriding since the ion current rate of increase diminishes with increased ion energy (Fig. B-10).

The chart also shows that increased r_o results in a beneficial decrease in power requirements. Resultant frequency changes are unimportant and no other parameters are affected. The primary limitation on r_o is the detrimental effect of large rod surface area on vacuum performance. (Rod radius is 1.16 x r_o. The diameter of the total cross sectional area of the instrument is 6.64 r_o.) For V between 2000 and 3000 volts, an r_o of about 1.0 cm appears to be a reasonable compromise.

It is obvious that L affects only $U_{A_{max}}$, which is proportional to L^2 (Eq. B9). It is therefore desirable to make L as large as possible to increase sensitivity. However, the radial energy component limitations (about 2.00 eV) imposed by power requirement limitations, discussed above, limit the sensitivity gain resulting from very long rods; few ions can be anticipated to have less than a few percent of their total energy in a radial component. A $U_{A_{max}}$ between 30 and 100 eV therefore appears adequate. This can be accomplished with a rod length of about 20 cm for the above selected values of r_o and V.

CONCLUSIONS

It is concluded that the next stage of development should involve the physical coupling of a quadrupole mass analyzer and the cold-cathode ion source. The present basic source configuration should be used and situated so that the quadrupole entrance aperture is at one of the positions of greatest intensity. Both analysis and experimental results indicate that a lens will not benefit this situation.

APPENDIX B

REFERENCES

B1. Redhead, P. A.: The Magnetron Gauge: A Cold-Cathode Vacuum Gauge. Can. J. Phys., vol. 37, 1959, pp. 1260-1271.

B2. Hobson, J. P.; and Redhead, P. A.: Operation of an Inverted-Magnetron Gauge in the Pressure Range 10^{-3} to 10^{-12} MM. Hg. Can. J. Phys., vol. 36, 1958, pp. 271-288.

B3. Hall, C. E.: Introduction to Electron Microscopy. McGraw-Hill, New York, 1953, pp. 63-64, p. 184.

B4. Ibid., p. 51.

B5. Gabor, D.: The Electron Microscope. Chemical Publishing Company, New York, 1948, p. 11.

B6. Hall, C. E., op. cit., p. 73.

B7. Zworykin, V. K.; et al.: Electron Optics and the Electron Microscope. John Wiley & Sons, New York, 1945, p. 439.

B8. Ibid., pp. 436-440.

B9. Hall, C. E., op. cit., p. 72.

B10. Zworykin, op. cit., p. 438.

B11. Klemper, O.: Electron Optics. University Press, Cambridge, England, 1953, pp. 4-64.

B12. Helmer, J. C.; and Jepson, R. L.: Electrical Characteristics of a Penning Discharge. Proc. of the I. R. E., vol. 49, 1961, pp. 1920-1925.

B13. Brunnée, C.; Delgmann, L.; Kronenberger K.: The Atlas Quadrupole Mass Spectrometer. (Paper presented at Mass Spectrometry Conference, ASTM Committee E-14, May 1963, in San Francisco.)